Active Control of Smart Grids

Brenda Rojas Delgado

in partial fulfillment of the requirements to obtain
the degree of Doctor in
Electrical Engineering, Electronics and Automation

Universidad Carlos III de Madrid

Advisors:

Ph.D. Mónica Alonso Martínez
Ph.D. Hortensia Amarís Duarte

Tutor:

Ph.D. Hortensia Amarís Duarte

Leganés, April 2019.

A Malula, donde quiera que esté.

ACKNOWLEDGEMENTS

To my mother, for giving me the life, and to my family, for loving and supporting me unconditionally.

To my closest friends, who have been loyal and supportive to me during all this journey to pursue my PhD candidature. Even when sometimes I was going crazy and with the desire of giving up, they raised me up to keep going.

To my "guapa" and her family, whom I consider that have been my other family during all these years living in Madrid. Without them, my life in this big city would have been tougher, and they represent the kind of people I would like to be surrounded by from now on.

To my supervisors Ph.D. Monica Alonso and Ph.D. Hortensia Amarís at UC3M, who were always supportive to me and believed in my capacity to accomplish this goal, besides of helping me to pursue the scholarship I have finally won to go to Uppsala this year.

To my supervisor Ph.D. Juan de Santiago at Uppsala University, whom has introduced me to the world of Wave Energy Conversion, and still collaborates me when it comes to scientifically validates my models, apart from his assistance with many issues everytime I went to work at there.

To the Electrical Engineering Department at UC3M and Division of Electricity at Uppsala University, for all of the support and guidance.

To Mustafa Amiryar, from University of London City, for kindly allowing me to use a figure of his authorship to describe the flywheel model employed in the researches undertaken in this thesis.

Lastly, I would like to give special thanks to the Unit of Hydrostatic Pressure in Closed Tanks and its research leader, Mikael Bergkvist. Without them, my staying at Ångström-laboratoriet would have never be the same.

To all of you, as the late Gustavo Ceratti would have said: Gracias Totales!

PUBLISHED AND SUBMITTED CONTENTS

These documents include contents that have been either submitted or published by the same author in:

- M. Alonso, H.Amarís, B. Rojas, D. Della Giustina, A. Dedè, Z. Al-Jassim "Optimal network reconfiguration for congestion management optimization in active distribution networks" Renewable Energy & Power Quality Journal, Vol.1, No.14, pp: 879- 884. May 2016. ISSN: 2172-038X.
  - Materials from this source is included in Chapter 5.
  - All material of this source included in this thesis is not pointed out with typographic means or reference.
- B. Rojas, M. Alonso, H. Amarís, L.González "Coordinated management of low voltage power networks with photovoltaic energy sources". International Journal of Smart Grid and Clean Energy, vol. 5, no. 4, October 2016: pp. 213-220. ISSN: 2315-4462.
  - All material of this source included in this thesis is explicitly pointed out at [1].
- M. Alonso, H. Amarís, L. González-Juárez, B. Rojas, D. D. Giustina, A.Dede. "Gestión de Congestiones en Redes Eléctricas Inteligentes". III Congreso Smart Grids. Mayo 2016. III Congreso Smart Grids 18 y 19 de octubre 2016. vol 1, pp: 1-6. ISBN:978-84-617-5031-3.
  - Materials from this source is included in Chapter 5.
  - All material of this source included in this thesis is not pointed out with typographic means or reference.
- L. González-Juárez, H. Amarís, ,B. Rojas, M. Alonso. "Control coordinado de tensión en redes inteligentes: desarrollo e implementación "Hardaware in the Loop"". III Congreso Smart Grids 18 y 19 de octubre 2016. vol 1, pp: 31-36. ISBN:978-84-617-5031-3.
  - Materials from this source is included in Chapter 5.
  - All material of this source included in this thesis is not pointed out with typographic means or reference.

- B. Rojas, M. Alonso, H. Amarís, J. de Santiago "Wave Power Output Smoothening by a High-Speed Kinetic Buffer". Energies, Special Issue "Marine Tidal and Wave Energy Converters: Technologies, Conversions, Grid Interface, Fault Detection, and Fault-Tolerant Control", 2019. *In review*.
  - Materials from this source is included in Chapter 4.
  - All material of this source included in this thesis is not pointed out with typographic means or reference.

Figure 4.12 (Chapter 4, Section 4.3, Subsection 4.3.1) is explicitly referenced and was authorized in its usage by its author, Mustafa Amiryar, from University of London City.

OTHER MERITS

These documents include contents that have been either submitted or published by the same author, but not included in the thesis.

- L. Gonzalez, H. Amaris, B.Rojas, M.Alonso. "Power-in-the-loop" simulation of an active distribution network". The 9th International Conference on Real-Time Simulation Technologies. MUNICH 7-8 JUNE, 2016.
  - This contribution is not included in this thesis

RESUMEN

Según la Agencia Internacional de la Energía, la energía procedente de fuentes renovables se ha visto incrementada en un 10% en los últimos años, situándose en el año 2017 en un 25%. La incorporación de la generación renovable en los sistemas de distribución puede dar lugar a flujos de potencia bidireccionales y congestiones en la red.

Integrar de forma eficiente las nuevas unidades de generación distribuida, así como los vehículos eléctricos y los consumidores finales en la gestión de los sistemas de distribución manteniendo la calidad del servicio es uno de los grandes retos a los que se enfrentan los operadores de las redes de distribución (DSO). Como consecuencia de este nuevo paradigma, algunos países de la UE han desarrollado códigos de red que permiten a dichas unidades participar en los servicios complementarios de la red a la que se encuentran conectados. Sin embargo, las herramientas empleadas por los DSOs han demostrado no ser eficientes en la resolución de congestiones en las redes de distribución, a pesar de disponer de recursos distribuidos capaces de dar respuesta a esta necesidad. Además, las unidades de generación distribuida de las redes de distribución podrían ser empleadas en la resolución de congestiones de las redes de transporte si se desarrollan herramientas de operación coordinada de las redes de transporte y distribución.

El objetivo de esta tesis doctoral es desarrollar métodos y procedimientos que permitan regular la tensión de las redes de distribución de media y baja tensión con alta penetración de generación distribuida. Las herramientas desarrolladas permiten a los DSOs regular la tensión de las redes de media y baja tensión mediante la gestión de los recursos energéticos distribuidos presentes en su red (generación distribuida, almacenamiento, vehículo eléctrico). Además, las herramientas desarrolladas permiten ofertar servicios complementarios de control de tensión a la red de transporte.

La aplicabilidad de la estrategia desarrollada se ha demostrado en una red eléctrica real de 140 nudos localizada en España, en condiciones normales de operación de las redes de media y baja tensión, así como ante contingencias en la red de media tensión. En cada una de las condiciones de estudio se ha analizado la respuesta de tres estrategias de control de tensión: control local descentralizado, control distribuido y control coordinado. A partir de los resultados obtenidos se puede concluir que asignar óptimamente las consignas de operación de las unidades de generación distribuida presentes en los sistemas de distribución permite minimizar las pérdidas de potencia en los sistemas de distribución, minimizar el tamaño de las unidades de inyección de potencia reactiva presentes en los mismos, así como mejorar la vida útil de los transformadores de conexión de los sistemas de media y baja tensión.

Palabras clave: Almacenamiento, Control coordinado, Energías Renovables, Redes Eléctricas, Respuesta de la Demanda.

ABSTRACT

According to the International Energy Agency, power generation from renewable energy sources has increased worldwide from 15% in 2004 to 25% in 2017. In some situations, installing sources of renewable origin onto distribution grids creates network congestions and distribution networks are not prepared enough to manage the bidirectional flow of this energy.

In some EU-countries, grid codes are being defined so that the distributed generation can supply complimentary services to the grid at the connection point when the distributed generation is connected to the distribution grid. Currently, there is a need of implementing tools that help distribution system operators to manage the distribution grids. These tools are beneficial for distributed generation integration, electric vehicles connection, and the participation of the energy end-users, as the grids help to maintain both power efficiency (i.e., electric losses reduction) and the electricity supply quality. The aforementioned aspects show that grid operators do not possess the right tools that allow them to solve congestions in their grids, even though they have distributed resources that allows them to solve these congestions. Moreover, they do not have the proper tools to coordinate its operation with the transmission systems operators and they also cannot provide the assurance of offering distribution networks' flexibility services in order to, eventually, solve congestion problems in higher voltage power networks.

The aim of this doctoral thesis is to develop methods and procedures that can improve the voltage regulation of medium voltage and low voltage distribution networks that have a high penetration of distributed energy resources. The developed methods will allow distribution network operators to manage their distributed energy resources (distributed generation, storage systems, electric vehicles) in almost real-time; in this way, the distribution grid can regulate both voltages at low and medium levels, and it can offer a complimentary service of voltage control to the transmission network.

The applicability of the proposed strategy is demonstrated in a real 140-node power network located in Spain, regarding normal operation in the medium voltage and low voltage networks and abnormal situations in the medium voltage network. In each situation, three voltage control strategies are compared: local decentralized voltage control, distributed voltage control, and coordinated voltage control. In view of the results, it can be concluded that the implementation of the proposed algorithm allows the power losses in the system to be minimized if a coordinated optimal assignation of the distributed generation units present in the whole system is undertaken.

Keywords: Coordinated Control, Demand Response, Smart Grids, Renewable Energies, Storage Systems.

CONTENTS

LIST OF FIGURES

LIST OF TABLES

LIST OF ACRONYMS

ADN	Active Distribution Network
ADS	Active Distribution Systems
AMI	Advanced Metering Infrastructure
AVR	Automatic Voltage Regulator
BACS	Building Automation and Control System
BESS	Battery ESS
CB	Capacitor Bank
CENELEC	European Committee for Electrotechnical Standardization
CIM	Common Information Model
CIS	Consumer Information Systems
CVC	Coordinated Voltage Control
CVC-LV	Coordinated Voltage Control - Low Voltage
CVC-MV	Coordinated Voltage Control - Medium Voltage
D-FACTS	Distributed FACTS
D-SFC	Distributed SFC
D-TCSC	Distributed TCSC
DER	Distributed Energy Resources
DFIG	Doubly-fed induction generator
DG	Distributed Generation
DMS	Distribution Management System
DOE	U.S. Department of Energy
DR	Demand Response
DSM	Demand-Side Management
DSO	Distribution System Operator
DSU	Demand Side Units
DVR	Distributed Voltage Regulator
D-STATCOM	Distribution Static Synchronous Compensator

EDSO	European Distribution System Operators' Association
ENTSO-E	European Network of Transmission System Operators for Electricity
EPRI	Electric Power Research Institute
ESOs	European Standardization organizations
ESS	Energy Storage System
EU	European Union
EV	Electric Vehicle
FACTS	Flexible Alternating Current Transmission System
FEES	Flywheel Energy Storage Systems
GHE	Greenhouse Emissions
GIS	Geographic Information Systems
GSC	Grid Side Converter
HBES	Home and Building Electronic Systems
HES	Home Electronic Systems
$high - T_c$	High-Temperature Superconductors
HPC	Hydraulic and Pneumatic Central
HVAC	Heating, ventilation, and air conditioning
ICT	Information and Communication Technologies
IED	Intelligent Electronic Device
IEA	International Energy Agency
IEC	International Electrotechnical Commission
IEEE	Institute of Electrical and Electronics Engineers
LCD	Line-droop Compensation Function
LP	Low-pass filter
LRS	Lysekil Research Site
LV	Low Voltage
MAS	Multi-Agent System
MPC	Model Predictive Control
MV	Medium Voltage
MV-SVR	Medium Voltage SVR

NIST	National Institute of Standards and Technology
OLTC	On-load Tap Changer
PCC	Point of Common Coupling
PMU	Phasor Measurement Units
PV	Photovoltaics
RES	Renewable Energy Source
RREE	Renewable Energies
RTU	Remote Terminal Units
SCADA	Supervisory Control And Data Acquisition
SFC	Switched Filter Compensator
SGAM	Smart Grid Architecture Model
SMES	Superconducting Magnetic Energy Storage
SOA	Service-Oriented Architecture
SOC	State-of-Charge
STATCOM	Static synchronous compensator
SVC	Static VAR Compensator
SVR	Static Voltage Regulator
TAC	Trading Agent Competition
TCP/IP	Transmission Control Protocol/Internet Protocol
THD	Total Harmonic Distortion
TSO	Transmission System Operator
TCR	Thyristor Controlled Reactor
TSC	Thyristor Switched Capacitor
UPFC	Unified power flow controller
UPQC	Unified Power Quality Conditioner
UPS	Uninterrupted Power Supplies
V2G	Vehicle-to-grid
VRB	Vanadium redox flow batteries
VPP	Virtual Power Plant
WEC	Wave Energy Converters

1. INTRODUCTION

1.1. Background

Distribution power systems have experienced an important evolution in the last years, as they have carried out a huge deployment of smart meters roll out mainly at low voltage (LV) levels. This deployment has allowed operators to establish a bi-directional communications infrastructure between grid operators and end-users, who can behave as energy producers in most of the cases. To date, the communication between the distribution grids operators and the clients have been undertaken mostly unidirectionally, where the monthly energy consumption is being registered at each installation mainly for billing purposes.

Currently, although the communications infrastructure is already established, and an elevated number of digital meters have been deployed throughout the LV grid, there is a little utilization of the potential offered by these distributed meters, as electric sensors which could be used to measure the electric variables at the connection point of each client. This causes the observability level of LV networks to remain very limited.

On the other hand, the installation of renewable energy power sources connected to the distribution networks causes congestions problems in the distributions networks for some situations, mainly due to the stochastic nature of renewable energy sources and because distribution networks are not prepared for handling a bidirectional power flow through their lines. In some EU-countries, new grid codes are being defined for distributed energy resources in order to allow DG unit to offer ancillary services to the grid at the connection point (PCC) [2]. At present, there is the need for tools that will help distribution grid operators to manage their grids. This would help the integration of DG, the connection of electric vehicles (EVs), and the participation of energy consumers, as doing this would can maintain both the efficiency (i.e., reduction of power losses) and the power quality, security and continuity of supply.

Growth expectations with regard to the DG connected to distribution grids can predict that future power systems will be characterized by a massive penetration of renewable energy sources (RES), mainly photovoltaic (PV) (Figure 1.1). This would also be accompanied by an increment of distributed energy storage systems connected to the grid, as well as the connection of a high penetration of electric vehicles. Likewise, this allows future network systems to establish, Demand Response (DR) programs jointly with the clients to improve the continuity of power supply, and to enlarge the penetration of renewable energy sources [3].

While this new situation has a set of implications that mainly affects to the distribution grids, the situation also influences transmission power systems. In the report delivered by the European Distribution System Operators' Association (EDSO) for smart grids [5],

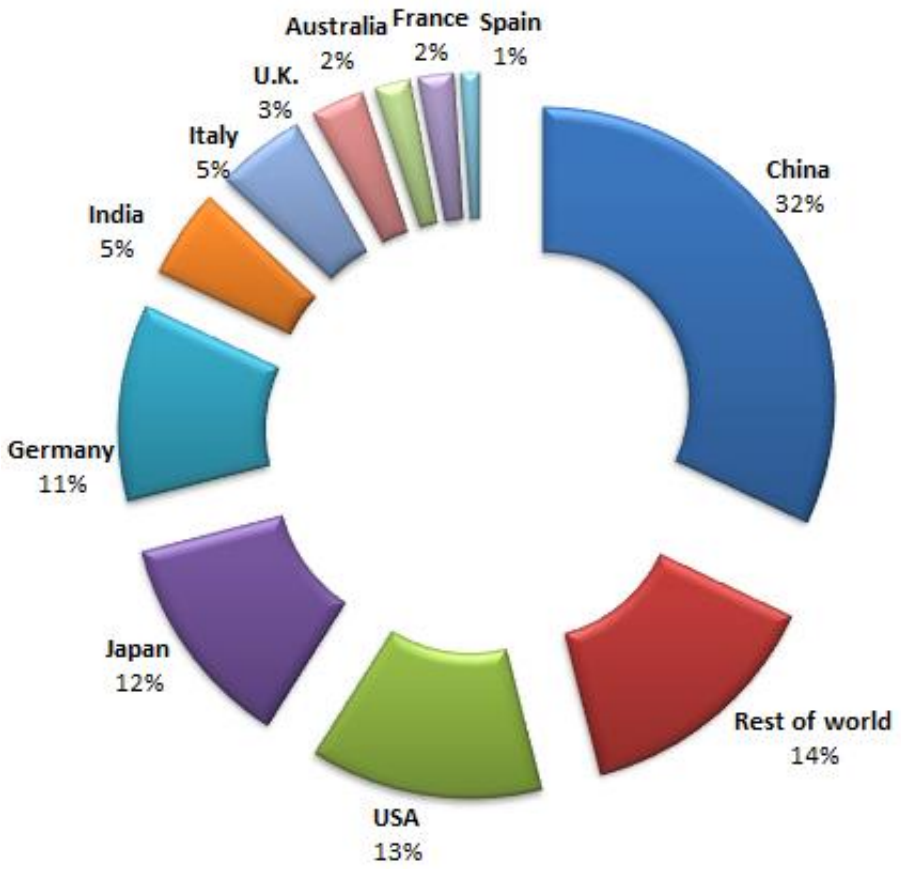

Fig. 1.1. Share of Photovoltaic power sources installed by the end of 2017 [4]

the European Network of Transmission System Operators for Electricity (ENTSO-E) express its interest in stretching the collaboration between the Distribution System Operator (DSO) and the Transmission System Operator (TSO). This is with reference to the flexibility that can come from having a DER unit connected to the distribution grid.

In many countries of the European Union (EU), there has hardly been any consideration in having TSOs and DSOs coordination between them regarding the ancillary services of voltage and frequency control. If it does exist, it is very limited and only applied to concrete situations [6]. Table 1.1 shows some examples of coordination between the TSOs and DSOs of several EU-countries related to the contract for services provided by the DERs connected to the distribution grid [6].

It is observed that, in most of the cases, the TSO directly contracts the flexibility services that exist in the distribution grid. This is done without the need of either a technical validation from the DSO who could verify that this resource does not produce congestions onto the distribution grid nor a notification. The main reason given is that the activation of the flexibility resources connected to the distribution grids is currently limited consequently, it does not have any relevant influence on distribution grids.

It was also found that in various EU-countries, distribution grids operators do not contract or utilize the flexibility services that are offered to them by the resources connected to their own distribution grids which could be used to solve their inherent congestion

	TSO contracting AS from DER directly connected to the DSO grid	DSO contracting local services from DER directly connected to the DSO grid	DSO contracting AS on TSO's behalf
Italy	✗	✗	✗
France	✓	✗	✗
Finland	✓	✗	✗
Spain	✓	✗	✗
Germany	✓	✗	✗
Denmark	✓	✗	✗
Norway	✓	✗	✗

TABLE 1.1. EXAMPLES OF ANCILLARY SERVICES CONTRACTS IN SOME EUROPEAN COUNTRIES

problems.

The above points reveal that at present, distribution grids operators do not employ the tools that allow them to solve the congestions that are present in their grids, even though they do have the distributed resources that allow them to solve these congestions. Moreover, they do not possess any tools that allow them to coordinate themselves with the TSOs in a way that can make sure the flexibility services contracted by the latter will not produce congestions in the distribution grids.

1.2. Motivation

According to the European Standard UNE-EN 50160 [7], voltages of the distribution grids must be kept within predefined variation margins. Nevertheless, the increment of the DG and the integration of the electric vehicle in the distribution grids can cause grid over-voltages and network congestions that would make necessary to implement control strategies for restoring nodal voltages at acceptable levels.

In recent years, a great number of existing pilots projects have improved the automation level at MV distribution networks. In these cases, substations of distribution grids have been automated in a way that is similar to how it is done for transmission networks [8]. Nevertheless, there are still many challenges to overcome for the distribution power systems to acquire real-time controllability on their own grids.

In the case of LV grids, the controllability level is even more reduced, The existing control actions are limited to the regulation of the on-load tap changer (OLTC) at the transformer located at the secondary substations (MV-LV). Moreover, at present, the DSO do not have the choice of either controlling the power injected by DG sources to improve

the voltage level, controlling the electric vehicle connection, or charging/discharging the energy storage systems connected to the grid.

The deployment of smart metering roll out in MV and LV distribution grids have allowed a bi-directional communications infrastructure to be implemented among the distribution grid operators, the clients, and the distributed energy resources (DERs), it would be feasible to send set-points to the agents capable of offering a voltage control service. In distribution grids, the components that can contribute to the voltage regulation, apart from the traditional methods, are as follows [9]:

- Distributed energy storage units connected to the MV and LV grids: these units can be owned either by the distributor MV-LV or by the client.
- Distributed generation source (normally PV): this is a local voltage regulation service that can be offered by the proprietary to regulate either active or reactive power that is injected to the grid.
- Demand management of the clients that can offer flexibility service (i.e., demand reduction in the presence of grid operators' requests).

In addition, static reactive power compensation devices can exist in MV grids; examples of these devices include static VAR compensators (SVCs), and distribution static synchronous compensators (D-STATCOMs). Scientific literature proves that many publications have proposes the usage of both deterministic [10] and heuristic optimization methods [1] for voltage control purposes.

However, one of the most critical aspects being currently considered is the definition of the information that must be exchanged among the different HV-MV and MV-LV grid controls [11]. There is uncertainty and lack of solutions, which makes this aspect one of the main challenges that has yet to be overcome.

1.3. Thesis Aim

The aim of this doctoral thesis is the development of methods and procedures that can improve the voltage regulation of MV and LV distribution networks with a high penetration of DERs. The developed methods will allow network operators to manage their distributed resources in almost real-time; such resources include DG, storage systems and electric vehicles. Doing so would allow the distribution grid to regulate both voltages at low and medium levels, and it would also offer a complementary ancillary service of voltage control to the transmission network. All this entails the development of voltage control techniques among the controllable devices present in the grid; this is done so that grid losses are minimized, and voltages are kept within the limits established in the normal functioning range. The developed techniques will also allow for the energy transference and the information exchange among the different voltage levels.

Framed around this global objective, the proposed specific objectives are as follows:

- To solve the problems of voltage regulation and bidirectional power flows in the operation and management of distribution grids.
- To know the network state in distribution grids (MV and LV) using the data gathered by the Advanced Metering Infrastructure (AMI).
- To develop optimization algorithms for the coordinated control of flexible devices present in the distribution grid (i.e. MV and LV) at different temporal ranges and for several penetration scenarios of RES.
- To define the energy and information that has to be exchange between the different MV and LV levels so that the LV grid can offer a complementary voltage service to the MV grid.
- To develop control models and techniques for wave energy plants that can be grid-connected at LV level.

This thesis proposes a coordinated voltage control architecture that allows the LV grid to provide support to the MV grid and that also makes it possible to control MV and LV grids in real-time. In this case, the tasks proposed to be developed are:

- Defining the coordinated control structure: relationship among levels, boundary nodes definition, interchange among levels (power, information), and so on.
- Define the exchanges of information and signal among the levels of the coordinated control.
- To design the control algorithms and compare them to classic local decentralized and distributed control techniques.
- To validate the control algorithms with real distribution grids (MV, LV) that include wind, PV and wave power sources.

The research suggested in this thesis will focus on the flexibility services that are offered by the DERs connected to DSO grid. Thus, there can be a way to control the PV energy sources and off-shore wave power plants connected to LV grid, as well as PV and wind emplacements connected to the MV grid.

1.4. Outline of the thesis

The doctoral thesis is structured in six chapters, including this chapter as the thesis introduction. Following the introduction:

- **Chapter 2** presents the state of the art of smart grids, and the chapter also identifies the current situation of the development of smart grids in different EU-countries, the challenges to overcome and the advancements that have been carried out with respect to demand management, roll-out smart metering deployment, smart grids' control techniques, consumers/prosumers situation, as well as the standards and the most cutting-edge communication technologies.

- **Chapter 3** provides a description of the voltage control techniques applicable to the smart grids, including decentralized, distributed and coordinated voltage control techniques. This chapter also presents mathematically deduced equations defining the PQ-capacity equations of both PV and wind energy units.

- **Chapter 4** describes the renewable technologies state-of-the-art of marine power installations. such as wave energy sources, and the chapter presents the elements that comprise the technologies, as well as the control techniques that can be applied at the off-shore wave farms. In addition, the chapter details the experimental wave farm known as the Lysekil Test Site (Sweden), which has been utilized to implement the developed control algorithms and filtering techniques proposed in this thesis.

- **Chapter 5** implements the developed algorithms into an existing power system located in Spain, which consists of four voltage levels that range from low to high voltage. In MV grids, the voltage controllers developed in Chapter 3 have been implemented, whereas in LV grids, the models and control techniques developed for the wave energy in Chapter 4, have been applied. This chapter compares the accuracy of decentralized local control, distributed voltage control, and coordinated voltage control in situations of normal operation and in situations of abnormal operation, such as emergency situations.

- **Chapter 6** presents the conclusions and contributions obtained from this doctoral thesis, and the chapter also sets out the possible future works to be further developed.

2. SMART GRIDS

2.1. Chapter introduction

This chapter presents a review of the state of art regarding smart grids. According to specialized literature, there is no consensus in standardizing the definition of a smart grid. This chapter gives an overview of the main smart grid actors and functionalities that appear in distribution networks. Special focus is given to the main challenges and barriers that limit the smart grid expansion, and this is done by analysing the actual development in some European countries. Moreover, one of the elements of the smart grids is the communication infrastructure and the standardization bodies. For this reason a review of the main standardization activities and architectural communication networks will be shown in this chapter.

To gather the conceptions which show what a smart grid is, the structure of this chapter is drafted as follows: Sections 2.2 and 2.3 present a definition of a smart grid and its state of the art, from its origins as a purely conventional power grid to its transition toward a smart entity. Sections 2.4 conceptualizes the actors that are participating in smart grids and Section 2.5 review the more relevant ICT standards.

2.2. Definition of Smart Grids

To date, a uniform definition on what a smart grid is that has not yet been conceived and universally accepted [12].

- In 2010, the International Electrotechnical Commission (IEC) pointed out that due, because there was no accepted ambit to decide which grids are smart and which ones are not, the term by itself was used as a marketing strategy rather than a technical term [13]. What is clear is that the "Smart Grids" concept refers to power networks modernization through Information and Communications Technology (ICT). This modernization allows the grid to be more flexible and it also facilitates real-time bidirectional communication between the active elements that are part of the power system and its control centers.
- International Energy Agency (IEA) has employed the term as a technical definition back in 2011, and the organization stated that the conceptualization of a Smart Grid is not so different from a conventional grid. This is due to both being compounded of the same main components, such as generation, transmission and distribution systems, end-users, and their respective interfaces. Nevertheless, the main difference between a conventional and a Smart Grid is that the latter possesses additional

components for managing the power flow between power suppliers and end-users bi-directionally, and it also operates the whole system as optimally possible, especially for digital technologies and storage systems[14]. It should be noted that this definition had not changed in the past five years [15].

– A definition of a smart grid is also provided by the U.S. Department of Energy (DOE). According to the DOE, a Smart Grids is a sensorized electric ecosystem in which cutting-edge ICT bi-directional technologies, as well as control, computing and power electronic systems, coexist and work together in order to guarantee both grid stability and power quality so that infrastructure aging can be delayed and that its enlargement can be postponed as much as possible [16].

These definitions refer to some of the existing definitions that have been given by International Working Groups; on academia's side, the concepts do not differ that much among one another. In [17], Smart Grids are described as a cohesive integration of power grids, intelligent systems (i.e., sensors), and ICT platforms. This definition is quite similar to the one in [16], with the difference being that the authors in [16] pointed out that these advancements were implemented over existing grids in order to smarten them. The main properties of a Smart Grid are resilience, adaptability, real-time dynamic interactivity, and a higher efficiency when compared to conventional grids [18]; other features include their capacity to store energy, establish communication channels, and make decision [12]. They also have a number of advantages; for instance, they can reduce losses, optimize the electric system's operation in both physical and economical terms, and offer economical benefits for the involved agents [19].

At the European level, the EU's "Strategic Research Agenda 2035" on Smart Grids [20] defines a "Smart Grid" as an electric grid that intelligently integrates the actions of all the users connected to grid. These can include consumers, electric sources, and prosumers, and the integration aim's to facilitate a reliable, economic, and efficient power supply.

On the other hand, the American organization Electric Power Research Institute (EPRI) [21] considers a Smart Grids to be an electric power network that uses millions of distributed sensors, which communicate with each other using advanced data acquisition and communication systems. Thus, an infrastructure of a Smart Grids allows a real-time analysis of the electric grid, as well as the distributed and dispersed computation in the whole grid in order to actively prevent blackouts in the distribution network.

After presenting several definitions of a Smart Grid, it can be stated that the main characteristics of a Smart Grid are as follows:

– A Smart Grid is not a revolution of the entire system within a power systems; instead, it consists of a natural evolution of the existing system by means of its progressive modernization.

– It is not a brand new electric super-grid: the physical infrastructure of the Smart

Grid network is the same as the one used in the conventional electric grids. What changes is the way that Smart Grid networks operate, in that it has a higher reliability and energy efficiency of power networks.

– It is not only an Advanced Metering Infrastructure (AMI) with millions of smart meters that are shared from end-users installations. A Smart Grid concept is broader than this in that it encompasses several topics such as Smart Metering, Control, Demand Side Management, Losses Minimization, Power Quality Improvement, Energy Efficiency Upgrading.

– It offers the possibility to decentralize the grid control in a distributed form, which means that in the case of unexpected behaviours, such as ground faults, the compromised area is isolated until the fault is located, and the energy service restored (FLISR), to operate in normal conditions. This property is known as resiliency [14].

– It allows consumers to participate in the energy market by becoming prosumers.

– It provides more information to energy suppliers and customers allowing them to decide how to use their energy supply efficiently.

– It uses communications technologies to optimize the resources connected to the smart grid [17].

In summary, some of the objective of a Smart Grids [22] are listed as follows:

1. Strengthening a grid and enhancing automation by improving its operation, upgrading power quality and minimizing network losses;

2. Controlling DG sources, thus allowing the correct functioning of small DG units to be in total harmony with the entire power system;

3. Improving the integration of intermittent generation and storage systems;

4. Tackling more advancements regarding electricity market's by enabling new services and functionalities both to energy retailers and to consumers in the market pool;

5. Actively managing the load demand, thereby allowing consumers to handle their own consumption more efficiently; and.

6. Promoting high penetration of electric vehicles by optimizing the connection of these new vehicles and dispersing loads to the grid and enabling the use of their energy storage functionalities.

Moreover, several benefits to both power systems and the involved stakeholders have been identified. Nevertheless, impediments to their definitive deployment are still present. Table 2.1 compares the advantages and disadvantages of a Smart Grid.

Advantages [23]	Disadvantages [22]
The usage of new and old assets is optimized altogether.	The lack of standard and mature technologies increases the risk of investment, and the limited pilot tests of sufficient scale make the estimates and assumptions to be considered as unreliable. Moreover, a lack of interoperability between different Smart Grid elements limits its whole deployment.
Self-adaptive maintenance schemes are promoted to prevent outages, the consequent power quality improvement is given to end-users.	Investment and operating costs are still too high, and there are still no economies of scale. On the other hand, the benefits that they intend to achieve are difficult to quantify and to be attributable to each agent.
Data storage and management as well as information networks are continuously increasing.	The data and volume of the information that will be collected about each consumer can cause privacy and security problems.
Innovation, load balance related services and new energy products are promoted.	The current regulatory frameworks deliver uncertainty in relation to the roles and responsibilities as well as the sharing of costs in the Smart Grid sector.
Renewable energies and advanced storage systems are integrated into electricity networks, which optimizes their usage and contribution to both electricity markets and system operators.	Uncertainty is found in relation to financial frameworks for DERs.
The active roles of the end-users within the entire power system are promoted. This results in peak shaving and energy efficiency, a reduction in greenhouse emissions, and increase in cap and trade savings.	Regulators have a lack of awareness regarding the role played by Smart Grids in promoting renewable energies, energy efficiency, reducing CO_2 and promoting investments in electricity networks.

TABLE 2.1. SMART GRID'S ADVANTAGES AND DISADVANTAGES

In short, Smart Grids are efficient, accommodating, motivating, quality focused, resilient, and full of potential. Most importantly, they are greener compared to their conventional counterparts [24]. In addition, their reliability, security, and generation-consumption matching allows them to be the basis for a Smart Zero Energy Community [18]. These features offer specific benefits to all the stakeholders in the electric systems by linking their objectives to achieve common objectives [14], [23]. Nevertheless, Smart Grids also has disadvantages such as cyber-security vulnerabilities, higher initial costs, rapid obsolescence, and potential consumer privacy violations [24].

2.3. Evolution of Smart Grids

There are several main factors that promoted the development of Smart Grids, such as the growing high penetration of renewable energies in power networks, the development of the DG in distribution networks, and the growing participation of the consumers in the production and management of their own energy. These aspects motivated the need of introducing ICT in the power grids, which leads to new opportunities and also challenges (e.g., prosumers and aggregators). Figure 2.1 shows the technical evolution of Smart Grids networks over the period of a decade.

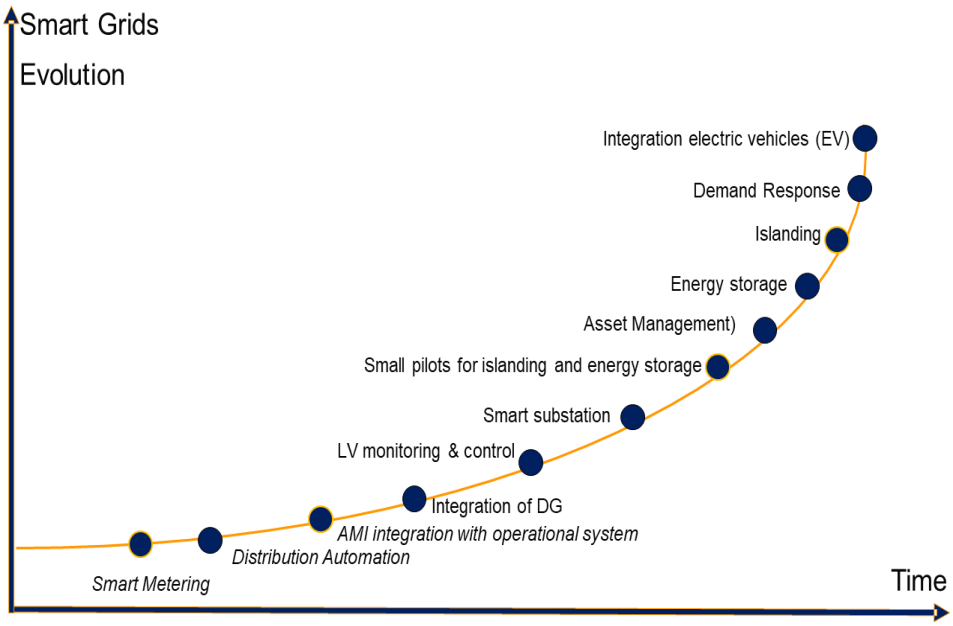

Fig. 2.1. Smart Grids Evolution

It can be stated that the starting point of Smart Grids networks appears with the development of projects related to telemetering deployment on LV and MV networks. This is known as "Smart Metering" and which has been mainly used for electricity tariff purposes and electricity billing. In 2017, the deployment of smart metering in diverse EU countries can be considered as nearly accomplished, as shown in Table 2.2 [25]. Such development is due to the national directives as set in the Spanish case [26]; due to these directives dis-

tribution companies are obliged to substitute 100% of their traditional energy meter with electronic ones before the end of 2018. Smart Grids deployment have been mainly carried out in LV distribution power systems and also in MV power systems (MV customers) but to a lesser extent.

In parallel to the development of the smart metering roll-out in the distribution grids, there were also some important advancements with regard of HV and MV substations that aim to increment their automation level. The automation has been developed in two levels:

- First, work is being done on developing advanced automation systems in distribution networks, such as the implementation of both ancillary services and the energy aggregator concept.
- Second, advanced applications are being developed to allow the monitoring and control of the whole grid and its distributed energy resources spread over the grid.

The automation of Smart Grids aims to dynamically integrate energy services through a real-time operation of the grid, thus allowing for energy-friendly services to be used with the traditional power grid. Such services include the ancillary services to the systems operators and the participation of the DERs in the market through aggregators. Data measurement, data control and data estimation can be combined, analysed and utilized at different levels in order to integrate multiple monitoring points. The concept of automation revolves around three areas:

- the design of the control architecture in the distribution grid automation,
- the design of the virtualization and aggregation of DERs through aggregators, and
- the utilization of the DERs on a large scale to manage the grid.

At present, all the automation systems work as vertical solutions, where each one of them is used for a specific purpose. Such systems include the SCADA/Distributed Management Systems (DMS), the monitoring solutions for secondary substations and the automatic management of smart meters. However, these automation systems are not capable of inter-operating among them to carry out general management, nor are they able to conduct the new tasks required by the future distribution networks. Hence, the integration of these systems and solutions can improve the monitoring of the entire distribution network in future networks.

From the DSO's point of view, the distribution system automation ameliorates with the incorporation of the flexibility services provided by the aggregator. The aggregator can interact with the DERs through a power management system which serves as a link between the monitorization and the remote control of a DG, a home-energy management

Country	Expected Roll-out Smart Meter by 2020 (%)	Roll-out period From	To	Deployment Strategy	Responsible party Implementation and ownership	Access to metering data
Sweden	100	2003	2009	Voluntary	DSO	DSO
Italy	99	2001	2011	Mandatory	DSO	DSO
Finland	100	2009	2013	Mandatory	DSO	DSO
Malta	100	2009	2014	Voluntary	DSO	DSO
Estonia	100	2013	2017	Mandatory	DSO	Central hub
Greece	80	2015	2018	Mandatory	DSO	DSO
Luxembourg	95	2015	2018	Mandatory	DSO	DSO
Spain	100	2011	2018	Mandatory	DSO	DSO
Ireland	100	2014	2019	Mandatory	DSO	DSO
Austria	95	2012	2019	Mandatory	DSO	DSO
Denmark	100	2014	2020	Mandatory	DSO	Central Hub
France	95	2014	2020	Mandatory	DSO	DSO
Lithuania	N/A	2014	2020	N/A	DSO	DSO
Netherlands	100	2012	2020	Mandatory with opt-out	DSO	DSO
Slovakia	23	2013	2020	N/A	DSO	DSO/Central hub
United Kingdom	100	2012	2020	Mandatory	Supplier	Central hub
Poland	80	2012	2022	Mandatory	DSO	Central hub
Portugal	N/A	2014	2022	N/A	DSO	DSO
Romania	80	2013	2022	Mandatory	DSO	DSO
Czech Republic	1	2020	2026	N/A	DSO	Central hub
Germany	23	2014	N/A	N/A	Meter operator/DSO	Meter operator/DSO

TABLE 2.2. EU SMART METERING ROLL-OUT

system (i.e., Building Automation System), and a micro-grids management system that can aggregate data and manage the DERs that are allocated near to clients. Similarly, the data of smart meters are gathered by the DSO, they can be analysed and can provide useful information to the clients.

The distribution grid automation hierarchy includes three levels namely: the primary, secondary, and tertiary levels. The controllers and primary protection devices are distributed in what is known as Intelligent electrical devices (IEDs), these work autonomously and offer a rapid response to signal reference variations.

The secondary level includes the coordination among various IEDs, such as the automatic coordination of DER controllers into a specified control area. Some of its functions include the following:

- a local voltage control (Volt/Var) in the control area,
- real-time control and management of the DERs,
- deployment of the Advanced Metering Infrastructure (AMI), and
- direct load control.

The tertiary level manages the entire system, and this management is generally based on the control systems and the operator action. Some functions being carried out in the tertiary level are as follow:

- long-term and short-term grid operation planning,
- demand-side management, and
- contingencies analysis.

A possible relationship between control schemes is depicted in Figure 2.2, which corresponds to the architecture scheme adopted in the IDE4L European project[27].

It should be noted that smart metering development and automation architectures expansion are the main pillars for all the subsequent technological evolutions.

2.4. Actors of Smart Grids

Based on the definition given by the National Institute of Standards and Technology (NIST) [28], a Smart Grid actor is understood as a device, a computer, a control unit, an individual or an organization that participates in the Smart Grid network. The actors have the capability of adopting operative decisions and communicating with other participants of the grid by means of the communication architecture. The actors that generally have a bigger participation in the Smart Grid networks are detailed in the following subsections; these include the DERs, consumers/prosumers, and market agents (i.e., aggregators).

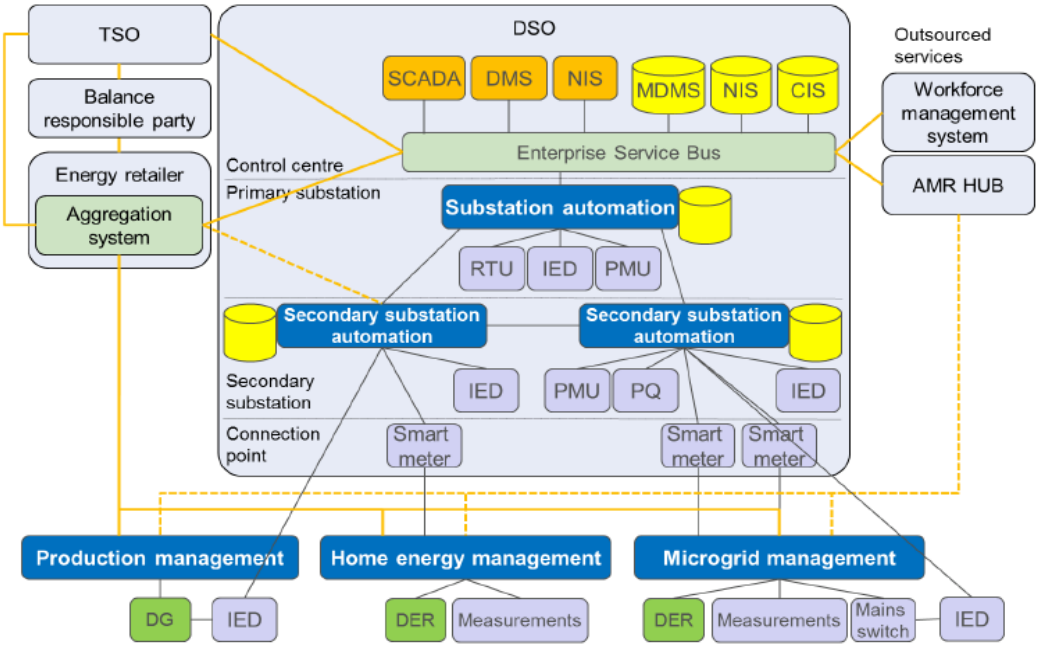

Fig. 2.2. Automation architecture for the grid active management [27]

2.4.1. Distributed Energy Resources

One of the main actors in the Smart Grids are the DERs, which are in charge of supplying the necessary functionalities so that distribution grids can become active entities. These include DG (e.g., PV and mini-wind), energy storage systems (e.g., electric vehicles and batteries), and distributed Flexible Alternating Current Transmission System (D-FACTS) devices for grid control purpose (e.g., voltage and frequency).

2.4.1.1. Distributed Generation

DG refers to the scattered energy resources that are directly connected into the distribution network and may sometimes be located near the consumption points (i.e., points of residential, industrial, and commercial clients). DG involves a wide range of technologies, including the microgeneration and renewable that are connected to the distribution grid. These are mainly classified as generation devices (e.g., micro-turbines, fuel cells, PV panels and wind turbines), whose typical rated power ranges from 3 to 10.000 kW [29].

DG units can be classified into controllable (i.e., dispatchable) and non-controllable (i.e., intermittent) generation sources. Dispatchable units are those which can be turned on and off when necessary, such as fossil fuel, and biofuel powered units; intermittent units are not controllable or predictable such as wind and solar.

Although not considered in [29], marine energy devices can be considered DG units since they are connected to distribution networks due to their location, size and intrinsic harmonic nature [30]. Although fuel cells are normally considered to be an innovative storage system, they are also categorized as both RESs and DG; one of the reason for

this is that they are being manufactured at capacity levels up to 200 kW with increased cost-effectiveness [29], [31], [32].

The most widely employed DG units in Smart Grids are shown in Figure 2.3

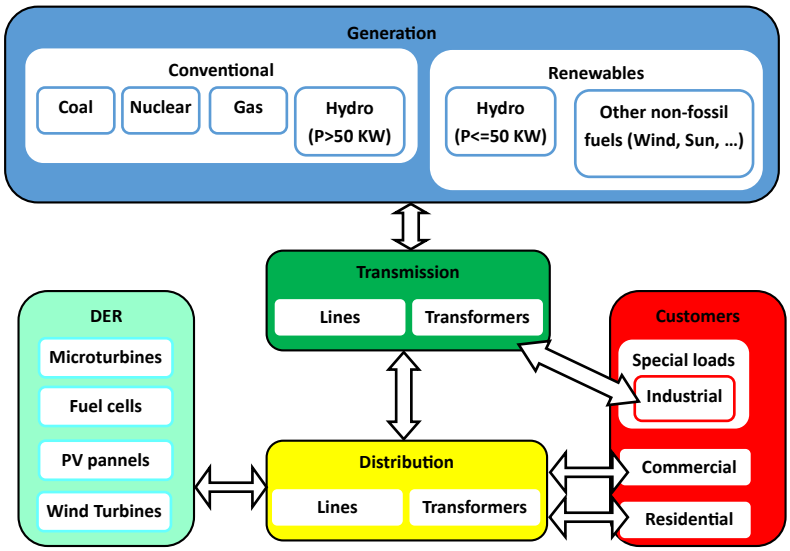

Fig. 2.3. Conventional Power Grid with Customer and DER Branches

2.4.1.2. Storage and Electric Vehicles

The transportation sector is one of the more important parties that is responsible for Europe's greenhouse gas emissions. The Clean Mobility package [33] proposed by the European Commission in November 2017 establishes a target of 15% reduction in the CO_2 emissions per kilometer (km) for new vehicles in 2025 and a 30% reduction in 2030. One of the main drivers for decarbonization and low emission from road transport is the deployment of electric vehicles. Electric vehicles offer relevant advantages compared to conventional fossil fuel vehicles, such as fuel savings as well as reduced greenhouse gas and pollutant emissions. The uptake of electric autonomous vehicles is being pushed by the following factors:

- The development of battery packs for electric vehicles is nowadays viable and the battery efficiency is continuously increasing.
- Smart cities demand sustainable mobility solutions.
- National and regional transport regulations have started to propose new strategies to promote the transport electrification.

The deployment of electric vehicles that started in 2009 focused on private electric vehicles. Initially, electric vehicles were intended to charge as soon as the electric vehicle is plugged-in at home (Figure 2.4). However, this type of uncontrolled electric vehicle

charging has important consequences in the electricity distribution network, such as a sudden peak demand or sudden overloading if the number of vehicles charging are increased at the same time.

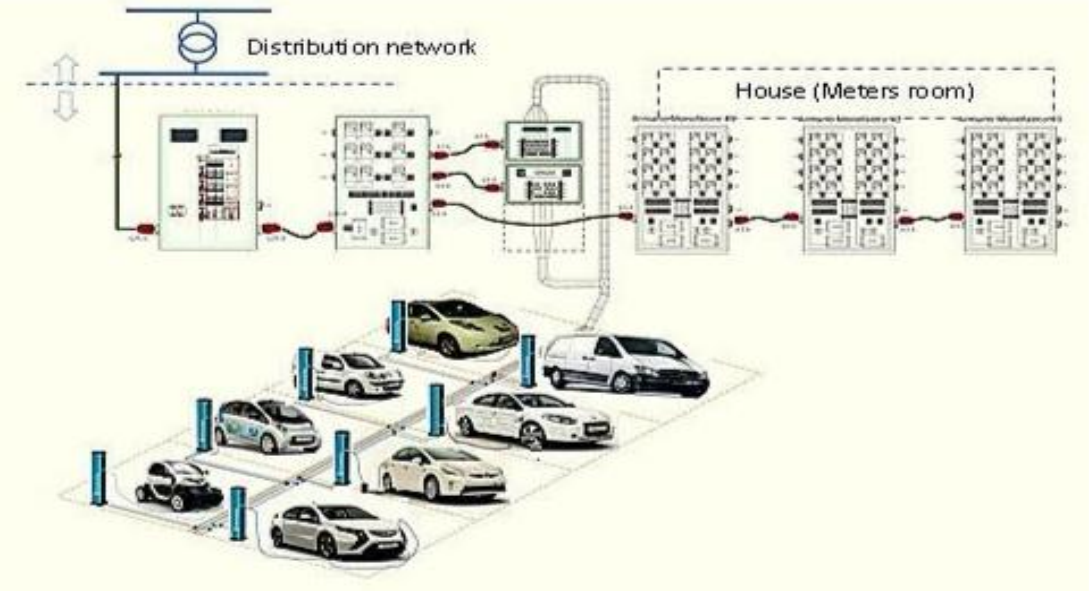

Fig. 2.4. Example of EV parking infrastructure [34]

The majority of studies on electric vehicles treated the vehicles as a moving electric load with the main function of charging batteries (i.e., Grid-to-Vehicle, or G2V function). However, an electric vehicle can also be considered as an electricity storage unit with the capability of providing power to the electricity distribution network when they are parked and connected to the grid (i.e., Vehicle-to-Grid, or V2G function). Electric vehicles can be considered as an energy storage capacity that can be controlled to inject power to the grid and vice-versa. This bi-directional flow of power was called V2G capability [35]. Since then, V2G capability has been applied to offer ancillary services to the networks operators or to perform demand response services. The International Council on Clean Technology [36] suggested that the electricity market regulation has to provide access to owners of electric vehicles so that they can offer V2G capabilities in future energy portfolios.

In the field of storage systems, the BRIDGE initiative stands out with its main objective in propelling the development of energy storage projects for the Smart Grids. In the report [37], which is framed inside the EU's Horizon 2020 Programme, the most widely used battery technologies are Lithium-ion batteries, followed by Sodium technologies (i.e., Sodium-ion and Sodium Nickel Chloride), lead technologies, Redox flow technologies and Nickel-Iron technologies (NiFe). Energy storage units are currently applied in all power sectors [37], and these provide energy services to transmission networks, distribution network, RES and customers (see Figure 2.5). Their application to RES units are mainly focused on operations related to power curtailment where they store the energy that cannot be injected to the network and ancillary services. Energy storage units are used in distribution networks to execute operations related to contingencies, inten-

tional islandings and load shifting in distribution grids. At customers installations, they are applied to DR purposes at PV self-consumption.

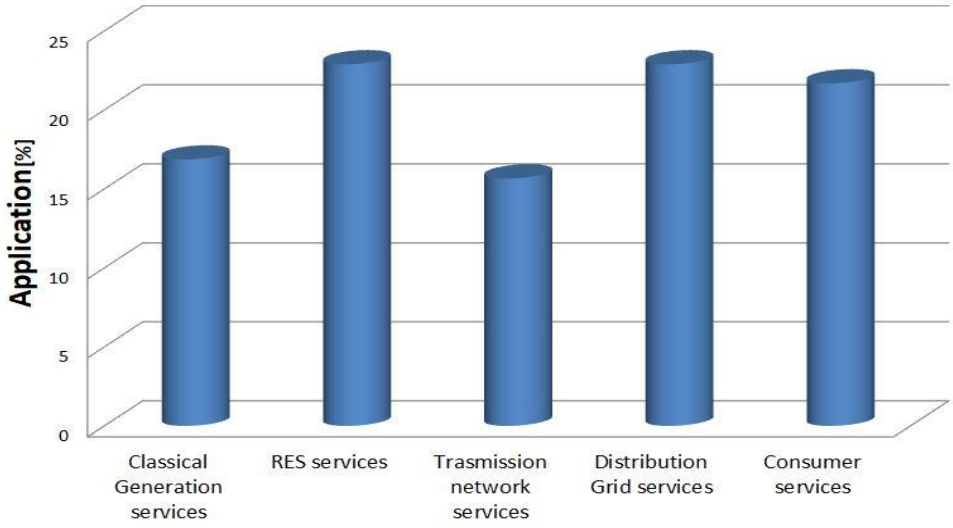

Fig. 2.5. Types of services provided by the storage systems framed inside the BRIDGE initiative [37]

Brand new storage systems, such as Vanadium Redox flow batteries (VRB), Sodium Sulfur (NaS) batteries, Superconducting Magnetic Energy Storage (SMES), and supercapacitors can provide up to 8 hours of autonomy. These systems enhance the power quality as well as voltage and frequency regulation. Meanwhile Flywheel Energy Storage Systems (FESS) with high energy density (up to 60 minutes of autonomy) can be activated in case of short outages [29].

2.4.1.3. D-FACTS

D-FACTS devices are included in the Custom Power Devices definition given in reference [38]. These are similar to the FACTS devices utilized in HV grids, with the main difference being that D-FACTS are used mainly in distribution grids. They are composed of a power electronic converter (i.e., DC/AC converter) and a storage unit; moreover, they can be connected both in series or in parallel at the connection point.

The topologies of the converters can be classified mainly in Voltage Source Converter (See Figure 2.6a) or Current Source Converter (See Figure 2.6b) .

D-FACTS devices are mainly used to give support to distribution grids needs, among which include voltage control, reactive power regulation and power quality improvement.

Depending on the application, they can be connected in parallel or in series.

- Devices with parallel connection are:
  - Static Var Compensator (SVC) and

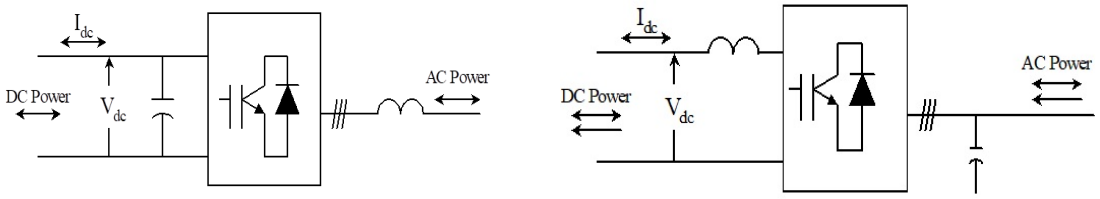

(a) Voltage Source Converter (b) Current Source Converter

Fig. 2.6. Power converters topologies

  - Distribution Static Synchronous Compensator (D-STATCOM)

- Devices with series connection are:
  - Dynamic Voltage Restoration (DVR)
- combination of the previous both:
  - Unified Power Quality Conditioner (UPQC)

Figure 2.7 depicts an example of how a DVR device is utilized to compensate voltage gaps in MV wind farms.

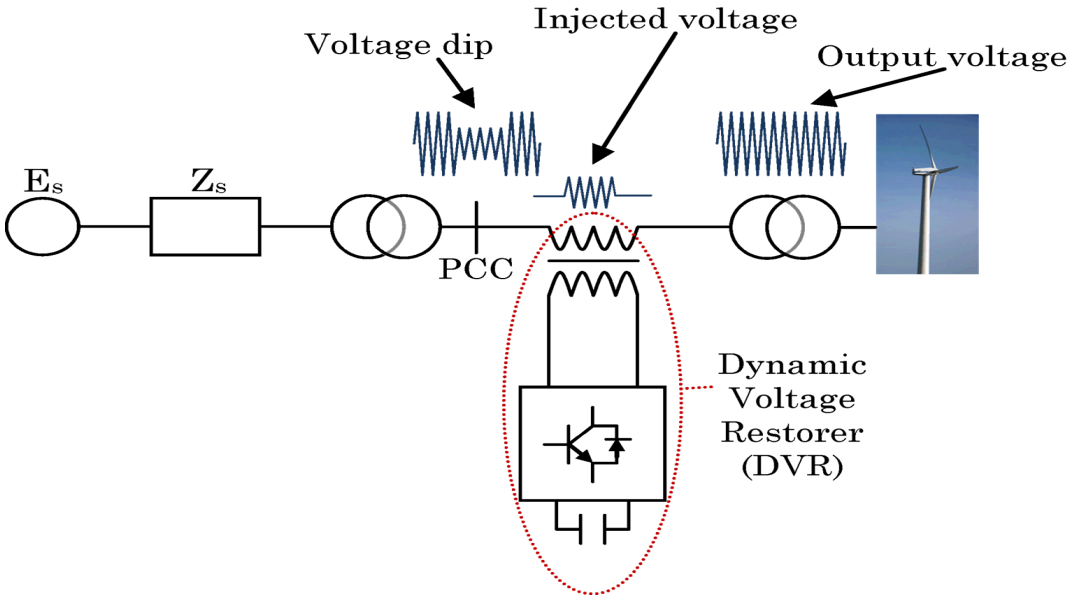

Fig. 2.7. Dynamic Voltage Restorer Scheme

2.4.2. Micro grids and Virtual Power Plants

A micro grid can be defined as a set of loads and DER units that are interconnected in the same electric region, either in LV or MV. It works as a unique controllable entity that can operate both isolated or grid-connected. The microgrids of the distribution network that cannot be connected to a stronger power system are known as isolated microgrids, and these are typically found either in rural zones or geographical islands. An isolated microgrid consist of DER units, loads, and control and measurement devices. The control architecture of the microgrid is composed by three hierarchical levels: Tertiary control, secondary control and primary control being possible to control the interrelation with the main grid, to control the microgrid, and later to control the individuals IEDs, respectively (see Figure 2.8).

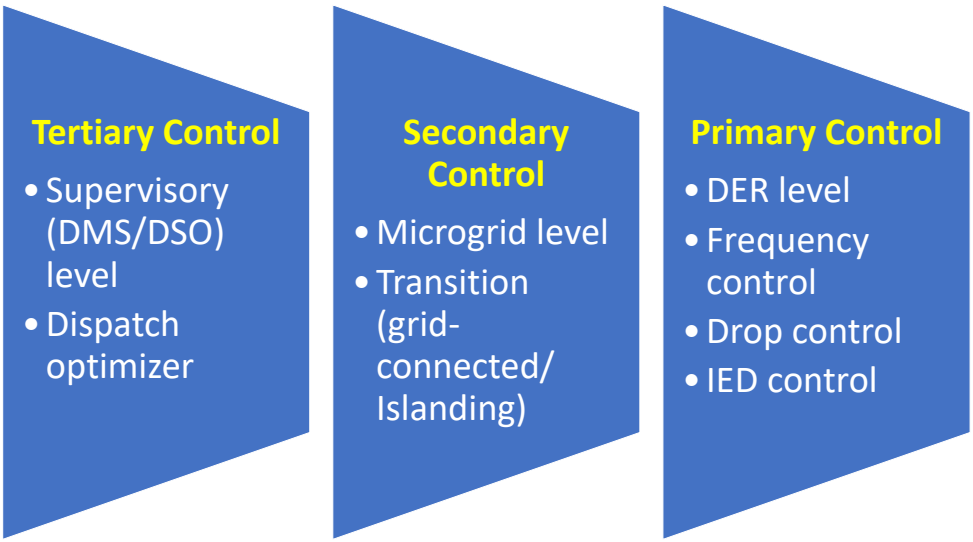

Fig. 2.8. Hierarchical Microgrid Control Architecture

Virtual Power Plants (VPPs) are differentiated from microgrids due to the fact that their components can be spread out in different geographic zones. Their working principle is based on a communication network, a measurement network and a system that makes it possible to control a set of DER units in an aggregated way; these DER units can also participate in the electricity market as a generation plant. Thus, a VPP can be defined as an aggregated set of DER units that are managed as a dispatchable unit with functions such as generation forecast, demand forecast, storage control, and the coordinated optimization of DG units, Table 2.3.

A VPP has three control schemes, namely centralized, decentralized, and coordinated, as depicted in Figure 2.9.

- In a centralized VPP control scheme, the VPP control unit carries out the complete control of all the controllable units of the grid (i.e., generation, storage, flexible loads).

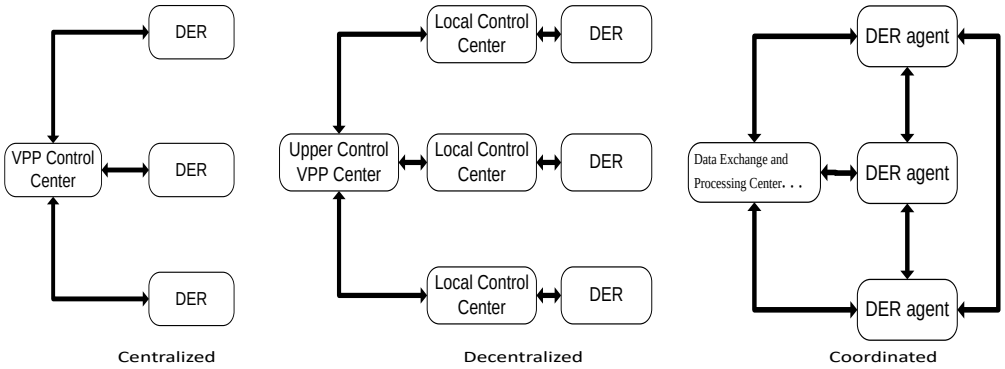

Fig. 2.9. VPP control architectures: (left) Centralized, (middle) Decentralized, (right) Coordinated

- For a decentralized VPP control scheme, the upper-level control unit assigns control tasks to the lower-level local control units, which controls all the controllable units under its control area.
- Lastly, in a coordinated VPP control scheme, the control is distributed among all the control agents. Here the central VPP control consists mainly of the communication signals that are interchanged between each agent and the information processing center.

Microgrids	Virtual Power Plants
Local power systems are made of different clustered DERs, and various storage systems that guarantee their stand-alone functioning when required. Among their provided functionalities there are SmartSource^{TM}and the interface SmartSwitch^{TM}; these allow plug-and-play independently of communications and a smooth changing of states between stand-alone and grid-connected operation. Industrial power systems are designed to cope with their key processes: these are used for UPS, DVRs, $high - T_c$, DERs and Power Electronics.	A group of DERs and flexible loads with control, optimization and monitoring is managed by a distant Energy Management System. A system such as this requires accurate short-term forecast systems, a robust front-end communication interface and bidirectional control systems protocols (IEC 61850).

TABLE 2.3. MICROGRIDS AND VPPS CHARACTERISTICS

2.4.3. Consumers

The Winter Package published by the EU in November 2016 [39], establishes imperative objectives that are to be reached by 2030. The package focused on three main areas,

namely prioritizing energy efficiency, fostering renewable energies integration in the electricity markets, and offering a fair treatment to consumers. As a results of this package, EU citizens have become an active actor within the power system by acquiring the following rights:

- They have the right to know their daily consumption and the ways to manage their own electric appliances use. This will be possible with the development and application of the smart homes.
- They have the right to adjust their own consumption according to the signal of electricity prices. Thus, the consumers will be able to respond in a coordinated form to the operator in the presence of the DR's actions and signals.
- They have the right and possibility to generate, store, and sell their own electricity; this turns them into prosumers.

Therefore, in the context of the Smart Grids, the consumer can adopt one of three roles:

– First, they have the choice to be a traditional consumer with a passive behaviour.

– Second, they can be an active consumer through of DR actions, and also through the development of the smart homes.

– Lastly, they can be a proactive consumer - also known as a "prosumer"- who can produce energy for their individual use (i.e., "self-production" or "self-consumption" and storage) or for the network (i.e., producer).

The DR actions provide consumers more power through either the control signals or economic incentives, which can make them modify their consumption at certain time periods. Depending on the type of consumer (see Figure 2.10), the signals can also affect their DG production and storage resources.

According to the indicators in the reports published by the EU [40], [41], the distribution of electricity consumption within the EU's residential sector is shown in the top box in Figure 2.11. The distribution corresponding to offices and commercial installations are depicted in the middle and bottom boxes, respectively.

From the point of view of the flexibilities that can be offered the different installations (i.e., residential. commercial, or small industries), the loads can be classified into the following groups:

- Non-shiftable or uninterruptible loads: these are loads with a consumption that cannot be reduced or planned throughout the day; examples include emergency lighting and security systems, cooking (household), plug loads (supermarket) or refrigerators (base performance).

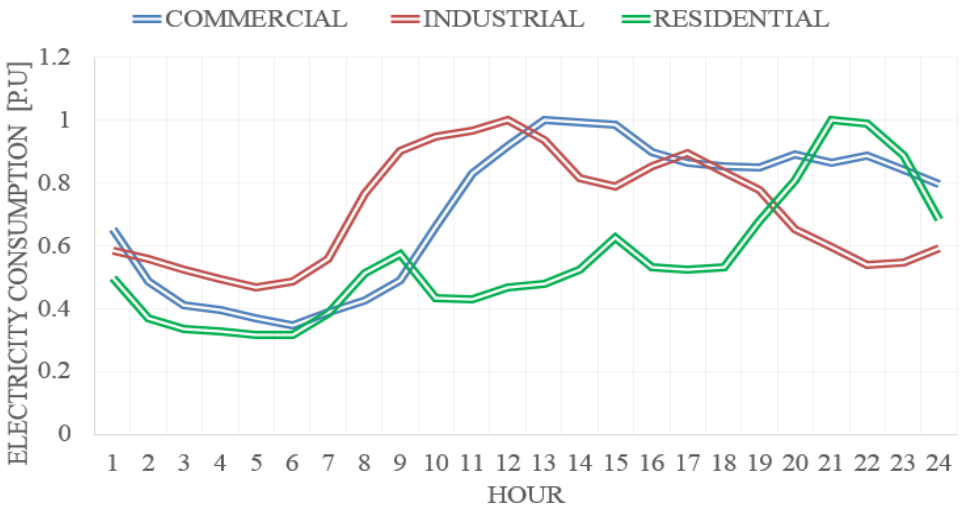

Fig. 2.10. Typical LV electricity consumers profiles (household, Commercial, Industrial)

- Shiftable loads: these include all the equipment that has start-up time which can be delayed and planned throughout the day. Examples in this category are dishwashers (where a delay up to 6 hours can be allowed during the start-up), washing-machines, dryers, HVAC heating and cooling systems, and water heating systems. In the residential sector, the freezer presents an operation cycle with a duration of 15 minutes and is activate every 45 minutes, whereas electric vehicles can be activated during charging operations [42], [43].
- Curtailable loads: these include loads that offer a reduced percentage of their own electricity consumption, such as lighting that has a fast speed response. In some instants of time, HVAC systems can also offer the capability of reducing their consumption by lowering the working point depending on the equipment thermal inertia.
- Storable loads: these correspond to the loads that makes it possible to store energy at periods in which the price is lower (e.g.,valley hours) so that the energy can be used at other time instances (e.g., peak period hours).

2.4.4. Prosumers

In the context of the Smart Grids, a "prosumer" can be defined as an entity or a LV electric grid user who can both produce energy and consume it. According to their role within the distributed power system, a prosumer can be classified as one of the following:

- Individual prosumer: these include individual clients who have self-production electric systems (i.e., PV plus storage) that offer the capability of both consuming and injecting electricity to the grid (see Figure 2.12a).
- Collective prosumer: these correspond to a set of individual installations that are connected to the same connection point of the electric grid; these installations

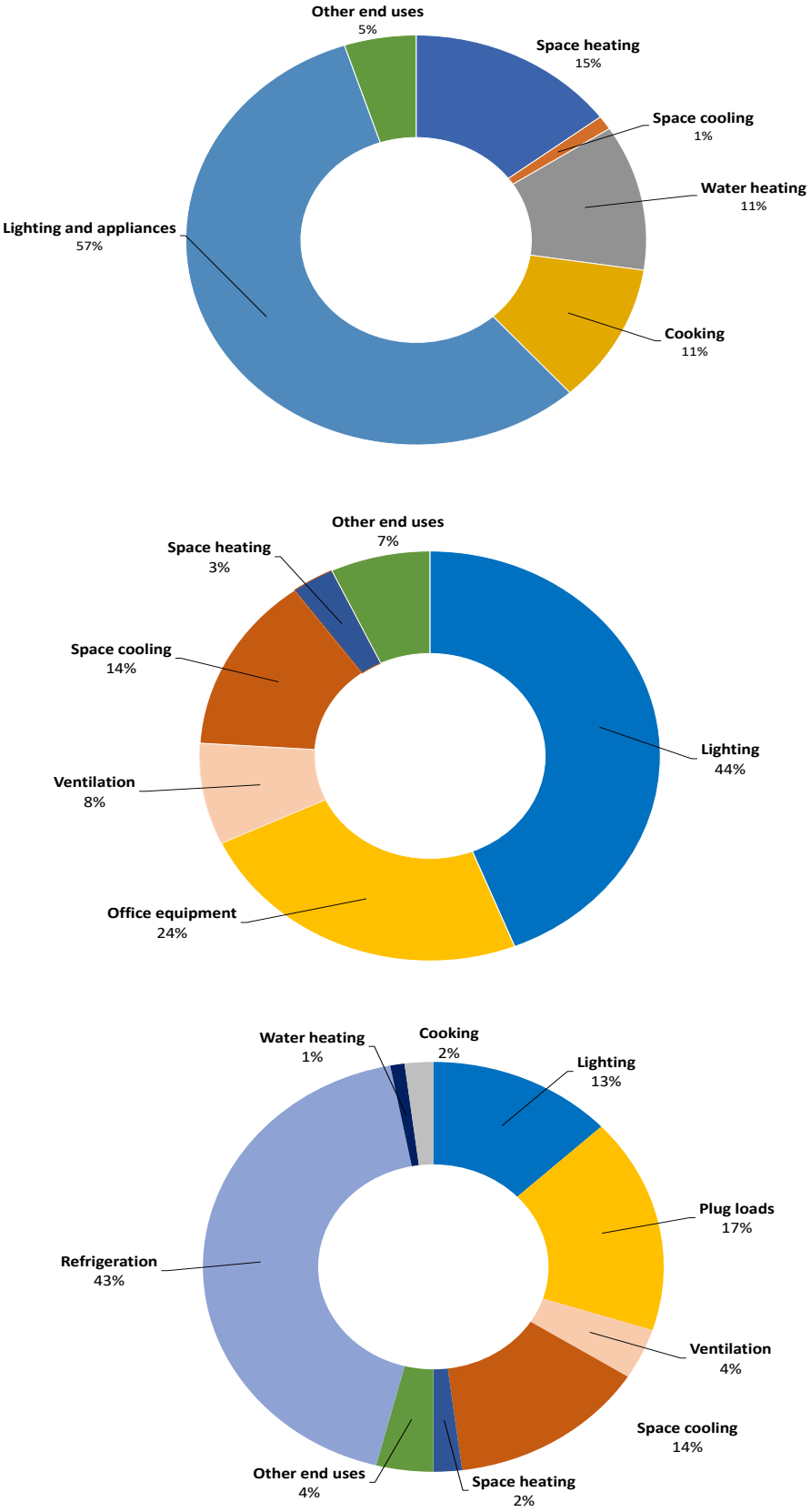

Fig. 2.11. EU -28 Electricity Consumption in 2016 by type of end-use EU28 – 2016.
(Top) Residential electricity consumption [40]
(Middle) Office building electricity consumption [40]
(Bottom) Supermarket electricity consumption [41]

would share a common set of generators that would commonly be PV panels and the generators would contain storage systems such as batteries (see Figure 2.12b).

- Shared prosumer: these refers to a set of clients who share their generation and storage equipment with the rest of their neighbouring installations (see Figure 2.12c).

The EU's Winter Package [39] highlights, the objective of achieving a higher participation of electric consumers by 2030. This is intended to push the electricity customers toward their conversion to active consumers, with the possibility to utilize their own produced energy (i.e., self-consumption) and, to let them to inject and sell their energy to the grid if feasible. One of the sectors that offer more expansion potential is the sector of residential prosumers, where both PV panels and storage systems can be used.

The active prosumer concept thus encompasses the individual and/or clustered consumers who require, store, or sell their generated energy, as long as these activities do not correspond with their main professional or commercial activity. The energy sold can be produced through the aggregators or by means of the joining within DR programs.

IEC Smart Grid Standardization Roadmap [13] in 2010 stated that prosumers have determined characteristics that depend on a number of factors, such as their communications requirements, their location on the power system, and their provided services.

According to their communication requirements, prosumers can have either in subsystems and inter-systems. Subsystems are further categorized into Process Automation and Smart Home and Building Automation. Process Automation is used for controlling and supervising manufacturing processes with their associated energy consumption and generation, whereas the HBES/BACS controls, monitors, optimizes, and manages a smart grid's components, such as its technical installations, DER, storage systems, electric vehicles (EVs), and co-generation plants.

For their part, the inter-systems of prosumers have four classifications: service, operation, markets and distribution. Service inter-systems are in charge of supporting operation functions, such as renewable energies forecasting. Operation inter-systems are compounded by DERs, including VPP, as well as flexible demand control and supervision; their functions can be divided into planning and control, and planning can involve weather, load and generation forecasting, unit commitment and side-by-side management. Within operation inter-systems, advanced metering for billing and network management couples both smart grid infrastructure and smart meters. Markets inter-systems schedule and trade information between power generators and market operators. Lastly, distribution inter-systems are used to communicate with DMS [13].

Although consumers can technically adopt a more active role and become a prosumer, there are still some barriers for its expansion [44]:

- One challenge is that currently there is no any adequate regulatory framework to facilitate its implementation. At present, no EU-country possesses a unique and

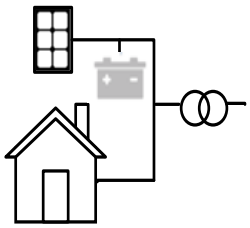

(a) Individual Prosumer

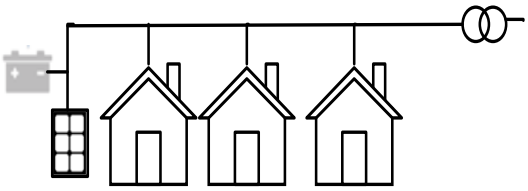

(b) Collective Prosumer

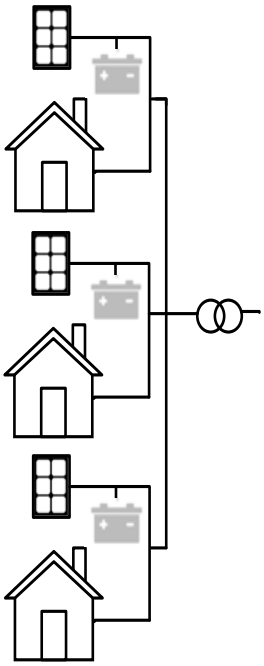

(c) Shared Prosumer

Fig. 2.12. Prosumers topologies

specific normative to regulate prosumers. For example, in Spain, the electricity sector law has self-consumption framed into the renewable energies legislation. In Hungary, prosumers are considered a "household power plant" but there is no mention of their role as consumers. Greek legislation regulates prosumers based on the ministerial order that promotes the installation of PV panels into buildings. Renewable energies production is not required in France, whereas in Norway, prosumers are considered as end-users with downstream consumption and production at the installation's connection point.

- Another challenge is that there is no clearly definition what the contracted power of prosumers should be at the European level. In Spain, the Real Decreto 900/2015 [45] limits the self-consumption capacity of the consumers, and it also establishes two types of users. Type 1 users are self-consumers with a maximum contracted power of 100 kW, whereas Type 2 users have a maximum contracted power higher

than 100 kW; the requirement is that these consumers develop the sale of the energy delivered to the grid as commercial activity. Lithuania limits the prosumer contracted generation power up to 10 kW, whereas in Portugal, four different prosumer categories are established depending on the contracted power prosumers are either below 200 W, between 200 W and 1.5 kW, between 1.5 kW and 1MW, or over to 1MW.

- Moreover, the economical benefits that users obtain are not well defined. In Spain, Type 1 prosumers (i.e., residential) do not receive any monetary compensation for the energy they deliver to the grid and the same applies to Slovenia. Conversely, in countries such as Italy, Denmark, and Portugal, the end-users who are categorized as prosumers receive a monthly compensation for the energy they deliver to the networks.

- Lastly, the grid usage costs are considerably high. These costs are associated with the usage of the grid in transporting and distributing energy. In countries such as Portugal and Belgium, costs are fixed for all the users, whereas in Spain, UK, and France, prosumers have to pay for these costs by means of variable costs' terms. For the particular case of Spain, the "sun tax" and "backup toll", require prosumers to assume some costs for the grid usage, including the cost in which these prosumers produce all of their consumption and do not require energy of the main network.

To reach a larger participation of end-users in the future so that more consumers become prosumers, the following next challenges need to be addressed:

– To promote the installation of PV energy onto LV installations' customers through an adequate RREE's Regulatory Framework.

– A regulatory framework needs to be defined; such a framework would bring economical benefits to the end-users who deliver energy to the grid, either as producers or consumers, without making a difference regarding to the installation's activity.

– The taxes that holds back the self-consumption (e.g., the sun tax in Spain) need to be eliminated.

2.4.5. Aggregator and market actors

An aggregator is a new Smart Grids actor that assumes the role of a service provider and coordinates the sale of the flexible demand that a set of electricity customers can provide to electricity markets (e.g., generators, consumers, prosumers, storage, microgrids, and VPPs). The main function of an aggregator is to coordinate the DR actions that individual clients offer by considering grid operators request, as well as electricity pricing signals.

Moreover, Demand Side Management (DSM) or DR can be defined as the planning and implementation of a set of measures aiming to influence the way that end-users consume their energy so that their consumption pattern can be modified. In this context, DR is defined as the capacity of that users have in modifying their own consumption pattern when responding to pricing signals. This capacity is also known as flexibility, and this relates to the offers by the controllable generation, storage and controllable load (i.e., load shifting and load curtailment) in both MV and LV networks. DR measures are categorized into two groups, namely "incentive based" and "price based" DR, as can be shown in Figure 2.13.

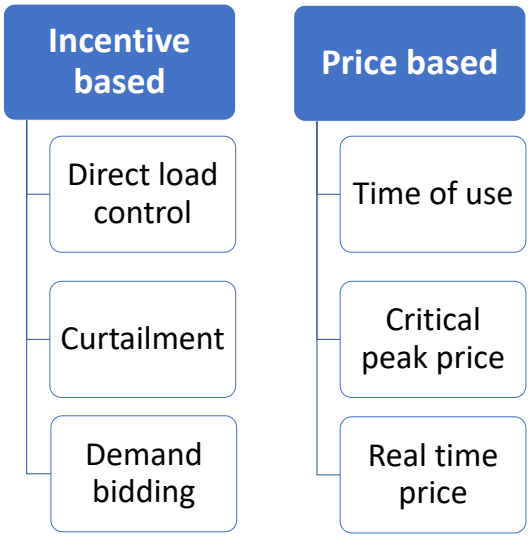

Fig. 2.13. Demand response actions

In the "incentive based" DSM schemes, consumers receive a supplement for changing their energy production/consumption in response to requests from network operators. On the other hand, users in the "price-based" DSM schemes would react dynamically to the variable signals coming from the electricity market.

Apart from the economical benefits that are provided to end-users, DSM measures offer the following benefits to the power systems operators:

- Grid losses are reduced by means of a reduction of the maximum power supplied.
- Local voltage control. The reduction of maximum powers can correct local voltage problems that are associated with excessive voltage drops.
- The reliability of power supply is improved by avoiding the blackouts and overloads in the grid, and this would help with to improve the continuity and security of electricity supply.
- Investments in the system are reduced and they are more efficient. The system's efficiency increases while its costs decrease by reducing the over-dimensioning of

both generation and power systems, which makes it possible to achieve a better use of the existing assets.

- There can be a greater penetration of the RES.
- There would be a smaller consumption at peak hours, as well as fewer Greenhouse Emissions (GHE).
- The consumption at valley hours can be increased, when the renewable generation is greater.

Unbundling an electricity system implies dividing it into separated operating, market and regulatory units. Having market-based units makes it possible to include the aggregators as a brand new retail agent; nevertheless, transmission and distribution system operators need to coordinate with one another in order to estimate better cost-benefits on a system-wide basis [14].

Even though the figure of the grid aggregator is a basic one for the DSM programs, there are still several barriers that present difficulties in its application. The Technical Report of Reference [46] showed that, the majority of EU-countries do not recognize the role of the aggregator dealing with the DSM. France and Switzerland are the only countries that already have a defined framework for the aggregators. In many countries, only large VPPs and retailers are allowed to aggregate (or cluster) and sell their flexibility to the electricity market. The current situation of some EU-countries with respect to DR development is summarized in Tables 2.4 and 2.5 [46].

2.5. Architecture and Standards of ICT

ICT plays an important part of the Smart Grids technologies, and their integration passes through the development of cutting-edge hardware (e.g., communication equipment, routers, relays, switches, gateway, and computers) and software (e.g., enterprise resource planning and customer information system). Their development trend is fast and evolutionary, which leads to rapid obsolescence. Although the development continually advances, these technologies have reached to a high enough maturity level to set standards. Two examples of these standards are the IEEE 802.22 and the IEC 61850. The IEEE 802.22 is responsible for transferring real-time big data generated by smart grids to their respective control centers, and the IEC 61850 uses TCP/IP protocol to allow data transference among electronic devices inside a smart substation [14], [47]. Based on concepts given in [47], the ICT for real-time performance is displayed in Table 2.6.

The general architecture of a Smart Grids is assumed to be the same as the landscape depicted in [13], which was drawn in accordance with the NIST Smart Grid Framework 3.0 in 2014 [28]. This is used as a standard for several authors such as [12], [47]. In this sense, the landscape is composed of seven domains customer, markets, service provider,

Demand response Development	Country	Situation by 2017
Commercially active	Belgium	• The aggregator requires the retailer agreement prior to load management. • Customers do not have the ability to choose their aggregated service provider, since they have to obtain the permission of their BRP/retailer. • DR can participate in the Primary and Tertiary Reserves, as well as in the Interruptible Contracts programme. • Wholesale markets are closed to DR.
	Finland	• Independent aggregators can only access the market in agreement with the consumer's retailer. • Both day-ahead and intra-day markets require a minimum size of 0.1 MW to participate.
	France	• The participation of consumers connected at the distribution level has been theoretically possible since January 2016. • Activations of DR programs are managed by the TSO based on the system requirement, providing rights to all retailers to offer variable tariffs.
	Great Britain (GB)	• All balancing is open to DR and aggregated load is accepted. • DR currently can only participate in the GB Day-ahead and Intra-day markets in the form of flexibility of retailers and a few very large industrial customers that are already trading members. • The markets are closed to independent aggregators.
	Ireland	• Aggregation is allowed, and the minimum bid size is 4 MW for Demand Side Units (DSU). • The TSO issues instructions to the DSU to reduce demand at an aggregate level, and the DSU has one hour to reduce its demand, and must be able to maintain this demand reduction for a minimum of two hours.

TABLE 2.4. DEMAND RESPONSE IN EUROPE ACCORDING SMART ENERGY DEMAND COALITION (SEDC)

Demand response Development	Country	Situation by 2017
Partial Opening	Germany	• Minimum bid size is 10 MW and opportunity costs are paid for generation but not for demand. • Day-ahead and Intra-day markets are open for consumers working with their electricity retailer through implicit and explicit DR.
	Denmark	• Retailers are in charge of DR aggregation. • There are no independent aggregators. • Only the largest consumption units (> 10MW) are able to participate.
	Austria	• DR is open only for Primary control.
Preliminary development	Poland	• Emergency DR Programme is the only DR programme.
Closed	Spain	• Aggregation is not legal in the Spanish electricity system. • The Interruptible Load programme for large costumers connected to HV networks is the only DR program in Spain. • Consumers can join the Time-of-Use (ToU) con-tracts for load shifting in response to price signals.
	Portugal	• DR is not allowed in the balancing market or the ancillary services. • The interruptible contracts programme is limited to large industrial consumers, connected to the HV grid. • Only generators with a production unit of at least 50 MW, can participate as a seller in the wholesale market.
	Italy	• Aggregators are not allowed in any of the key markets. • The enrolment of interruptible loads requires a minimum size of 1 MW to participate. • Aggregation is not allowed.

TABLE 2.5. DEMAND RESPONSE IN EUROPE ACCORDING SMART ENERGY DEMAND COALITION (SEDC) (CONTINUATION)

Sensing and measurement	Smart sensors collect information from the state-measure modules; they also serve as a communication link between devices and IEDs.
Smart Metering	The main function of smart meters is to inform end-users about real-time prices according to their terms of usage. They form an interface called Advanced Metering Infrastructure (AMI) that is also composed of database systems, network protocols, applications, GIS and CIS.
Demand response	Color codes are used for each power grid voltage level; a similar scheme was used to establish DR, which depend on energy demand of the involved end-users. The main function is help to shift consumption level (i.e., peak shaving and valley filling).
Quality of Services (QoS)	• Smart grids should provide stored energy for buffering purposes in case of outages • Based on this point, a letter code can be implemented, and it would depend on the consumer's QoS requirement.
Phasor Measurement Units (PMU)	PMU measures a voltage's magnitude and angle at the system's frequency. When synchronized to a GPS, they turn into synchrophasors.
Database Structure	Smart grids are distributive due to the complexity of their databases in containing temporal, frequency and geographical information, data processing is required to be transactional. This is the final step for smartening a grid [48]

TABLE 2.6. KEY TECHNOLOGIES FOR REAL-TIME COMMUNICATION IN SMART GRIDS

operation, generation, transmission and distribution; these can be seen in the NIST conceptual diagram in Figure 2.14 [28].

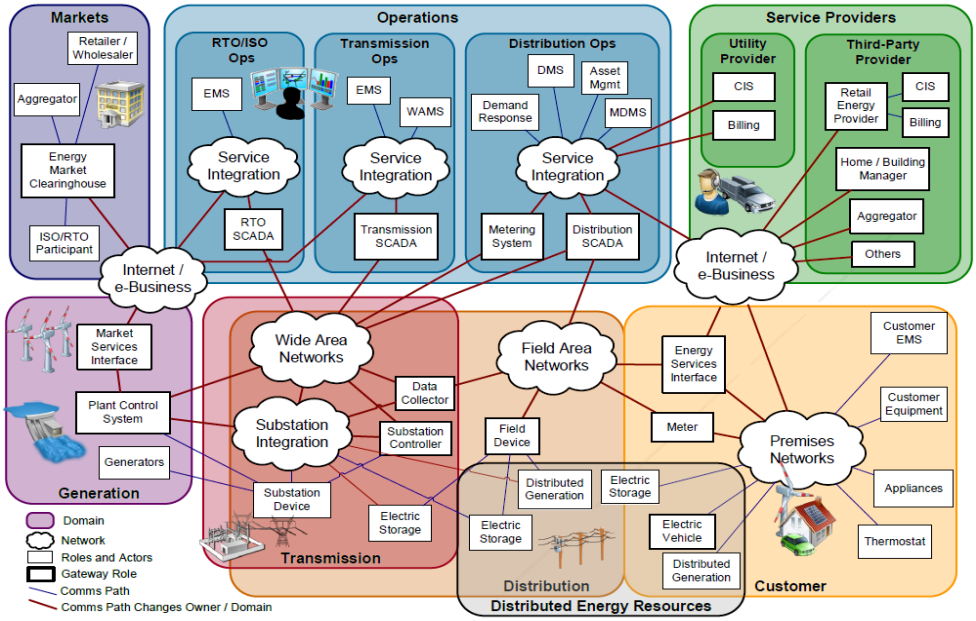

Fig. 2.14. NIST Conceptual Domains for Smart Grid Information Networks [28]

The lower domains are the ones that form the power grid infrastructure. These are referred to as bulk generation, transmission, distribution, and Customer; their flow is bidirectional and their common path is known as the electrical flow interface. The upper domains are formed by markets, operators and service providers (i.e., aggregators with clustered customers). From here, several secure communication interfaces are outlined. In between the path from upper to lower domains, there is a central upper domain known as operation, and its main function is to gather information for controlling and monitoring all the lower domains.

Due to their nature, customers have two options for reaching electricity market. The first one consist of passive consumers who are attached to their own service providers, and the second involves becoming prosumers, who have enough autonomy to compete for market prices by themselves depending on their installed capacity. Service providers communicate simultaneously to operators and markets domains to fix their service prices after the auction processes in the daily and intra-daily markets are closed [12], [13], [17].

A similar focus based on the layers that ended up in creating a Multi-Agent System (MAS) is founded in [17]. Comparatively, the equivalent of and electric domain is referred to as an agent, which is defined as an entity capable of autonomous and flexible decision-making depending on the information received from their built-in intelligent interfaces with the rest of the entities.

A MAS has three different action layers, namely the deliberation, coordination, and reactive layer.

- The deliberation layer contains the agents capable of performing wide-area monitoring and control, which helps to plan the behaviour of a down-stream layer's agent for a long period of time.
- The coordination layer contains the agents that has main function of establishing priority order regarding which fault event from the reactive layer should be firstly attended to by deliberation layer.
- Lastly, the reactive layer contains all the resilient components placed in the lower electric domains.

From this three-layer architecture, a seven-agents control architecture was conceived [14], [17], whereas another three-layered architecture was analysed in [49] that was based on the power trading agent competition (TAC) simulation tool proposed in 2013 [50]. In this latter model, two of the layers coincide with the upper domains (i.e., the market domain) and lower domains; the third layer is directly assumed to be the same as the communication interfaces described in [13]. Both models are depicted in Figures 2.15a and 2.15b, respectively.

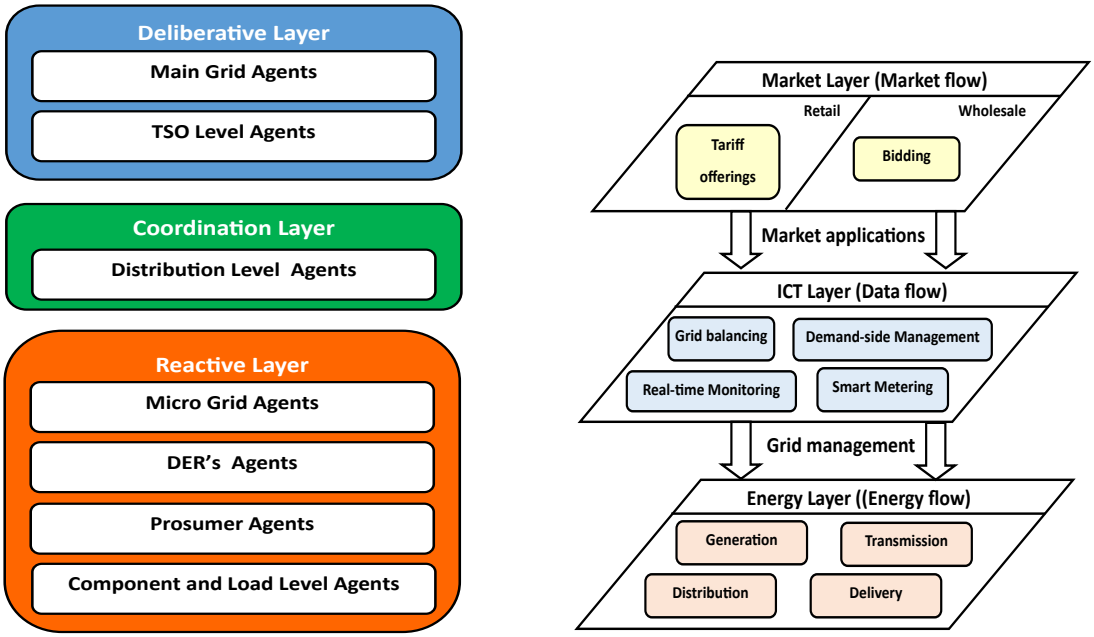

(a) Multi-Layer Smart Grid Architecture with seven agents

(b) Power-TAC-based three-layered Smart Grid Architecture

Fig. 2.15. Multi-layer Smart Grids Architecture Models

Nevertheless, the smart grid architecture is not only defined by layers or domains but also by the components and their sub-architectures [47], [51], their functions and sub-functions [13], [52], as well as the sector they are referred to [13]. Some examples of interoperability architectures in [13] include IEC 62357 Reference Architecture, service-oriented architecture (SOA), advanced EMS, IEC 61968 compliant interface, four-layered

next-generation CIM, and HES. In terms of communications interface, database structure described in Table 2.6 has an architecture that is the same as the one established by IEC 61850 Standard. In other words, it has five layers that are stacked from the inside to outside; starting from the innermost layer, these layers are referred to as Data Attribute, Data Object, Logical Node, Logical Device (LDx) and Physical Device (IEDx) [47]. This has a model that is quite similar to the TCP/IP Protocol. By contrast, the situation recognition, situation comprehension, and situation projection requirements that are derived in the creation of a Situational Awareness (SA) architecture designed for SCADA systems are present in Smart Grids [53].

From the point of view of communications architecture, it is important to have a set of standards that allow the different devices to interoperate with each other. The main standardization organizations are the International Electrotechnical Commission (IEC) IEC 61970/61968, IEC 62325 IEC 61850, the European Standardization Organizations (ESOs) and the European Committee for Electrotechnical Standardization (CENELEC). These are actively working to define a standardization process for the Smart Grids. In this aspect, the Smart Grid Architecture Model (SGAM) developed by the CEN/CENELEC/ETSI Smart Grid Coordination Group (SGCG) is highlighted; their objective is to design a general architecture that is useful for the different requirements for European Smart Grids. This SGAM [54] is one of the Europeans Open Standards Technical Model, which is constituted by Five Interoperability Layers (Business, Function, Information, Communication and Component), the same number of electric domains (Generation, Transmission, Distribution, DER and Customer Premise), six sectoral zones (Market, Enterprise, Operation, Station, Field and Process), diverse Frameworks, Sub-Functions, Data Model and protocols.

The SGAM model depicted in Figure 2.16 allows to obtain an automation system model for the distribution grids. This model incorporates the substation's protection, measuring, and control elements, as well as components belonging to the associated installations (i.e., substation transformers, lines and loads). Figure 2.17 shows how automation systems are grouped depending on the domain that encompasses each unit when the SGAM functional diagram is followed.

At the distribution level, the functions that stand out are feeder automation and substation automation. The typical operations that can be carried out are protection, network reconfiguration, or power quality control.

The IEC 61850 Standard covers all the necessary fields for modelling the operations and functions into a distribution substation. For example, the IEC 61850-7-4 Standard allows modelling the information level, whereas the IEC 61850-8-1 defines the communication level inside the substation.

Similarly, the IEC 61850-7-1420 and the IEC 61850-7-4 Standards allow the DER's information level to be modelled. Depending on the type of DER technology, the following standards can be applied:

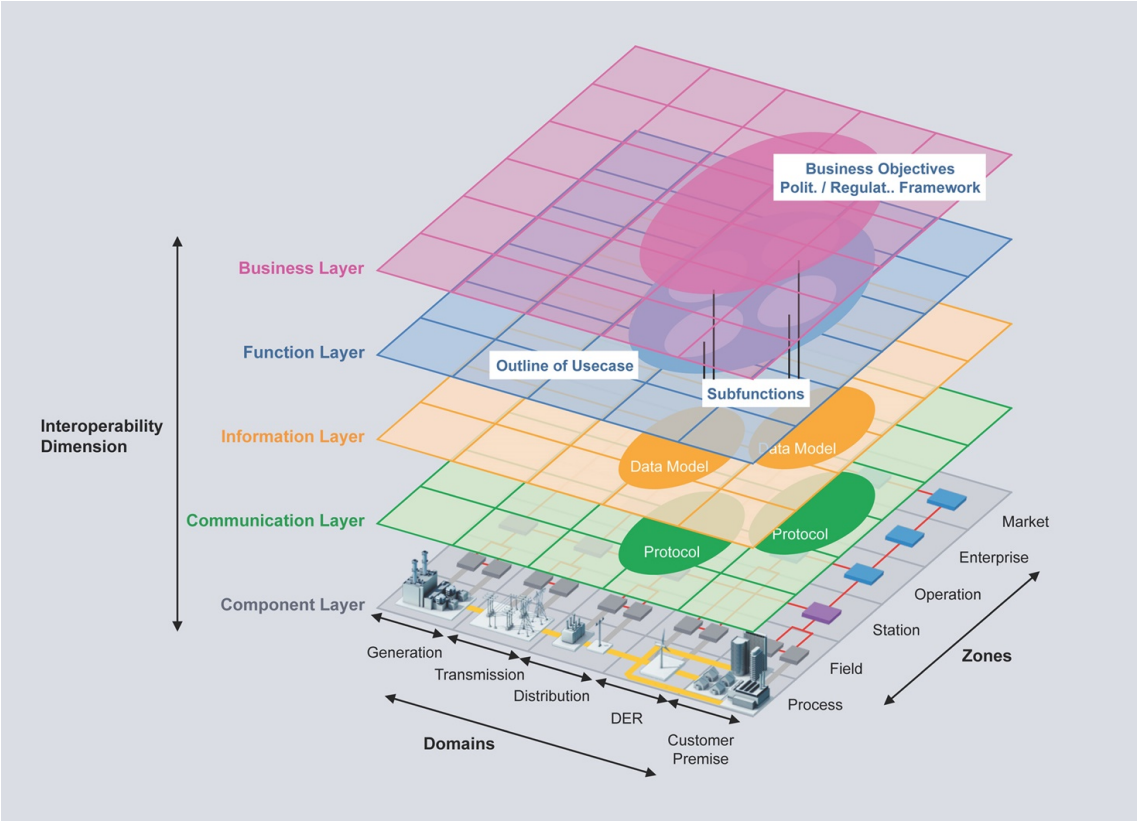

Fig. 2.16. The SGAM framework [54]

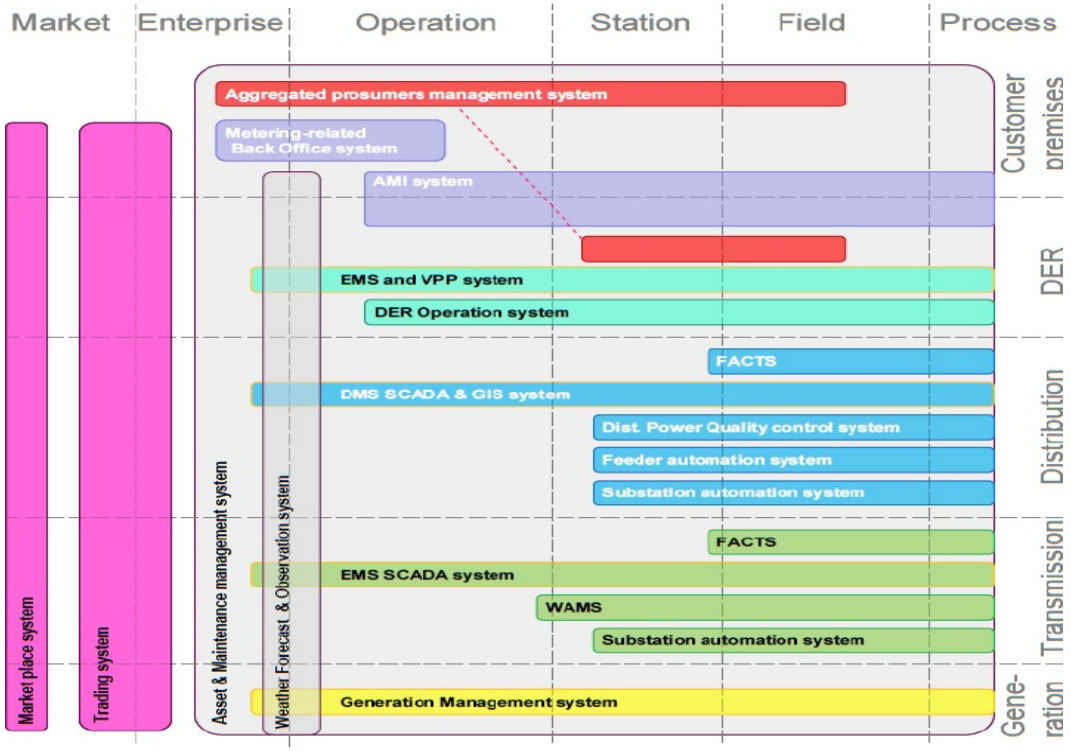

Fig. 2.17. SGAM function group diagram [54]

- IEC 61850-7-420, which contains a description of the logical nodes of the DER units;
- IEC 61400-25-2 / 3, which defines the exchange of information for the control and monitoring of wind power plants;
- IEC 61850-90-7, which defines the object-oriented modelling of DER power converters and is focusing mainly at PV inverters.
- IEC 61850-90-9, which defines the models for electrical energy storage systems, and
- IEC 61850-90-15, which presents the hierarchical architecture to be implemented in distribution networks with multiple DER units.

Finally, depending on the geometry given by the field of action for each component and their interoperability, Smart Grid architectures and sub-architectures can be classified as semantic, circular and holonic. A holonic Smart Grid refers to an Smart Grid behaving as an holon; which can be considered something that is both a whole and a part [47], [55].

2.6. Summary

This chapter presented, a review of the state-of-the-art regarding Smart Grids. The chapter analysed the technological evolution of Smart Grids and the main actors that adopt a predominant role with respect to their operation. This study highlighted the various situations that Smart Grids currently face within the EU; this include Smart-Metering roll-out, actions that have been taken to implement DR, and the greater or lesser facilities that can be offered to the prosumers. Similarly, the main inconveniences and barriers when it comes to enlarging the existing prosumer base have been highlighted.

This chapter also covered the subject of the communications infrastructure, as well as the standardization actions that have been carried out in the EU so that interoperability among devices, generalization, and facilitation of the necessary tools for fulfilling Smart Grids projects can be achieved, as proposed with SGAM Model.

The standardization part revolves around the IEC 61850 Standard, which is composed of 10 different parts covering DG, storage systems, control architecture, and the modelling and exchange of information into the Smart Grids.

Lastly, this chapter focused on the distribution Smart Grids, specifically both MV and LV levels since these voltage levels are the ones that involves consumers/prosumers, DER units and microgrids.

3. SMART GRIDS VOLTAGE CONTROL

3.1. Chapter Introduction

Distribution grids currently face a new paradigm where new entities appear, such as DG, storage units, flexible loads, and electric vehicles. In addition to these generation and energy demand systems, there are also electric distribution grids lately that are equipped with communication systems; these aim to allow users to know the real-time consumption and production regarding generation and demand units, while establishing the directionality of power flows. As a result of this evolution, distribution grids have become active distribution networks, which are capable of managing the controllable elements available in the system to improve the network operation [56].

The increase of generation units connected to the MV and LV grids produces voltage problems and network congestions' issues in both MV and LV grids [57]. Because of this, the concept known as "fit and forget" that was frequently employed by the Distribution System Operators (DSOs) is no longer valid here, which makes it necessary to implement solutions that can manage the controllable units connected to MV and LV networks. One of the most remarkable problems per specialized literature are the over-voltages generated in the LV systems when DG overcomes the demand. These problems can be propagated to the MV grid and even in some situations, to the transmission grid.

With the above in mind, it is therefore necessary to develop control schemes of the electric grids that can manage MV and LV networks in a coordinated manner and can also locally control the distributed generation, storage, and flexible loads. There are three main schemes with regard to power systems control that are found in the literature; these schemes are centralized control (which is principally used in conventional electric grids), decentralized local control, and coordinated control.

3.2. Impact of distributed generation on electricity networks

Conventional LV distribution networks follow a radial topology with a main substation with one or several feeders, and the loads are connected to these feeders. The minimum voltage in these grids is found at the final nodes of the feeders, whereas the maximum value is found in the main transformer at the secondary substation. The way in which voltage has been controlled and maintained within the established limits involves the on-load tap changers (OLTC) of the main transformer located at the secondary substation.

Nevertheless, the incorporation of DG units into the electric grids have a huge impact on the voltage profiles of the distribution networks, especially at the LV level.

Figure 3.1 shows the voltage profile of an LV grid, which is made up of a substation

and two feeders. In the red feeder, the connected loads are considered to have either no regulation capacity or no DG units. On the contrary, the green feeder has both controllable loads and DG units.

As can be seen in Figure 3.1, when no power is injected by the DG units, the voltage profile of both the conventional feeder (in red) and the one with controllable loads (in green) decrease as they move away from the substation. Conversely, when there is power injection coming from the DG units connected to the green feeder, an augmentation of the voltages in the nodes begins, which leads to over-voltages which do not respect the limits established by grid regulation. Thus, in looking at the voltage profiles shown in Figure 3.1, it can be concluded that it is necessary to regulate the voltages in the distribution grids with DG units (i.e., over-voltages) and those without DG units (under-voltages).

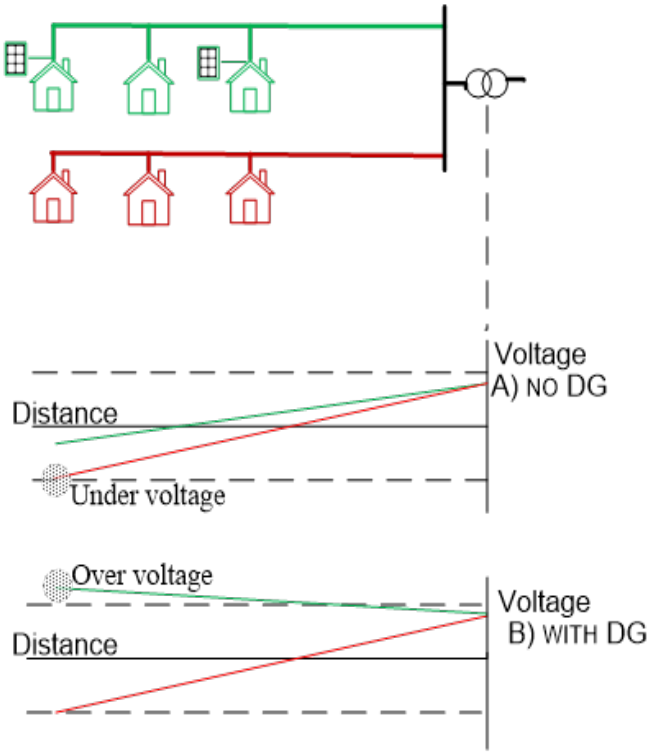

Fig. 3.1. Voltage profile of an LV network with presence of DG units and controllable loads

Unlike the MV grids, LV grids are characterized by being very resistive with a characteristic elevated R/X. Thus, the suppositions used in the MV voltage lines are not applicable on LV grids.

In Figure 3.2, the electric line that is shown presents a series line impedance $Z = R + jX$, and it connects two nodes whose voltages are $\overrightarrow{U_1} = U_1\angle\theta_1$ and $\overrightarrow{U_2} = U_2\angle\theta_2$, respectively. In the Node #2, there is a load connected that demands power; this is expressed as $P + jQ$.

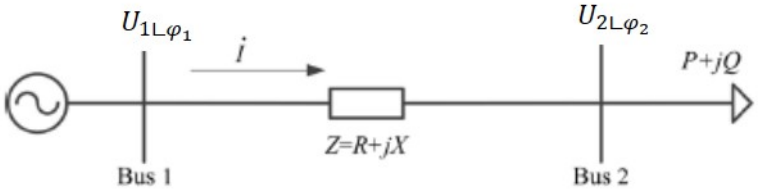

Fig. 3.2. Single-line Diagram of a Distribution Line

The voltage drop that is produced in the line has the expression given in (3.1).

$$\Delta\overrightarrow{U} = \overrightarrow{I}(P + jQ) = \left(\frac{P + jQ}{\overrightarrow{U}_2}\right)^* (R + jX) = \frac{PR + QX}{U_2} + j\frac{PX - QR}{U_2} \tag{3.1}$$

In the particular case of MV and HV networks, where lines present a mainly inductive impedance, the voltage drop in the line can be approximated by (3.2), with the grid nodes voltages being controlled by means of the injected reactive power.

$$\Delta\overrightarrow{U} = \frac{QX}{U_2} + j\frac{PX}{U_2} \approx |\Delta\overrightarrow{U}| = \frac{QX}{U_2}. \tag{3.2}$$

However, as a consequence of the elevated resistive value of the LV lines, the voltage drop effect cannot be cancelled due to the line resistance. Thus, a voltage drop in a line belonging to a LV grid can be calculated with (3.3):

$$\Delta\overrightarrow{U} = \frac{PR + jQR}{U_2} \tag{3.3}$$

From (3.3), it can be deduced that a voltage drop in LV grids is no longer dependent on the reactive power that flows throughout the grid in the way as with MV grids, and thus, the injection and control of the reactive power will not be the only methods to control voltage in LV networks.

By applying a derivative to (3.3) with respect to the power in (3.4), it can be deduced that for the same value of both the injected active and reactive powers in a LV grid, the impact caused by the injected active power is greater than the one caused by the injected reactive power. This is a consequence of the elevated R/X ratio on these networks. Consequently, to regulate the voltage in LV grids it will be necessary not only to regulate the reactive power injection/absorption in var sources but also to regulate the active power injected by the DG and even regulate the active power demanded by flexible loads if DR actions are available.

$$d|\Delta\overrightarrow{U}| = \frac{\delta|\Delta\overrightarrow{U}|}{\delta P}dP + \frac{\delta|\Delta\overrightarrow{U}|}{\delta Q}dQ = \frac{R}{U_2}dP + j\frac{X}{U_2}dQ \tag{3.4}$$

LV grids can present two clearly distinguishable behaviours with respect to voltage profiles:

- First, the hours where the power injected by the DG units are above the system's demand, over-voltages can be produced, and thus it will be necessary to carry out a control over the active power injected to the system.
- Conversely, when there is no power injected by the DG units for an elevated demand condition, this would cause under-voltages problems. The solution here is to employ voltage control mechanisms such as on-load tap changers (OLTCs) or Capacitor Banks (CBs), which will allow voltage profiles to be maintained within the established limits.

Hence, it can be concluded that the voltage control of LV grids with a presence of DG units can be carried out by two methods namely using the active power control of the controllable units (i.e., DER and flexible demand) and the utilization of conventional voltage and reactive power control units.

3.3. Traditional voltage control devices

In Distribution networks it can be located DER devices (either controllable or controllable), storage systems, reactive power compensators, as well as flexible loads. Together with these new elements of distributed power systems, there are conventional voltage-control units, such as OLTC, CBs, and in some cases SVCs. The operation of all these components bring benefits to the power system usually these are referred to as "ancillary services", and they depend largely on the location, size and controllability of the devices. Power systems control schemes must be able to regulate both the delivered/absorbed active and reactive power from these components, so that network's nodal voltages keep between the limits established by the corresponding normative [7], [58].

Considering the elements to be controlled by the voltage control schemes, the variables that may be used include the following:

- active and reactive power delivered by the DER units,
- the reactive power injected by the capacitor banks,
- the tap position of the OLTCs, and
- the set-points of both STATCOM and SVC.

The voltage regulation in the grids with DG units depends on the controllability offered by DG units in the system at each instant of time. Thereby, the DG units connected to the grid by means of power electronics offer a regulation capability of the injected reactive power that help to improve the voltage level at the Point of Common Coupling (PCC). The coordination among the controllable units will allow the network's general behaviour to improve, especially the nodal voltage profile.

Nevertheless, the incorporation of the DG units to the power systems also implies some challenges. One such challenge stands out is the problem of over-voltages caused by an excess of production from DG units under low demand situations or the problem of bidirectional power flow which can produce the tripping of the network relays [59].

As seen in Section 3.2, on LV networks where R/X ratio is elevated, it is not enough to regulate the nodal voltages by exclusively employing reactive power control devices as it is normally done in HV and MV networks. Rather, they have to work jointly and coordinately with other elements such as AVRs, OLTCs, as well as controlling the active power injected/absorbed to the grid by controlled generators and flexible consumers. The following subsections presents a description of the most utilized devices for voltage control.

3.3.1. On-Load Tap Changer

A typical power system is composed by different transmission and distribution networks with different voltage levels and various step-up and step-down power transformers located at primary and secondary substations. Transformers are usually equipped with tap regulators (i.e., AVR) that allow the transformation ratio to be changed in order to maintain the voltage levels in its windings at the reference level without needing to interrupt the power supply.

The voltage control is located at the transformer windings with tap regulations and is connected to the load and it is managed by means of a dynamic voltage regulator, as shown in Figure 3.3. In the event where voltage variations are higher or lower than the set point, a time relay operates. Once the relay waiting time has elapsed, which is usually several seconds, the tap changing mechanism is activated to a new tap position until the voltage gets back within the normal working zone, or until the tap limits are reached. The activation delay between tap positions is adjustable, with the typical values ranging from 30 to 60 seconds. In the case of elevated voltage variations, the required time delay for passing through all the tap positions can reach up to 2 minutes. The longer the tap changers' delay is, the longer the available time is for taking corrective voltage measures.

In looking at the operating characteristics of the OLTCs equipped with mechanical AVRs, these devices are classified as slow voltage regulation elements. Thus, they are used as a backup of other faster voltage control units.

In the past recent years the Line-droop Compensation Function (LCD) has been used to operate the regulation taps of the OLTCs. The OLTCs with conventional control mechanisms, are capable of regulating the voltage on the transformer's secondary winding, but they are not able to control the voltage of other points of the electric grid. Instead, those OLTCs equipped with the LCD function can widen the voltage control range to others grid nodes. From the reading of the voltage and current gathered at OLTC's secondary winding, the LCD function estimates the voltage drop to be between the transformer's

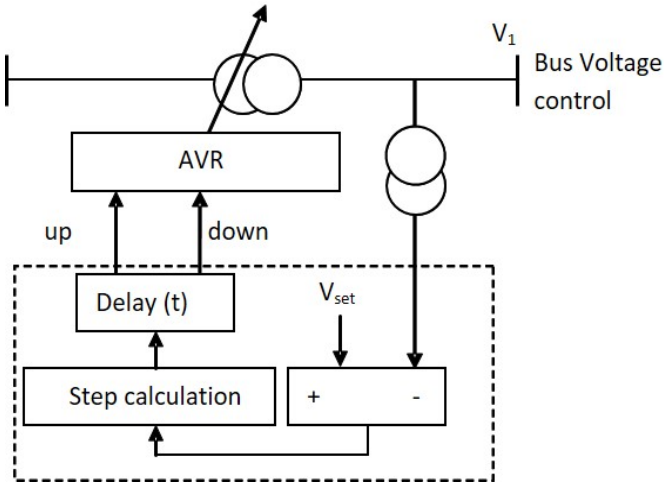

Fig. 3.3. Dynamic regulator of a transformer with tap changers

secondary winding and the other specific nodes. If some of the voltage estimations in the system's nodes are outside the limits established by the regulation, the OLTC adjusts the tap position in order to set the nodal voltage within the limits [57]. The OLTC's basic operation with LCD function is shown in (3.5).

$$\Delta tap = \begin{cases} +1 & \text{if } (U_{min} \prec U_L) \cup (U_{max} \prec U_H) \\ -1 & \text{if } (U_{min} \succ U_L) \cup (U_{max} \succ U_H) \\ -1 & \text{if } (U_{min} \prec U_L) \cup (U_{max} \succ U_H) \cup (\Delta U_{max} - \Delta U_{min} \succ U_{step}) \\ +1 & \text{if } (U_{min} \prec U_L) \cup (U_{max} \succ U_H) \cup (\Delta U_{min} - \Delta U_{max} \succ U_{step}) \end{cases} \tag{3.5}$$

Where:

U_L is the allowed minimum voltage; U_H is the allowed maximum voltage; U_{step} is the voltage variation at each one of the OLTC steps; Δtap is the position of the transformer regulator tap, with ΔU_{max} and ΔU_{min} calculated according to (3.6) and (3.7).

$$\Delta U_{max} = U_{max} - U_H \tag{3.6}$$

$$\Delta U_{min} = U_L - U_{min} \tag{3.7}$$

3.3.2. Capacitor Banks (CBs)

The usage of CBs is widely extended in power networks. These elements are mainly used for several purposes, such as elevating the voltage at certain points of the electric network and compensating the power factor of the loads connected to the distribution network. They also allow generators to work with a unitary power factor, and they can also control the voltage profiles of the distribution grids.

Capacitors are generally shunt connected, although they can also be found connected in series in a network line. The connection or disconnection of these elements is usually done by mechanical switched Capacitor providing a reactive power proportional to the square of the voltage at the connection point.

The main drawback with capacitors is the reactive power rating of the device for different working conditions and demand variations. This is solved with the connection of several capacitors in parallel (CBs) which would either connect or disconnect the required number of steps for the optimal functioning of the system, and this would be done through the usage of voltage relays. If the relay detects a reduction of the voltage below the threshold, a capacitor step is connected to elevate the voltage level at the connection point. The main inconvenient of this configuration lies in the usage of the relays, these mechanical elements are subjected to fatigue, which implies the need of maintenance and slow-action. The constitution of the capacitor banks makes them incapable of giving a proper answer to the over-voltage or under-voltage problems that are derived from abrupt demand or generation oscillations. These oscillations can be produced in the Smart Grids networks, as a results of the intermittence in the renewable generation.

3.4. D-FACTS

Most of the power electronics components have helped to develop newer and more efficient control systems. Smaller versions of these components have been later used to control the performance of both transmission and distribution systems; these already have a considerable penetration of renewable energies and DERs [29]. D-FACTS devices are applied in distribution networks, and this is done mainly at MV level [29], [60], [61].

Among the several D-FACTS devices encountered in the market, the most important ones are listed as follows [29], [61]:

- The MV-SVR helps to push load voltages up when source voltages have dropped, regardless of whether the fault occurs at transmission or distribution level. These devices help to avoid operational power breakdowns as long as the control is achieved within a range which is going from a quarter to a half cycle.
- The MV-SVCs is mainly used in distribution systems with DER, particularly with a strong presence of PV plants. These devices help to improve the quality and stability of the power system as well as the lower instabilities produced by transient flows [61].
- The D-SFC stabilizes voltages, improves the power factor and mitigates THD.
- The D-STATCOM aims to regulate voltages, compensate the harmonics that come from the current wave distortion, control reactive power, and serve as an uninterrupted source of power when used as a backup for storage systems.

- The DSSC allows for active-power-flow-control, so that power losses are diminished.
- The D-TCSC: provides system steadiness and control [61].

There are different configurations for reactive power compensation in distribution networks. One configuration is to have CBs, SVCs, and STATic synchronous COMpensator (STATCOM) connected in parallel to the electric grids. These devices can be utilized as a complement or backup for the reactive power delivered by the DG units, so that voltage profiles of the Smart Grids can remain within the established limits. This would create a reactive power flow in the system that counteracts the effects of the power that is injected over the voltage nodes of the grid [62].

3.4.1. Static Var Compensator

In the same way as CBs, SVCs are basically reactive power compensation components. Their connection or disconnection is dynamically regulated by electronic control devices. Unlike CBs, SVCs are fast-response elements that can improve the voltage profile at the connection point almost instantaneously. Another feature of these devices is that they dynamically adjust the reactive power injection as the conditions of the network change.

SVCs began to be utilized in the 1970s and they can be found connected to both transmission and distribution power systems. Their main applications include: temporary over-voltages control, prevention of voltage collapses, transient stability improvement, mitigation of electromechanical oscillations in transmission grids, unbalanced systems' equalization, and flickers reduction on the proximities of variable loads in the distribution networks.

There are two main topologies of SVC namely the thyristor controlled reactor (TCR) and the thyristor switched capacitor (TSC).

- The TCR scheme is equivalent to a system formed by a capacitor that is connected in parallel with a variable reactance (see Figure 3.4a). The reactive power that is injected in the point of connection is composed of the one injected by the capacitor connected in parallel and the regulation of the one absorbed by the reactor. For this kind of control, two thyristors are connected in anti-parallel; in order to control the conduction angle.
- In the TSC configuration, the CBs is connected to the power system using thyristors (See Figure 3.4b). It is the simplest configuration when it comes to utilize power-electronics-based devices to compensate the reactive power. The connection or disconnection of the capacitors that put together the bank is made through two thyristors connected in anti-parallel, namely one for each conduction cycle.

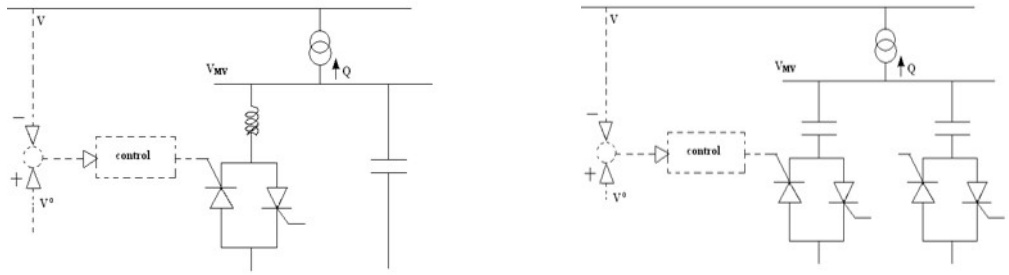

(a) TCR Configuration

(b) TSC Configuration

Fig. 3.4. SVC's representative schemes

Figure 3.5 shows the Voltage-Current characteristic curve of the SVC devices in the PCC. As it can be noted, SVC devices present a wide performance range in steady-state, but their response under low voltage levels is very limited.

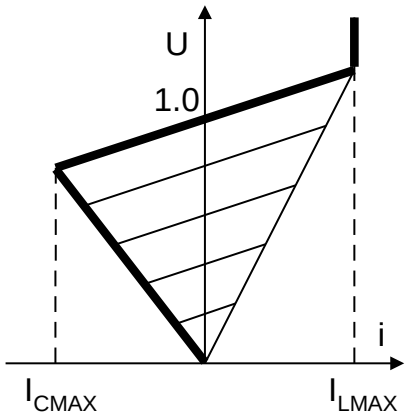

Fig. 3.5. V-I characteristic of a SVC device

3.4.2. STATic synchronous COMpensator (STATCOM)

The working principle of a STATCOM is based on a voltage source converter. These devices belong to the Flexible AC transmission systems (FACTS) family, and their main function is to dynamically exchange reactive power with the grid in the PCC.

Figure 3.6 depicts a STATCOM scheme, which is compounded by an electronic converter, a storage energy element, and a control system. The control system is the part in charge of maintaining the voltage of the DC-stage to a constant reference, and it also calculate the triggering angles of thyristors or IGBT devices in order to inject the reactive power that is needed in each working condition of the system [63]. By adequately controlling both the magnitude and angle of the converter's voltage output, the STATCOM can exchange both the active and reactive power with the system. Through the voltage source converter, the STATCOM is capable of regulating both the voltage magnitude and

phase, as well as the frequency of the PCC. In doing all this, STATCOM devices present themselves as an answer to reactive power flow problems and voltage control in both transmission and distribution electric grids, although it should be noted that for the latter grids, Distributed STATCOMs are used (D-STATCOMs). These devices allow the power factor to be corrected, and they also allow for harmonic filtering when they are connected in parallel with a disturbing client.

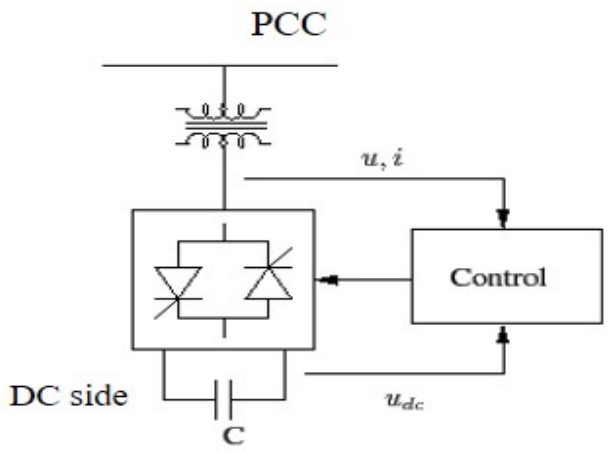

Fig. 3.6. STATCOM scheme

Among their most remarkable features, they have two outstanding characteristics.

- First, they have the capability to deliver reactive power even for very reduced voltages, thus allowing the voltages to increase in situations with abnormally low values. This supposes an improvement with respect to the performance of the SVCs (see Figure 3.7).
- Secondly, they have fast-response capability, which makes these devices an ideal solution for voltage control applications, in conjunction to their ability in supplying constant capacitive current.

In addition, STATCOMs can be utilized where a rapid and continuous reactive power control may be required. In these situations, STATCOMs can perform the following functions:

- regulation and effective control of the voltage,
- reduction of temporary over-voltages,
- increase of the transient stability margin,
- single-phase balance among loads, and
- reduction of the rapid voltage fluctuations (i.e., flicker control).

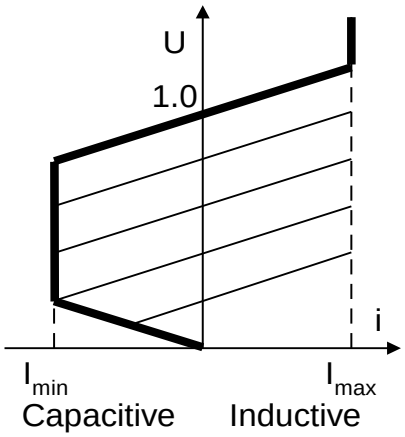

Fig. 3.7. V-I characteristic of a STATCOM device

3.5. Distributed generation reactive power control

DGs units are elements that can be used for voltage control in smart grids. Generally, these units have enough capability to manage both the active and reactive generated power, and in this way they are able to support the voltage control of networks with different R/X ratios.

Wind farms and photovoltaic installations are connected to the grid through power electronic converters providing to the grid an active and reactive power capability which can be use for voltage control purposes. These technologies are the ones that will be shown in this chapter.

3.5.1. Wind turbines

Nowadays, wind power installations are formed mainly by variable-speed wind turbines. Among them, the most outstanding is the Doubly-Fed Induction Generator (DFIG) which is depicted in Figure 3.8. The main characteristic of this machine is its connection to the grid through converters, this connection makes it possible to control the active and reactive power injected to the grid at the connection point.

Doubly-fed machines are formed by an asynchronous machine of wound rotor and back-to-back power converters linked by a common DC-link, as it is shown in Figure 3.8 [64].

In wind farm installations, the production curtailment will depend on the available technology in the wind machine. In the case of machines with no-pitch control, the production curtailment is carried out when disconnecting the machine by means of relays that check the voltage at the PCC. If there are pitch-controlled machines, the power output of the machine can be controlled through the blade's angle of rotation, so that the voltage can remain within the established limits [65].

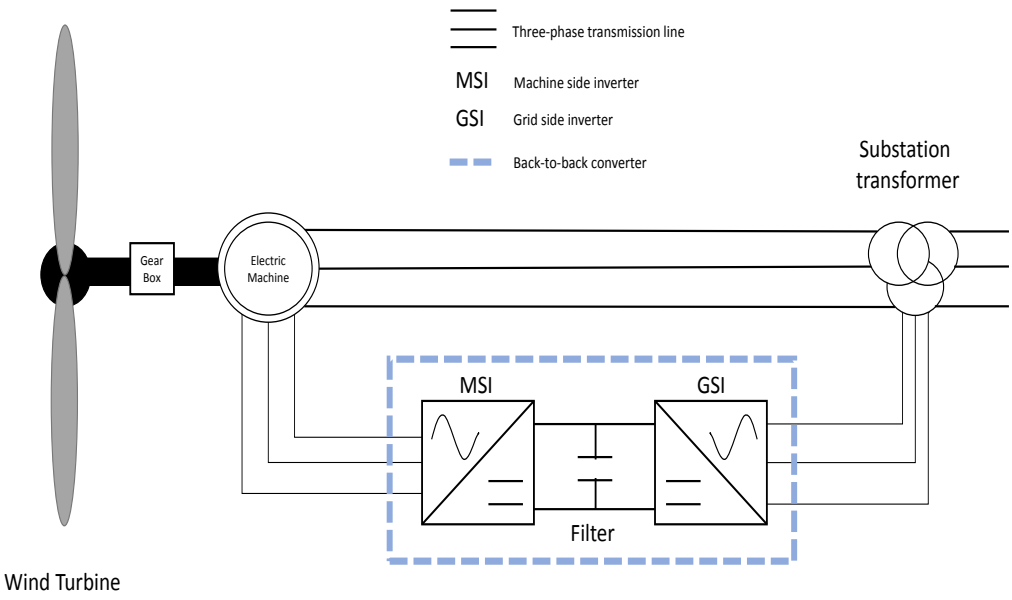

Fig. 3.8. Wind Turbine Model with Doubly-Fed Induction Generator (DFIG)

Incorporating both generation capacity and power control of the converter at the grid side expands the limits associated with the performance capability of this machine. From here, the study develops upon the steady-state behaviour of this machine as well as its PQ performance curve.

In the case of DFIG machines, voltages on both stator and rotor can be expressed as (3.8) and (3.9):

$$(R_s + j\omega_1\sigma_s L_0)I_s + j\omega_1 L_0(I_s + I_r) = U_s \tag{3.8}$$

$$\left(\frac{R_r}{s} + j\omega_1\sigma_r L_0\right)I_r + j\omega_1 L_0(I_s + I_r) = \frac{U_r}{s} \tag{3.9}$$

The equivalent circuit of the machine is shown in Figure 3.9.

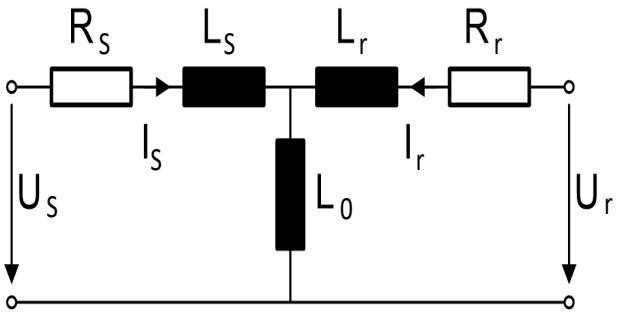

Fig. 3.9. Equivalent circuit of the DFIG Wind Turbine

The magnetization current of the machine can be determined from the both stator and rotor currents, as seen in (3.10):

$$I_{ms} = (1 + \sigma_s)I_s + I_r \tag{3.10}$$

The voltage in the stator can be obtained in function of the magnetization current of the machine I_{ms}, which is expressed in d-q axes, and refers to the stator flux, according to Figure 3.10 and (3.11).

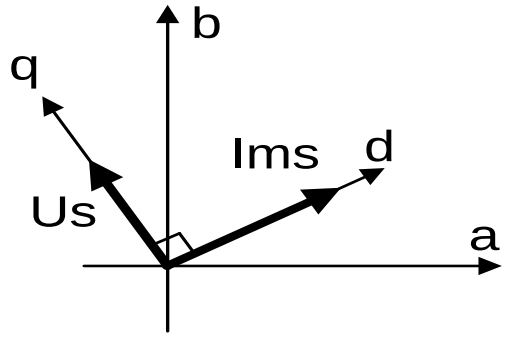

Fig. 3.10. Stator Magnetization Current referred to d-q axes

$$U_s = j\omega_1 L_0 I_{ms} \tag{3.11}$$

The active power delivered by the machine to the grid corresponds to the power contribution given from the stator, and the power delivered from the rotor, both by means of (3.12) - (3.15):

- Active power delivered by the stator

$$P_s = -I_{ms}\omega_1 L_0 I_{sq} \tag{3.12}$$

- Active power delivered by the rotor

$$P_r = sI_{ms}\omega_1 L_0 I_{sq} = -sP_s \tag{3.13}$$

- Total active power delivered by the machine, expressed in d-q coordinates

$$P = P_r + P_s = V_s I_{sq}(s - 1) \tag{3.14}$$

- Total reactive power delivered to the grid by the machine, which corresponds to the power delivered by its stator

$$Q_s = -\Im\{V_s I_s^*\} = -V_s I_{sd} \tag{3.15}$$

It is necessary to point out that the reactive power delivered by the grid converter is normally null, but this converter can be over-dimensioned (S_c) so that can be capable of giving reactive power to the grid, and it can do this apart from the active power delivered to the grid by the rotor P_r, in (3.16).

$$Q_c = \pm\sqrt{S_c^2 - P_r^2} = \pm\sqrt{(V_c I_c)^2 - P_r^2} \tag{3.16}$$

V_c and I_c refer to the maximum grid converter's voltage and current, respectively.

Under these conditions, the reactive power delivered to the grid by the DFIG machine is expressed as (3.17):

$$Q = Q_s + Q_{c,grid} \tag{3.17}$$

The PQ diagram corresponding to the DFIG machine are defined by the following limits:

- Maximum admissible current in the rotor, (3.18)

$$\left[\frac{P}{S_0^{Ir}(S-1)}\right]^2 + \left[\frac{Q_S - Q_0^{Ir}}{S_0^{Ir}}\right]^2 = 1 \tag{3.18}$$

  Where S_0^{Ir} and Q_0^{Ir} are given by (3.19) and (3.20).

$$S_0^{Ir} = \frac{U_S L_0}{L_S} Ir, max \tag{3.19}$$

$$Q_0^{Ir} = \frac{U_S^2}{\omega_1 L_S} \tag{3.20}$$

  Where P and Q_S are the active power delivered by the wind turbine and the reactive power delivered by the stator, respectively. In equations (3.19) and (3.20), U_s refers to the stator voltage, L_s is stator inductance, and L_0 corresponds to the machine mutual inductance, Ir, max is the maximum current admissible in the rotor, ω_1 is the machine synchronous speed and S is the slip velocity.

- Maximum admissible current in the rotor, (3.21)

$$\left[\frac{P}{S_0^{Ur}(S-1)}\right]^2 + \left[\frac{Q_S - Q_0^{Ur}}{S_0^{Ur}}\right]^2 = 1 \tag{3.21}$$

  Where S_0^{Ur} and Q_0^{Ur} are given by (3.22) and (3.23).

$$S_0^{Ur} = \frac{U_S L_0}{S_\alpha} U_{r,max} \tag{3.22}$$

$$Q_0^{Ur} = \frac{1+\sigma_R}{\alpha} U_S \tag{3.23}$$

  Where U_R and $U_{r,max}$ are the current and maximum current in the rotor, respectively, and σ_R is the rotor leakage factor.

- Maximum admissible current in the stator, (3.24)

$$\left[\frac{P}{S_0^{Is}(S-1)}\right]^2 + \left[\frac{Q_S}{S_0^{Is}}\right]^2 = 1 \tag{3.24}$$

Where S_0^{Is} is given by (3.25).

$$S_0^{Is} = U_S I_{S,max} \tag{3.25}$$

Where U_S and $I_{S,max}$ are the voltage and maximum current in the stator, respectively.

From the working limits fixed by voltages and currents in both the rotor and stator, PQ curves can be obtained; these curves make it possible to determine the performance point of the DFIG machine, as depicted in Figure 3.11.

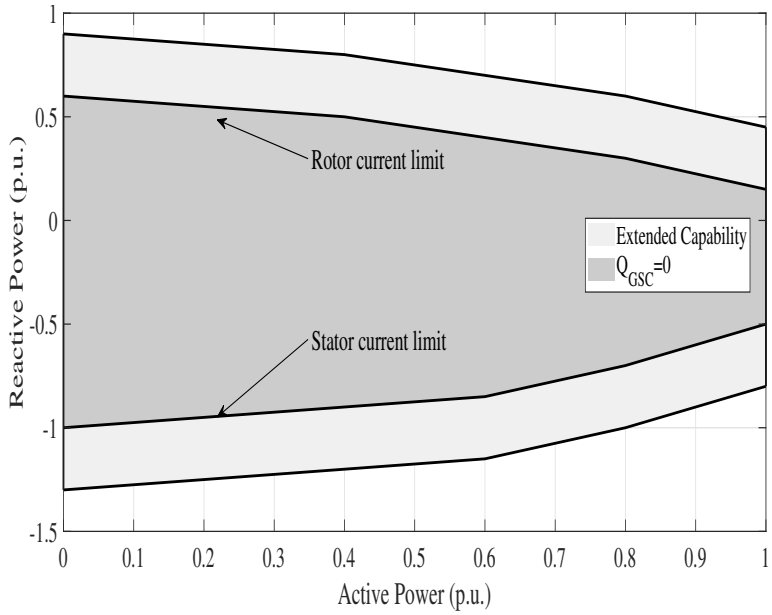

Fig. 3.11. P/Q curve of a DFIG machine plus the GSC

3.5.2. Photovoltaics units

In general, PV units are designed to work at a unitary power factor when they are joined with their grid-side connected inverter [66]–[68]. Under this assumption and the fact that the inverter size is rated to the nominal power of the PV installation, it is not possible to deliver reactive power to the grid integrating at the same time the maximum available active power to the grid. To solve this problem, two main options are considered. The first one is to reduce the active power delivered by the installation in order to inject reactive power. However, this option supposes a reduction in the economical benefits that an owner can obtain. The second solution involves over-dimensioning the grid-side connected inverter so that, at rated power, the PV converter still has enough capacity to inject reactive power to the system. This second option has a cost associated with the inverter's over-sizing.

To alleviate over-voltages problems on grids with an elevated R/X ratio, it is necessary to limit the active power delivered by the units, as seen in Section 3.2. In the case of the PV units, there are different methods that aim to control the output power in function of the voltage at the PCC. One of the most extended methods is the one shown in Figure 3.12, in which there are two operational voltages delimiting the performance of the installation. While the voltage at PCC is lower than the minimum value (Vmin), the PV installation will provide the maximum available power depending on the current irradiance. When Vmin is reached, the PV installation begins to reduce its own production; this leads to a negative slope trajectory that will end up being completely cut off once the maximum magnitude (Vmax) is reached. Thus, in the range between Vmin and Vmax, a curtailment of the PV generation will be produced, which entails a reduction of the economical benefits of the installation's owner in favour of maintaining the PCC's voltage within the established limits.

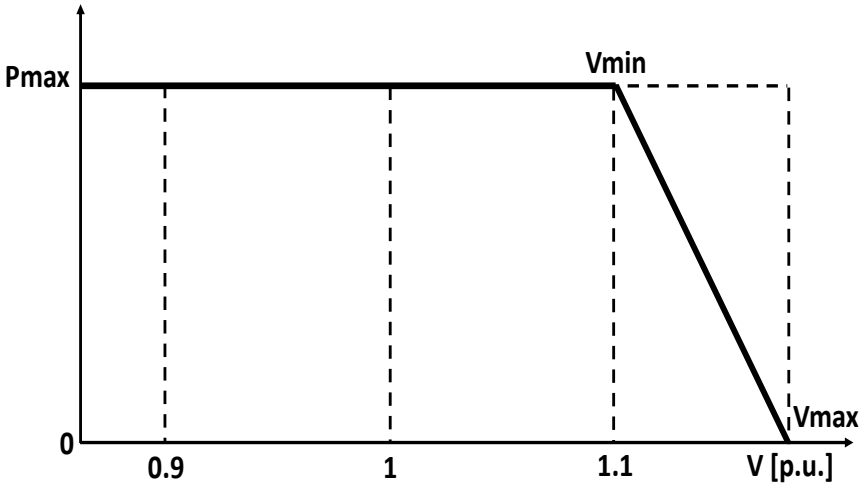

Fig. 3.12. Local control of the PV unit's active power

The reactive power control to be applied in the PV power inverter can be carried out using four strategies, namely fixed Q, fixed cosφ, cosφ, and the Q strategies [69]:

- **fixed Q**: in this strategy the reactive power exchange between the inverter and the grid at the PCC is constant, and it is independent of the value that is taken by other variables in the system. This control method requires a deep study of the grid in order to determine the required reactive power value to be maintained for every situation.

- **fixed cosφ**: in this strategy the PV installation's power factor is maintained at a constant value so that the reactive power injected to the system will depend on the active power that it is produced by the installation. Both fixed Q and fixed cosφ

control strategies will have the problem of injecting reactive power to the grid in occasions where it was not needed causing voltage problems in the grid.

- **cosφ (P)**: in this control strategy the power factor of the installation is limited in function of the injected active power.
- **Q (V)**: in this strategy, also known as Volt-Var, the reactive power exchange between the PV inverter and the grid will be determined by the voltage at the PCC.

Figure 3.13 shows a PQ diagram of the four control strategies applied to the PV inverter [69].

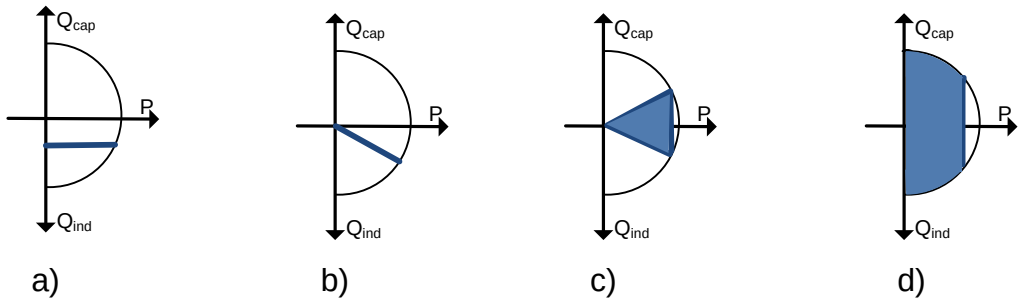

Fig. 3.13. PV inverter's control strategies [69]

Control strategies known as cosφ (P) and Q (V), are local control strategies applied in PV inverters. Nevertheless, if the grid connected to the PV emplacement has communication with a central control unit, it is possible to establish operative set-points for the PV unit's inverter.

In the case of PV installations, the capacity curves of the PV can be obtained from the voltage, current and power limits of each one of the installation's components. Some studies have investigated this topic [70]–[72], and their conclusions are shown in (3.26) and (3.27):

- The inverter's current limit refers to the maximum current that can flow through the inverter, and it limits the power that can be delivered to the grid. Eq. (3.26) shows the equation to calculate the current injected by the PV installation to the grid, which correspond to a circle centered at (0,0) with a ratio equivalent to $U_{g_{PV}} * I_{PV}$.

$$I_{PV} = \frac{\sqrt{P_{PV}^2 + Q_{PV}^2}}{U_{g_{PV}}} \tag{3.26}$$

  Where I_{PV} is the single-phase that can be delivered by the inverter to the grid, $U_{g_{PV}}$ is the single-phase voltage in the network connection point of the installation, P_{PV} and Q_{PV} represent the active and reactive power injected to the grid, which have values that will be limited by the maximum current that is injected by the inverter.

- The inverter's voltage limit refers to the maximum voltage at the point of connection; this is presented as a new constraint that is associated with the power that can be transmitted to the grid. Eq. (3.27) shows the relationship between both active and reactive power, as well as the voltage at the network connection point, representing an ellipse.

$$U_{PV} = \sqrt{P_{PV}^2 + \left(Q_{PV} + \frac{U_{g_{PV}}^2}{X_{PV}}\right)^2} - \frac{U_{g_{PV}}}{X_{PV}} \tag{3.27}$$

  Where U_{PV} is the voltage of the PV installation, which depends on the voltage registered at the DC-link prior to it passing through the DC/AC power inverter. X_{PV} is the reactance seen from the power inverter terminals.

Figure 3.14 shows the capability curve of the PV installation, where the voltage and current limits in relation to the power inverter connected to power grid are depicted.

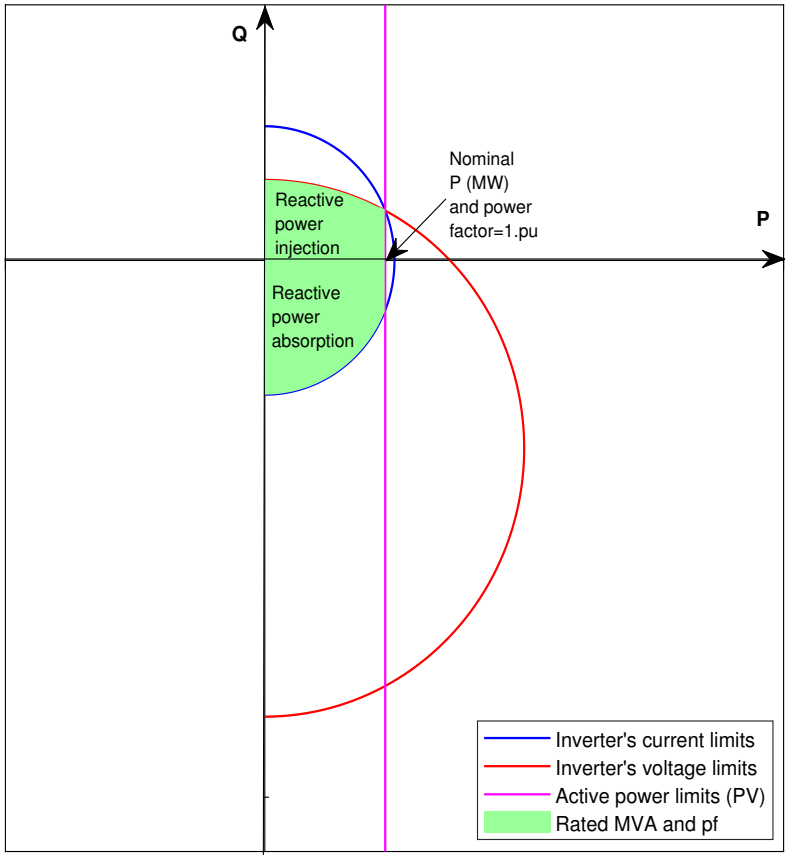

Fig. 3.14. P/Q curve of photovoltaic generation with power inverter

3.6. Load and production curtailment

As demonstrated in Section 3.2, the voltage control on LV grids where the effect of the line resistance over the line reactance is higher, it can be more adequate to control the

active power than the reactive power.

The DSM of the LV systems is presented as a promising alternative to the voltage control in systems that have a strong presence of DG units. The possibility of connecting or disconnecting loads makes it possible to counteract the sudden variations suffered by the production coming from the DG units in the system. In this manner, the effect of the generation variations on the nodes voltage is minimized.

To carry out this demand response, it is necessary to have a wide and complex communications network that allows controlling the flexible loads or sending the price signals to the costumer. Nowadays, this technological deployment can be realized in the Smart Grids, where the demand response programs emerge as an efficient alternative for voltage controlling in low voltage distribution network.

In the group of flexible loads is important to give priority to the thermal loads such as cooling or HVAC systems. Their connection or disconnection has no determinant effect over the consumption habits of the LV grid clients.

As a complement to the capacity of some LV system's load to store energy, the option of directly controlling the loads of some flexible clients is presented. This is done so that, in situations of low or null DG generation and high demand, which causes undervoltages problems a reduction of the energy demanded by the flexible loads can be carried out (i.e., load shedding). This type of demand response direct control offers a number of advantages, such as the avoidance of overloads in lines and in power transformers. Nevertheless, to conduct the voltage control using DSM, it is necessary to develop an economic environment that can provide benefits to the consumers who make their services available.

In some occasions, voltage problems in the Smart Grids networks cannot be solved through the mechanisms previously described. In such situations, it is possible to carry out a reduction of the active power generation in the units present in the system. Because of this, the production curtailment may experience a decrease of the benefits for the owners with DG installations, and thus it is necessary to develop economic tools, the same that are used for the demand control of the consumers. These tools aims to facilitate the participation of the DG in this kind of voltage control.

The reduction of the generation can be implemented in small hydraulic installations, since it is only necessary to modify its input water flow. In the case of HPC installations, where the process is governed by the heat demand, this method turns into something more complicated to achieve, although in some occasions the thermal process is separated from the electric process, and there would be storage units of the heat generated in the thermal process.

In principle, these controls would be autonomously and located on each of the system's production units, although they can also react to the set-points determined by a centralized control strategy.

The incorporation of energy storage devices into the Smart Grids is presented as a feasible alternative to the curtailment of DG units production, as the devices can store excess energy inside these units. This energy excess is generated by the DG units, and the storage of this energy allows it to be delivered to the grid afterwards when there is the need to restore the voltages to the range established by the regulation.

In general, the local control applied to the batteries is done through control loops (Figure 3.15), and it is mainly applied to [73]:

- In grid over-voltages situations, the grid operator can request DG units for a reduction in their production. The surplus energy that has been curtailed at DG units can be stored into batteries until their maximum State of Charge (SoC) is reached.
- In grid under-voltages situations, the system operator can ask the batteries for a partial discharge of their stored energy once an under-voltage is detected. In this way, the system voltage can be restored within the range established by the regulations.

Real ESS have been widely used, and lately these systems has been combined to achieve even greater improved results, as proven by many authors [32], [74]–[79].

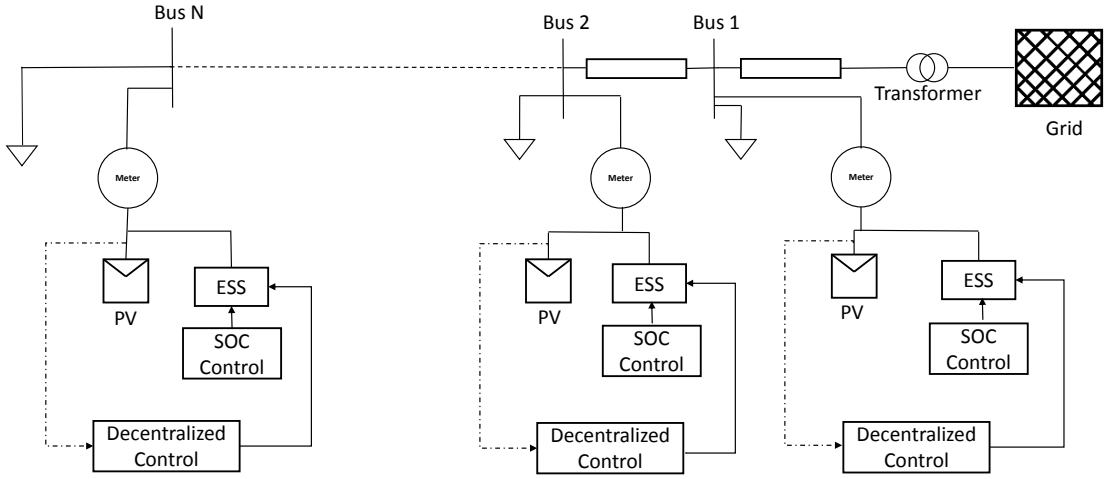

Fig. 3.15. Decentralized Storage Strategy proposed in [80]

3.7. Voltage control schemes for Smart Grid networks

The increment of the number of flexible distributed resources that have been incorporated to transmission and distribution power systems has made control systems to evolve towards brand new architectures. Such architectures are capable of integrating all the devices optimizing the system operation, thus increasing the penetration of renewable energy sources. In this way, distribution electric grids are becoming Active Distribution

Systems (ADS). These networks are grids that have a capacity of managing all the devices present in the system.

The main difference between the existing schemes is the location of the logic or intelligence that is in charge of controlling the whole system. Therefore, in the centralized controls, the intelligence is found across one device only, which would be known as the central controller. In decentralized schemes, the control systems are scattered throughout the controllable units.

The following subsections detail the main control schemes that are gathered from the specialized literature. In most of the cases, these schemes will use the flexible elements that were previously described in Section 3.6.

3.7.1. Centralized control scheme

Centralized voltage control has a control unit known as a DMS which is capable of using the information gathered about the network state to determine the working set-points of the controllable units present in the system. These set points allow to optimize the operation of the systems encompassed into the Smart Grids.

The network monitoring is carried out by means of sensors, namely smart meters or the Remote Terminal Units (RTU) spread over the system. With the available measurements, it would be necessary to use of a state estimator that can determine the state of the power system and also employ the output of such an estimator as the input of the optimization process that is implemented in the control center.

The centralized control schemes need to have a robust communications infrastructure in charge of transmitting the information gathered by the measurement units to the control center. This control mechanism will be very sensitive to both the data transfer speed and the communication failure. Supervisory Control and Data Acquisition (SCADA) systems are currently set up in the distribution grids and are used by the central control to gather information regarding the state of the grid.

Set-point allocation is carried out by the control center using an optimization process that is in charge of determining the working set-points of the controllable elements in the system. There are four kinds of objectives in the optimization process [76]:

- Objectives focused on the nodal voltage (i.e., maintaining the voltage within the established limits, or minimizing the voltage deviation with respect to a given set-point).
- Objectives related to the integration of DER units into the system (e.g., maximizing the power delivered by the DG units or reducing their power curtailment).
- Objectives directed to prolonging the life cycle of the elements present in the system, which can mean minimizing the number of operations carried out by either

OLTCs or CB devices.

- Objectives related to the system's operative efficiency (e.g., such as minimizing the power losses).

The optimization process is completed with a set of constraints, which are mainly associated with the working limitations of the devices present in the system, as well as the load flow equations. The optimal power flow is a tool that is typically used for solving the optimization undertaken by the central control; this central control determines the optimal performance of the controllable units by considering the restrictions imposed by the grid.

Because the centralized control outputs are the controllable units' set-points, the centralized control need to be coordinated with the local control schemes that are assigned to both the generation and flexible loads units present in the system. In this way, it can be possible to execute the control actions of the power of the controllable units established by the control center.

Figure 3.16 shows an example of centralized control scheme. Its implementation is usually applied in small MV systems with several controllable units, a communication architecture and a central control center. This type of system has a central unit that receives the measurements recorded by the measurement units that are present in the system, and the central unit also estimates the state of non-telemetered units. Once the grid optimization algorithm is executed, this system sends the working set-points to the controllable elements.

The main drawbacks of centralized control schemes are the following:

- Centralized control schemes require an extensive and expensive communications architecture that is in charge of transmitting measurement, network breakers state from the RTU to the control center. This will require millions of data to transfer through the communication infrastructure in almost real time operation.
- Failures in the data communication will produce failures in the state estimation and optimization process. Consequently the voltage control will fail.
- For a correct performance of the voltage control it is necessary to implement several additional process, such as a state estimation algorithm, load and production forecasting algorithms and algorithms for estimating the demand of non-telemetered customers.
- The greater the number of units to be controlled in the power system, the greater the computational complexity of the centralized voltage control process. This is all due to the large number of variables that need to be determined, which slows down the optimization process, and this sometimes cannot be resolved by traditional methods.

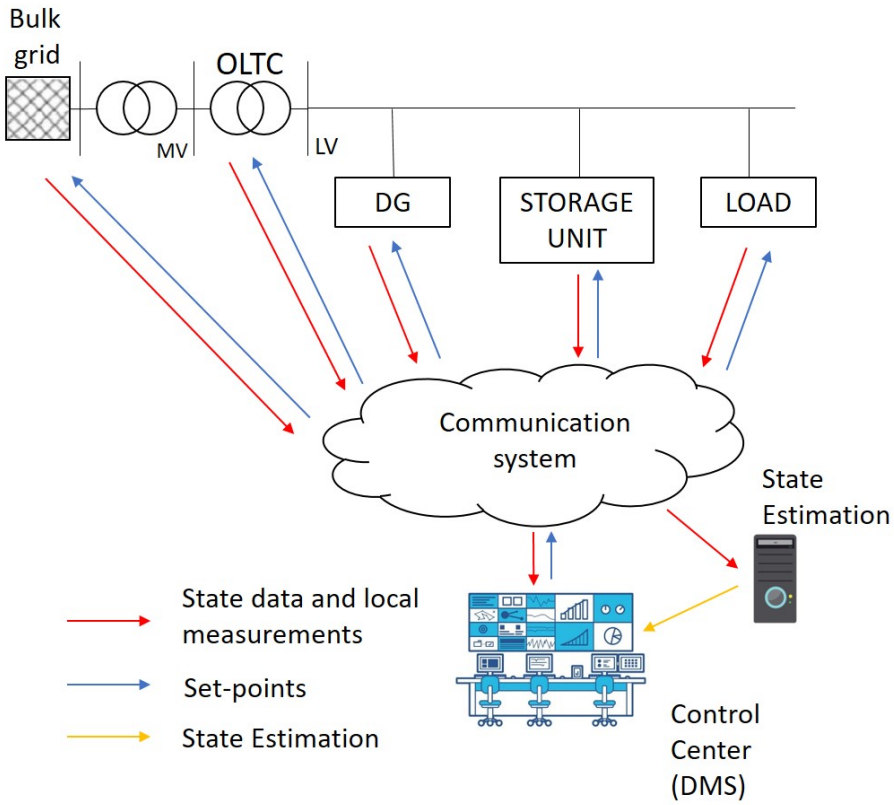

Fig. 3.16. Centralized Voltage Control

- In addition, the centralized control has to assume a huge uncertainty in the system's operation as a result of the uncertainty regarding the variables to be controlled. These variables include intermittent DG production, electric vehicles, storage systems, dynamic loads, network reconfiguration.

Nevertheless, the use of centralized control schemes by DSOs in power systems with a few controllable units may lead to a bigger integration of their DER, and this can lead to a subsequent improvement in the power system's hosting capacity [81].

A number of studies have addressed the use of centralized control strategies in controlling power networks. In [82], a strategy that contemplates charge/discharge operation of ESS is developed, which is done in conjunction with conventional voltage control schemes, such as OLTCs and SVRs. The strategy aim to minimize the number of operations performed by the tap changer, reduce system's losses, and provide the study grid's peak demand under conditions of PV generation's high penetration. In [83], both PV generation and demand forecasts are used for reducing the number of operations of the transformer's tap changer by means of the reactive power optimization delivered by the PV units. However, there is no power curtailment when the maximum reactive power is delivered. The authors in [84] employ power injection capacity attributed to V2G systems to improve the operation of the grid. This strategy minimize the active power curtailment on the DG units as well as the operations on the OLTC tap changer. The voltage control

is undertaken in three steps: first, the demand of the EVs needs to be fulfilled, followed by minimizing the energy delivered by the DG unit, and then lastly controlling the grid voltage through the management of the power delivered by the EVs and DG units. In [85], the voltage control in an unbalanced distribution grid with high penetration of PV units is firstly carried out controlling the power injected to the grid by the ESSs. When these ESSs no longer deliver enough active power to maintain the voltage within the established limits, the reactive power injection capacity of the PV inverters is utilized to improve the voltage profile. In this study, the control of the batteries is performed by the central controller instead of the storage owners. In [86], Ji, et. al. developed a centralized control that sends voltage set-points to each DG local controller according to which the reactive power that must be delivered by the DG units is established.

3.7.2. Decentralized Local Voltage Control

Given the high computational cost in which centralized control schemes frequently incur and the need of having robust communication systems, the adoption of decentralized control systems was developed.

A power grid with a decentralized architecture is characterized by having one controller per each plant's subsystem, and thus the actuators would conduct their activities based on the local measurements. Given the nature of this control scheme, there is no need to have a communication infrastructure among the DERs that are present in the system, since the control is locally and works autonomously at each of the units [87]. In decentralized systems, the voltage control only needs to have the local measurements gathered at the PCC of the DER units where the generation set-point fitting process is located; the voltage control would normally use "droop control" according to which the power delivered by each one of the units is proportional to its nominal power [88]. The utilization of the unit's local control allows the decentralized schemes to offer a local-and-fast response in solving possible voltage problems that can come up in the electric grid [89]. Moreover, autonomous decentralized control systems present themselves as a robust, flexible and easily scalable alternative in the distribution power systems [90].

Optimizing the operation of controllable devices, such as DG units, EVs, BESS and HPs, is carried out by means of droop functions that allow the employment of their flexibility to be maximized [73]. This would utilize the voltage and currents control and measure parameters at the device's PCC.

There are also some disadvantages in decentralized control schemes. The lack of communication among controllable units lead to poor functioning of the system. In addition, the decentralized control architecture does not take into consideration the dynamic behaviour of the loads, and it only presents a partial relationship between both the active and reactive power generated by the DG units [88].

Figure 3.17 shows the scheme of local decentralized control. In this architecture,

each of the controllable units present in the system is provided with a controller; this controller is capable of determining the necessary set-points for maintaining the voltage within the established limits.

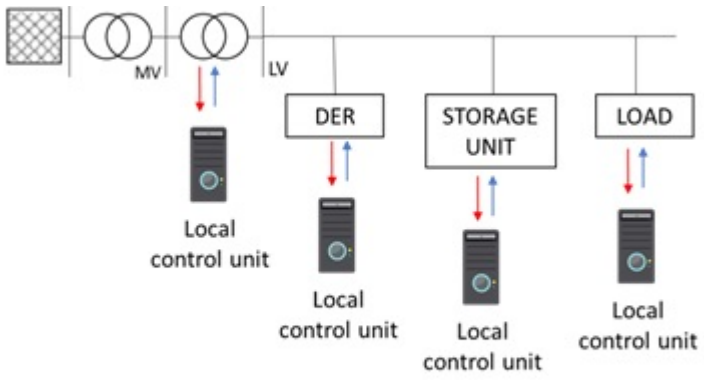

Fig. 3.17. Decentralized Local Voltage Control

From the previously presented arguments, it can be concluded that local decentralized control schemes currently present a low performance in large MV networks where there are hundreds of elements to be controlled. This is due to the increasing number of elements to be controlled in the system. This scheme is, mainly utilized in microgrids, where the number of controllable units is smaller in comparison to those within distribution power networks.

Decentralized control strategies has various advantages. They can provide privacy preservation to customers and avoid communication traffic congestion.

In [91], decentralized control was applied on the DG units in the system. The objective in that paper was not only to control the nodal voltage using the DG units but also to guarantee that the power injected by these do not lead to a violation of the established voltage limits. Ochoa et. al. [92], developed diverse local control strategies of the DG units with the aim of minimizing the impact of reactive power flow from HV to MV networks. It is deduced that the network losses increase in those situations where DG were operating with a constant power factor. The research in [90] proposes a decentralized control in which the active/reactive power delivered by the DG units is used to maintain the voltage within the established limits, this subsequently allows the units to offer complementary services to the distribution grid. Another example of how a decentralized control works is seen in [80], where the control strategy is focused on adding storage systems coupled to distributed generators in one feeder in order to form a bunch of partially closed loops. This scheme represents a wider version of the one proposed in [93], but it is a less complex system in terms of loads than the one presented in [94]. The objective function deals with minimizing the cumulated charging power of the energy storage, this is subjected to a maximum allowed voltage on the feeders, a peak PV power share, and both minimum and maximum ESS charge/discharge power. With this arrangement, storage charging is prioritized during peak hours, so that it would be possible to achieve a peak shaving that

aims to reduce voltage overloads and at the same time obtain active power curtailment and grid enlargements.

3.7.3. Coordinated control scheme

The coordinated control scheme merges the functionalities of both centralized and decentralized schemes. The coordinated control architecture is composed of various levels, and each one of them uses a control scheme in function of the area that must be controlled. Conventional transmission power systems use this control scheme, and three control levels with different scheme and performance times can be differentiated.

- The primary control is the most inferior and the fastest scheme. It is in charge controlling the network's controllable units locally and it would be considered as a local decentralized control. In the coordinated control scheme, the primary control acts on each unit to be controlled based on the set-point received by the control of the intermediate level area (i.e., secondary control), as well as the measures gathered at the PCC of the unit to control.

- The secondary control is the intermediary level control and it is in charge of performing the voltage control at a determined area. This voltage control is carried out based on the measures gathered at the nodes of the area to be controlled, as well as the availability or flexibility of the system's controllable units. The secondary control optimally sets up the set-points of each one of the controllable devices, and it does this based on the state of the area to be controlled and the flexibility of the units present in the system. In this way, the nodal voltages keep within the established limits without any network congestions. These optimal set-points will be sent to the primary controllers in charge of of each controllable units in local control. From the above points, this secondary control can be considered to be a centralized one.

- The tertiary control is placed at the superior level. The objective is to control the power flow among the areas controlled by secondary controllers; it does this by considering voltage and overvoltage constraints of the system and thus minimizing power losses. In the past, conventional power systems were provided with both primary and secondary controllers.

Figure 3.18 shows the general scheme that represents a coordinated control.

Similar to the centralized control, the coordinated control scheme requires, of a wide communications infrastructure. The secondary controls carry out a bidirectional communication with the tertiary and the primary control. Secondary control sends information to tertiary control, namely the information regarding to state of the units that it controls; in return, it receives information on the reference power signal that should be exchange among the different secondary areas. With the primary control, the secondary control

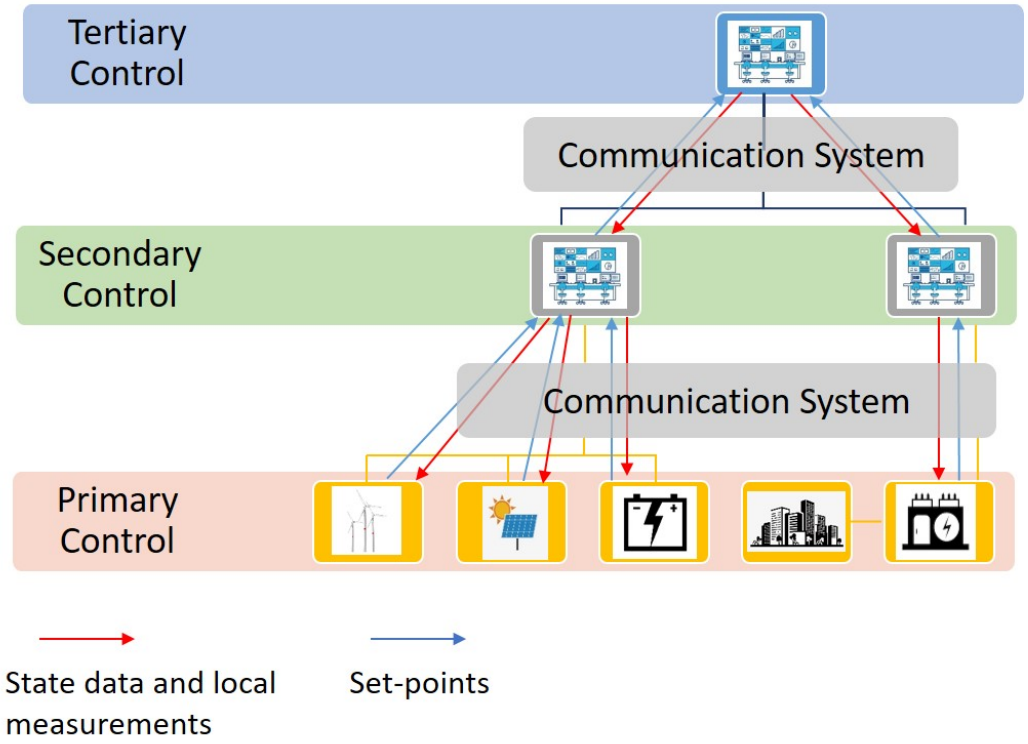

Fig. 3.18. Coordinated Voltage Control

exchanges information about the set-points of the controllable units in this area, and it receives data information about the measurements gathered by smart meters, RTUs, DER state and other monitoring sensor located at the controlled area. For its part, the primary control takes care of either managing the set-point tracking established by the secondary control or of modifying the set-points of the control unit if it is required by the secondary control.

In [95], the authors presented a coordinated voltage control scheme applied to a system with high penetration of PV and ESS units. When the voltage is above the established limits, batteries in the system are charged to avoid to do a curtailment of the active power that is delivered by the PV units. The energy stored by the batteries will be later discharge to the grid when the voltage in the system is below the established limits. The study in [96] presented a coordinated control scheme in grids with DG units based on model predictive control (MPC). The voltage control was carried out by means of DGs units, ESS, and OLTCs present in the system. To improve the technical-economical operation of the system, the coordinated control is performed depending on the voltage at each node of the grid. While the system is working within the established voltage limits, DGs units are controlled by a model predictive control to inject the maximum available power to the grid. Conversely, when the voltage is out of limits, a corrective control that establishes the optimal reactive power generation set-points of the DG units goes into operation; the aim of this control is to restore the system's voltage to the limits imposed by the regulations. Moreover, the corrective control performs a power curtailment on the DG units if it is needed to restore the system's voltage. Wang et. al [97] used a distributed ESS system to

improve the voltage profile of the LV systems with a high penetration of PV units. As in [96], batteries are charged with the excess of energy delivered by PV units at hours when the production is greater and overloads are manifested, while the discharge cycle will be undertaken at those hours in which under-voltages are present in the grid. The ESSs are controlled locally, based in the set-points established by a distributed control.

3.7.4. Distributed Voltage Control

A problem that has been highlight is the poor functioning of decentralized local control, and this problem is derived from the lack of communication, namely from coordination among devices. To address this issue, it is possible to use an evolution of these devices that incorporates a communications network known as peer-to-peer or distributed. Here, the controllers associated with each one of the system's local units communicate, among themselves, with neighbouring devices. This new control scheme makes it possible to improve the operation of Smart Grids by means of determining the set-points of each local controller, and this would be based on the state of the adjacent units. In spite of needing a vast communications grid, the number of parameters to transfer in the communication network does not increase [73]. The main advantage of the distributed control schemes is that due to the communication among neighbouring devices, it is possible to undertake an optimization of the system's operation in small areas of the system. In this manner, distributed control schemes present themselves as a solution that involves the compromise between the central controllers and local controllers. The central controller requires large communications networks and large traffic information for the optimal operation of power systems. Decentralized controllers are not able to perform a voltage control in a whole area because they only control the voltage at their connection point.

Distributed control schemes are also known as Multi-Agent Systems (MAS). These systems are considered as agents for each one of the local controllers of the devices installed in the system, and these devices are also capable of acting autonomously to improve the state of the nearby environment.

Figure 3.19 depicts the operative scheme of a distributed control, in which the entities controlling DG units, ESSs, loads, and OLTCs are each considered to be a system agent.

There are many advantages in using distributed control systems, as noted in [98], [99]. First, this system accelerate power equipment installation and start-up processes; it can improve the reproducibility of the processes as well as the long-term power stability and consistency. Moreover, such a system is scalable and modular, and it can cope with LV networks variability in a way that centralized and decentralized systems may not be able to. Furthermore, the system allows optimization to be combined with learning techniques. IT can also achieve a better performance and controller complexity reduction, unlike centralized and decentralized control systems. Lastly, it can be considered as a special case of distributed systems.

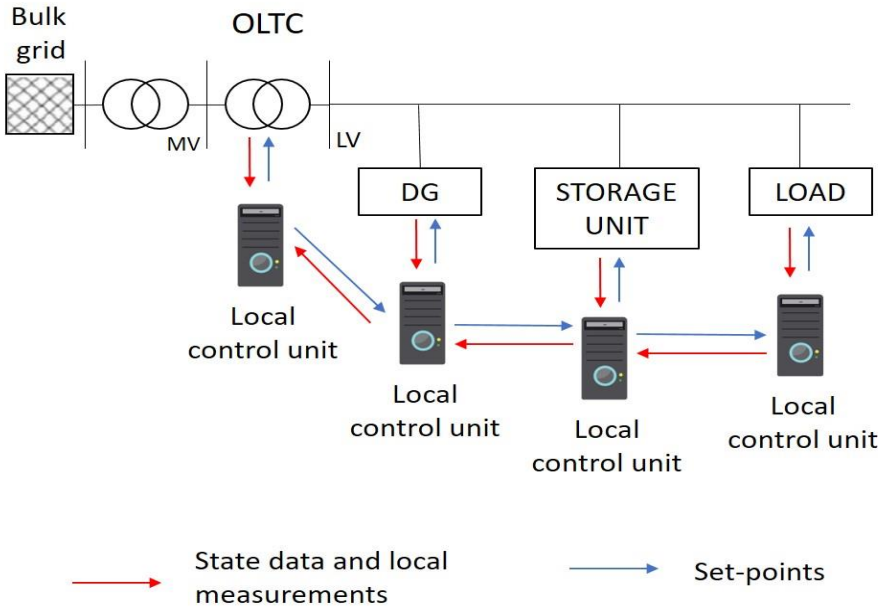

Fig. 3.19. Distributed Voltage Control

There are also disadvantages, and the main ones include cyber-security constraints, customer-privacy possible violation, and limited decomposition of more complicated problems into easier-to-drive entities.

3.7.5. Hierarchical voltage control

Before incorporating DG to the electrical system, this kind of management strategy was only applied downstream. Currently, a hierarchical control system is considered to be the most similar to a genealogical tree where all of the family members are geographically split, since it is modular and scalable (see Figure 3.20). Nevertheless, total scalability can be guaranteed if control processes are different at the lowest levels only. Boundaries are split into smaller parts that match the size and features of their subsystems, and limits regarding to the number of control processes per level are imposed, otherwise scalability is only partial, although it is still effective.

In these kind of systems, bi-directional power and communication flows are controlled for each level of the tree. These systems can be considered as a special case of a multi-level scheme [100], based on its properties, modern hierarchical control systems can be coordinated or they can contain all of the aforementioned control schemes within. Diverse multi-level hierarchical control approaches, can be found in [100]–[103].

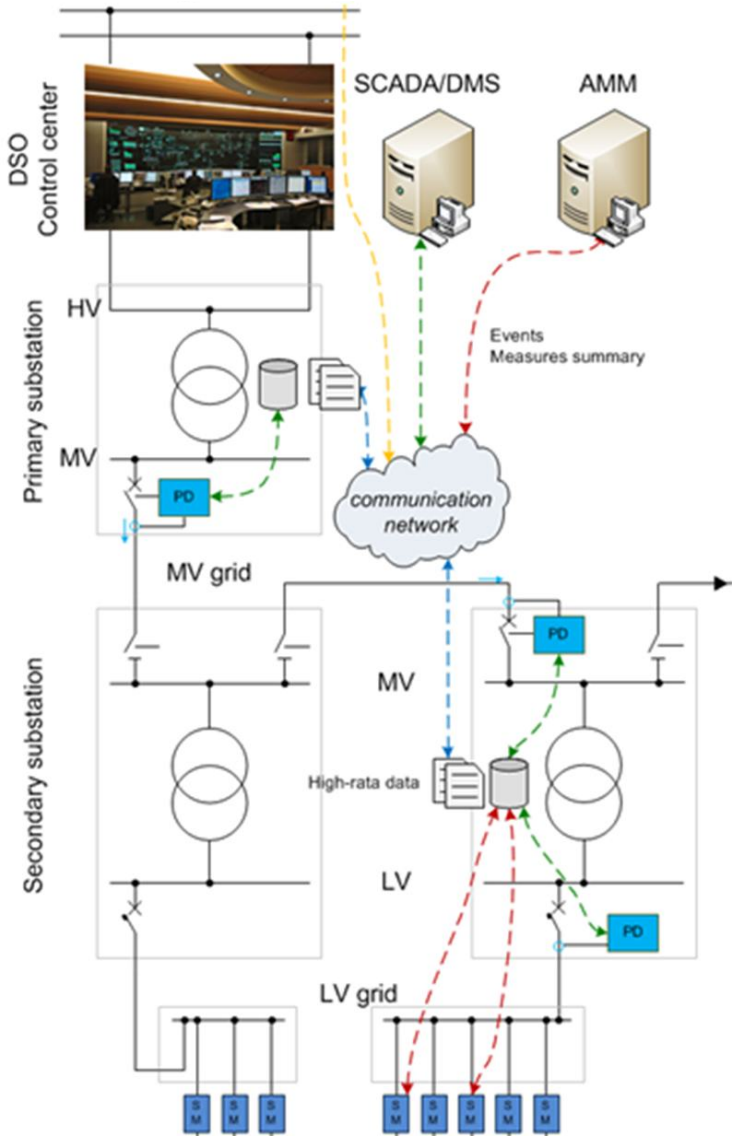

Fig. 3.20. Example of Hierarchical control [103]

3.8. Summary

This chapter provided a review of the state of both the elements and schemes that are used for Smart Grids voltage control.

Firstly, the study determined which variables influence the system the most when it comes to performing voltage control on grids with a high R/X ratio, such as with LV networks. Based on the results obtained, it is concluded that in LV distribution networks which are mainly resistive the impact of active power regulation in nodal voltages is greater than the effect of reactive power regulation.

Smart Grids voltage control can be carried out using conventional voltage control elements, such as OLTCs, CBs, SVCs, or STATCOMs. Nevertheless, new elements in the Smart Grids (i.e., DERs and controllable loads) can be used for voltage control purposes. Some of the possibilities to control a smart grid are the following: the active power control

of flexible loads, the regulation of the PQ capability of grid-connected DG units, and the possibility of ESSs to store surplus energy of DG units when production is high and to discharge this energy to the grids in situations of under-voltages in the networks.

With respect to the control schemes, this chapter conducted an analysis of the most representative schemes, namely the centralized, local decentralized, distributed and hierarchical schemes. In dealing with the high number of elements needing to be controlled at Smart Grids, both the coordinated and hierarchical control strategies are presented as viable alternatives to control nodal voltages. The coordinated control reports the same advantages offered by the centralized control when it comes to managing several components simultaneously. At the same time, it also shares its benefits with local decentralized control; with these benefits, final control of the system's manageable is carried out locally, based on the set-points established by the coordinated control.

4. WAVE ENERGY INTREGRATION IN DISTRIBUTION NETWORKS

4.1. Chapter introduction

This chapter presents a hybrid model of wave power installation combined with a flywheel. The main objective of the model is to improve the quality of the energy delivered by the wave farm that is being grid-integrated afterwards. Firstly, the chapter details a state-of-the-art description of both technologies as well as the way they are modelled. The second part of this chapter is dedicated to the development of the hybrid model that is aimed to improve the wave installation's power output. The validation of the model will be carried out with real raw data obtained from a wave energy emplacement located at Lysekil, Sweden (Lysekil Research Site, LRS). Finally, the chapter shows how the proposed joint model, that is, WEC-Flywheel, is capable of tracking the active power set-point that is established by the grid operator.

4.2. Wave Energy Converters

4.2.1. State of the art

Humanity is given a great challenge ahead when it comes to facing and mitigate climate change and global warming, as it continues to contribute to its own progress and development. In the midst, the energy sector constitutes the main pillar in which renewable energies play a key role. Wave energy represents 0.24% of renewable energies [104], with an estimated power of 92 PWh/year [105]. It should be noted that water encompasses 70% of Earth's surface, of which oceans, seas, and bays accumulate about 96.54% of total water worldwide [106]. With these data in mind, wave energy may be seen as a good alternative for the generation of electric power in the future. At the moment, there are 1.7 GW of marine emplacements under construction and 0.5 GW of commercial grid-connected arrays. The lack of large marine plants makes it difficult to predict the future of this technology. Nevertheless, marine energy by 2020 is expected to have a growth with forthcoming global projects accounting for 838 GW and over 16,2 GW of planned capacity at different stages with respect to wave energy and tidal energy, respectively [105].

Among the main characteristics of wave energy, are highlighted the following:

- Wave energy resource is three times the size of the currently available resources, which is almost double of the amount of energy density and it offers higher forecast accuracy when compared to wind and solar renewable sources. Wave energy can be

considered a second type of solar energy, since waves rise as a consequence of the wind, and the wind in turn, it also lifted due to temperature changes. Thus, a solar intensity of $0.1 - 0.3 kW/m^2$ is transformed in a power flow intensity of $2 - 3 kW/m^2$ in the vertical plane in the direction of the wave [107].

- In taking into account the direct relationship between the electricity demand and the temperature as well as the relationship between both solar and wave energy, the electricity production by means of this technology is presented as a good alternative when it comes to tracking the seasonal demand curve of the consumers [108].

- Considering the annual production ratio, marine converters work 90% of the hours of the year, which is significantly greater than the 20-30% of the other renewable generation technologies, such as solar and wind [109].

Nevertheless, the main technical concerns nowadays are the following:

- Grid integration and power quality as well as optimum control strategies are required to improve the grid integration. Both aspects have a strong connection with the marine variability resource, even though wave energy forecast produces more accurate values, and their devices deliver power up to 60% times more than wind and solar ones.

- The proximity of the emplacements to less populated main land which generally have weak grids would need enlargements in the near future. In addition, there is the need to cope with weak grids and their associated issues, such as: voltage regulation, frequency levelling, power factor correction and harmonic mitigation. For this, several alternatives to smooth power output have demonstrated to be effective in hydro power and wind power installations. These techniques could be modified in order to be applied into wave energy installations [30], [110].

Figure 4.1 shows an example 1-minute time interval the power output that corresponds to the WEC installation submerged at the Lysekil Marine Platform in Sweden, which is composed of three clustered linear generators. In the figure, the variability manifested by the electricity coming from the marine installation is shown. As it can be noted, marine production presents peak powers of 16.71 kW, which is equivalent to more than 5.8 times the mean power delivered to the grid in the portrayed time interval, which is measured to be 2.88 kW. There is a great irregularity found in the WEC's power production, as a consequence of the wave resource variability, and this irregularity makes the grid integration of this technology difficult to achieve.

Hence, despite of the advantages that wave energy presents and the availability of its resources, it is necessary to overcome a series of challenges in order to improve the current developments on power extraction and grid integration, as well as the costs of the installations [111]:

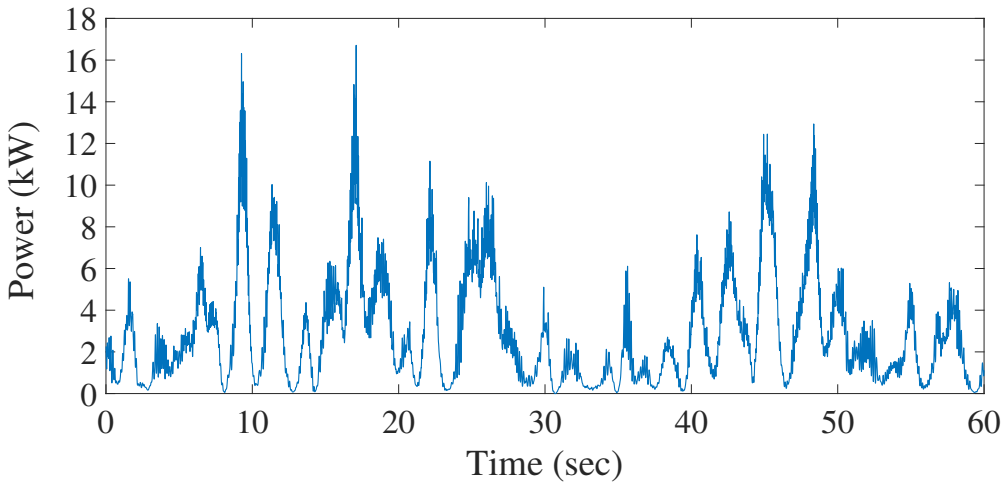

Fig. 4.1. WEC's power output for the Lysekil wave farm

- Marine resource is characterized by the height and frequency of the waves, which experience constant variations, whereby marine installations power output does not comply with quality criteria required in the electric grids. To improve the quality of the delivered energy, it is possible to install storage systems in the marine emplacements or even to group wave the energy converters in a way so that power output's oscillations of some units can be compensated by the power output of other units in the same clusters.

- Waves direction is very changeable, and for this reason it is necessary to carry out exhaustive studies to determine the optimal location of the marine generation's units mooring systems.

- Considering the variations in the wave resource density, generation units must be designed for values with a higher occurrence frequency. Nevertheless, there could be cases in which wave resource's frequency could be 100 times higher the design power of the installation, which entails marine installation's attrition.

- With respect to grid-connection requirements, there are no grid codes regulating the coupling of converters with marine generation emplacements, and therefore the codes that have been used for wind installations are applied instead. However, the variability of the power output that marine installations inject to grid must be considered, as it makes them different from other types of installations. Firstly and given the great oscillation present in the power output of the marine installation, it is necessary to determine whether the restrictions imposed by the grid codes can have considerably different values of mean or peak power. In addition, due to the variability in the electric generation of the marine emplacements, it is not possible to directly apply the requirements of generation slopes that are used in other renewable energies technologies.

- Regarding the dynamic behaviour of the machine and the grid stability, the impact

of the great variability in the power output of a small marine generator can be much higher than the impact of a large wind generator that has an output power with lower percentage of oscillation. Thus, the size of the electric machine cannot be used as a criterion in the development of grid codes.

- To drive the development of the marine energy, and to reduce costs associated with it, the hybrid systems in which the marine energy is installed close to off-shore wind farms are being used, so that it is possible to share the point of grid connection.

Based on the previous arguments, it is necessary for there to be a huge investment in the development of marine energy so that it can become generation systems for the electric grids they are connected to and the costs of these installations can be reduced. If marine energy finally manages to take off as an alternative power generation system, it is estimated 10% of the energy consumed by the European Continent could be supplied solely by marine energy by the year 2050.

4.2.2. Wave resources availability

Figure 4.2 shows the estimated total power produced by wave energy in different continents as well as the vast potential attributed to wave energy worldwide as expressed in kW per length unit, where length is measured on the wave crest or throughout the shoreline direction [112]. The best locations for wave generation are those that present a potential ranged from 20 kW/m to 70 kW/m, these are mainly located at latitudes between 30º and 60º of each hemisphere. Given that waves originate from the wind and that simultaneously wind is produced due to changes of temperatures, it can be said that wave power production will be affected by the thermal changes experienced seasonally throughout the year. Moreover, seasonal changes are lower in the Southern Hemisphere, which means the coasts of South America, Africa, and Oceania which present a greater wave power potential. This low variation in the available resource allows the performance of the generators to be optimized better; this is done by increasing the number of hours in which the marine resource is the singular resources that the installation has been designed for.

Wave resource density can be calculated depending on the wave front's length (P_{w_f}) in (4.1) or from wave crest's measurement ($P_{w_{cm}}$) in (4.2), where ρ corresponds to the water density (1000 kg/m^2), g corresponds to Earth's gravity constant, A to wave amplitude, T to a wave's period, and H is considered to be double the wave's amplitude [113]. Waves power flow represents the mean power passing through an area of 1m wide and infinite depth in the perpendicular sense.

$$P_{w_f} = \frac{1}{8\pi}\rho g^2 A^2 T \tag{4.1}$$

$$P_{w_{cm}} = \frac{1}{32\pi}\rho g^2 H^2 T \tag{4.2}$$

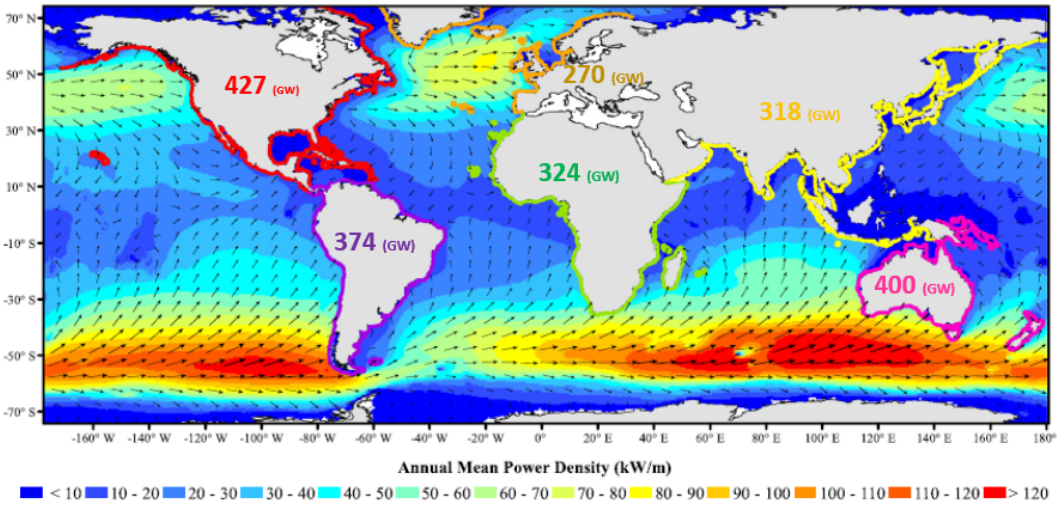

Fig. 4.2. Wave resource - Mean annual density [112]

4.2.3. Wave power technology

The first patent related to wave energy conversion into its electric form dates backs to 1799 and this was developed by Pierre-Simon Girard. However, it is not until the 1940s when Yoshio Masuda undertook the first studies on wave energy production, which later propelled its development as a competitive technology. Despite the fact that in 2009, there were roughly a thousand patents related to energy extraction from wave resource [113], wave energy is still at its initial development stage. To date, several R&D programs [114]–[118] and research projects [119]–[121] have been carried out, and marine technologies have been investigated [105], [116], [122], [123]. Early-stage design requirements demand the undertaking of multiple studies in regular wave conditions [124]–[128]. Once optimal solutions in these conditions are achieved, real waves are used as input data to prove the prototypes' efficiency once they are already built [126], [129]–[131].

Wave resource transformation into electrical energy is conducted by means of three main processes, namely resource capture (i.e., front-end interface), resource transformation or power take-off (PTO) conversion, and electricity generation, as depicted in Figure 4.3.

As with other renewable technologies, there are many wave energy converters (WECs). WEC systems can be classified according to the emplacement location, wave resource catchment, and the transformation of the latter into electricity.

4.2.3.1. Classification of WEC systems according to the location

According to the location of the emplacement, the seabed depth establishes three types of installations, as depicted in Figure 4.4. The types are namely installations that are shoreline (or onshore), installations corresponding to those located on the coast line, and installations near the shore and off-shore.

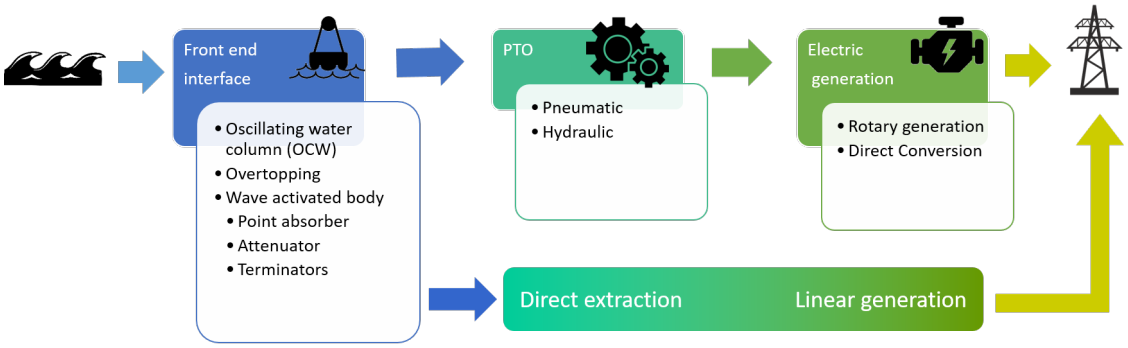

Fig. 4.3. Transformation of wave resources into electrical energy

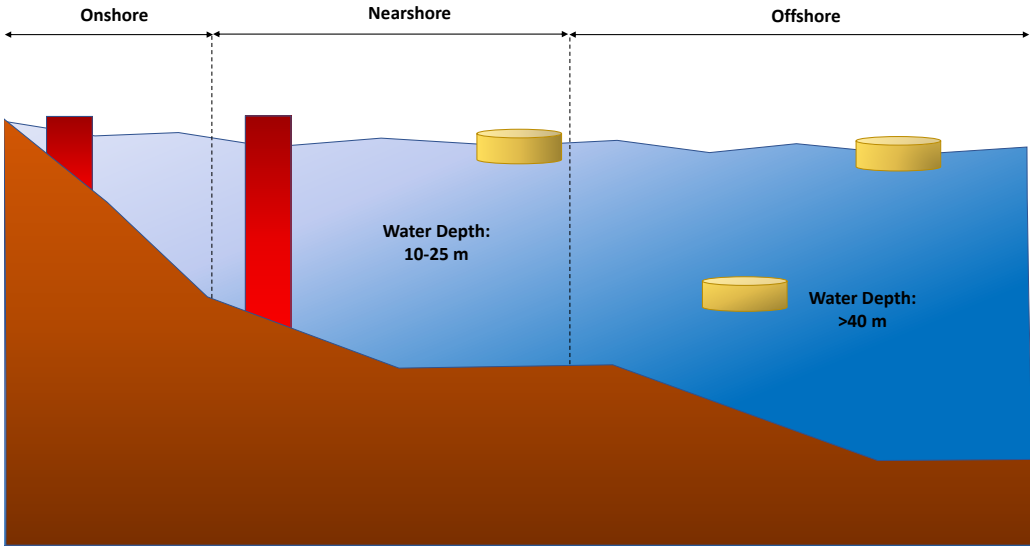

Fig. 4.4. Classification of the WECs by location [113]

4.2.3.2. Classification of the WEC systems according to the capture of the marine resource: front end interface

With respect to wave resource capture, there are numerous developments in this field that can be grouped into three main categories Oscillating Water Column (OWC), overtopping, and Wave Activated Body (WAB)

- OWC is considered as the first device that is utilized in the conversion of the wave resource into electrical energy. They are composed of a partially-submerged chamber that allows a water column to be created and its height goes up or down depending on the movement of the waves. Water column height variation is determinate by the waves and the variation makes the air in the lower part of the chamber flow toward the upper part of the chamber, where a marine turbine (i.e., Wells turbine) coupled to an electricity generator is found. These devices are usually utilized in onshore installations and can be anchored either to the littoral or to the seabed rocks.

Some examples of the OWC include the LIMPET, OE buoy, and Mighty Whale [132]. Figure 4.5 shows an example of this technology.

- Overtopping are devices composed of a semi-submerged structure that can store water when waves pass over them. The pressure exerted by the water column inside the structure activates a wave turbine connected to an electricity generator. The most representative example of this technology is the Wave Dragon as depicted in Figure 4.5.

- Finally WAB devices can be classified into attenuators, point absorbers, and terminators. WAB devices are provided with a buoy that floats on the waves of the marine surface. The perpendicular movement of the buoy with respect to the seabed activates the transformation of the energy in the waves into electrical energy. The main difference between WAB devices and the other devices is in the device size and its disposition with respect to the direction of the waves that have an impact on the device.

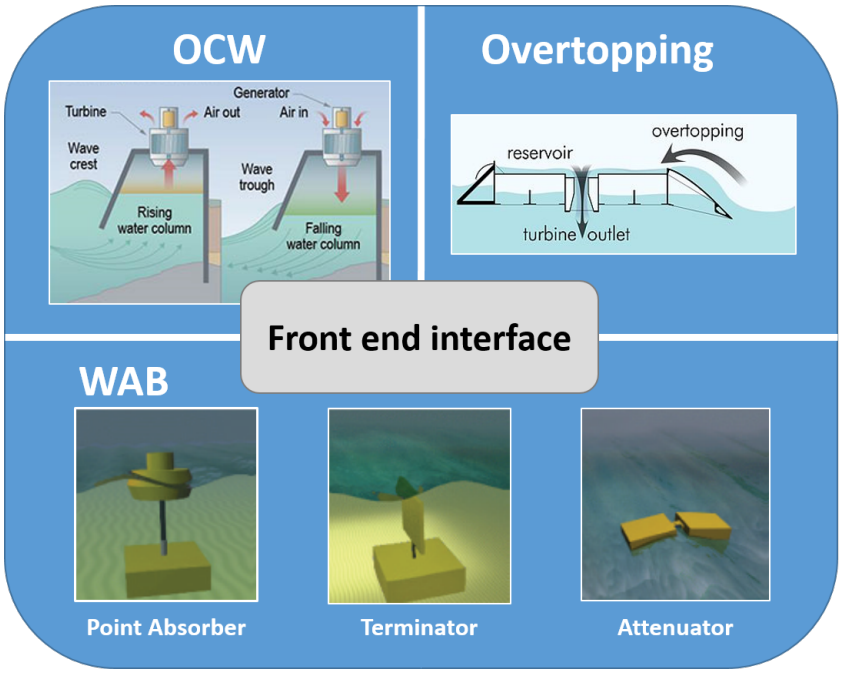

Fig. 4.5. Front-end interface types [107], [133], [134]

When the absorber device is smaller than the wave length, it is known as point absorber. One example of this technology is the device that was developed by Uppsala University [135]. On the other hand, when the predominant direction of the waves is perpendicular to the device, it is known as terminator (e.g., Wave Roller and Oyster [136], [137]). Finally, there are attenuators, which are devices that are situated parallel to the wave propagation direction; the most representative example of this is Misspedd [138]. Figure 4.5 shows an example of these devices.

4.2.3.3. Classification of WEC systems according to the transmission technology

Regarding the conversion between the wave-induced mechanical movement and the generation of electricity, three types of transmission technologies are identified, namely pneumatic technologies, hydraulic technologies, and direct drive systems.

- Pneumatic technologies are employed in installations where the wave motion implies an air mass movement inside of a chamber. The chamber is wide open at its lower part which is submerged into the sea, while its upper part is connected to a turbine that transforms the oscillation of the waves into a mechanical motion for its posterior conversion to electrical energy. This type of installations will therefore utilize OWCs to capture the wave resource. Figure 4.6 shows the working scheme of a WEC device with a pneumatic PTO.

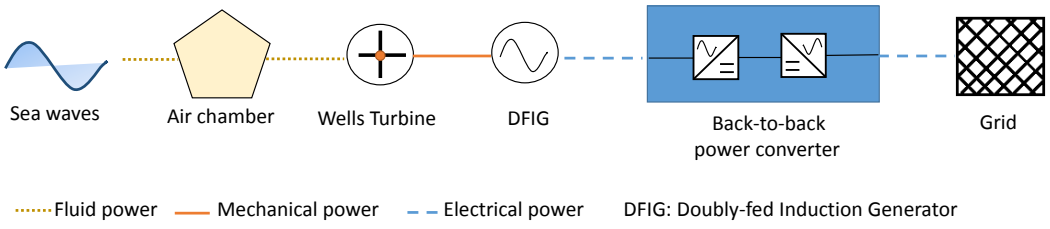

Fig. 4.6. Pneumatic PTO [139]

- For hydraulic technologies, PTO installations are the most extended because they present greater facility with respect to the control and rectification of the installation's power output. There are two types of hydraulic transmission systems, one type utilizes turbines to convert wave motions to mechanical movement, and the other type stores hydraulic energy. In the first system, a hydraulic turbine transforms the wave oscillations into mechanical movement. The connection between the turbine and an electrical generator allows the energy contained in the waves to be converted to its electrical form (see Figure 4.7). The second type of hydraulic transmission is the one used for the catchment systems such as terminators. These systems comprised by several cylinders joint altogether by means of mechanic joins that allow motion in all directions. The relative movement between the cylinders that compose the terminator modifies the pressure exerted on the oil contained inside the hydraulic system's pistons, which stores the wave energy in the form of hydraulic energy. Finally, the stored hydraulic energy is converted to electrical energy through hydraulic generators. Figure 4.8 shows the working scheme of a WEC device with a hydraulic PTO known as the terminator.

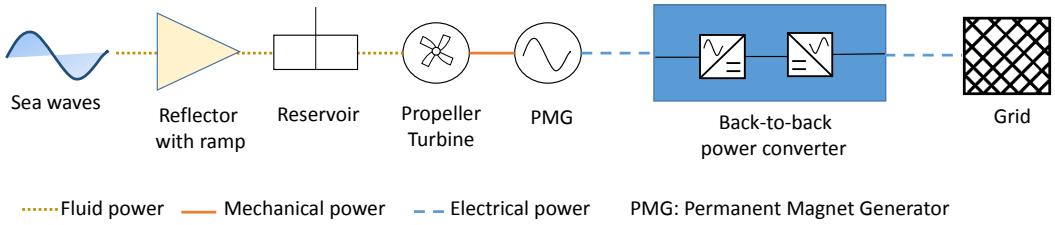

Fig. 4.7. Hydraulic PTO (Wells) [139]

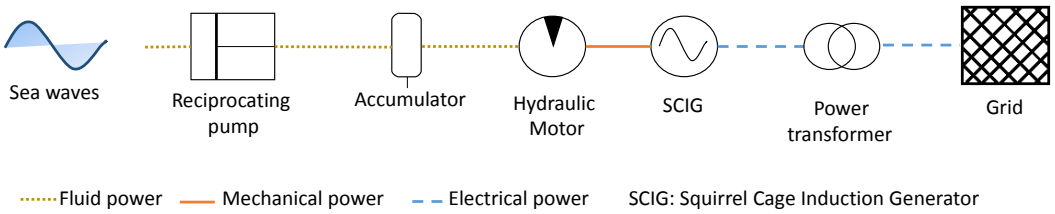

Fig. 4.8. Hydraulic PTO (Terminator) [139]

- There is one final PTO configuration in which the wave energy conversion into its electric form is carried out in the same device. This is known as direct drive systems, which mainly utilize point absorbers as wave energy capturer. These systems do not possess intermediate mechanical devices for electricity generation, as in the case of pneumatic and hydraulic PTOs, which makes them structurally simpler and more efficient since their losses are smaller. It is possible to use rotative generators to transform wave energy into electricity due to the wave's low variation speed and the great force it transmits to the generator, but low speed linear generators are the most adequate for this purpose. Linear generators are directly coupled to the buoy to generate electricity. Direct driven systems mainly use Linear Permanent Magnet Synchronous Generators (LPMSG), which comprise a magnetic translator and a stator. Wave motion is transmitted from the translator to the LPMSG. The magnetic translator slip with respect to the stator creates a magnetic field; the stator voltages are induced from this field and no other mechanical or hydraulic stage is needed throughout the process. Because of the translator motion is taken place at waves speed, it is necessary to incorporate electronic converters to the installation, so that its power output is adequate for the grid requirements. Figure 4.9 shows a scheme of an all-electric PTO system.

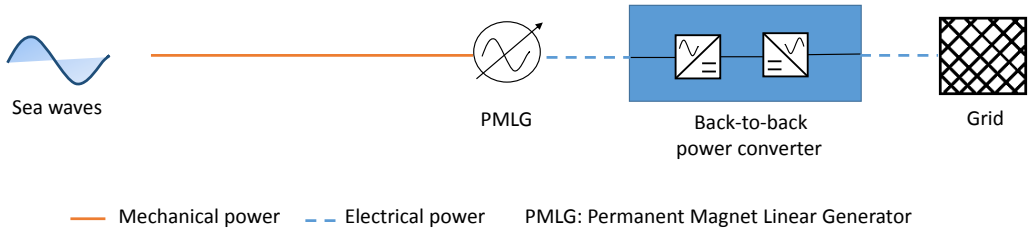

Fig. 4.9. All-electric PTO [139]

4.2.4. Mechanical model of a point-absorber WEC

Some wave installations, such as the Lysekil Test Site in Sweden [140], are made of a point absorber that floats onto the marine surface plus a linear generator anchored onto the sea bottom. This generator converts waves motion into electrical energy; the connection between the point absorber and the linear generator is carried out through a wire that transmits the buoy motion to the generator rotor. The linear generator is composed of a piston that sometimes acts as a rotor; it captures the waves motion due to its connection with the buoy. The piston is hosted inside a cavity that uses springs in its upper part. These springs are used to facilitate the piston motion and to delimit its trail. Finally, the piston chamber is partially surrounded by the linear generator's stator; this means that for very high waves, the piston motion can exceed the linear generator's stator dimensions, which limits the machine power output. Figure 4.10 portrays the WEC installed at Lysekil.

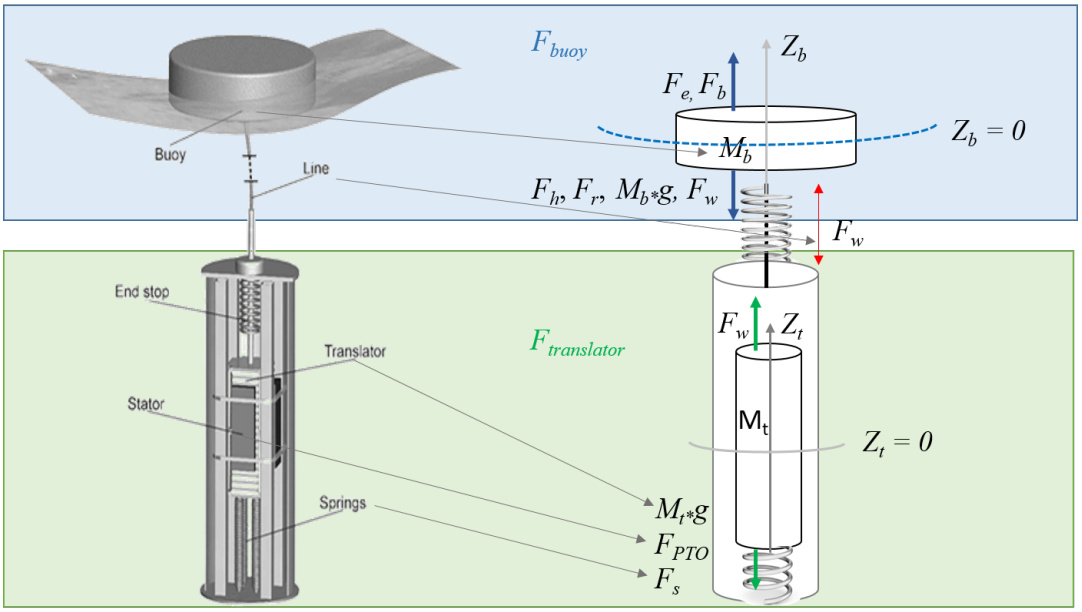

Fig. 4.10. Lysekil WEC unit and forces [135]

The waves motion and the connection to the linear generator produces a set of forces around the buoy [141]. A close look at Figure 4.10 can reveal how the forces are divided between those acting around the buoy and those acting around the translator.

The forces acting around the buoy are the excitation force (F_e), the radiation force (F_r), the hydrostatic recovery force (F_h), the buoyancy force for still water (F_b), the force exerted by the buoy weight, and the one exerted by the cable connecting the buoy to the linear generator mobile part (translator) (F_w). There forces are described in the following:

- The excitation force (F_e) produced by the waves is horizontally incident in the buoy. It can be expressed as the convolution between the function that represents the excitation force impulse (f_e), and the incident wave elevation in the center of the buoy (η), as seen in (4.3).

$$F_e(t) = f_e(t) * \eta(t) \tag{4.3}$$

- The radiation force (F_r) is provoked by the buoy vertical oscillation in the absence of waves. Eq. (4.4) shows the relationship between the radiation force's response impulse which is known as the delay function of K(t) and the buoy's vertical speed, which is given as $\dot{y}(b)$.

$$F_r(t) = -K(t) * \dot{y}_b(t) \tag{4.4}$$

- The hydrostatic recovery force (F_h) represents the response of the buoy to small displacements from its gravity center with respect to the marine surface as a response to the waves motion. In other words, this force accounts for the small variation in the buoy draft as it moves with the waves. Eq. (4.5) shows the relationship between the hydrostatic force, the water density (ρ), the Earth's gravity constant g, and the volume of the additional buoy that is submerged inside the water, ΔV_{sub}. When $\Delta V_{sub} = 0$, the equilibrium point of the buoy is on the marine surface.

$$F_h(t) = \rho g \Delta V_{sub}(t) \tag{4.5}$$

- To find the net force around the point-absorber buoy, a number of considerations are firstly needed. Firstly, there is the direction of predominant waves only. Another consideration is that the buoy has a cylindrical shape. In addition, the set of WECs can be modelled as a one-dimensional mass-spring damping system. Considering all this points in relation to the linear theory of waves, the net force acting around the point-absorber buoy, $F_{buoy}(t)$, is given by (4.6) using the Newton's Second Law, where F_e is the excitation force of the waves that have an impact on the buoy, $F_b = \rho g \Delta V_{sub}(t)$ is the buoyancy force for still water, F_h is the hydrostatic force, F_r is the radiation force, $M_b \cdot g$ is the force exerted by the buoy height, and F_w is the

force exerted by the wire connecting the buoy to the linear generator's mobile part (translator).

$$F_{buoy}(t) = M_b \cdot \ddot{y}(t) = F_e(t) + F_b - F_h(t) - F_r(t) - M_b \cdot g - F_w \tag{4.6}$$

Several forces are acting around the translator, namely F_w (the one exerted by the cable connecting the buoy to the linear generator's mobile part),the electromagnetic force (F_{PTO}) from the rotor due to the waves motion, F_s (the force exerted by the springs of the beginning and end of the accommodation of the translator), and $M_t \cdot g$, which is the force exerted by the translator's weight.

The net force applied to the WEC's translator ($F_{translator}$) is given by (4.7):

$$F_{translator}(t) = m_p \cdot \ddot{x}(t) = F_w - F_{PTO} - F_s - M_t \cdot g \tag{4.7}$$

In (4.4) - (4.10), the motion, speed and acceleration of both buoy mass and piston are given by $y(t)$, $\dot{y}(t)$, $\ddot{y}(t)$, $x(t)$, $\dot{x}(t)$, and $\ddot{x}(t)$, respectively.

$$F_{PTO}(t) = \gamma(\dot{x}) A_{fac}(t) \dot{x}(t) \tag{4.8}$$

where $\gamma(\dot{x})$ is the damping coefficient and A_{fac} is the effective contact area between the stator and rotor or translator, as defined in (4.9):

$$A_{fac}(t) = \begin{cases} 0 & \text{if } f|x(t)| \geq \frac{1}{2}(l_t + l_s) \\ 1 & \text{if } f|x(t)| \leq \frac{1}{2}(l_t + l_s) \\ \frac{1}{L_t}\left(\frac{1}{2}(l_t + l_s) - f|x(t)|\right) & else \end{cases} \tag{4.9}$$

where l_t and l_s correspond to translator and stator longitude, respectively.

Finally, the WEC's instantaneous power output can be calculated from 4.10:

$$P_{output_{WEC}} = F_{PTO}(t) * \dot{x}(t) = \gamma(\dot{x}) A_{fac}(t) \dot{x}(t)^2 \tag{4.10}$$

4.2.5. Electric WEC model with LPMG

The LPMSG modelling can be done by utilizing the Park relation [142], with induced voltages in dq0 axes being expressed in accordance to (4.11) and (4.12), where R_s is the stator resistance, Ψ_d and Ψ_q correspond to the flux created in the stator and rotor, respectively, ω_r is the rotor spin angular speed that can be calculated depending on its slip speed in (4.13), with λ being the stator pole width.

$$u_d = R_s i_d + \frac{d\Psi_d}{dt} - \omega_r \Psi_q \tag{4.11}$$

$$u_q = R_s i_q + \frac{d\Psi_q}{dt} + \omega_r \Psi_d \tag{4.12}$$

$$\omega_r = \frac{2\pi \dot{x}}{\lambda} \tag{4.13}$$

Linkage fluxes in both d and q axis are calculated with 4.14 and 4.15.

$$\Psi_d = L_s i_d + \Psi \tag{4.14}$$

$$\Psi_q = L_s i_q \tag{4.15}$$

Due to the translator spin's speed and frequency varying in function of the sea conditions, it is necessary to utilize electronic converters to control the installation performance.

With the aim of reducing losses in the machine, the i_q current can be cancelled. Thus, active power at the LPMSG input is given by 4.16, and the force that the generator exerts on the buoy can be calculated from 4.17, where τ is the pole pitch of the LPMSG. In doing this, the force that LPMSG applies to the point absorber can be controlled from the current that is registered in the q axis.

$$p_{PTO} = \frac{3}{2} \omega_r \Psi i_q \tag{4.16}$$

$$F_{PTO} = \frac{p_{PTO}}{\dot{x}} = \frac{3\pi}{\lambda} \Psi i_q = \frac{3\pi}{2\tau} \Psi i_q \tag{4.17}$$

The possibility of controlling the force that generators applies to the point absorber allows the complete performance of the device to be optimized, and it also allows maximize the energy extracted from the marine resource. Nevertheless, some problems are found. First, the reactive control presents high ratios between the peak power and the mean power extracted from the installation. There may be cases in which bi-directional flows appear, because of the cycles in waves motion, and there can also be large displacements between the buoy and the PTO system.

To address this problem, there is a second generator control method, known as linear damping. This method employs a simpler LPMSG model, in which its inductive component is cancelled; this component is considered a passive circuit in which only the resistance of the generator is weighted up. With this new passive control, problems derived from reactive control are avoided. Because of the maximum power being extracted when the machine works resonantly with the frequency of waves, nulling the impedance's reactive component entails a reduction of the installation's power output.

4.2.6. Wave power output signal improvement

Converting wave energy into electricity implies three fundamental steps: wave resource absorption, wave power transmission, and electricity generation. However, wave power is a non-controllable and intermittent energy source. Wind and solar are capable of generating constant power, while the marine generation power can be maintained at intervals between 4 and 15 seconds [143]. This huge variability in the power output attributed to wave energy emplacements makes it necessary to carry out a fourth step with respect to the conversion process. The application of signal conditioning devices in this state is particularly crucial in the installations that use direct driven wave energy converters. The reason for this is that there is no mechanical stage between the wave resource absorption and the electricity generation that can absorb the oscillations occasioned by waves motion.

Consequently, grid integration becomes one of the main challenges that wave energy needs to deal with. Without Power Smoothing Systems (PSS), variations in the power output of wave energy emplacements are transferred to the electric grid they are connected to. This causes grid frequency fluctuations, flicker problems, harmonics, and violation of the thermal limits of the elements used in the on-shore connection of these installations [144]. It is also important to emphasize that wave installations are usually connected to weak grids. Weak grids are uncapable of maintaining the power quality established by grid operators when the energy generated by WEC units is delivered to them.

To improve the wave power output, several techniques have been implemented, and these can be classified based on whether they use electric energy storage to accomplish their goal or not [110].

About those techniques that do not employ storage systems coupled to WECs:

- The first approximation consists on clustering a set of WECs to the same point of power delivery in order to generate power that can be injected to the grid with fewer oscillations. This power output aggregation also improves the on-shore connection system [145]. Studies have shown that when a wave farm's power output is aggregated, the same is great for regular wave condition than for irregular waves when proper measurements are taken at a real emplacement [146].

- WEC units are connected to the electric grid by means of electronic devices. The active control of the PTO system with the usage of these devices allows the power output of a grid-connected marine emplacement to be improved [147].

- Additionally, hybrid systems can be utilized to improve the electric power output injected to the grid destined to wave farms [144]. These systems comprise off-shore wind farms together with wave energy emplacements.

- In the cases where the PTO system be can hydraulic, it is possible to reduce the output power oscillations of the installation using water accumulators at sea level

in the hydraulic system [148]. The system utilized by the overtopping catchment systems allows for a small power output regulation. Nevertheless, storing wave energy in its hydraulic form in other types of installations means an increase in installation costs and in maintenance frequency in order to obtain a lower energy efficiency in the facility, and to limit usable seabeds to certain geographic locations [144].

According to the ESSs that are used to mitigate short-term voltage fluctuations, DC capacitors of grid-connected converters are utilized in [149] to smoothen the installation's power output. The greater the installed WEC power is, the greater the size of device is. In [124], supercapacitors are used to improve wave farm power output at laboratory instances; regular waves are considered here only, as their behaviour differs greatly from real waves, (see Figure 4.11). Super-capacitor connection and control is carried out by means of a DC/DC converter that can accommodate the output power of the supercapacitor to the wave farm DC stage.

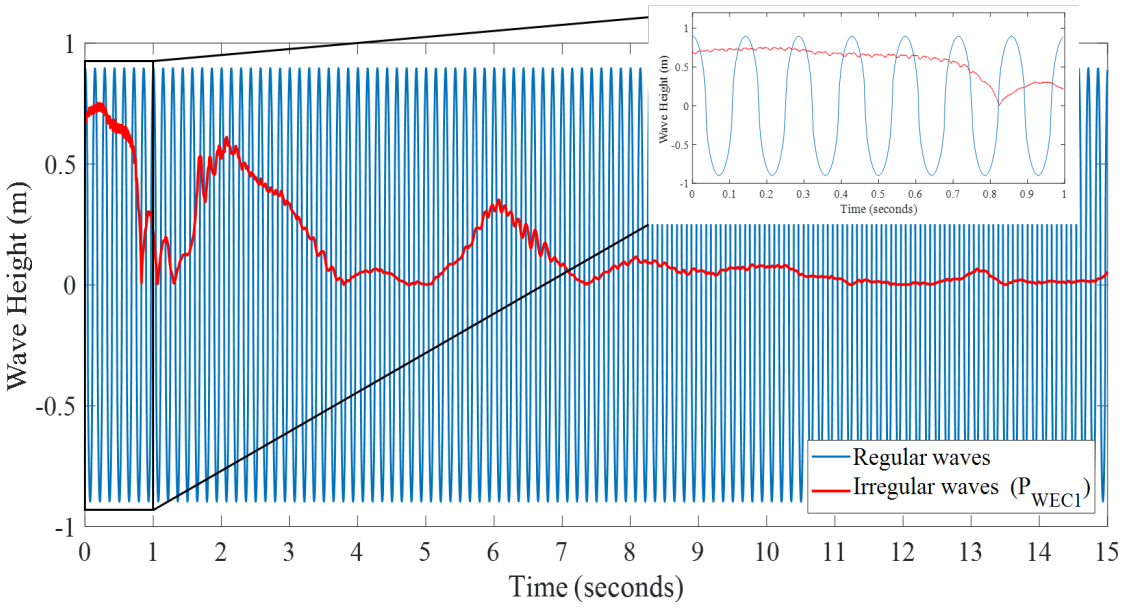

Fig. 4.11. Regular and real wave height comparison

However, a storage system subjected to high charge-discharge cycles and low-power density is also not adequate to mitigate short-term wave fluctuations. Its requirements in the time scale seconds are different from other RES, seeing that the reaction time must be very fast and needs several hundreds of charge-discharge cycles each day [150].

Other technologies have been proposed since 2001 to smoothen the output power from the marine farm, such as placing a flywheel after the generation output. There are advantages of using a high-speed FESS over a low-speed one or even over other storage systems. The main advantages include a linear proportionality to its mass, higher power and energy density, and easiness in coping with load changes. It can also be easily locate onshore and off-shore; it is eco-friendly, and the charge-discharge regime does not affect

its lifetime too much [31]. The authors in Norway [151] and Sweden [152] concluded that for real wave data gathered from farms located in both countries, high-speed flywheel prototypes usage leads to low total losses, but for low-speed ones the global efficiency of a FESS is equal or higher than any other storage system, with the exception of chemical batteries.

Lastly, different approaches regarding filtering the output wave power have been also proposed, whether this is done passively or actively [153]–[157]. In [155], the authors investigated how filtered wave-to-wave frequency and wave height affect the power extraction based on data gathered from three locations. They produced a list of marine resources that listed the devices capable of tuning themselves and their responses in accordance to the wave conditions, according to the EPRI [158]. Their results show that the mean and standard deviation of the correlations between the wave frequency and/or the wave height experience a reduction that is proportional to the filter's frequency. Finally, a power ratio in which a filtered power signal is contrasted with its non-filtered equivalent shows that the larger filter's frequency can lessen this ratio, thereby allowing a longer time interval that is required to retune the device so that it can achieve an optimum power extraction. In [156], the authors produced an algorithm that is enhanced by input wave data, which were gathered from one out the three wave height sensors deployed throughout their model-scaled wave tank. This was done to optimize the sea water pump. A FFT analysis is applied over the irregular wave input signal in order to select the frequency components that gives the maximum volume of water; this leads to the optimum volume of air inside the compression chamber. With this arrangement, pumping process is improved. In the case of wave energy converters, the algorithm must guarantee a balance between input and output power, thereby avoiding the saturation or drain of the ESS [124].

4.3. Flywheel Energy Storage Systems

4.3.1. State of the art

Power systems are currently experiencing a high penetration of small stochastic DG units. Energy storage systems present themselves as a good alternative to address the great variability associated with the production of this units and their impact on the quality of energy delivered to the grid. This is due to the fact that they can either deliver a great amount of energy at short-time periods or provide energy to the power systems at higher time periods [159]. According to [31], there are at least 11 types of energy storage systems with different specifications and market share. Out of all these, batteries are the cheapest and most extended storage system, but flywheels represent a strong competition on the whole.

A FESS consists of a rotational mass that is capable of storing a kinetic energy directly proportional to the square of its central axis' rotational speed. For energy production

purposes, these rotational masses either store or deliver electricity by means of converting the kinetic energy into electrical energy when coupled to a motor or generator.

The main components of a FESS are as follows [79]:

- The primary component is a rotating mass capable of storing a kinetic energy that is strongly dependent on its rotational speed; this is commonly known as flywheel. The greater the size of the flywheel, the greater the stored energy is.
- An electric machine is in charge of transforming the electric signal into flywheel spin velocity; this is done so that it absorbs or delivers energy as it acts either as a generator or motor.
- Power electronics are used for controlling the performance of the electric machine.
- Magnetic bearings are magnets that hold the flywheel's weight.
- An external inductor is used for improving the Total Harmonic Distortion (THD) that is created by the generators of the permanent-magnets in the electric machine.

Several types of electrical machines that accompany the flywheel when the charge/discharge process occur, can be used. These types of machines are as follows: Permanent magnet synchronous machine (PMSM) [160], Brush-less direct current machine (BLDCM) [161], Induction machine (IM) [162], Switched reluctance machine (SRM) [163], Homopolar machine (HM) [164], Synchronous machine(SM) [165] or Bearingless machine (BM) [166]. Rotor bearings are classified as Permanent (Passive) magnetic bearing (PMB), Active magnetic bearing (AMB) and Super conducting magnetic bearing (SMB). Mechanical bearings have fallen practically in disuse since their magnetic counterpart started to be implemented. A universal structure of flywheel and its components can be found in [79], but this design is prone to undergo some changes depending on the desired configuration (see Figure 4.12).

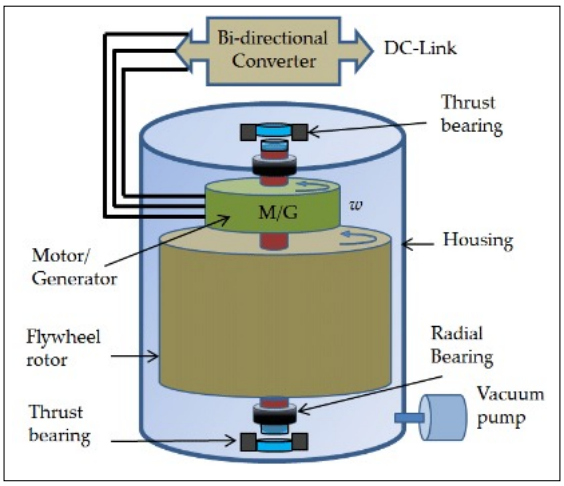

Fig. 4.12. Structure and components of a flywheel [79]

In terms of the electrical interface needed for reaching grid connection, several electric power interfaces have been implemented based on wind energy installations. The back-to-back topology represents a scheme in which there is an AC/DC converter after the grid that is coupled with a flywheel storage system, and there is also placed after an AC/DC converter. This topology is seen in [167].

Flywheels also have several applications aside from merely ensuring power quality and load management, as seen in Figure 4.13 [150], [168]–[170].

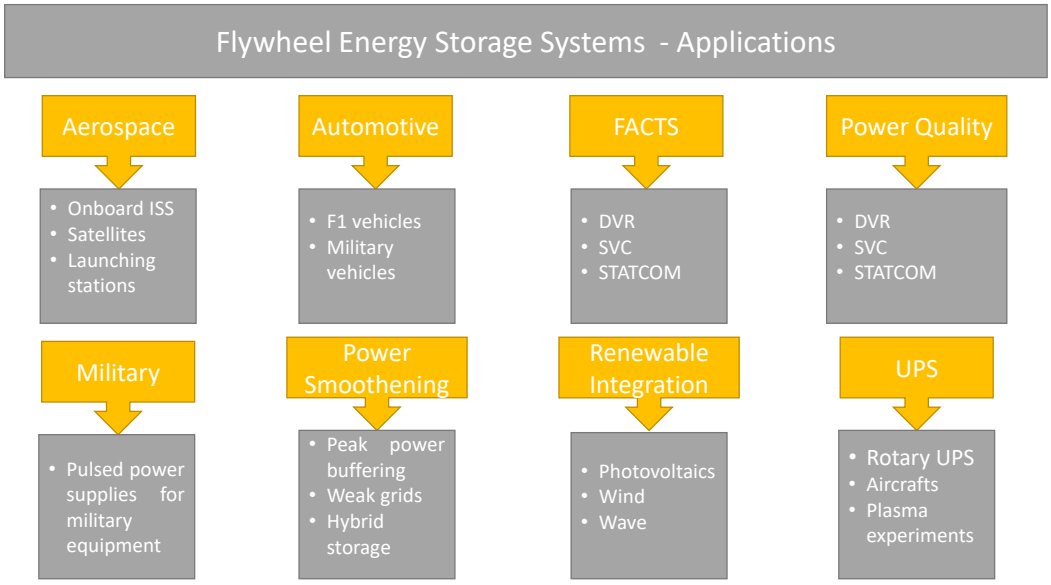

Fig. 4.13. Applications of Flywheel Energy Storage Systems

Lastly, flywheels present some advantages when compared to electrical batteries.

- First, flywheels and batteries share similar life cycles (over 100,000 times), but flywheels do not required chemical components or cycles of charge/discharge in contrast; this means they cause less impact to the environment and their maintenance needs are considerably shorter [31], [150].
- Moreover, flywheels have a higher power and energy densities [150].
- The also have a shorter charging time. This brings a power output that can even come from primary sources with a high variability in a short period of time, such as wind and wave power; on the other hand, this trait facilitates their design for load variation [150].
- Furthermore, they have a higher efficiency (90-95%) [79], considering that for the same number of cycles, advanced Lead-Acid batteries have an efficiency between 75 and 90%, whereas Li-ion ones register an efficiency around 87% and to% [31].

- In short, flywheels systems offer a great variability: from low to high speed, from metallic to composite rotating cylinders, and with or without brush-less magnetic bearings [150].

4.3.2. Flywheel components

Figure 4.12 depicts a typical flywheel's structure and components. Three sub-structures are clearly differentiated, namely a vacuum pump, a DC-link, and flywheel housing. The vacuum pump regulates the air emptiness inside the flywheel housing, and the DC-link is connected to the motor/generator inside the housing by mean of a bidirectional AC/DC converter.

Flywheel housing has several components, namely the flywheel rotor and, the motor/-generator which converts the kinetic energy stored/delivered by the flywheel rotor into electrical energy. This energy is later sent to the DC-link when it is working in generator mode; both rotating masses are connected by means of their central shaft, whereas the electrical connection between the housing and rotating components is achieved by both thrust and radial bearings, which can be brushless or not depending on the technology.

4.3.2.1. Flywheel rotating-mass

The flywheel rotating-mass is the key component of the FESS, and it consists of a disc capable of storing the electrical energy in the form of kinetic energy. This energy storage makes it possible to smoothen the power output of the installations with a high resource variability. The material that the disc is made of is extremely important when it comes to establishing the operative characteristics of the device. In the beginning, steel was used to manufacture flywheels, but this material presents stress limitations. In 1970s, composite materials began to be utilized for flywheels manufacturing; these materials can work at high speeds and can support great fatigues due to rotational stress. In this way, composite-based flywheels are used for functionalities that require performance speeds superior to 10,000 rpm, with a small size, while the ones made of steel are utilized for those applications that do not require such high speeds (up to 10,000 rpm).

Power and energy are decoupled in flywheel storage systems. The power rate is defined by the electric machine that is coupled to the flywheel. Kinetic energy, E_k, is defined by the moment of inertia J and the square of rotational speed ω, as shown in (4.18).

$$E_k = \frac{1}{2} J \omega^2 \tag{4.18}$$

From (4.18), it can be deduced that, to increment the kinetic energy stored in the flywheel, actions over its moment of inertia or its angular speed can be exerted. The moment of inertia is dependent on the mass and the disc ratio of the flywheel, as given in

(4.19). It should be noted that the mass is the function of the material density (ρ_m) and that the discs which make up the flywheel's rotating-mass used to be cylindrical. Given these two points, the volume is directly proportional to the ratio r and the height h. Moreover, the moment of inertia can be calculated according to (4.20).

$$J = \frac{1}{2}mr^2 \tag{4.19}$$

$$J = \frac{1}{2}\rho_m \pi h r^4 \tag{4.20}$$

Likewise, the useful energy can be obtained by two different ways. The first way is by means of the range go from maximum to minimum rotational speed, as depicted in (4.21). The second one, which is given in (4.22), is based on the moment of inertia's decomposition for a hollow cylinder, where m is the cylinder mass, r_{outer} is the outer radius, and r_{inner} is the inner radius [79].

$$E_k = \frac{1}{2}J(\omega_{max}^2 - \omega_{min}^2) \tag{4.21}$$

$$E_k = \frac{1}{2}m\omega^2(r_{outer}^2 - r_{inner}^2) \tag{4.22}$$

4.3.2.2. Magnetics bearings

Magnetic bearings are located inside the FESS cavity, specially at the upper and lower part of the disc that contains the flywheel rotating-mass. Their main function is to hold the weight of the flywheel disc, and therefore it can be considered the main mechanical component of the FESS. The flywheel disc is sustained in between the two magnetic bearings due to the repelling electromagnetic forces that are generated inside the housing, and there is no need for them to be in contact with the disc. For this reason, flywheels that employ magnetic bearings have lesser friction forces than their mechanical version; in addition, they can reach a higher spin and higher response speeds, and they also have a higher lifecycle and capacity with a minimum maintenance [159]. To limit the friction of the elements contained in the housing, the housing is filled with low-pressure air or helium [171]. The main inconvenience with magnetic bearings is their control mechanism. When there are failures in the control system or overloads, it is necessary to have an ancillary system with magnetic bearings.

There are currently three types of magnetic bearings, namely passive, active, and superconducting.

- Passives: are those used with ancillary services because they present instabilities in their performance. The main advantages of these elements are their low friction losses and low costs [172].

- Actives: are those used as ancillary bearings to reduce the rotor vibrations. Their main advantage is that they present higher controllability and higher lifecycles than the passive ones, but active magnetic bearings do present higher losses due to the existence of bias currents. Combining active and mechanical bearings is a good choice in terms controllability, stability, viability, and costs [167].

- Lastly, superconducting magnetic bearings are the most widely utilized type in applications that require great velocity, since they are more stable with, a larger lifecycle and lower losses. The main inconvenience with them is their working temperature, because the operating temperature are considerably below normal levels, it is necessary to provide FESSs with a cryogenization system that can generate these temperatures, which causes a rise in the device's cost [167].

4.3.2.3. Electric machine

Electric machine plays a key role in the FESSs because they act as the electromechanical device in charge of establishing the energy flux that flows between the flywheel and the grid. At the same time, it convert the electrical energy into mechanical energy, and vice versa. In other words, the electric machine works as a generator when the electric grid demands energy to the flywheel, and in which case the speed of the flywheel is reduced; when the machine needs to act as a motor to store energy in the flywheel the acceleration in the device is increased. Permanent Magnet Synchronous Machines (PMSG) are most commonly utilized in the FESS because they present lesser rotor losses, higher energy densities and higher efficiency. They are used in applications that require working speeds of about 50,000 rpm, but there are developments that are currently able to reach ultra-high velocities (150,000 to 300,000 rpm) [173]. IM are a good alternative when the application requires lower speeds, as they are robust, reliable, and comparatively cheaper. In the past recent years, DFIM have been utilized in FESS applications, which allows the size of the converters in charge of their control to be reduced [174]. Homopolar Synchronous Machines (HSM) has a better performance due to lower rotor losses and the materials used for their construction. In addition, it is possible to use the rotor of these electric machines as an ancillary storage device in the FESS. HSMs can work in the range of 30,000 to 60,000 rpm with an efficiency of 83% [175].There are also other types of machines used in the design of the FESSs, such as: IM, Switched Reluctance Machine (SRM), Axial-Flux Permanent Magnet (AFPM), and a brushless DC machine.

4.3.2.4. Electric interface

Figure 4.14a shows the basic electric scheme of a flywheel device. As it can be noted, the flywheel disc is connected to an electric machine that performs electromechanical conversion. The connection of the electric machine to the grid is carried out by a back-to-back converter. Before grid-connection, a filter is placed into the machine; this filter

is used for improving the power quality that the device injects into the grid. In general, the flywheel's electronic converters performs an AC/DC/AC conversion, with the back-to-back configuration being the most commonly used for FESS [167]. The grid-side converter converts the AC voltage to DC. After the DC stage, the machine-side converter converts the DC voltage again to AC. Because the electric machine works as a generator or a motor, grid-connected converters are bi-directional. The converter placed at the machine side is in charge of controlling the speed and the flow of the electric machine through the active power adjustment. On the other hand, the converter placed at the grid side takes care of maintaining the DC voltage between both converters. When the electric machine works as motor, the machine-side converter works as a power inverter, while the grid-side converter works as a rectifier. When working as a generator, the machine-side and grid-side converters work as rectifier and inverter, respectively. When the flywheel is utilized to improve the power output of the DG-units, which can be wind and wave, the flywheel can use the machine-side converter only, and it connects to the DC-link which corresponds to the backup DG converter (see Figure 4.14b). In this case, the grid-side converter should consider the rated capacity of both the DG and the flywheel [167].

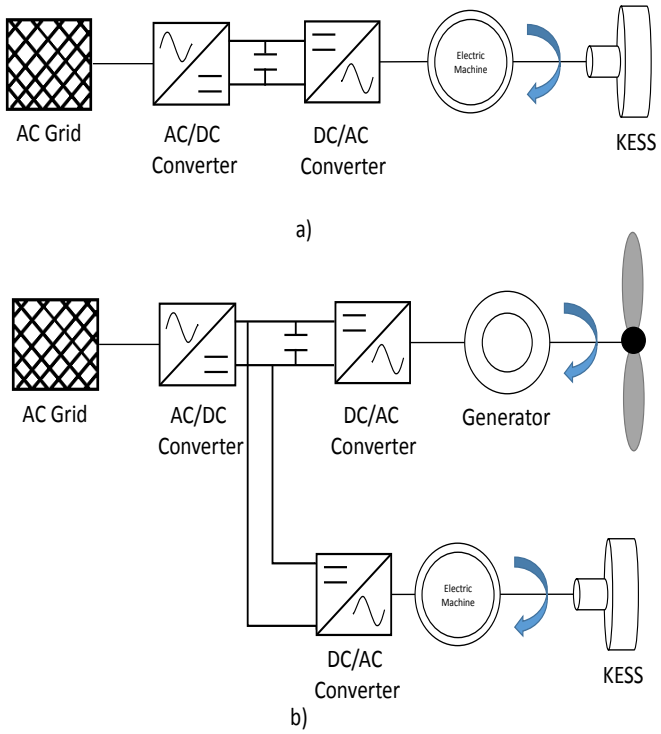

Fig. 4.14. Basic electric schemes of a grid-connected flywheel

4.4. Lysekil Research Site

4.4.1. Location

Based on the classification established by [176], the Lysekil wave farm (Lysekil Research Site, LRS) can be included within the group of the last "pre-commercial stage gate requirements test sites". The installation is located on the west coast of Sweden, at 100-km from the south-western part of Götemborg city and 2-km from the coast of Lysekil city. The location encompasses a surface of 40,000 m^2 with the coordinates of 58^o 11' 850"N 11^o 22' 460"E and 58^o 11'630"N 11^o 22" 460"E, a sea bottom is placed at a depth of 24-25 m, and optimal conditions are created for WEC devices mooring [177]. The location of the Lysekil facility is surrounded by islands; this allows the facility to have a good sea state, even in winter, with an energy density of 2.6±0.3 kW/m [178]. Figure 4.15 shows the location of the installation and, the sea state in the surroundings of the LRS. Figure 4.16 shows the wave climate matrix that corresponds to the Lysekil wave farm location.

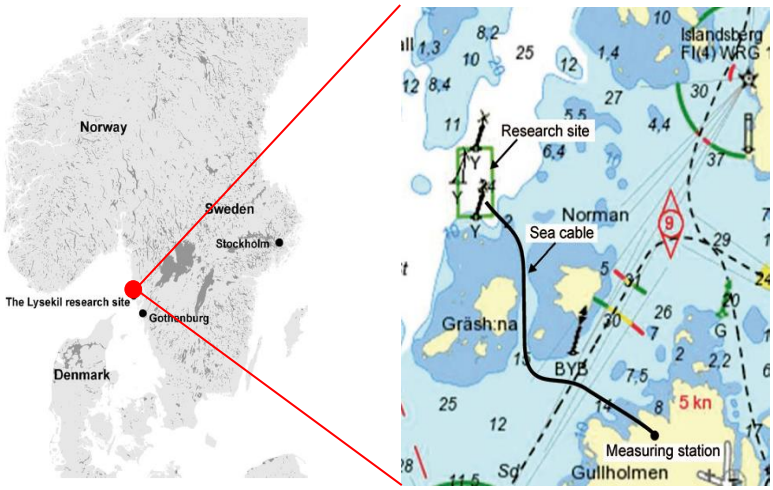

Fig. 4.15. Location and state of the sea at the Lysekil marine facility [177], [179]

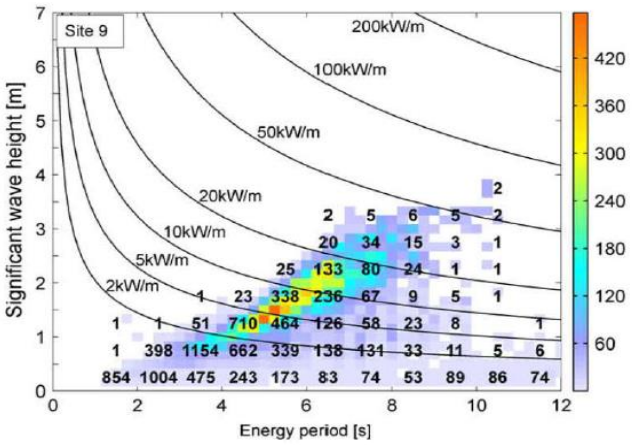

Fig. 4.16. Wave climate matrix at Lysekil research site [180]

LRS started its operation in 2003, and the first measurements taken with respect of the sea state where in 2004. In March 2006, LRS installed the first buoy, known as L1; it was connected through a 2.9-km long wire to the measurement substation that is located on the Hermanö island at the southern point of the LRS. In 2009, two WEC devices, namely L2 and L3, were installed, which altogether with the L1 prototype were connected in cluster to a marine substation in order to deliver energy to the grid [181]. Together with the WECs, 21 environmental buoys were installed in 2007; the intention was to measure the impact of the WEC units in the marine surroundings of the installation and vice versa. Between 2009 and 2010, 5 new WEC units, L4, L5, L7, L8 and L9, were installed. In 2015, three more WEC units (L10, L11 and L12) were also installed; since November 2015 all of them are currently grid-connected, with an installed capacity of 200 kW [181]. At present, more than 10 WEC models have been analysed at the LRS [182]. The LRS is completed with a measurement tower installed in the summer of 2008; it was situated 150-m away from LRS. The measurement tower is provided with a camera that makes it possible to correlate the images taken of the waves motion with the installation's power output. As listed from left to right, the components in the LRS scheme and the scheme itself is shown in Figure 4.17 namely the observation tower, the biological buoy, the buoy for the measurement of the sea state by means of the waves characteristics, the WEC coupled with its energy catchment buoy and the linear generator for electricity conversion, the marine substation and the off-shore measurement station.

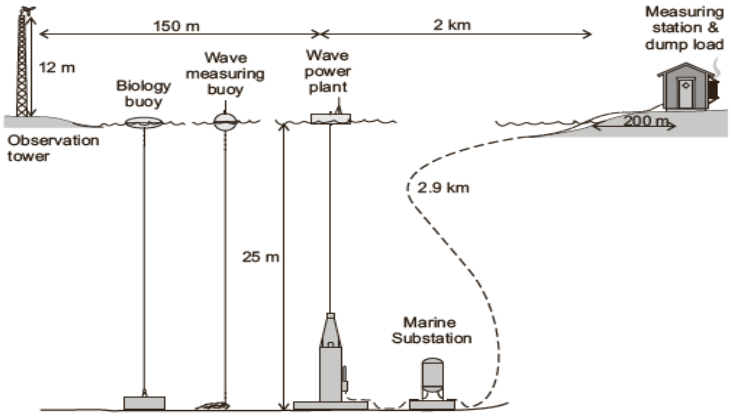

Fig. 4.17. Outline of the basic components of LRS [183]

4.4.2. Technology used

In the LRS, point absorbers are used to extract energy from the waves, while the conversion of wave energy into electrical energy is performed using the direct driven linear generator (DDLG). The movement of the waves is transmitted from the point absorber towards the generator translator through a cable. To improve the performance of the generators for extreme wave conditions, WEC units are provided with springs in their upper part that limit the translator motion inside the DDLG's cavity. Because the LRS is

a research installation, several DDLGs (Figure 4.18a) and point absorber buoys (Figure 4.18b) have been tested [140].

(a) (b)

Fig. 4.18. DDLG (a) and point absorber (b) buoys at LRS [140], [177]

The technical characteristics of both L1 and L9 models are shown in Appendix A [177].

4.4.3. Marine substation

The LRS installation is grid-connected through a marine substation, with a rated power of 96 kVA, and a 2.9-km long wire (see Figure 4.19) that is used for the configuration of the first WEC units [179].

The wave power generators are provided with a 12-Ω dump load, which oversees the dissipation of the energy delivered by the WEC units when they are disconnected from the substation.

The power output of each WEC unit is rectified inside a six-diode bridge converter. In the marine substation's DC stage, the three WEC units are interconnected in parallel. The electrolytic aluminium capacitors in the DC stage allow the output signal that is sent from the installation to the inverter to be smoothened. The AC voltage at the output of the inverter is increased to the grid voltage (1,000 V). This is done using a Y-Y power transformer that is provided with tap regulation (80-100-125-250/1,000 V), and a tap changing mechanism compounded of off-load circuit breakers [179]. Appendix A.3 shows the characteristics of the marine substation. The elements that make up the substation are confined within a $3m^3$ nitrogen filling at a 3-bar pressure.

The marine substation is completed with an auxiliary system, a resonant circuit, and a measurement station. The main function of the auxiliary system is to distribute the power

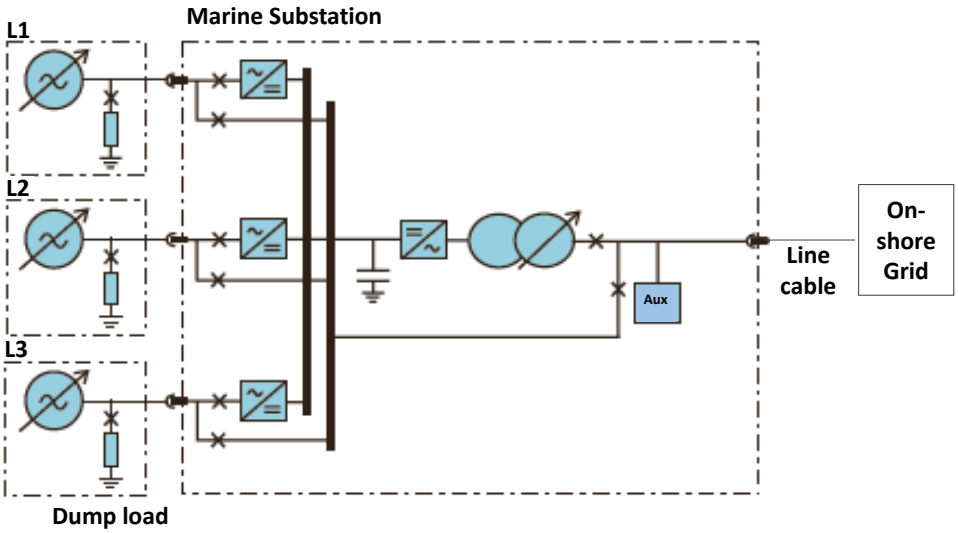

Fig. 4.19. Electrical diagram of the LRS on-shore connection [184]

generated by the WEC units between the control systems and the circuit breakers. This installation is fed by the WEC generators, or it can be fed from the off-shore system when feeding from WEC generators it is not possible. The resonant circuit allows the production of the installation to be incremented. Lastly, the measurement station is supplied with different loads so that the LRS performance and its remote control can be widely studied.

This entire system was subjected to several control mechanisms, such as Programmable Automation Controllers (PACs) for both the marine substation and the power inverter, and a Data Acquisition System, which was implemented for gathering electrical outputs from each wave converter [185].

4.5. Lysekil Research Site modelling for power output smoothen

4.5.1. Input data

Data used in this research were gathered from three linear generators with an attached cylindrical buoy each (L1, L2 and L3). Their model and parameters can be found in Appendix A. The time series of the power measured after the linear generators' rectifier were sampled at 256 frames per second, which accounts for a 1-hour input data (921600 frames in total). Data used were gathered by Uppsala University on July 20, 2009 at 22:00h. A boxplot analysis was carried out to determine the trends in each phase of the three generators, as shown in Figure 4.20. It is seen that median value is close to zero in each phase of the generators. Moreover, for the number of outliers coming out from the quartiles, it can be noted that the wave energy converters were subjected to reiterated overloading conditions, and their influence over the power output should not be dismissed [186], [187]. It is important to point out that when there are dips in the power output, its value is almost zero; this is due to the voltage level present in the DC bus, and

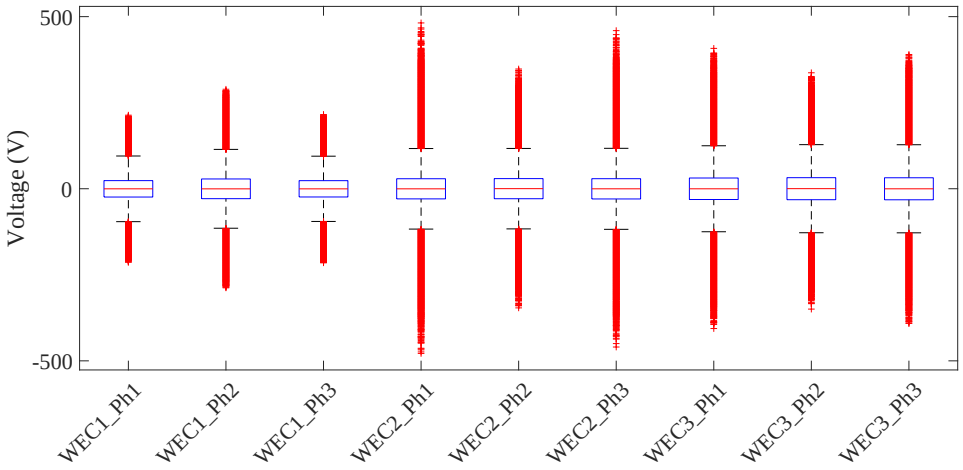

Fig. 4.20. Boxplot analysis over each phase of the wave converters (WEC1, 2 and 3)

consequently the translator needs to reach a high speed as well to confront this condition and deliver energy to the system [186]. This point was validated with the results gathered in Figure 4.21 for Generator 1 with a sample time of 20 seconds.

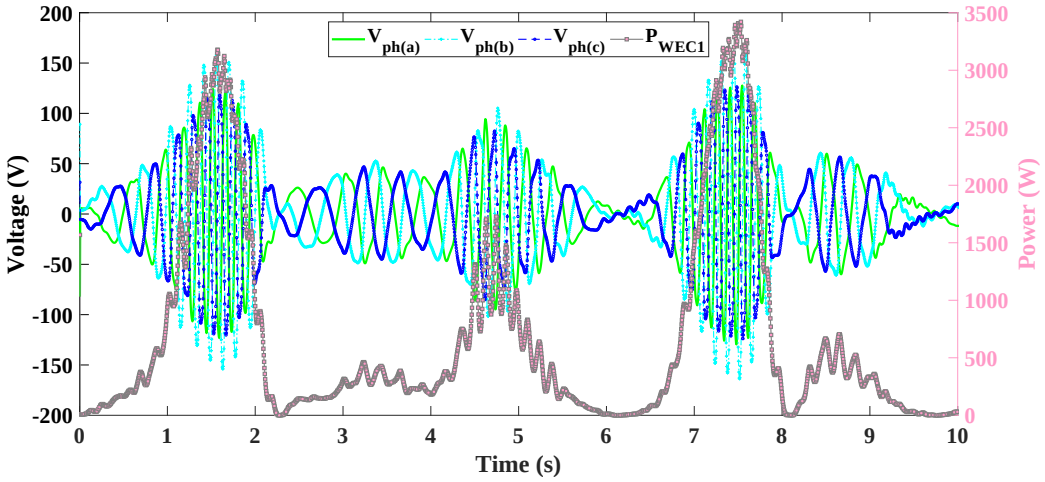

Fig. 4.21. Voltages and power of $PWEC_1$

4.5.2. LRS modelling

4.5.2.1. General description

The general structure of the Lysekil Wave Farm and the proposed wave power smoothing system is shown in Figure 4.22, which includes a wave farm, a filter, a Kinetic Energy Storage System (KESS), and DC/AC converter, and a marine transformer. Each block in the wave farm is described as follows:

1. The wave power farm consists of WEC's (see Subsection 4.2.2). For wave power output smoothing, the WECs are modelled with the measurement data collected in

the three WECs located at the Lysekil Test Site (see Figure 4.22, WEC's Block) [182].

2. Filter: The purpose of the filter is to create a reference signal for the FESS in order to store wave energy in this device. For accomplish that, the filter decomposes the input signal (power from WECs) into two components: one that corresponds to the smoothen power output, and the rest which corresponds to the fluctuation part of the signal and which must be stored into the FEES (Figure 4.22, Reference signal Block).

3. The KESS is formed using a high-speed flywheel, that it is connected to the DC-link (see Figure 4.22, FESS Block).

4. The DC/AC inverter is an IGBT inverter that transfers the smoothen generated power from the DC-link to the transformer. The inverter's control improves the wave farm output filling up the power valleys with the stored energy in KESS (see Figure 4.22, Grid Side Converter Block).

5. Marine transformers are used for integrating the wave power output to the on-shore power grid. The transmission network existing in the Lysekil emplacement consists of two power transformers, with five winding taps, connected at each extreme of a submarine transmission line. In this study, only the first transformer is considered [188].

The aforementioned elements can function collectively to feed an isolated or a grid-connected system.

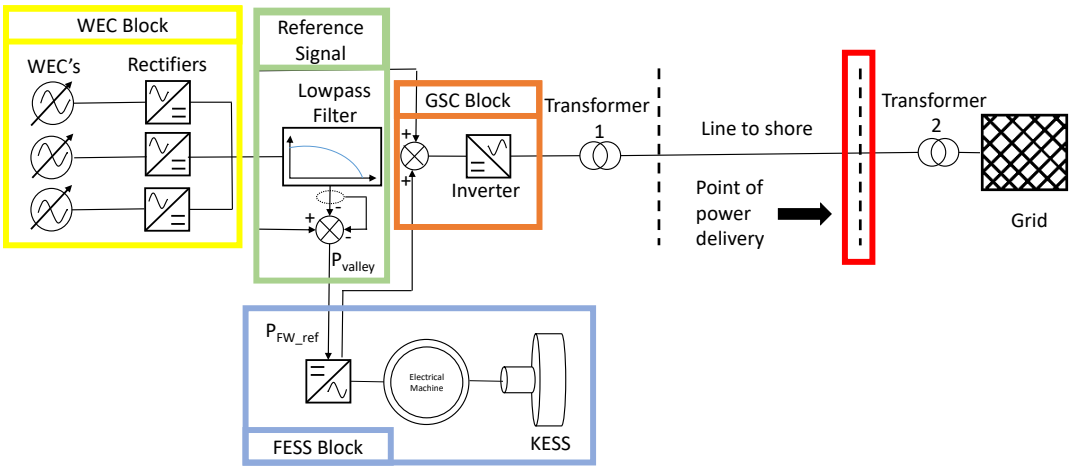

Fig. 4.22. Circuit diagram applied on linear wave energy system located in Lysekil Test Site

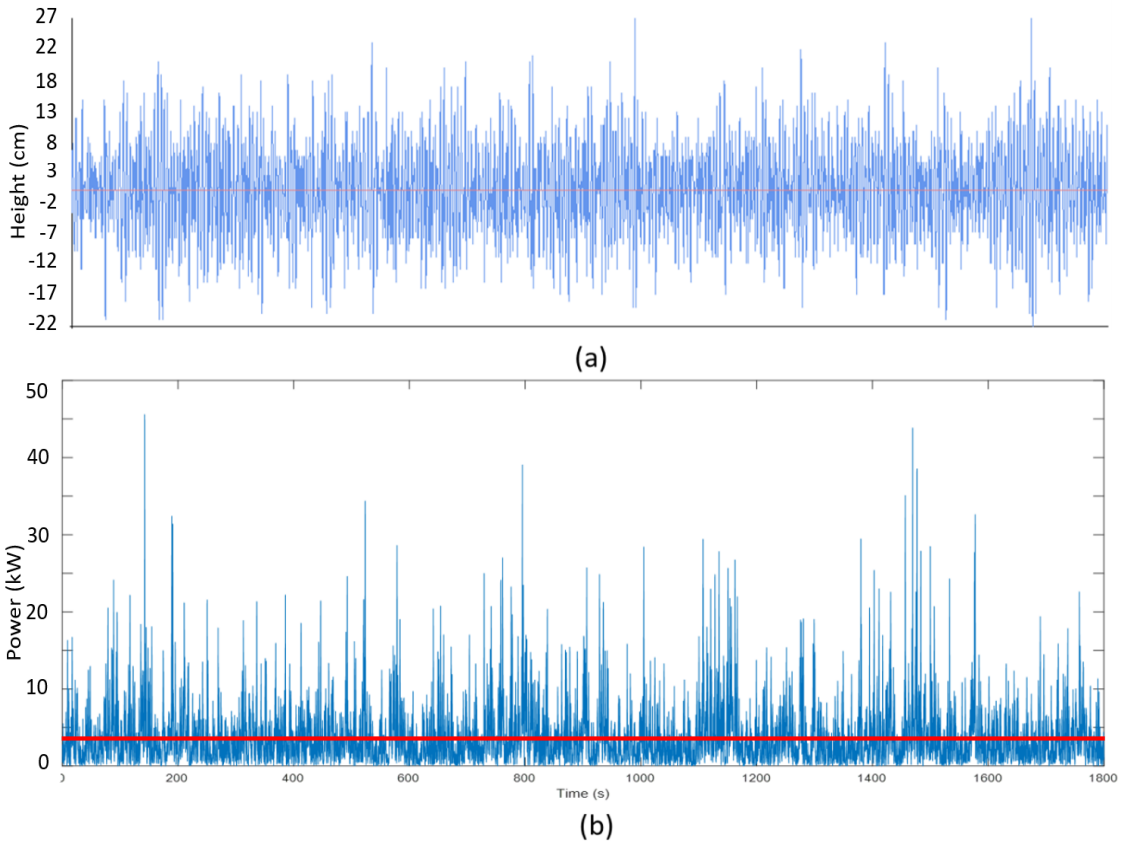

Fig. 4.23. Buoy wave elevation (a) and WEC's power output (b) for the Lysekil wave farm

4.5.2.2. WEC unit

Real power measurements of the three WEC's units are used to demonstrate KESS's capability to smooth wave power output. The measurement was done July 20, 2009 at 21:00; signals are sampled to 256 Hz [189]. Figure 4.23 shows the sea state in terms of (a) the buoy wave elevation and (b) WEC power output registered for the first half hour of study. The measurements that allows the lower part of the figure to be depicted correspond to the power output of the wave farm after the rectifier. As it can be seen, the hour of study corresponds to a calm sea, with a high wave range between 27 and -22 cm and a medium power output of 2.55 kW.

4.5.2.3. Flywheel model

In this doctoral thesis a the parameters of a flywheel prototype developed by Uppsala University was used. This prototype comprises a hollow cylinder, radial magnetic bearings, and an electric machine that is capable of acting either as a motor or a generator. The kinetic energy that FESS delivers is governed by (4.18), and it has an established maximum discharge depth of 25% with respect to the FESS' storage capacity.

The FESS is able to store electrical energy in the form of kinetic energy. The wave energy power output smoothening process will be carried out in terms of power, and therefore the flywheel will take the losses equations described in this section into account.

To minimize the device's losses, this study takes two series of considerations into account for the development of the model:

(a) First, the flywheel rotor is located inside a chamber, and it is suspended by magnetic bearings that allows them to work at quasi-vacuum conditions. Therefore stand-by losses are minimized [190].

(b) Secondly, the PMSM that is used as a motor/generator is composed of a coreless stator [191].

Finally, losses can be grouped and categorized as drag losses, electric machine losses, and magnetic bearings losses.

– Drag losses occur when the FESS model is operated between 15 and 30 krpm. At this speed range, the air in the flywheel chamber develop turbulent velocity regime. Under this condition, the power dissipated due to drag losses between a rotating cylinder in a concentrically cylindrical case can be expressed as (4.23), [192]:

$$P_d = \omega R F_d \tag{4.23}$$

where R is the cylinder radius and F_d is the frictional force on the cylinder. The force induced by the viscous drag is expressed as (4.24):

$$F_d = \lambda \rho \pi R^3 L \omega^2 \tag{4.24}$$

where λ is the friction factor or drag coefficient, ρ is the density and L is the cylinder length.

– For electric machine losses, the FESS model that is used considers an electric machine whose stator is coreless, and thus the main source of losses in the machine is joule losses in (4.25):

$$P_i = RI^2 \tag{4.25}$$

– Lastly, magnetic bearing losses associated with the magnetic bearing in charge of sustaining the flywheel rotor can be classified as hysteresis losses or eddy losses. At high flywheel speeds, the eddy losses are the ones that predominate over the hysteresis losses [193]; thus for the developed FESS model, magnetic bearing losses

are calculated according to (4.26), and these losses are directly proportional to the square of flywheel work speed.

$$P_{eddy} = K_{eddy}\hat{B}^2 f^2 \tag{4.26}$$

where K_{eddy} is a constant depending on both the geometry and the material used in the magnetic bearing's design, $\hat{B}$ is the maximum magnetic flux, and f is the flywheel work frequency.

4.5.2.4. Grid connection

Both the KESS and WECs are connected to the grid through a GSC that is rated to the nominal power of the KESS and WECs farm. The GSC is considered to have a constant efficiency of 98.5% (see Figure 4.22). The 2.9 km sea transmission line connected between offshore and onshore substations is pi-model with a line resistance of 0.21 Ω/km. The point of power delivery is placed in the primary winding that correspond to the offshore transformer (Transformer 1).

4.6. LRS power output smoothening

The power output smoothening process developed in this thesis has three main steps. In the first step, the power output of several WECs are clustering. Next a filter is applied to the output signal of the clustering process in order to determine the power that must be stored in the flywheel. In the final step, a valley filling power output is developed in order to achieve the reference power signal given by a grid operator.

Figure 4.24 shows the complete block diagram of the proposed power output smoothening process. The blue box corresponds to the first step, and the red boxes correspond to the second step; the green box corresponds to the last step of the power smoothening process developed in this thesis.

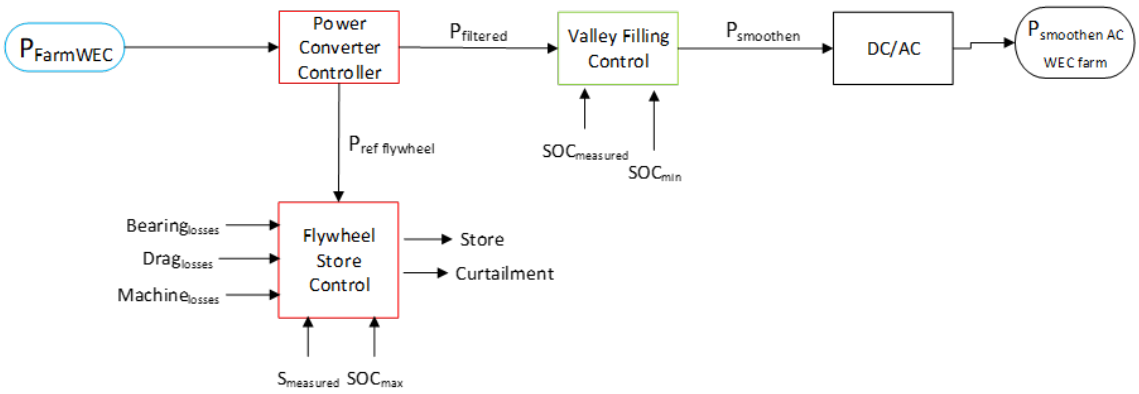

Fig. 4.24. Block diagram of the power output smoothening process

4.6.1. First stage: generators clustering

In this stage, the study analyses the effect of clustering generators over several parameters. To do this, each of the generators (WEC1, WEC2, and WEC3) and their delivered wave active power are studied separately. Later, the clustering is made with every two generators. Finally, the three converters are aggregated altogether to a common node.

The effect of the wave active power aggregation is summarized in Table 4.1 and it was examined in the context o the key performance indicators (KPI's) described as follows:

1. Peak Power, Average Power and Peak/Average Ratio

   The great the number of clustered generators on an aggregation node, the great the peak and average power are. Nevertheless, a lower peak/average ratio is achieved when generators are aggregated when compared with individual performance.

2. Normalize Standard Deviation (nSD) In order to have a better understanding of the standard deviation of the time data set, the standard deviation has been normalised by the mean output power of each WEC or WEC array. The normalized standard deviation is measured in p.u., and it gives a measure of the relative power output fluctuations, which is a more intuitive value than absolute fluctuations. Figure 4.25 shows the effect of the total clustering over the total nSD, and the results show that wave converters clustering process lower the nSD of the total signal when compared to individual ones. Calculations were carried out for a continuous time data set measured on July 20, 2009 at 22:00h.

3. Point of delivery KPIs.

   Table 4.1 shows additional KPIs that describe the system's behaviour on the point of energy delivery. From the results, it can be concluded that clustering WEC units improve power quality from the entire wave farm in terms of the peak/average ratio and standard deviation. Nevertheless, the power quality associated with the signal that is delivered to the grid is not completely improved. Consequently, additional techniques need to be carried out in order to achieve this goal; these techniques include filtering and valley filling, and their procedures are fully shown in the following.

4.6.2. Second stage: filtering and KESS stage

To further improve the power output signal from the wave farm at Lysekil, two filtering techniques have been tested namely Windowed Integrator (WI) as a continuous filter, and a low pass (LP) filter as a discrete technique.

	Peak P_{shore} (kW)	Mean P_{shore} (kW)	Peak/Ave. P_{shore}	Normalized Standard Deviation	Energy to shore (kWh)	Grid Losses (Wh)
WEC1	9.94	0.81	12.28	1.54	0.81	0.85
WEC2	40.82	1.29	32.71	1.75	1.25	2.42
WEC3	30.09	1.35	22.32	1.52	1.35	2.48
WEC (1+2)	42.83	2.06	20.82	1.23	2.05	4.120
WEC (1+3)	33.98	2.16	15.75	1.12	2.15	4.260
WEC (2+3)	45.30	2.60	17.45	1.16	2.59	6.20
All WECs	45.58	3.41	13.39	0.96	3.4	8.840

TABLE 4.1. WAVE POWER DATA ANALYSIS FROM THE THREE GENERATORS AND THE EFFECT OF AGGREGATION

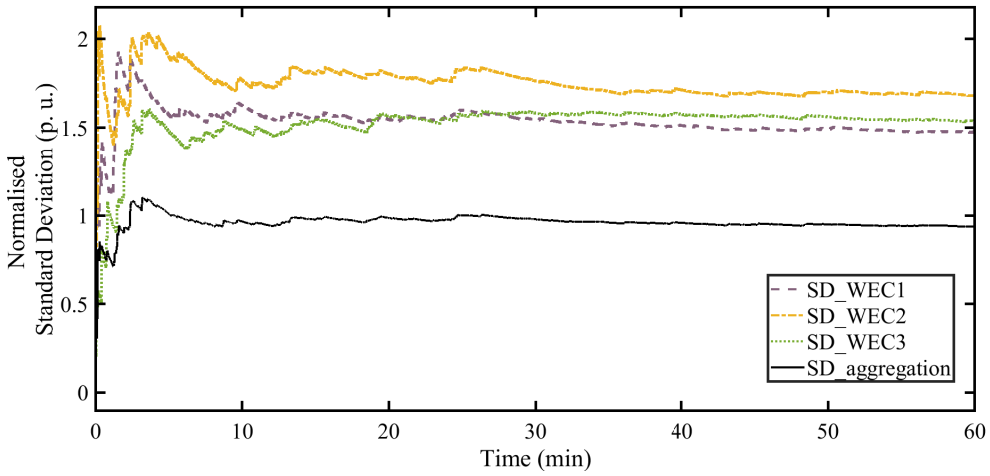

Fig. 4.25. Results of the aggregation over the Normalised Standard Deviation

4.6.2.1. Windowed Integrator smoothening stage (WI)

In this stage, the sum of the power signals coming from the three wave converters emplaced in the Lysekil Test Site were used as a continuous signal over a sliding time window of fixed length. By applying a WI in the clustering point, that corresponds to the power aggregation from the wave farm, the power output is considerably smoothened. KPIs of the WI analysis are shown in Table 4.2.

4.6.2.2. Low-Pass (LP) filter smoothening stage

When using a discrete low-pass filter, the power smoothness depends on the filter parameters. The optimal filter depends on the sea state, and the control algorithms should adapt to different sea conditions. For this reason, it would be necessary to apply adaptive filters to oversee the whole filtering process. In this installation, the smoothing process is carried out by three filtering stages. Consequently, it is possible to design a simplified filter in

charge of the second stage of the smoothing process, thus offering minimum complexity for its implementation in the real installation. The proposed filter is compounded by a low pass filter with a zero-order hold block. The combined filter is governed by (4.27) where f_{fil} is the filter's frequency. Figure 4.26 shows the block diagram of the filter control step.

$$T = \frac{1}{2\pi f_{fil} s + 1} \tag{4.27}$$

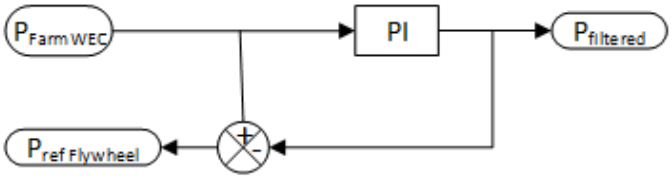

Fig. 4.26. Block diagram of the filtering process

In this step, a low pass filter with a cut-off frequency initially tuned in at 256 Hz is used. Table 4.2 shows the most representative KPIs for 256 Hz cut-off frequency, the WEC clustering and WI; it is inferred that a low pass filter with a frequency value up to 256 Hz is enough to obtain a remarkable reduction in most of the involved KPI's over the results obtain by WI.

Figure 4.27 shows the difference between the signal filtered with WI and LP plus zero order hold, both tuned at 256 Hz. Raw data is also drawn for comparison purposes as well.

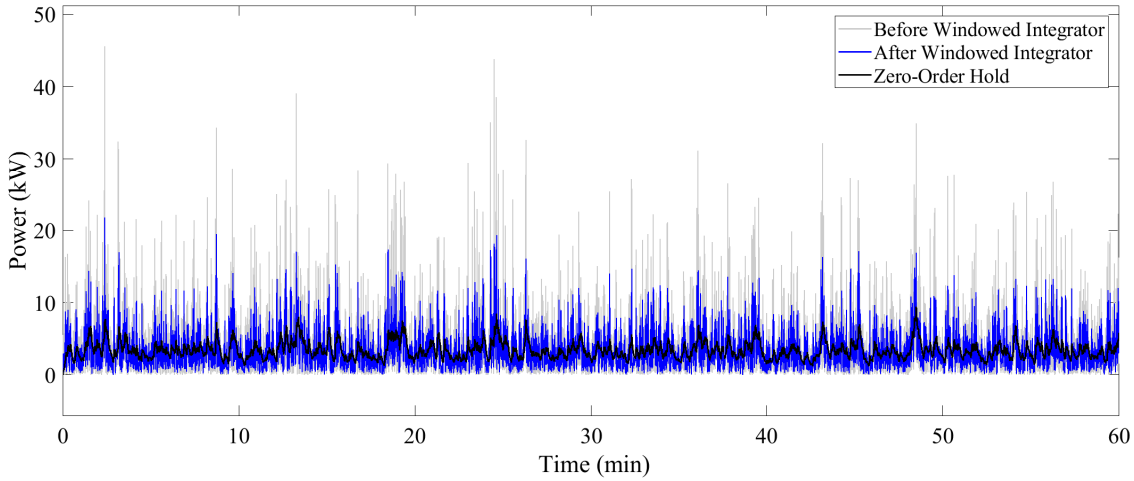

Fig. 4.27. Results of the filtering control system over the wave power output

4.6.2.3. Flywheel smoothening stage

As previously mentioned, the wave power plant offers large oscillations for short-time periods. For this reason, the storage to be used should meet certain criteria, such as quick

Filter	Peak P_{shore} (kW)	Mean P_{shore} (kW)	Peak/Ave. P_{shore}	Energy to shore (kWh)	Normalized Standard Deviation
Windowed Integrator	21.58	3.40	6.35	3.39	0.75
Low pass filter	9.23	2.52	3.66	2.72	0.58

TABLE 4.2. SUMMARIZED RESULTS FOR DIFFERENT FILTERING TECHNIQUES

charge/discharge cycles with no electrochemical degradation, high power density, and high capability of making stipulate definition [194].

In this research, a high-speed buffering is applied to the wave power prototype located at the Lysekil Test Site. The Lysekil flywheel is modelled as a hollow cylinder presented in [168]. The size of the flywheel can be selected according to the energy required, based on a minimum and maximum threshold.

Figure 4.28 shows the block diagram of the flywheel store control and the charge and discharge control strategy of the KESS is shown in Figure 4.29. A reference signal ($P_{ref_{FW}}$) is used to control the charge and discharge mode of the flywheel. The difference between the output power of the WEC array ($P_{WEC_{farm}}$) and the filtered power (P_{fil}) is used as $P_{ref_{FW}}$ of the flywheel. In the cases, where the $P_{WEC_{farm}}$ is larger than P_{fil}, $P_{ref} = P_{WEC_{farm}} - P_{fil} > 0$, the difference between both signals is stored in the KESS, and the flywheel is in charging mode. Once the KESS achieve its maximum SOC (0.9 p.u.), the excess power is curtailed, $P_{curt} = P_{ref_{FW}} - P_{nom_{FW}}$. If $P_{ref_{FW}} = P_{WEC_{farm}} - P_{fil} < 0$, then the KESS is in discharge mode and the power injected in the system is equal to Pref . KESS discharges energy until the SOC_{min} limit is achieved. In this study the SOC_{min}=0.25 p.u. If SOC_{min} is reached, there is the possibility to inject energy from the KESS into the system, so the complete P_{WEC} is sent to shore. The charge and discharge control strategy lets the power output fluctuation to reduce. This control strategy will be coupled with the inverter controller to smoothen the wave power farm output.

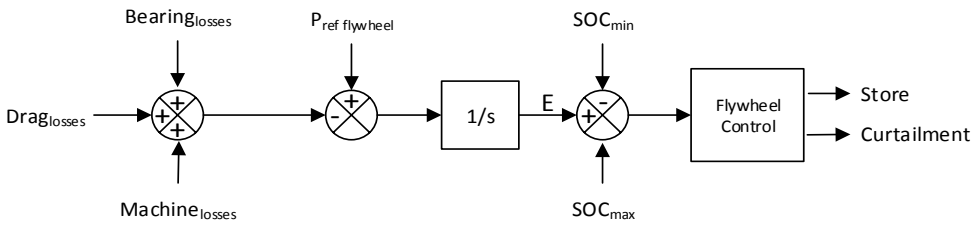

Fig. 4.28. Block diagram of the FESS store control process

Figures 4.30 and 4.31 show an example of the control strategy in two different periods of time. The lines in Figure 4.30 (i.e., A, B and C) and the lines in Figure 4.31 (i.e., D, E and F) represent the time intervals in which the flywheel performance experi-

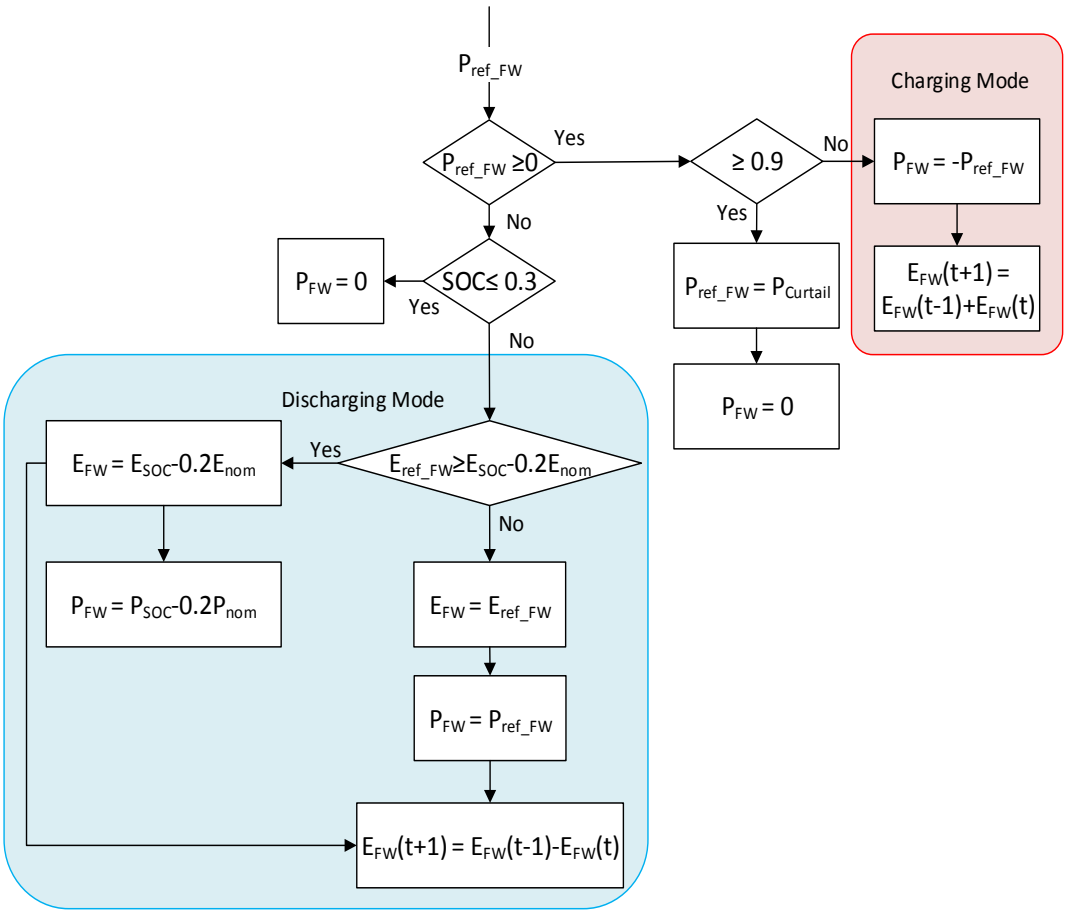

Fig. 4.29. KESS control flowchart

ences a change. The space between point A and B corresponds to a KESS charge mode, in which the reference signals is positive (orange line). Once the KESS achieves the maximum SOC (0.9*SOC_{nom}), at line B, the power is then curtailed, and the power to shore keeps constant with the energy feed by the KESS. At point C, the reference signal becomes negative, and the KESS system is in discharge mode. Figure 4.31 shows a period of time with KESS charge and discharge mode around the minimum KESS SOC. At the initial instance portrayed in Figure 4.31, the FESS's SOC is situated at its minimum value (0.25*SOC_{min}). In the first instance of the simulation which is up to line D the installation's power output (blue line) roughly follows the output reference signal of the wave emplacement once filtered. This is due to the fact that KESS suffers constant charge/discharge cycles around its SOC_{min}, and this is caused by the zero-crossing oscillations associated with the KESS' reference signal. The KESS is charged during the time interval ranged from line D to line E, due to a positive reference signal, which allows the wave installation to maintain a constant power output of 3 kW until the time instance of line F is reached. From this point, it is noted that the KESS does not possess enough stored energy to keep the installation's power output at a constant value, and this it tracks back the filtered signal of the power output.

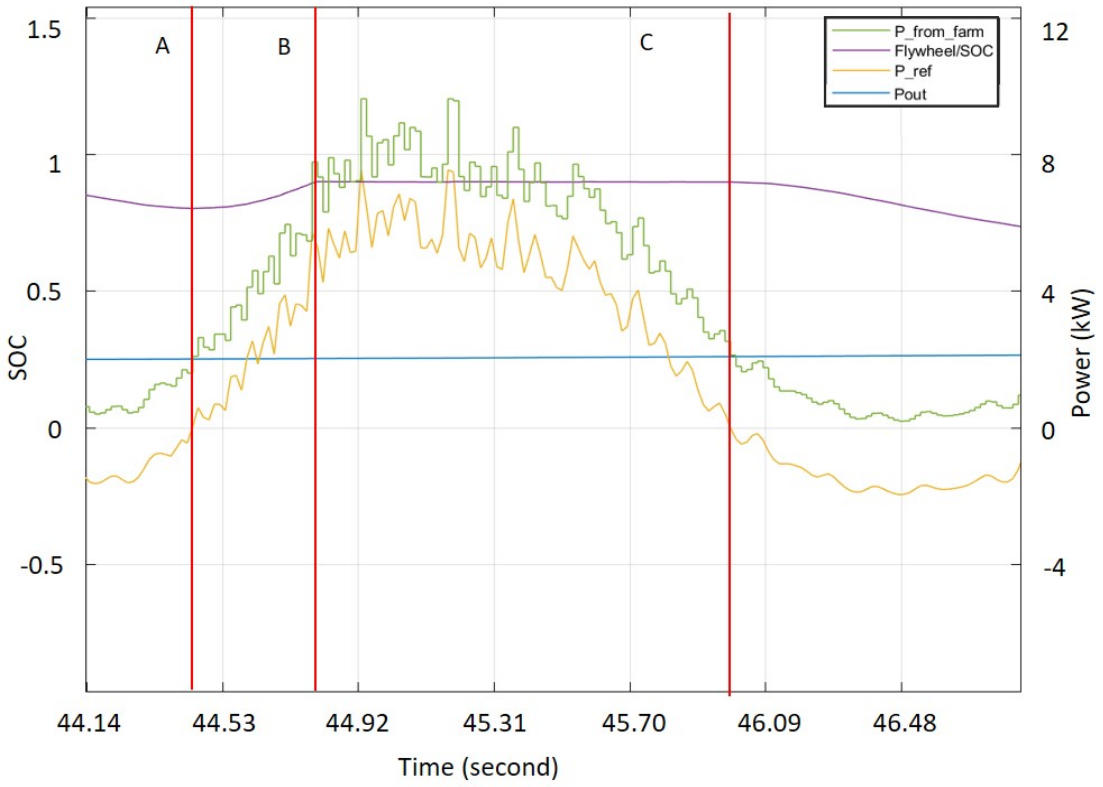

Fig. 4.30. Example of the KESS Control's performance I

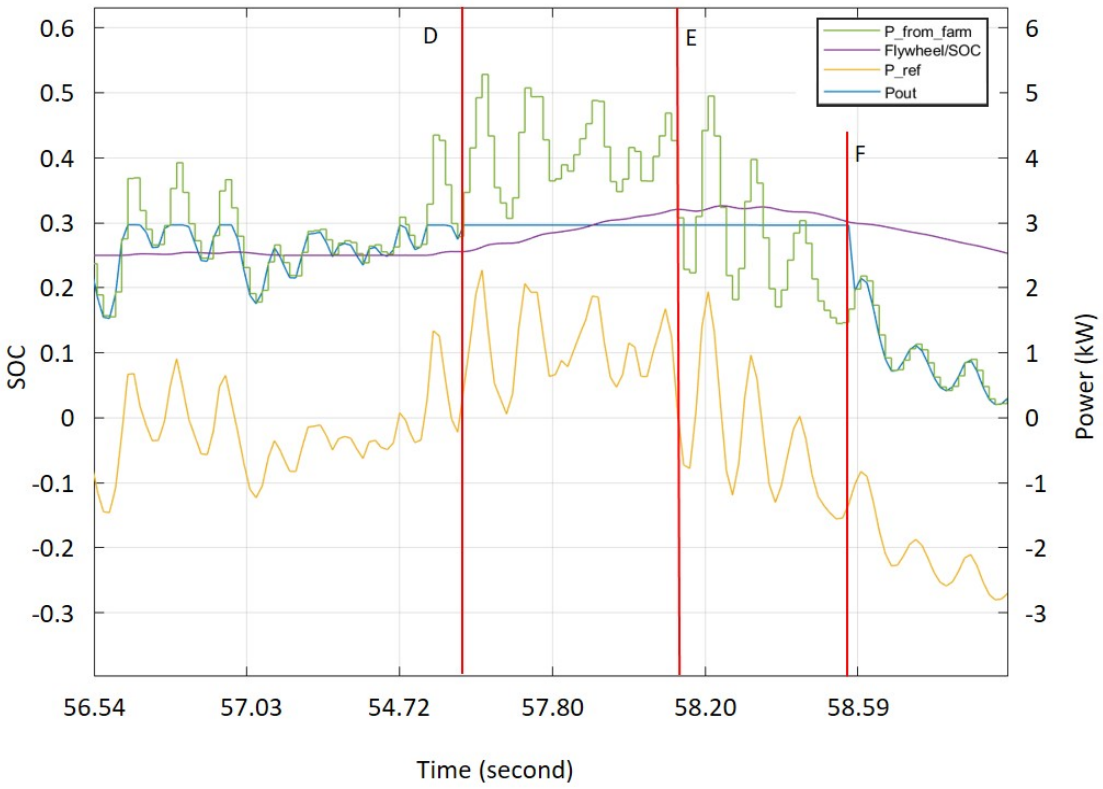

Fig. 4.31. Example of the KESS Control's performance II

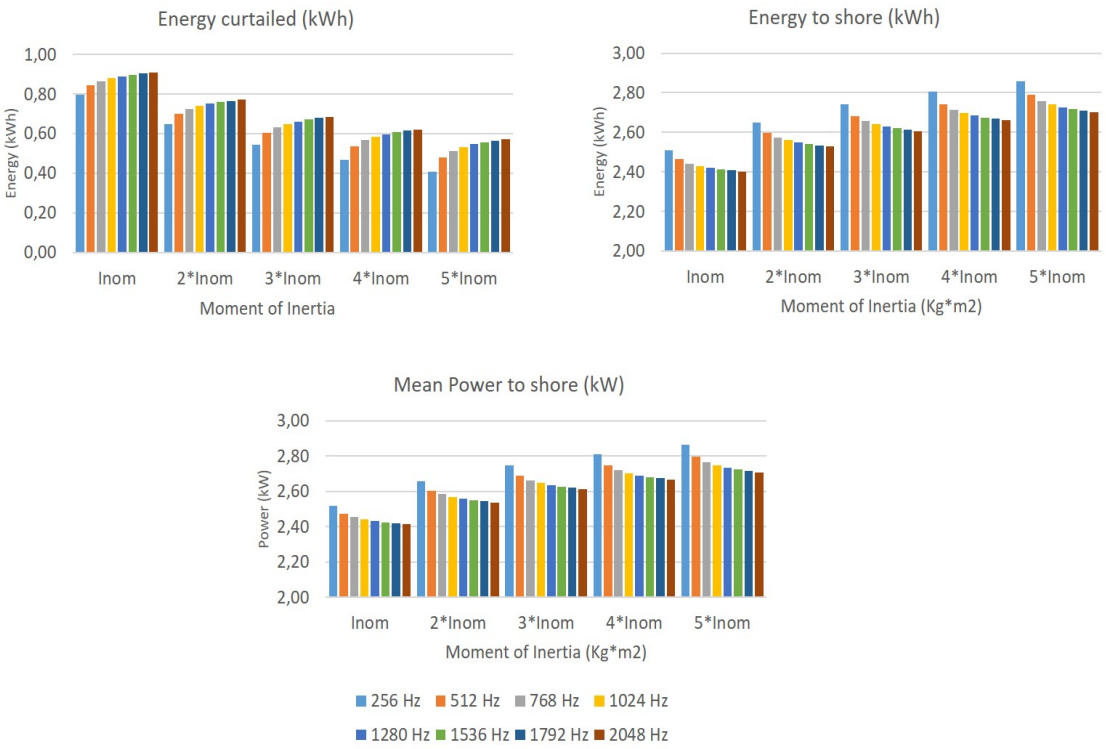

Fig. 4.32. Energy curtailed, energy to shore and mean power to shore comparison between different filtered frequencies and flywheel moment of inertia.

There are several simulations that were performed (see Figure 4.32), and these simulations involved a filtered frequency range from 256 Hz to 2048 Hz and a flywheel with a moment of inertia varying between (I_{nom}, 5*I_{nom}). It must be noted that the flywheel control is linked to the filter control. Consequently, the optimal flywheel size depends not only on the inverter capacity but also on the cut-off frequency filter. It can be therefore deduced that a filter with a cut-off frequency of 256 Hz is the frequency that offers minimum curtailment, maximum energy to shore, and a greater mean power to shore.

Once the optimal filter frequency for this installation is selected ($f_{fil_{opt}}$ = 256 Hz), a new study with a moment of inertia between 1 and 8 times the nominal inertia moment is done. The objective of this study is to determine the optimal size of the flywheel.

Figure 4.33 shows the results for this study tacking into account the relative improvement of three KPIs. It can be seen that for a flywheel with a moment of inertia greater than 5 times the nominal one the relative improvement in the energy curtailed, the energy send to shore and the grid energy losses are keep constant. It can be concluded that the best size of the flywheel for this application is the one with a moment of inertia of $I_{fw_{opt}}$ = 5*I_{nom}. For the optimal flywheel size, the cylinder height is calculated with (4.28), where h is the height in meters of the prototype located at Lysekil Test Site [195], [196]:

$$h_{FW_{opt}} = \frac{2 * E_{FW_{max}} * h_{ref}}{I_{FW_{opt}} * \omega_n^2} \tag{4.28}$$

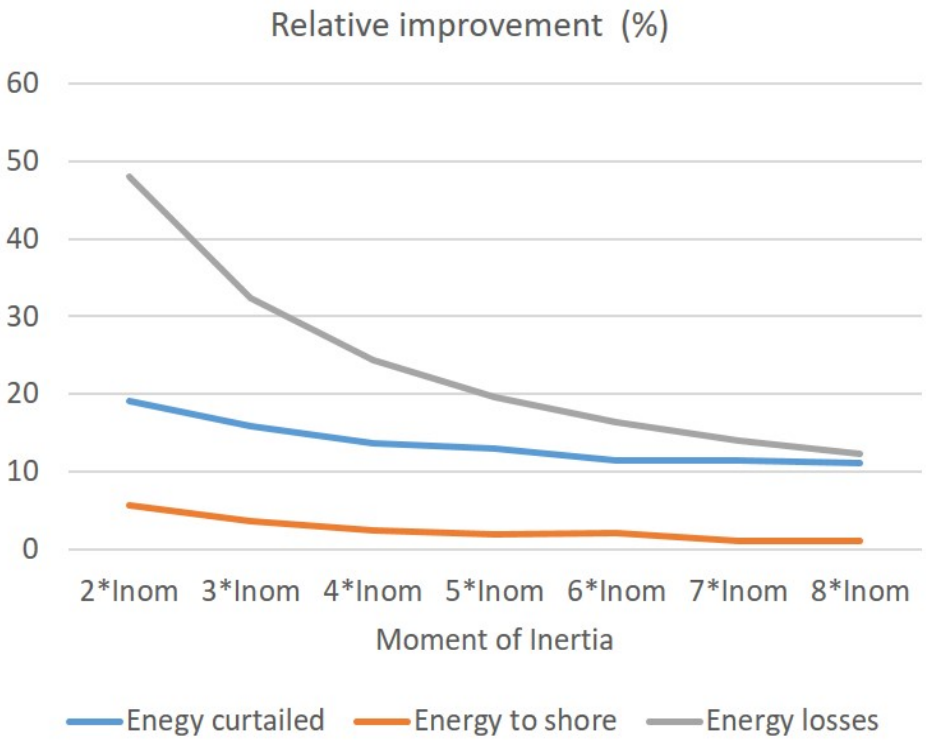

Fig. 4.33. KPIs' relative improvements

The optimal cylinder height is $h_{FW_{opt}} = 0.9 * h$, where h_{ref} is flywheel's height of the original prototype, $E_{FW_{max}}$ is the maximum energy delivered by the flywheel, and $I_{FW_{opt}}$ is the optimal moment of inertia of the device. The operating speed ranges from $\omega_{min} = 15krpm$ to $\omega_{max} = 30krpm$, respectively, with a minimum and maximum SOC of $SOC_{min} = 25\%$ and $SOC_{max} = 90\%$.

4.6.3. Valley filling using moving average process

Several power outputs improvements have been achieved by clustering WEC units, filtering the output farm power, and incorporating a KESS to the marine system. In the final step of the proposed novel approach for power output smoothening, a valley filling of the output signal is achieved using a moving average after the filtering stage; that is developed by a sliding window (see Figure 4.34). Moving average filtering (P_{MAve}) improves the Pref of the KESS unit. In this final step, the input reference to the flywheel is calculated as the difference between the output power of the WEC farm and the moving average output of the filtered signal, $P_{ref_{FW}} = P_{WEC_{farm}} - P_{MAve}$. In order to look for the optimal window length, three different times slots have been studied: window lengths of 1, 2 and 5 minutes.

Results shown in Table 4.3 demonstrate that a window length of 5 minutes improves the quality of KPIs, mainly the Peak/Mean ratio and nSD. Moreover, this duration can also minimize grid connection losses. Figure 4.35 shows a 5-minutes comparison between the

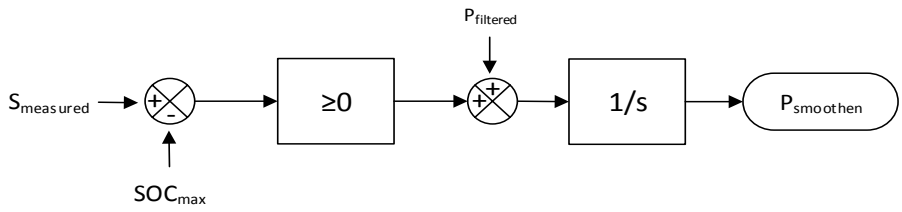

Fig. 4.34. Block diagram of the valley filling control process

power to shore with a filtered signal and three moving average window length studies. As it can be noted, using a moving average filter with a window length of 5 minutes can improve the smoothening of the power to shore signal.

	Peak P_{shore} (kW)	Mean P_{shore} (kW)	Peak/Ave. P_{shore}	Grid Losses (Wh)	Curtailed energy (kWh)	Energy to shore (kWh)	Normalized Standard Deviation
LP Filter + KESS	7.561	2.95	2.56	4.37	0.42	2.96	0.48
1-min WL	6.62	2.77	2.39	3.77	0.61	2.77	0.46
2-min WL	5.89	2.73	2.15	3.62	0.64	2.74	0.44
5-min WL	4.57	2.68	1.70	3.47	0.70	2.68	0.43

TABLE 4.3. WINDOW LENGTH STUDIES

4.6.4. Active power control

The above sections described both the filters and the flywheel that have been used to improve the LRS's output signal. This subsection analyses the capacity of the proposed hybrid wave-flywheel system for tracking a certain power set-point given by the grid operator. The blue-coloured curve in Figure 4.36 shows the WEC output power delivered to grid, while the red-coloured curve shows the power delivered by the grid-connected wave-flywheel set. It can be seen that the hybrid wave-flywheel system can deliver the 2-kW set-point established by the grid operator, and this occurs in 95% of the studied hour. When the figure is zoomed in, the power output of the WEC is shown in more detail, and it can be seen the power is delivered to the grid and the flywheel SOC (yellow curve). It can also be seen that at the time intervals in which the flywheel does not have enough stored energy, the hybrid installation is not capable of tracking the set-point established by the grid, and at this point, there is the need of regulating the energy stored in the flywheel.

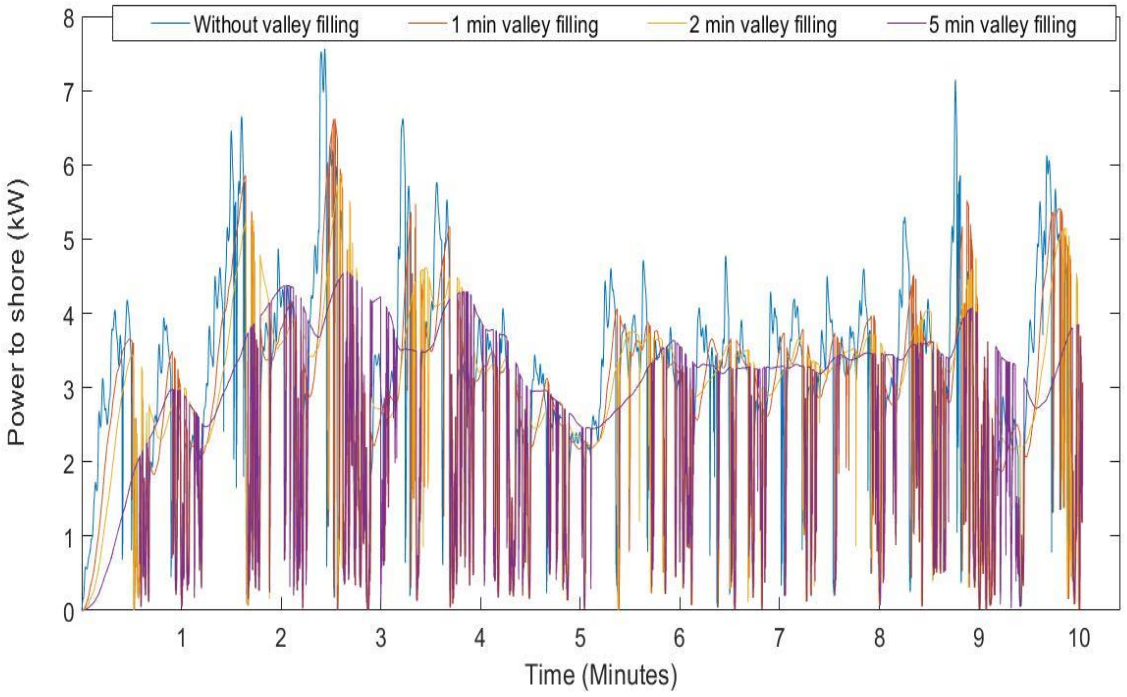

Fig. 4.35. Power to shore comparison for different window lengths

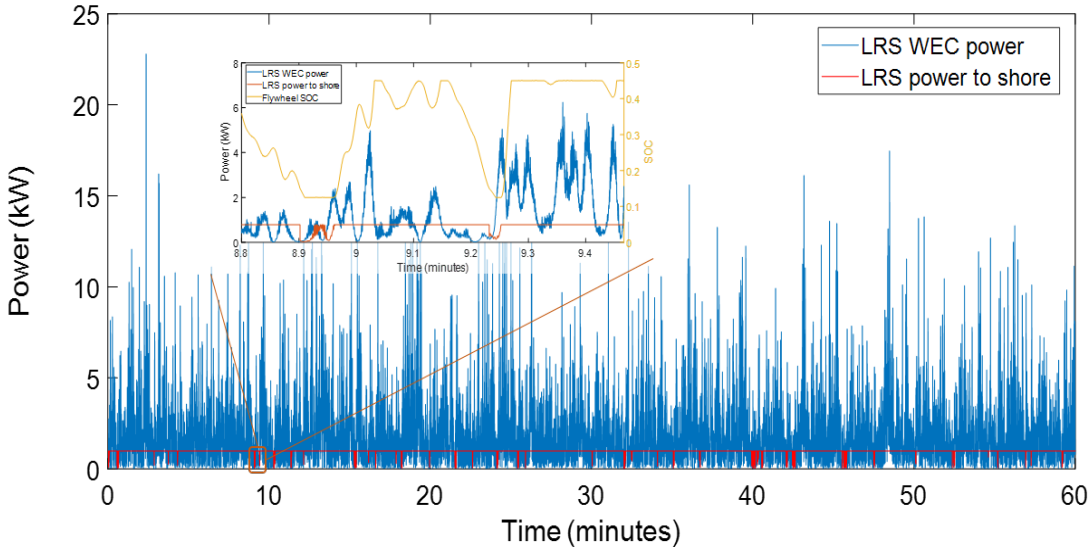

Fig. 4.36. Power-to-shore following a grid set-point

4.6.5. Discussion and conclusions

Table 4.4 summarizes the KPIs associated with the main studies throughout this section, and these KPIs have much to do with the improvement of LRS's power output.

	Peak P_{shore} (kW)	Mean P_{shore} (kW)	Peak/Ave. P_{shore}	Grid Losses (Wh)	Curtailed energy (kWh)	Energy to shore (kWh)	Normalized Standard Deviation
WEC clustering	45.58	3.41	13.39	8.84	–	3.40	0.96
WI	21.58	3.40	6.35	7.33	–	3.39	0.75
LPF at 256 Hz	9.23	2.52	3.66	12.72	–	2.51	0.58
KESS (3.18 kg.m^2)	9.23	2.91	3.17	4.37	0.36	2.92	0.49
5-min WL	4.56	2.68	1.71	3.47	0.70	2.68	0.44

TABLE 4.4. SUMMARIZED RESULTS FOR DIFFERENT SMOOTHENING STAGES

In analysing Table 4.1 and Table 4.4 the following conclusions can be obtained.

1. First aggregating a group of generators onto one cluster resulted in a dropped Peak/Average ratio and it improved nSD.

2. In addition, two clustered wave generators share the same magnitude order when peak values are referred to; this mean a notable increase of both energy losses and energy delivered to the grid (to shore). This can be seen from the results in Table 4.1 when the aggregation of Generators 2 and 3 was carried out.

3. Furthermore, the cut-off frequency of the low pass filter is critical for the smoothing process. The study found an optimal cut-off frequency, at 256 Hz, which not only filters the output power but also reduces the energy curtailment. Increasing the cut-off frequency of the filter above this optimal value does not decrease losses in the substation or flywheel, but it increases energy curtailment which it is not efficient.

4. Moreover, increasing the moment of inertia of the flywheel that is, increasing the cylinder height reports a considerable decrease of the energy curtailment. Nevertheless, a proper criterion in choosing the cylinder size could be based on the related improvement in the energy that is delivered to the shore and curtailed energy. This optimal value is achieved for a moment of inertia that is equal to 3.18 kg.m^2, which corresponds approximately to a flywheel size that is roughly 10% of the inverter's size.

5. In conclusion, regarding all the analysed KPIs, almost most of them are considerably decreased if the aforementioned smoothening techniques are carried out, such as peak power to shore, peak/mean power to shore ratio, normalized standard deviation and grid connection losses. This findings are a clear indicator of the effectiveness of the proposed simulated approach.

4.7. Summary

This chapter presented an analysis about the possibilities that wave energy can offer as a competitive renewable energy source, when it is compared to other renewable sources that are more conventional. Both the wave resource availability worldwide and the different components of a wave installation were given, including the power take off wave resource's and transformation devices, as well as the electricity generation from it. The chapter also described the equations that model the set that comprises point-absorber wave energy converter and a linear generator.

Wave generation is quite oscillating given the nature of its primary resource, and thus it is necessary to have a final stage of power/voltage output smoothening of these installations before grid-integration. Flywheels are found to be a good alternative for the smoothening process. This chapter investigated a state-of-the-art study related to flywheel technology, and this was done by indicating the different components that encompass the device and its modelling equations. It was confirmed that utilizing flywheel systems coupled to wave farms entails an improvement of the installation's power output, and the grid integration of this technology is improved accordingly.

It is worth highlighting that the developed models and control strategies have been applied to data from a wave emplacement located at the Lysekil Research Site. The chapter described the LRS, its location, the devices of the site, and the experienced evolution of the installation since its start-up in 2003.

To validate the methods and technologies developed in this chapter, real measurements gathered from the Lysekil Wave Farm were utilized in the proposed wave farm models and control strategies achieving the smoothening of the output power of this installation. The three stages are summarized as follows.

- In the first stage, a set of WECs was aggregated, and the aim was to improve the power output by means of the compensation of oscillations among the units of the wave farm. However, from the obtained results, it can be observed that the power quality after this first smoothening stage is not good enough for grid-integration purposes, which makes it necessary to develop other measures to compensate for these oscillations.

- In the second stage, a filter to the DC-link corresponding to the wave power system was incorporated, leading to the conclusion that a smoother power output is reached

when a low pass filter plus a zero order hold with a frequency of 256 Hz is coupled to the DC-link. The filter has been designed for the Lysekil Wave Farm.

– In the third stage, a flywheel with a charge/discharge control scheme was incorporated. This setup allowed the oscillating power of the system to be stored, and at the same time it also achieves power output smoothening. The energy stored inside the flywheel is the energy that comes after the low pass filter that was designed in the second stage. On the other hand, the optimum moment-of-inertia's magnitude for the experimental device developed by Uppsala University was determined. The study concluded that the optimum value is 3.18 kg.m^2, which allowed other characteristics of the flywheel device (e.g., disc's height) to be determined simultaneously.

– In the fourth final stage, a moving-average filter was used to improve the output signal that was delivered by the flywheel. In this aspect, a 5-minute window length filter was ascertained; in this time duration the quality of the power delivered to the grid was notably upgraded.

Finally, the study verified that the control scheme developed in the hybrid WEC-flywheel installation can control the reference power set-point that is established by the network operator to which it is connected.

5. ACTIVE CONTROL OF SMART GRIDS

5.1. Chapter introduction

The objective of this chapter is to develop a tool for the coordinated voltage control in MV and LV networks which allows to optimize the bidirectional power exchange between medium and low voltage levels and also the efficient DER operation on each voltage level.

To date, the proposed voltage control schemes have been centered on MV grids only. Traditionally, the voltage control in distribution grids have been carried out by regulating the On-Load Tap-Changers (OLTC) of Power Transformers located at the primary and secondary substations and by locally controlling the reactive power compensation devices and capacitor banks (CBs).

This chapter describes a new voltage control architecture based on the coordinated control structure that can be implemented at MV (primary substation) and LV (secondary substation) networks. Such a proposed control structure enables the flexible resources of LV grids to serve as a backup system to the MV grids, thus regulating the active/reactive power exchange among boundary nodes that are situated between both voltage levels.

The proposed coordinated control addresses the problems associated with decentralized schemes dimensioning and the inherent lack of communication among distributed systems. Results obtained after implementing the developed coordinated control tools will be compared to two other voltage control methods of a more traditional nature used in electrical networks, namely the methods of local decentralized and distributed control.

5.2. Voltage optimization and reactive power regulation

In the current process of evolution toward Smart Grids, the voltage control is encompassed within the energy efficiency upgrading of distribution power systems [197]–[199]. Voltage control in smart grids can be achieved by means of two different processes, namely Volt-Var control (VVC) and voltage optimization (VO).

1. VVC makes possible to have a local voltage control in the nodes where OLTCs and CBs are normally installed. The aim of the VVC is to keep grid node voltages within the established limits [7].

2. VO carries out an optimum coordination among the devices aimed for voltage control, such as OLTC units and reactive voltage sources (e.g., CBs, D-FACTS). The coordination among controllable units can be performed either in centralized or distributed mode.

From the point of view of voltage control, incorporating RES to the distribution power systems lays out two different situations to DSOs:

1. On the one hand, RES units are generation sources with a power output that can experience high variations in short time periods; this leads to voltage oscillations at grid nodes forcing to regulate voltage control dynamically [200], [201].

2. On the other hand, many RES units offer the possibility to regulate the injection of the reactive power they generate, so that this reactive power capacity regulation could be used as a voltage control element [201], [202].

5.2.1. Local decentralized voltage regulation

A local voltage control is usually applied at generation sources where the control unit takes voltage measurements at the generation connection point (PCC) to determine the working set-points of the controlled generator. Because the local control only employs the measurements gathered at the PCC and does not establish any communication with the DSO, it is considered to be a decentralized control, and it would be immune to failures occurring at the communication systems. However, because the actions carried out by the local control are oriented to solve voltage problems existing in the grid's connection point, the individual operation of the local controlled units can reach to non optimal network situations [202].

There are various types of grid codes and regulations that serve to establish interconnection and interoperability criteria for the RES units present in the distribution systems. Among these, the Standard IEEE 1547-2018 is one of the more relevant [66].

Figure 5.1 depicts the minimum requirements of the PQ curve that correspond to the RES units connected to the distribution systems, according to the IEEE 1547-2018. Three operation zones of the RES units that depend on the active power output of the installation can be differentiated.

- If $P_{gen} \leq 0.05 P_{rated}$, RES units do not inject or absorb reactive power.
- If $0.05 P_{rated} \leq P_{gen} \leq 0.2 P_{rated}$, RES units must be capable of at least injecting or absorbing between 11% and 44% of the rated apparent power of the installation (S_{rated}).
- If $P_{gen} \geq 0.2 P_{rated}$, the reactive power injection or power absorption of the RES units must be, at least, 44% of the rated apparent power of the installation (S_{rated}). Because it is not possible to exceed the generation capacity of the RES devices, power curtailment could be performed in these circumstances where delivering a higher amount of reactive power would be necessary. The active power curtailment will be carried out according to the reactive power voltage control that is used in the RES device.

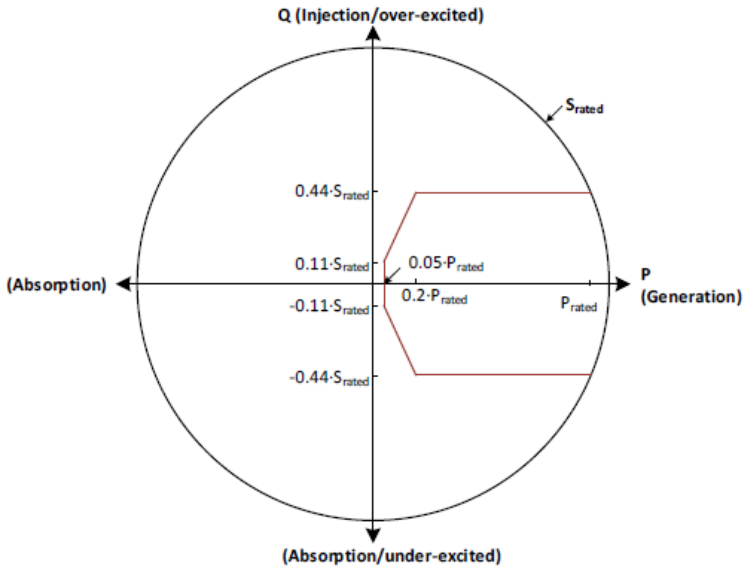

Fig. 5.1. Reactive power capabilities of RES units, category B, IEEE 1547-2018 standard [66]

In the normal operating conditions of the system, the IEEE Standard 1547-2018 establishes the operation characteristics and criteria of the RES units that are required to participate in the voltage control of the power system. Thus, for a high penetration of the RES units (IEEE 1547-2018 , Category B), such units must be capable of offering voltage control to the DSO based on five different mechanisms organized in two families according to several features, namely the utilized power used, whether they are active or reactive, and whether they perform the voltage control.

5.2.2. Voltage control by means of the Volt/Var reactive power control

IEEE Standard 1547-2018 establishes four methods to carry out voltage control by means of controlling the reactive power injected by the RES units. There are namely the constant power factor mode, the voltage-reactive power mode, the active/reactive power mode, and the constant reactive power mode.

- **Constant power factor mode**: the DSO imposes the power factor set-point of the RES units. This allows the possibility for voltage control at the RES connection point (PCC).
- **Constant reactive power mode**: the DSO establishes the reactive power injection/absorption set-point of each RES unit when a constant reactive power control is executed. The DSO would perform this while respecting the limits imposed by the PQ capability of the RES unit according to IEEE 1547-2018 standard as represented in Figure 5.1.

– **Voltage-reactive power mode**: in this operation mode, RES units can control its reactive power injection to the grid according to the voltage measurements at the RES connection point. The relationship between the voltage and reactive power is a continuous piecewise linear curve, as shown in Figure 5.2. Five zones are mainly distinguished:

- If $V_L \leq V_{bus} \leq V_1$, the RES unit must inject reactive power to the system with a value Q_1.
- If $V_1 \leq V_{bus} \leq V_2$, the RES unit must begin to linearly diminish its injected reactive power so that it reaches a voltage value V_2, from which, the reactive power contributed to the system by the RES unit is null.
- If $V_2 \leq V_{bus} \leq V_3$, the RES unit does not make any reactive power contribution to the system because the voltage at the connection node is close to the reference value.
- If $V_3 \leq V_{bus} \leq V_4$, the voltage measurement at the connection point is superior to its reference value. In this case, the RES unit must absorb reactive power to try to reduce the voltage value at the RES connection point.
- Finally, if If $V_4 \leq V_{bus} \leq V_H$, the RES unit must keep the reactive power absorption Q_4, which has a default value of $0.44.S_{rated}$(abs).

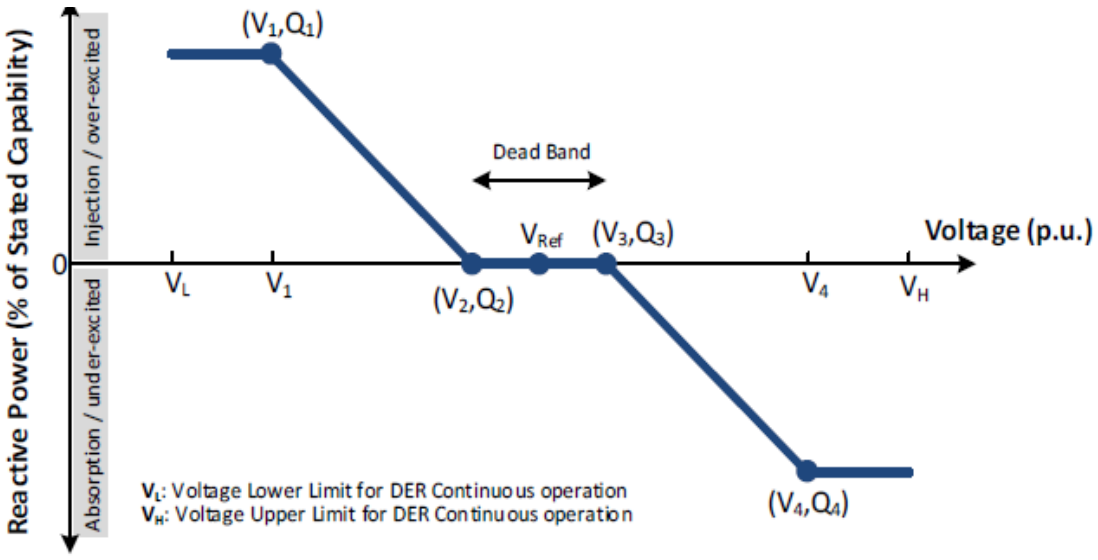

Fig. 5.2. Voltage-reactive power control mode [66]

Table 5.1 shows the values by default, as well as the range of values for each voltages that delimits the performance zones corresponding to the Volt/Var control, based on the voltage levels and limits established by the ANSI C 84.1 Standard [203].

Settings	Min. value	Default value	Max. value
V_{ref}	0.95* V_{nom}	V_{nom}	1.05* V_{nom}
V_1	$V_{ref} - 0.18 * V_{nom}$	$V_2 - 0.08 * V_{nom}$	$V_2 - 0.02 * V_{nom}$
Q_1	0	0.44*$S_{rated}(inj)$	S_{rated} (inj)
V_2	$V_{ref} - 0.03 * V_{nom}$	$V_{ref} - 0.02 * V_{nom}$	V_{ref}
Q_2	S_{rated} (abs)	0	S_{rated} (inj)
V_3	V_{ref}	$V_{ref} + 0.02 * V_{nom}$	$V_{ref} + 0.03 * V_{nom}$
Q_3	S_{rated} (abs)	0	S_{rated} (inj)
V_4	$V_3 + 0.02 * V_{nom}$	$V_{ref} + 0.08 * V_{nom}$	$V_{ref} + 0.18 * V_{nom}$
Q_4	S_{rated} (abs)	0.44*S_{rated} (abs)	0

TABLE 5.1. PERFORMANCE ZONES CORRESPONDING TO THE VOLT/VAR CONTROL

– **Active/reactive power mode**: In this control mode, the RES unit regulates the generation/absorption of reactive power according to the active power generation/absorption to the grid. Figure 5.3 portrays a continuous piecewise linear curve that represents the active/reactive operation mode established by the IEEE Standard 1547-2018. Similar to the voltage-reactive power control functioning mode, there are five working zones for the RES units as follows:

□ If $0 \leq P_{gen} \leq P_2$, the RES unit does not deliver any reactive power to the system.

□ If $P_2 \leq P_{gen} \leq P_3$, the RES units must begin to absorb the reactive, following a linear relation between both the active and reactive power output of the RES units.

□ Lastly, if $P_{gen} \geq P_3$, the reactive power absorbed by the RES units must be kept constant at a value Q_3.

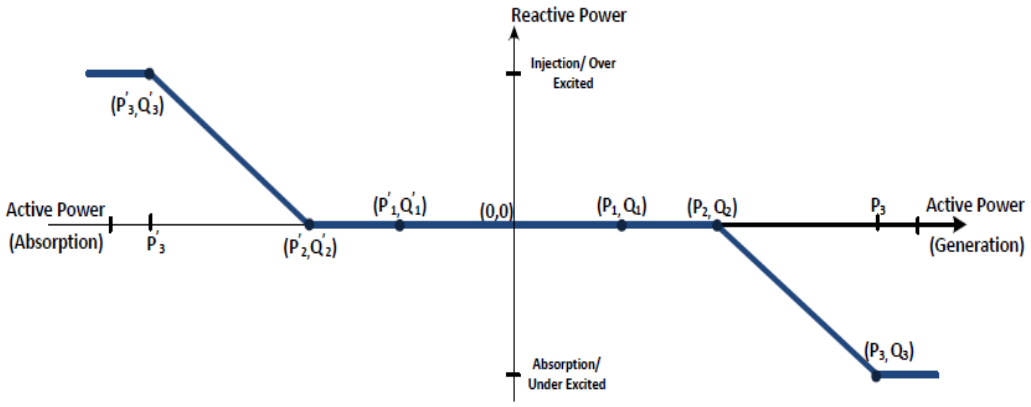

Fig. 5.3. Active-reactive power control mode [66]

Table 5.2 summarizes the default and admissible range of power values P_2, P_3 and Q_3 as established by the IEEE Standard 1547-2018, and are based on the voltage levels and limits imposed by the ANSI C Standard 84.1 [203].

Settings	Min. value	Default value	Max. value
P_2	$0.4{*}P_{rated}$	$0.5{*}P_{rated}$	$0.8{*}P_{rated}$
P_3	$P_2 + 0.1 * P_{rated}$	P_{rated}	P_{rated}
Q_3	S_{rated}(abs)	$0.44{*}S_{rated}$(abs)	S_{rated}(inj)

TABLE 5.2. ACTIVE POWER-REACTIVE POWER SETTINGS FOR NORMAL OPERATING PERFORMANCE, CATEGORY B - RES

5.2.3. Voltage control by means of the Volt/Watt active power control

The DSO can request the RES units to regulate its active power injection according to the voltage value at the RES connection point. Figure 5.4 shows the linear relation between the voltage and the active power output of a RES generation unit.

- If $V_{bus} \leq V_1$, RES units may inject to the grid all its available power generation capacity.
- If $V_1 \leq V_{bus} \leq V_2$, RES units must linearly reduce the active power that is injected to the system until a value V_2 is reached.
- If $V_{bus} \geq V_2$, the RES unit must keep the injected active power to the minimum value that is established by the IEEE Standard 1547-2018.

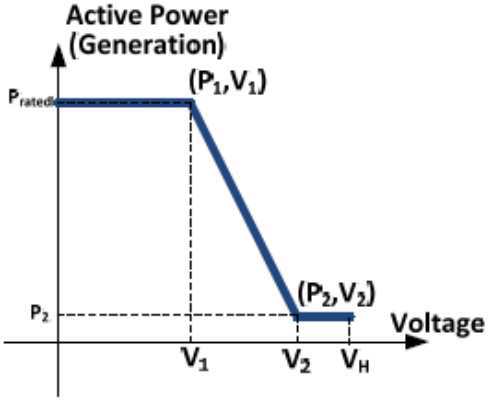

Fig. 5.4. Active power-voltage control mode [66]

Table 5.3 depicts the limit values and default values as established by the IEEE 1547-2018. These correspond to the active power-voltage control mode and are based on the voltage levels and limits imposed by the ANSI C 84.1 [66], [203].

Settings	Min. value	Default value	Max. value
V_1	$1.05 * V_{nom}$	$1.06 * V_{nom}$	$1.09 * V_{nom}$
P_1	N/A	P_{rated}	N/A
V_2	$V_1 + 0.1 * V_{nom}$	$1.1 * V_{nom}$	$1.1 * V_{nom}$
P_2	P_{min}	$\min(0.2 * P_{rated}, P_{min})$	P_{rated}

TABLE 5.3. VOLTAGE-ACTIVE POWER SETTINGS FOR CATEGORY B RES [66]

Grid-connection requirements established by the IEEE 1547-2018 for the RES units allows these to present themselves to the DSOs as a new voltage control elements. The voltage-reactive power, active/reactive power and active power-voltage control modes allow RES units to perform a decentralized local control, which occurs when there is lack of communication between RES units and the DSO.

5.2.4. Local decentralized voltage control applied in MV networks with RES penetration

Among the local decentralized control modes established by the IEEE Standard 1547-2018, the voltage-reactive power control mode is selected to perform voltage local control on the RES units that are connected to MV grids.

To set the linear relations between the voltage at point connection of the RES units and their reactive power output, the following steps are taken. Firstly, the study uses the limits imposed by the capacity curves of both wind turbines and PV units developed in Chapter 3 (see Figures 3.11 and 3.14, respectively). Secondly, piecewise linear curve defines the RES reactive power output injection/absorption according to the voltage at the RES connection point according to the IEEE 1547-2018 (see Figure 5.3). Finally, the voltage limits have been stated to the ones standardized by the Spanish regulation, which considers an admissible voltage margin of ±5% with respect to the rated voltage [204]. Eqs. (5.1) and (5.2) gives the local reactive power regulation proposed for wind and PV units located in the MV grids, respectively.

$$Q_{output_{WT}} = \begin{cases} \alpha_1^{WT} * S_{rated}(inj) & V_{bus} \leq 0.96 * V_{nom} \\ m_1^{WT} * (V_{bus} - 0.96 * V_{nom})(inj) & 0.96 * V_{nom} \leq V_{bus} \leq 0.98 * V_{nom} \\ 0 & 0.98 * V_{nom} \leq V_{bus} \leq 1.02 * V_{nom} \\ m_2^{WT} * (V_{bus} - 1.02 * V_{nom})(abs) & 1.02 * V_{nom} \leq V_{bus} \leq 1.04 * V_{nom} \\ \alpha_2^{WT} * S_{rated}(abs) & V_{bus} \geq 1.04 * V_{nom} \end{cases} \quad (5.1)$$

Where:

- $\alpha_1^{WT} = 0.48$ it is the coefficient used to determine the maximum reactive power injection,

- $m_1^{WT} = 24$ it is the slope of the piecewise linear curve between V_1 and V_2 (see Figure 5.3),
- $m_2^{WT} = 50$ it is the slope of the piecewise linear curve between V_3 and V_4 (see Figure 5.3),
- $\alpha_2^{WT} = 1$ it is the coefficient used to determine the maximum reactive power absorption.

$$Q_{output_{PV}} = \begin{cases} \alpha_1^{PV} * S_{rated}(inj) & V_{bus} \leq 0.96 * V_{nom} \\ m_1^{PV} * (V_{bus} - 0.96 * V_{nom})(inj) & 0.96 * V_{nom} \leq V_{bus} \leq 0.98 * V_{nom} \\ 0 & 0.98 * V_{nom} \leq V_{bus} \leq 1.02 * V_{nom} \\ m_2^{PV} * (V_{bus} - 1.02 * V_{nom})(abs) & 1.02 * V_{nom} \leq V_{bus} \leq 1.04 * V_{nom} \\ \alpha_2^{PV} * S_{rated}(abs) & V_{bus} \geq 1.04 * V_{nom} \end{cases} \quad (5.2)$$

Where:

- $\alpha_1^{PV} = 0.44$ it is the coefficient used to determine the maximum reactive power injection,
- $m_1^{PV} = 22$ it is the slope of the piecewise linear curve between V_1 and V_2 (see Figure 5.3),
- $m_2^{PV} = 40$ it is the slope of the piecewise linear curve between V_3 and V_4 (see Figure 5.3),
- $\alpha_2^{PV} = 0.8$ it is the coefficient used to determine the maximum reactive power absorption.

5.2.5. Local decentralized voltage control in LV networks with RES penetration

In the voltage control of the LV grids, the available RES units are regarded as small-sized PV units that have the capacity of regulating their active/reactive power injection to the grid at the connection point according to the voltage-active voltage control mode. Considering that LV grids are characterized by presenting a greater R/X line ratio (see Chapter 3), it is possible that the regulation of the active power injected to the grids has a stronger influence on the voltage control than reactive power regulation. Because of this, the voltage-active power control mode defined by the IEEE 1547-2018 is applied for active power regulation on the RES units present in the LV grids, according to the Figure 5.4. For the proposed local control on the LV systems under study, the linear relation

between the PV installations' active power output and the voltage at the connection node of the same is given by (5.3).

$$P_{output_{PV}} = \begin{cases} P_{rated} & V_{bus} \leq 1.04 * V_{nom} \\ m_{LV} * (V_{bus} - 1.04 * P_{rated}) & 1.04 * V_{nom} \leq V_{bus} \leq 1.05 * V_{nom} \\ 0 & V_{bus} \geq 1.05 * V_{nom} \end{cases} \tag{5.3}$$

where $m_{LV} = 10$ is the coefficient used to determine the slope of the line that relates the active power output of the RES unit to the voltage at the connection point.

5.2.6. Distributed voltage optimization

It is possible to coordinate the operation set-points of each one of the controllable devices, according to certain grid optimization criteria in those cases where there is a communication architecture between the RES control equipment and the DSO control center. In this situation, grid optimization is performed independently for each voltage level according to certain grid optimization criteria (e.g., minimizing losses, improving voltage profiles, and diminishing the number of the transformers' tap changes). Traditionally, HV transmission networks regard MV distribution power networks as non-controllable load/-generation, connected at the primary substations between both power grids. For the case of MV distribution grids, the HV transmission power network is represented as a voltage source that feeds the grid of the lower voltage level [205].

In the case of MV and LV grids, the same working principle applies. The MV grid voltage control optimizes the operation of its controllable devices by considering the consumption/generation of the LV grids as non-controllable. Likewise, in the LV grid, the voltage control optimizes the controllable devices connected to the same grid.

The optimization procedure proposes a voltage control scheme namely the distributed voltage optimization as two independent optimization sub-problems:

- **MV grid optimization**: the optimization is achieved by means of determining the working set-points of the controllable devices that are present in the MV grid. This is done so that the voltage at its nodes keeps within the established limits according to certain optimization criteria defined for the MV network. When MV grids are being optimized, the LV grids are represented as a load/generation and their value is the one recorded by the measurement stations in the border knots between both networks.
- **LV grid optimization**: the algorithm here aims to coordinate the working set-points of the controllable devices of the grid (e.g., OLTC, CB, RES) that are present in the LV network, which allows the voltage within the established limits to be maintained.

The MV grid control for voltage optimization is set according to (5.4):

$$\begin{aligned} \min \quad & f_{MV}(\boldsymbol{u_{MV}}, \boldsymbol{x_{MV}}) \\ \text{s.t.} \quad & g_{MV}(\boldsymbol{u_{MV}}, \boldsymbol{x_{MV}}, \boldsymbol{\Omega_{LV}}) = 0 \\ & h_{MV}(\boldsymbol{u_{MV}}, \boldsymbol{x_{MV}}) \geq 0 \end{aligned} \tag{5.4}$$

Where:

- $\boldsymbol{u_{MV}}$ represents the state variables' vector of the MV systems.
- $\boldsymbol{x_{MV}}$ represents the state variables' vector of the MV systems.
- $\boldsymbol{\Omega_{LV}}$ is the vector that contains the aggregated power demand of the LV networks connected to the MV network, and it can be obtained either by real-time measurements at the secondary substation or by forecasting techniques.
- $\boldsymbol{g_{MV}}$ represents the equality constraints associated with the resolution of load flows of the MV grids.
- $\boldsymbol{h_{MV}}$ represents the inequality constraints associated with the operation limits of the controllable devices that are present in the MV grids.

For the LV grid's voltage optimization purposes, (5.5) is used:

$$\begin{aligned} \min \quad & f_{LV_D}(\boldsymbol{u_{LV_D}}, \boldsymbol{x_{LV_D}}) && D = 1...N_{LV} \\ \text{s.t.} \quad & g_{LV}(\boldsymbol{u_{LV_D}}, \boldsymbol{x_{LV_D}}) = 0 && D = 1...N_{LV} \\ & h_{LV}(\boldsymbol{u_{LV_D}}, \boldsymbol{x_{LV_D}}) \geq 0 && D = 1...N_{LV} \end{aligned} \tag{5.5}$$

Where:

- $\boldsymbol{u_{LV}}$ represents the state variables' vector of the LV systems.
- $\boldsymbol{x_{LV}}$ represents the state variables' vector of the LV systems.
- $\boldsymbol{g_{LV}}$ represents the equality equations associated with the resolution of load flows of the LV grids.
- $\boldsymbol{h_{LV}}$ represents the inequality equations associated with the operation limits of the controllable devices that are present in the LV grids.
- D represents a LV system and N_{LV} the number of LV systems connected to the LV network.

In this thesis the proposal of the distributed voltage control scheme it is based on two optimization independent process where nodal voltage will be considered as the state variables, while the controlling signals will be the set-points of the controllable devices

connected to MV and LV networks. High fluctuations in the nodal voltages of the power systems entail high energy losses in the power system. Because of this, power losses minimization is one of the main objectives to be achieved in the voltage control schemes, and this is used in the distributed control scheme proposed in this chapter for the optimization of both MV and LV grids [206].

As can be seen from (5.4) and (5.5), MV and LV grid optimization schemes are working independently. The only information that MV and LV grids interchange is either the real-time measurements or the forecasted load/generation at the secondary substations.

5.3. Coordinated voltage optimization

5.3.1. Introduction

In recent years, distribution power systems have faced a new paradigm in which voltage problems and bi-directional power flow appear as a consequence of the incorporation of DG units [202], [207], [208]. The interest for decarbonization has also come to LV systems, and more consumers of these grids are becoming prosumers that is, elements of the power systems capable of consuming and generating electricity produced through small-scaled PV generation systems [209]. Consequently, DSOs are finding overvoltage problems in LV grids at time intervals in which PV generation increases and LV demand is low, which occurs at central hours on the day [210].

Similarly with the interconnection problems between MV and HV grids [211], the over-voltage problem that is manifested in the LV grids with the increment of the LV grids' microgeneration units is translated to the MV grids. Besides, there will also be an injection of power in the border nodes shared by the MV-LV networks where there would traditionally be energy demand or exportation from the MV grids toward the LV grids [197], [212], [213].

From the above, it is necessary to coordinate the functioning of the LV and MV units so that the LV units can offer ancillary services to the MV grid [201], [213].

The possibility of controlling LV grids in terms of voltage and power flows would allow such grids to become a new controllable energy resource at the (MV-LV) [213]. This new flexibility offered by the LV grids allows them to bid to DSO the utilization of the energy required from LV grids to address active/reactive power requirements in the MV network.

This new vision of the LV grids as a flexibility resource for the MV grids makes if possible to improve the performance of both networks and to reduce the number of operations to be performed over the conventional voltage control devices that are connected to the MV grids, thus maximizing the lifespan of the same devices [202], [214]. Under these new operative conditions it is necessary to establish a major coordination among MV and LV grids, because the aforementioned traditional control schemes are not able to offer the

possibility of a coordinated management between both voltage levels [205].

In this new distribution network concept, it is necessary to supply DSOs with tools that are capable of adequately managing the future systems. By doing this, the new generation units can be integrated under safe and stable operative conditions, and this would improved the power quality and security of the energy delivered to end-users [198], [202].

As from the mentioned above, this thesis proposes a new coordinated voltage control algorithm to be applied among MV and LV grids that allow LV networks to offer ancillary services to the MV grid. The voltage control will be carried out by means of two processes, namely the coordinated voltage control of MV grids (CVC-MV) and the coordinated Voltage Control of the LV grids (CVC-LV).

- **CVC-MV**. Firstly, the optimum PQ assignation of the RES units that are present in the MV grid is determined, as well as the required optimum flexibility in the border nodes between the MV grid and LV networks. This is done by means of the CVC-MV algorithm.
- **CVC-LV**. Secondly, the optimum assignation of the RES units that are present in the LV systems is established; this is done based on the required flexibility setpoint determined by the upper level in the border node (MV-LV) using the CVC-LV algorithm. The MV system is regarded by the CVC-LV as an energy source with a required voltage reference signal at the secondary substation (MV-LV) and a required exchange flexibility signal at the secondary substation (between MV and LV networks).

5.3.2. Theoretical mathematical description

5.3.2.1. Coordinated power flow equations

An electric system can be represented as a graph $\mathcal{G}(\mathcal{N}, \mathcal{E})$, where $\mathcal{N}$={1,. . . ,n} denotes the system's nodes and $\mathcal{E} \subseteq \mathcal{N}x\mathcal{N}$ makes reference to the lines connecting such nodes. Eqs. (5.6) and (5.7) allow the power flow along the lines of a power system to be calculated.

$$P_i - V_i \sum_j V_j(G_{ij}cos(\theta_i - \theta_j) + B_{ij}sin(\theta_i - \theta_j)) = 0 \quad \forall i, j \in \mathcal{N} \tag{5.6}$$

$$Q_i - V_i \sum_j V_j(G_{ij}sin(\theta_i - \theta_j) - B_{ij}cos(\theta_i - \theta_j)) = 0 \quad \forall i, j \in \mathcal{N} \tag{5.7}$$

Where:

- P_i is the active power balance demanded at the node i^{th}.
- Q_i is the reactive power balance demanded at the i^{th} node.

– V_i and θ_i are the module and phase of the nodal voltage at the bus i^{th}.

– V_j and θ_j are the module and phase of the nodal voltage at the bus j^{th}.

– G_{ij} and B_{ij} are the conductance and susceptance of the line that connects the node i^{th} with the node j^{th}.

The power balance in a node can be calculated according to (5.8) and (5.9):

$$P_i = P_{l_i} - P_{g_i} \quad 0 \,\forall i \in \mathcal{N} \tag{5.8}$$

$$Q_i = Q_{l_i} - Q_{g_i} \quad 0 \,\forall i \in \mathcal{N} \tag{5.9}$$

Where:

– P_{l_i} is the active power demanded in the node i^{th}.

– Q_{l_i} is the reactive power demanded in the node i^{th}.

– P_{g_i} is the active power generated in the node i^{th}.

– Q_{g_i} is the reactive power generated in the node i^{th}.

Let us consider a power system that comprise a MV network, where there are connected a D number of LV grids (see Figure 5.5) and, where $\mathcal{N}_{MV}$ and $\mathcal{N}_{LV}$ represent the set of nodes of the MV and LV systems, respectively, being $\mathcal{N}_{MV}, \mathcal{N}_{LV} \subseteq \mathcal{N}$. The set of nodes that are found to be in the border between both systems will be denote with the set $\mathcal{N}_b \subseteq \mathcal{N}$ (boundary MV-LV, Figure 5.5). The red arrows depict the bi-directional power flows exchange in the border nodes between the LV grids and the MV grid, being S_i^b the complex power exchanged between the MV grid and each LV grid. Because of the incorporation of generation units to the LV grids, the power flow exchange in the border nodes can be bidirectionally, that is, from the MV toward the LV grid and vice versa.

The pairs (P_i^{MV}, Q_i^{MV}) and (P_i^{LV}, Q_i^{LV}) represent the active and reactive power flexibility exchange required in the border node i_{th}, which can be calculated by means of the conventional power flow equations from (5.10) to (5.13). These are applied to each of the MV and LV systems respectively, where the node $i \in \mathcal{N}_b$ (being $\mathcal{N}_b \subset \mathcal{N}_{MV}$ and $\mathcal{N}_b \subset \mathcal{N}_{LV}$), and Y_{ij} represents the admittance of the line that connects the node $i - j \in \mathcal{E}$.

$$P_i^{MV}(t) - Re\left(V_i(t) \sum_{j \in \mathcal{N}_{MV}} V_j^*(t) Y_{ij}^*\right) = 0 \quad \forall i \subset \mathcal{N}_b \tag{5.10}$$

$$Q_i^{MV}(t) - Im\left(V_i(t) \sum_{j \in \mathcal{N}_{MV}} V_j^*(t) Y_{ij}^*\right) = 0 \quad \forall i \subset \mathcal{N}_b \tag{5.11}$$

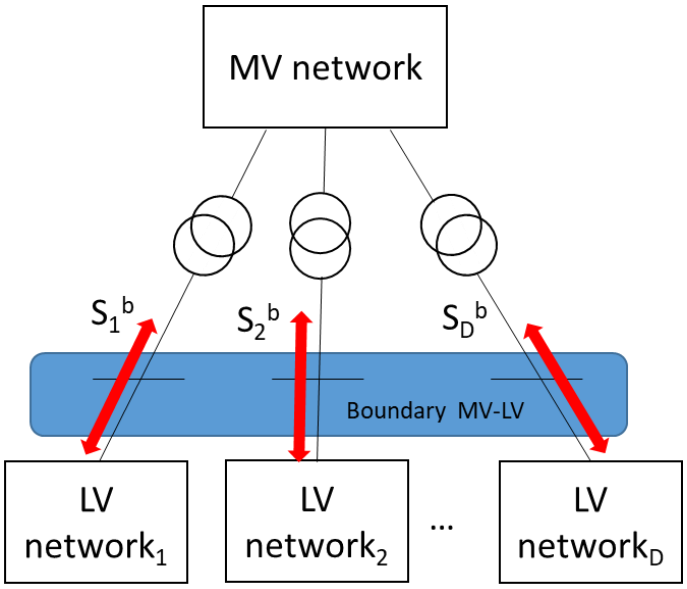

Fig. 5.5. Information and power exchanged in distribution networks

$$P_i^{LV}(t) - Re\left(V_i(t)\sum_{j\in\mathcal{N}_{LV}} V_k^*(t)Y_{ij}^*\right) = 0 \quad \forall i \subset \mathcal{N}_b \tag{5.12}$$

$$Q_i^{LV}(t) - Im\left(V_i(t)\sum_{j\in\mathcal{N}_{LV}} V_k^*(t)Y_{ij}^*\right) = 0 \quad \forall i \subset \mathcal{N}_b \tag{5.13}$$

The MV set of nodes ($\mathcal{N}_{MV}$) can be split into two different sets: the one composed by the border nodes between the MV grid and the LV grids ($\mathcal{N}_b$) and the other one composed by the rest of the nodes ($\mathcal{N}_{MV}^*$). Consequently, the power exchange across the MV system lines, excluding the border nodes, can be expressed according to (5.14) and (5.15).

$$P_i^{MV}(t) - Re\left(V_i(t)\sum_{j} V_j^*(t)Y_{ij}^*\right) - Re\left(V_i(t)\sum_{k\in\mathcal{N}_b} V_k^*(t)Y_{ik}^*\right) = 0 \quad \forall i,j \subset \mathcal{N}_{MV}^* \tag{5.14}$$

$$Q_i^{MV}(t) - Im\left(V_i(t)\sum_{j} V_j^*(t)Y_{ij}^*\right) - Im\left(V_i(t)\sum_{k\in\mathcal{N}_b} V_k^*(t)Y_{ik}^*\right) = 0 \quad \forall i,j \subset \mathcal{N}_{MV}^* \tag{5.15}$$

Analogously, by decomposing the set of nodes belonging to the D_{th} LV system $\mathcal{N}_{LV_D}^*$ in two sub-sets: one composed by the i_{th} node corresponding to the boundary with the MV grid ($k \in \mathcal{N}_b$) and the other one composed by the rest of the downstream nodes $\mathcal{N}_{LV_D}^*$, the power flow equations in the LV network (excluding the border node) can be formulated

according to (5.16) and (5.17).

$$P_i^{LV}(t) - Re\left(V_i(t)\sum_j V_j^*(t)Y_{ij}^*\right) - Re\left(V_i(t)\sum_{k\in\mathcal{N}_b} V_k^*(t)Y_{ik}^*\right) = 0 \quad \forall i, j \subset \mathcal{N}_{LV}^* \tag{5.16}$$

$$Q_i^{LV}(t) - Im\left(V_i(t)\sum_j V_j^*(t)Y_{ij}^*\right) - Im\left(V_i(t)\sum_{k\in\mathcal{N}_b} V_k^*(t)Y_{ik}^*\right) = 0 \quad \forall i, j \subset \mathcal{N}_{LV}^* \tag{5.17}$$

Lastly, the power exchange between the MV and LV grids can be calculated by (5.18) and (5.19), where P_i^b and Q_i^b represent the balance of the power demanded in the border node i at a instant of time t.

$$\begin{aligned} P_i^b(t) - Re\left(V_i(t)\textstyle\sum_{j\in\mathcal{N}_{MV}^*} V_j^*(t)Y_{ij}^*\right) - Re\left(V_i(t)\textstyle\sum_{j\in\mathcal{N}_b} V_j^*(t)Y_{ij}^*\right) \\ -Re\left(V_i(t)\textstyle\sum_{k\in\mathcal{N}_{LV}^*} V_k^*(t)Y_{ik}^*\right) = 0 \quad \forall i \subset \mathcal{N}_b \end{aligned} \tag{5.18}$$

$$\begin{aligned} Q_i^b(t) - Im\left(V_i(t)\textstyle\sum_{j\in\mathcal{N}_{MV}^*} V_j^*(t)Y_{ij}^*\right) - Im\left(V_i(t)\textstyle\sum_{j\in\mathcal{N}_b} V_j^*(t)Y_{ij}^*\right) \\ -Im\left(V_i(t)\textstyle\sum_{k\in\mathcal{N}_{LV}^*} V_k^*(t)Y_{ik}^*\right) = 0 \quad = 0 \quad \forall i \subset \mathcal{N}_b \end{aligned} \tag{5.19}$$

Finally, (5.14) to (5.19), represent the set of equations that correspond to the power flows across the network lines (MV and LV), and the power exchange between both systems at the border node (secondary substation).

5.3.2.2. Coordinated management optimization

The objective of the coordinated control strategy over the MV and LV grids is to improve their operation in both normal and abnormal working conditions (contingencies). This involves employing the flexibility offered by the RES units that are present in both voltage levels. The participation of the RES units of the LV systems allow them to provide the MV grids with flexibility in the exchanged power through the border node between both networks. This flexibility of the LV systems can be expressed as (5.20):

$$S_b = P_b + j * Q_b = |S_b|\angle_{\theta_b} \quad \forall b \subset \mathcal{N}_b \tag{5.20}$$

The formulation of the coordinated optimization problem of the MV and LV networks

is shown in (5.21):

$$\begin{aligned} \min \quad & f_{MV}(\boldsymbol{u_{MV}}, \boldsymbol{x_{MV}}, \boldsymbol{\Omega_{LV}}) + \sum_{D} f_{LV_D}(\boldsymbol{u_{LV}}, \boldsymbol{x_{LV}}, \boldsymbol{\Omega_{MV}}) \qquad D = \quad 1...N_{LV} \\ \text{s.t.} \quad & g(\boldsymbol{u}, \boldsymbol{x}, \boldsymbol{\Omega}) \;=\; 0 \\ & h(\boldsymbol{u}, \boldsymbol{x}) \;\geq\; 0 \end{aligned} \tag{5.21}$$

Where (5.21) shows the objective function of the coordinated voltage optimization problem of the distribution grids, which comprises the MV grid optimization and the LV grid optimization. The equality constraints of (5.21)) correspond to the load flow equations of the MV-LV grids, as well as the set of constraints in the boundary node in (5.19) to (5.24). On the other hand, the inequality constraints of (5.21) are associated with a number of factors, namely the operation limits of the controllable devices connected to the distribution grid, the thermal limits of lines and transformers, and the voltages on the nodes of the MV-LV grids. The sets $\boldsymbol{u}$ and $\boldsymbol{x}$ gather the state and control MV-LV variables, respectively. The set $\boldsymbol{\Omega}$ represents the information interchanged among the MV and LV grids, and it is composed of the flexibility required by the MV system to the LV systems, according to (5.22).

$$\boldsymbol{\Omega} = [P_b, cos(\theta_b)] \quad \forall b \subset \mathcal{N}_b. \tag{5.22}$$

The objective function (5.21) can be divided into $D + 1$ subproblems:

- A subproblem corresponding to the optimization of the MV grid that can be expressed according to the objective function in (5.23).

$$\begin{aligned} \min \quad & f_{MV}(\boldsymbol{u_{MV}}, \boldsymbol{x_{MV}}, \boldsymbol{\Omega}) \\ \text{s.t.} \quad & g_{MV}(\boldsymbol{u_{MV}}, \boldsymbol{x_{MV}}) \;=\; 0 \quad \forall MV \subset \mathcal{N}^*_{MV} \\ & h_{MV}(\boldsymbol{u_{MV}}, \boldsymbol{x_{MV}}) \;\geq\; 0 \quad \forall MV \subset \mathcal{N}^*_{MV} \\ & g_b(\boldsymbol{u_b}, \boldsymbol{x_{MV}}, \boldsymbol{x_{LV}}, \boldsymbol{x_b}, \boldsymbol{\Omega}) \;=\; 0 \quad \forall b \subset \mathcal{N}_b \\ & h_b(\boldsymbol{u_b}, \boldsymbol{x_b}) \;\geq\; 0 \quad \forall b \subset \mathcal{N}_b \end{aligned} \tag{5.23}$$

- D subproblems corresponding to the optimization of the LV networks which can be expressed according to the objective function in (5.24), where $\boldsymbol{\Omega_D}$ is the flexibility requested by the MV network to the Dth LV grid.

$$\begin{aligned} \min \quad & f_{LV_D}(\boldsymbol{u_{LV_D}}, \boldsymbol{x_{LV_D}}) & & & D = \quad 1...N_{LV} \\ \text{s.t.} \quad & g_{LV_D}(\boldsymbol{u_{LV_D}}, \boldsymbol{x_{LV_D}}) & = 0 \quad & \forall LV \subset \mathcal{N}^*_{LV} & D = \quad 1...N_{LV} \\ & h_{LV_D}(\boldsymbol{u_{LV_D}}, \boldsymbol{x_{LV_D}}) & \geq 0 \quad & \forall LV \subset \mathcal{N}^*_{LV} & D = \quad 1...N_{LV} \\ & h_{b_D}(\boldsymbol{u_{b_D}}, \boldsymbol{x_{b_D}}) & = \Omega_D \quad & \forall b \subset \mathcal{N}^*_b & D = \quad 1...N_{LV} \end{aligned} \tag{5.24}$$

5.3.3. Coordinated structure

The voltage control proposed in this chapter establishes a coordination among the MV grid and the different LV grids connected to the MV grid. Between both controls centers, information will be exchanged regarding to the required power flexibility exchange between the two networks, as well as the voltage set-point at the boundary point between both networks.

Figure 5.6 depicts the scheme of the proposed coordinated control structure. In this figure, the dotted blue lines represent the flow of information of the data corresponding to the power load measurements, as well as the measurements of the power generated by the DG units of both MV and LV systems. The information relative to the consumption and generation in the MV grid is measured and stored in the corresponding SCADA system, while for the LV grids the informations is stored in LV data servers. The DMS of the MV grid oversees a number of tasks, such as carrying out the generation and demand forecasting in the MV grid, as well as the state estimation of the grid from the measurements stored onto the SCADA system. From this information, the DMS executes the coordinated voltage control (CVC) that corresponds to the MV grid so that the working set-points of the devices in charge of undertaking the CVC in such a grid can be determined, as well as the required flexibility in the border nodes shared with the LV grid. The working set-points of the MV grid's RES and the set-points at the boundary nodes are sent to both the corresponding devices and the DMS of the LV networks (DMS-LV), which are represented in Figure 5.6 with dotted red lines. Each DMS-LV uses the generation and demand forecasts that correspond to the PV units and loads that are in each network; it also uses the required flexibility information in the border node with the MV grid, that is given by the CVC-MV in order to execute the CVC-LV and to determine the working set-points of both PV units and CBs.

The flowchart of the proposed CVC is shown in Figure 5.7. The orange-shadowed elements correspond to the MV grid voltage control, and the green-shadowed elements refer to the LV grid voltage control.

The CVC is executed when an activation signal is send either from the DSO-MV or from a programmed sequence. The algorithm starts with the optimization of the MV grid. The MV grid voltage control requires their corresponding data to be loaded, as well as the generation and demand forecast in all the nodes of the grid by the time horizon, in which it would be necessary to perform the voltage control. The execution of the MV-VO provides various information namely the working set-points of the RES units that are present in the MV grid, the set-points in the border nodes among the MV grid and each of the LV grids in terms of flexibility in the power exchange, and the voltage reference signal at each border node. All these MV-VO outputs are stored while the CVC for each LV grid is performed ($CVC - LV_D$).

The CVC-LV is executed for each LV grid connected to the MV network. In each LV grid, the CVC-LV loads the information corresponding to the grid, the generation and

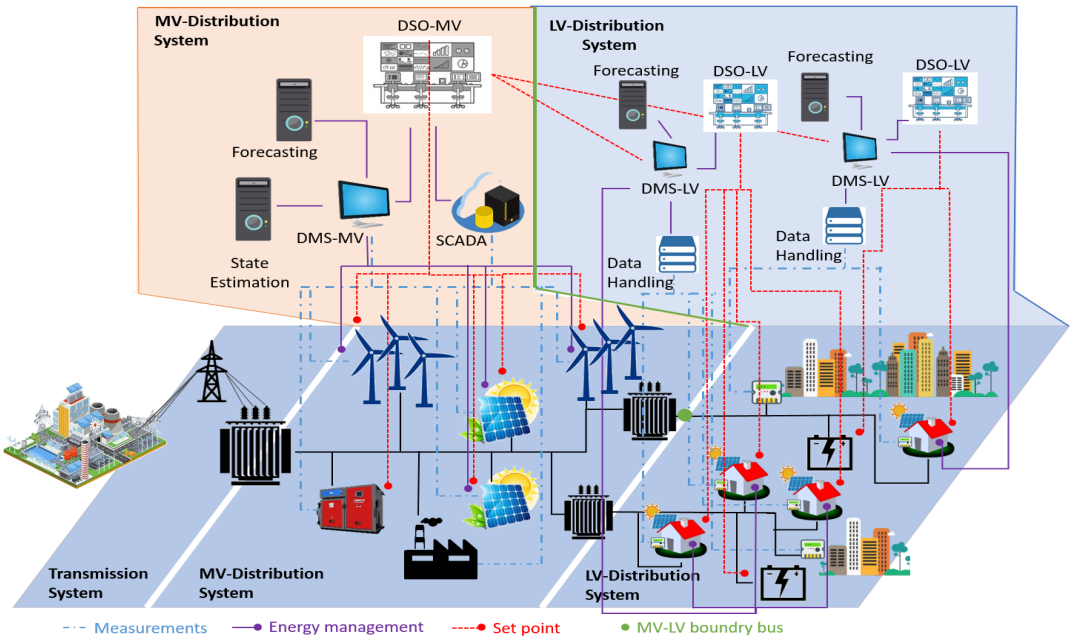

Fig. 5.6. Information and power exchanged in distribution networks

demand forecasts, and the set-points required by the CVC-MV in the border node between the MV grid and the LV_D grid (voltage reference signal at the secondary substation and power flexibility exchange) for the time horizon of action of the CVC. After the data loading procedure, the VO of the LV_D grid is performed, and the output of the VO is stored that is, the set-points of the RES units corresponding to the LV_D system and the reactive power compensation devices. If the obtained result for each CVC-LV accomplishes the interconnection set-points with the MV grid, the set-points of the RES units connected to both the MV network and the LV networks are sent to the primary controllers of such units. Otherwise, if some of the CVC-LVs have not reached an optimum solution that fulfills the set-points specified by the CVC-MV at the boundary, it will be necessary to execute the whole process again, including the set of data used by the CVC-MV, as the power exchange established by the CVC-LV of these LV systems cannot track the set-point given by the CVC-MV.

5.3.4. Medium voltage optimization algorithm (CVC-MV)

The MV grid optimization algorithm (CVC-MV) is in charge of determining the working set-points of the RES devices that are present in the MV network. It also determines the optimum voltage signal and required flexibility in the border nodes of the LV grids connected to the MV grid (secondary substations).

The CVC-MV uses as inputs the daily 24 hours-ahead forecast of wind, PV and wave resources. These information is used to estimate the maximum power capability by each DG units present in the MV network.

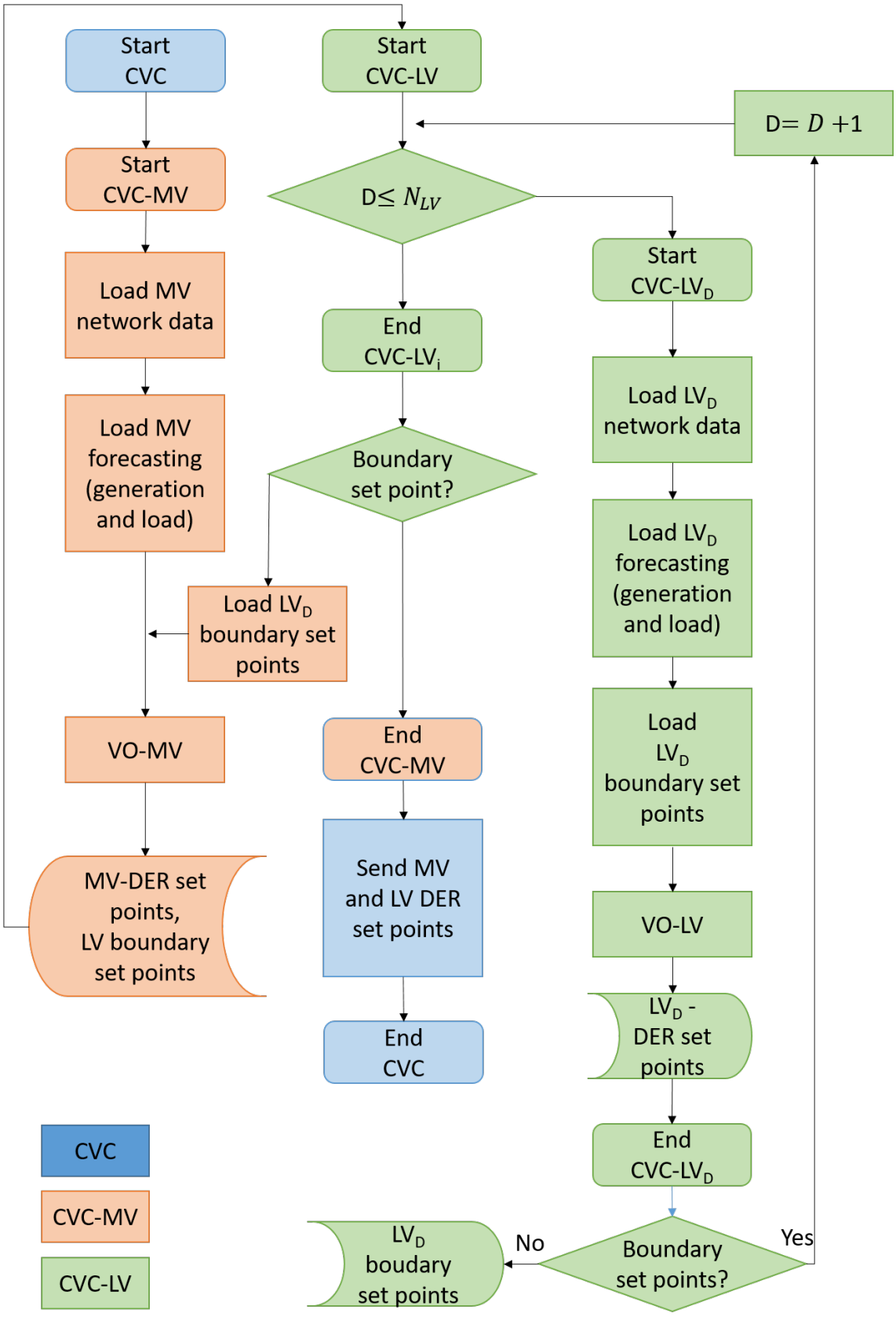

Fig. 5.7. Information and power exchanged in distribution networks

5.3.4.1. Input data for the medium voltage controller

To undertake the MV grid optimization process, it is necessary to firstly present the following input data:

- Day-ahead short-term load and generation forecast in the MV grid, with i being each one of the nodes of this grid:
  - $P_{load_{MV_{i,h}}}$, $Q_{load_{MV_{i,h}}}$ refer to the day-ahead short-term load forecast for each MV consumer.
  - $S_{gen_{DG_{MVmax_{i,h}}}}$ refer to the day-ahead short-term generation for each MV renewable energy source.
- Aggregated active and reactive power at each LV secondary substation. The LV systems connected to the MV grid will be modelled as a generator with a load, with j being each LV grid and k being the sub-index denoting the nodes of a grid j:
  - $P_{load_{LV_{j,h}}}$, $Q_{load_{LV_{j,h}}}$ refer to the aggregated day-ahead short-term load forecast at the LV secondary substation, where $P_{load_{LV_{j,h}}} = \sum_{k=1}^{j_k} P_{load_{LV_{k,h}}}$ and $Q_{load_{LV_{j,h}}} = \sum_{k=1}^{j_k} Q_{load_{LV_{k,h}}}$, $P_{load_{LV_{k,h}}}$ and $Q_{load_{LV_{k,h}}}$ being the active and reactive load demand for each LV user (consumer/prosumer/generator) at each k node that correspond to the LV grid j.
  - $S_{gen_{DG_{LVmax_{j,h}}}}$ refer to the aggregated day-ahead short-term generation forecast at the LV secondary substation. The PV units' power factor of the LV grids will be given a range between 0 to 1, where $S_{gen_{DG_{LVmax_{j,h}}}} = \sum_{k=1}^{j_k} S_{gen_{DG_{LVmax_{k,h}}}}$, $S_{gen_{DG_{LVmax_{k,h}}}}$ being the forecast of maximum hour generation of the renewable generation unit k of the LV system j.

5.3.4.2. MV Variables

The set of variables used in the MV-grid coordination algorithm of $x^{MV}(t)$ are as:

- set-point of the DG units connected to the MV grid ($S_{DG}^{MV}\ \forall DG$),
- set-point of the D-FACTS connected to the MV grid ($Q_{D-FACTS}^{MV}\ \forall D-FACTS$),
- flexibility requirements (P, Q) in each secondary substation (frontier point) MV-LV ($P, \cos_\theta\ \forall MV-LVfrontier$).

5.3.4.3. Objective function

The optimization of the MV grid is performed based on two main objectives: minimizing the active power losses in the MV system, and minimizing the power curtailment on the distributed generators that are present in the MV grid. This is according to the bi-objective function given by (5.25):

$$\begin{aligned} \min \quad & F(x^{MV}(t)) = \alpha f_{MV}(x^{MV}(t)) + \beta g_{MV}(x^{MV}(t)) \\ \text{Being:} \quad & \\ & f_{MV}(x^{MV}(t)) = \sum_{\substack{L \in N_{MV} \\ Bus_{MV}}} P_{loss} = \sum_{L \in N_{MV}} g_L(V_i^2 + V_j^2 - 2V_i V_j \cos\theta_{ij}) \\ & g_{MV}(x^{MV}(t)) = \sum_{i=1} (P_{DG_{imax,h}} - P_{DG_{i,h}}) \end{aligned} \tag{5.25}$$

where $L = (i, j), i \in N_{b_{MV}}$ are the MV system's nodes and $j \in N_{i_{MV}}$ are the adjacent nodes the node i of the MV system, including the node i. Likewise, $l = (m, n), m \in N_{b_{LV}}$ corresponds to the nodes of the LV system, and $n \in N_{m_{LV}}$, including the m^{th} node. N_{MV} represents the set of lines belonging to the MV system, while N_{LV} represents the set of lines belonging to the LV system. The conductance of the lines of MV (L) and LV(l) grids are represented by g_L and g_l, respectively. Nodes' voltages of the MV and LV systems are denoted as $V_{bus}\angle\theta_{bus}$, where V_{bus} is the amplitude and $\angle\theta_{bus}$ is the angle of the voltage at each node of the MV and LV grids, being $bus \in N_{b_{MV}}, N_{b_{LV}}$. Thus, θ_{ij} and θ_{mn} correspond to the phase difference among the nodal voltages of the lines $L = (i, j)$ and $l = (m, n)$, respectively.

The coefficients α and β correspond to the weights assigned to each components that is included in the individual objective functions to be optimized.

The solution given by the MV grid optimization algorithm establishes the set-points that correspond to each controllable RES devices that are present in the MV grid, as well as the power to be interchanged with the LV grids (secondary substation).

5.3.4.4. MV constraints

The MV grid control algorithm considers the following constraints when it comes to looking for the optimum assignation of both the generation delivered by the DG units and the reactive compensation devices.

Firstly, equality constraints corresponding to the load flow equations will be depicted (5.26) and (5.27), then the inequality constraints associated to generation units, reactive compensation devices, OLTCs and voltage at the nodes among both networks will be shown.

– Load flow equations

$$P_{ik} = V_i \sum_{i=1}^{N} V_k(G_{ik} \cos\theta_{ik} + B_{ik} \sin\theta_{ik}) \tag{5.26}$$

$$Q_{ik} = V_i \sum_{i=1}^{N} V_k(G_{ik} \sin\theta_{ik} - B_{ik} \cos\theta_{ik}) \tag{5.27}$$

where P_{ik} and Q_{ik} represent the active and reactive power that flows from the node i toward the node k, respectively. Voltage at a node i is given by $V_i \angle \theta_i$. The admittance of the line that connects the node i with the node k is expressed as $G_{ik} + jB_{ik}$.

– DG units limits

The constraints associated with the working capacity of the PV installations is given by (5.28) and (5.29), which corresponds to the inverter's maximum current and voltage:

$$I_{PV_{min}} \leq I_{PV} \leq I_{PV_{max}} \tag{5.28}$$

$$U_{PV_{min}} \leq U_{PV} \leq U_{PV_{max}} \tag{5.29}$$

In addition, the power generated by the PV installations cannot surpass their rate capacity as given in (5.30):

$$0 \leq S_{PV} \leq S_{PV_{max}} \tag{5.30}$$

In the case of DFIG wind farms, the constraints associated with their PQ curves are represented by the limits in the voltages and currents of stator and rotor, as given from (5.31) to (5.33).

$$I_{R_{min}} \leq I_R \leq I_{R_{max}} \tag{5.31}$$

$$U_{R_{min}} \leq U_R \leq U_{R_{max}} \tag{5.32}$$

$$I_{S_{min}} \leq I_S \leq I_{S_{max}} \tag{5.33}$$

The maximum generation of the wind installation will become limited by its rated capacity in (5.34):

$$0 \leq S_{wind} \leq S_{wind_{max}} \tag{5.34}$$

– Reactive power compensation limits

  The limits of D-FACTS devices are given by their maximum reactive power capacity, as seen in (5.35).

$$S_{D-FACT_{min}} \leq S_{D-FACT} \leq S_{D-FACT_{max}} \quad \forall D-FACT \in N_{D-FACT} \tag{5.35}$$

– Thermal limits of lines and power transformers

  The coordinated control algorithm must be capable of determining the optimum assignation of the DG units that are present in the system without surpassing the thermal limits of both lines and power transformers, as given in (5.36) and (5.37).

$$S_{line} \leq S_{line_{max}} \quad \forall line \in N_{MV} \tag{5.36}$$

$$S_{pt} \leq S_{pt_{max}} \quad \forall pt \in N_{pt_{MV}} \tag{5.37}$$

– Nodal voltage limits

$$V_{bus_{min}} \leq V_{bus} \leq V_{bus_{max}} \quad \forall bus \in N_{b_{MV}}, N_{b_{LV}} \tag{5.38}$$

  In (5.38), V_{bus} represents the voltage module for each grid node in both MV and LV grids, and it will be established by the regulatory standards of the country which the grids belong to.

– Power Flexibility exchange at the border node between the MV network and the LV networks

  The power Flexibility exchange will be given by the active power interchanged between the MV network and each LV grids; it is also determined by the $\cos\varphi_D$ that correspond to such a power exchange.

  The optimum active power exchange among the MV grid and the LV grids is calculated by means of (5.39), where P_{LV-MV} represents the power exchange in the border node between the MV and LV grids.

  - When $P_{LV-MV} > 0$, the LV network exports energy to the MV network.
  - On the contrary, when $P_{LV-MV} < 0$, the LV network imports energy from the MV network.

  $P_{gen_{DG}}$ is the active power generated by the DG units in the LV grids; $P_{load_{LV}}$ the total active power demand of the LV grid, and $P_{losses_{LV}}$ the active power losses in the LV grid.

$$P_{LV-MV} = P_{gen_{DG}} - P_{load_{LV}} - P_{losses_{LV}} \tag{5.39}$$

$$P_{LV-MV_{min}} \leq P_{LV-MV} \leq P_{LV-MV_{max}} \tag{5.40}$$

The limits of power exchange in the border node in (5.40), is given by the conditions of maximum and minimum generation that is delivered by the DG units corresponding to the LV system.

The exchange flexibility is given by the $\cos\varphi_D$ of each power exchange between the MV grid and the LV grids, and the limits is imposed using (5.41).

$$0 \leq \varphi_D \leq \frac{\pi}{2} \quad \forall D = 1, ..., N \tag{5.41}$$

5.3.5. Low voltage optimization algorithm (CVC-LV)

The LV grid optimization algorithm (CVC-LV) is the algorithm in charge of allocating the required power flexibility, received by the CVC-MV, at the secondary substation MV-LV among the flexible resources connected to the LV network. It will thus be necessary to execute such an LV algorithm for each LV networks.

Like the MV algorithm, the LV grid optimization algorithm has a 24-hours time horizon, and it performs a simulation for each hour of the day.

The output of the LV algorithm is the set-points of both all the controllable DG units and the CBs connected to the LV grid.

5.3.5.1. Input data for the low voltage controller

To carry out the optimization of each of the LV networks, it is necessary to have the following input data:

- Day-ahead short term load and generation forecast is needed, where j represents each LV network and k refers to each one of the nodes of the j^{th} LV network:
  - $P_{load_{LV_{jk,h}}}$, $Q_{load_{LV_{jk,h}}}$ refers to the day-ahead short term load forecast for each LV consumer, and
  - $S_{gen_{DG_{LVmax_{ijh}}}}$ refers to the day-ahead short term generation forecast for each DG source connected to the LV network.
- At the secondary substation (MV-LV frontier point), the following data are needed:
  - $S_{LV_j-MV} = P_{LV_j} + jQ_{LV_j}$, where P_{LV_j}, Q_{LV_j} and S_{LV_j} correspond to the active and reactive power transfer set-point at the frontier point between the LV and MV networks. This set-point has been calculated at the upper level controlled by the CVC-MV.

Such complex power should be fulfilled by the controllable LV flexible sources (i.e., flexible demand and flexible LV generation) while considering the non-controllable sources (i.e., non-flexible demand and non-flexible LV generation) and LV network losses, as given in (5.42).

– Voltage Set point at the secondary substation. This set-point has been calculated, previously, in the control superior level by the CVC-MV.

$$S_{LV_j-MV} = \sum S_{flex-gen} + \sum S_{non-flex-gen} - \sum S_{flex-load_j} - \sum S_{non-flex-load_j} - \sum S_{losses} \tag{5.42}$$

5.3.5.2. LV Variables

The set of variables used in the LV coordination algorithm of $x^{LV}(t)$ are as follows:

– $P_{DG_{j,k}}$ and $\cos\theta_{DG_{j,k}}$ refer to set-points of the DG controllable units that are connected to node k of the j^{th} LV network, and these are determined by the flexibility of each DG unit, and

– $Q_{CB_{j,k}}$ refers to a set-point of the controllable reactive power compensation units that is connected to node k of the j^{th} LV network.

5.3.5.3. Objective function

The aim of the LV grid's optimization algorithm is as follows. For each operation point, the algorithm determines the set-points of each controllable generation unit and reactive compensation device connected to the LV network. This makes it possible to minimize the deviation between the MV-LV power set-point that is received from the upper level to be interchanged and the injected power from the MV-LV border nodes (5.43).

$$\begin{aligned} \min \quad & F(x^{LV}(t)) = \gamma f_{LV}(x^{LV}(t)) + \rho g_{LV}(x^{LV}(t)) \\ \text{Being:} & \\ & f_{LV}(x^{LV}(t)) = P_{LV_j} - P_{sub_j} \\ & g_{LV}(x^{LV}(t)) = Q_{LV_j} - Q_{sub_j} \end{aligned} \tag{5.43}$$

The coefficients γ and ρ give weights to the individual objective functions that are to be optimized.

5.3.5.4. LV constraints

In the LV grid's optimization process, the study considers a number of items, namely the equality constraints that are associated with the equations of power flow, the inequality

constraints given by the nodal voltage limits, and the overloads of lines and power transformers. In addition, it is also necessary to consider the constraints that are associated with the performance of RES devices connected to the LV grid, as well as the constraints that have to do with the power exchange among the MV grid and the LV grid.

– Load flow equations
  To solve power load flow equations, the same equations for the MV optimization process in (5.26) and (5.27) will be used.

– Power power exchange at the secondary substation connecting the j^{th} LV network and the MV network
  The active and reactive power injected through the j^{th} substation that connects the MV network with the j^{th} LV system is given by (5.44) and (5.45).

$$P_{sub_j} = \sum_{k}^{Bus_j} (P_{DG_k} - P_{load_k}) - P_{loss_k} \tag{5.44}$$

$$Q_{sub_j} = \sum_{k}^{Bus_j} (Q_{DG_k} - Q_{load_k}) - Q_{loss_k} \tag{5.45}$$

  Where:

  - P_{DG_k} and Q_{DG_k} represent the active and reactive power generated by DG units connected to the k^{th} node of the j^{th} LV grid.
  - P_{load_k} and Q_{load_k} are the active and reactive power demanded by the loads connected to the k^{th} node of the j^{th} LV grid.
  - P_{loss_k} and Q_{loss_k} are the active and reactive power losses of the j^{th} LV system.

– Thermal limits of lines and power transformers
  Thermal limits of lines and power transformers must be respected for each solution achieved by the LV grid's optimization algorithm, which can be determined using (5.46) and (5.47).

$$S_{line} \leq S_{line_{max}} \quad \forall line \in N_{LV} \tag{5.46}$$

$$S_{tp} \leq S_{tp_{max}} \quad \forall tp \in N_{tp_{LV-MV}} \tag{5.47}$$

– Voltage limits

$$V_{bus_{min}} \leq V_{bus} \leq V_{bus_{max}} \quad \forall bus \in N_{b_{LV}} \tag{5.48}$$

  Where (5.48) represents the voltage amplitude for each LV grid's node, and according to [7], the voltage of each LV grid's node must be ranged about 0.93 and 1.07 p.u.

– DG generation units' limits
DG generation units present in the system can neither surpass the apparent power established by the maximum available resource at the hour under study, nor their rated capacity. This is determined by (5.49).

$$0 \leq S_{DG_{j,k}}(t) \leq S_{DG_{max_{available_{j,k}}}}(t) \quad \forall \text{ DG present in the } j^{th} LV network \tag{5.49}$$

The active and reactive power injected to the LV grids' DG units must not surpass the limits established by (5.50) and (5.51).

$$0 \leq P_{DG_k} \leq S_{DG_{k max_{available}}} * cos(\varphi_{DG_k}) \tag{5.50}$$

$$0 \leq Q_{DG_k} \leq S_{DG_{k max_{available}}} * sin(\varphi_{DG_k}) \tag{5.51}$$

The working range is given as $0 \leq cos(\varphi_{DG_k}) \leq 1$.

– Reactive power compensation devices limits
LV systems will be provided to CBs for reactive power compensation purposes. The injection of these are conditioned by (5.52).

$$Q_{CB_{min}} \leq Q_{CB} \leq Q_{CB_{max}} \quad \forall CB \in N_{CB} \tag{5.52}$$

5.4. Description of the network being studied

The system under study belongs to one portion of the Spanish power system, and corresponds to a zone between the localities of Ávila and Segovia. The system comprises 140 nodes, and different voltages levels ranged from 0.38 to 380 kV are distributed among the nodes. Data corresponding to the system are found in Appendix B [34], [216].

– The MV clients connected to 380 kV and 15 kV levels demand 122.71 MW and deliver 6.74 Mvar. The generation mix of the MV grid comprises three PV farms that have an installed capacity of 7.5 MVA, 5 MVA and 10 MVA, and two wind farms with an installed capacity of 31.5 MVA each.

– Each 15-kV node is connected to a 15kV/0.380kV secondary substation.

Figure 5.8 depicts a reduced scheme of the network to facilitate the visibility of the MV grid. The gray-colored box shows only the nodes corresponding to the 380 kV, 220 kV and 45 kV MV levels.

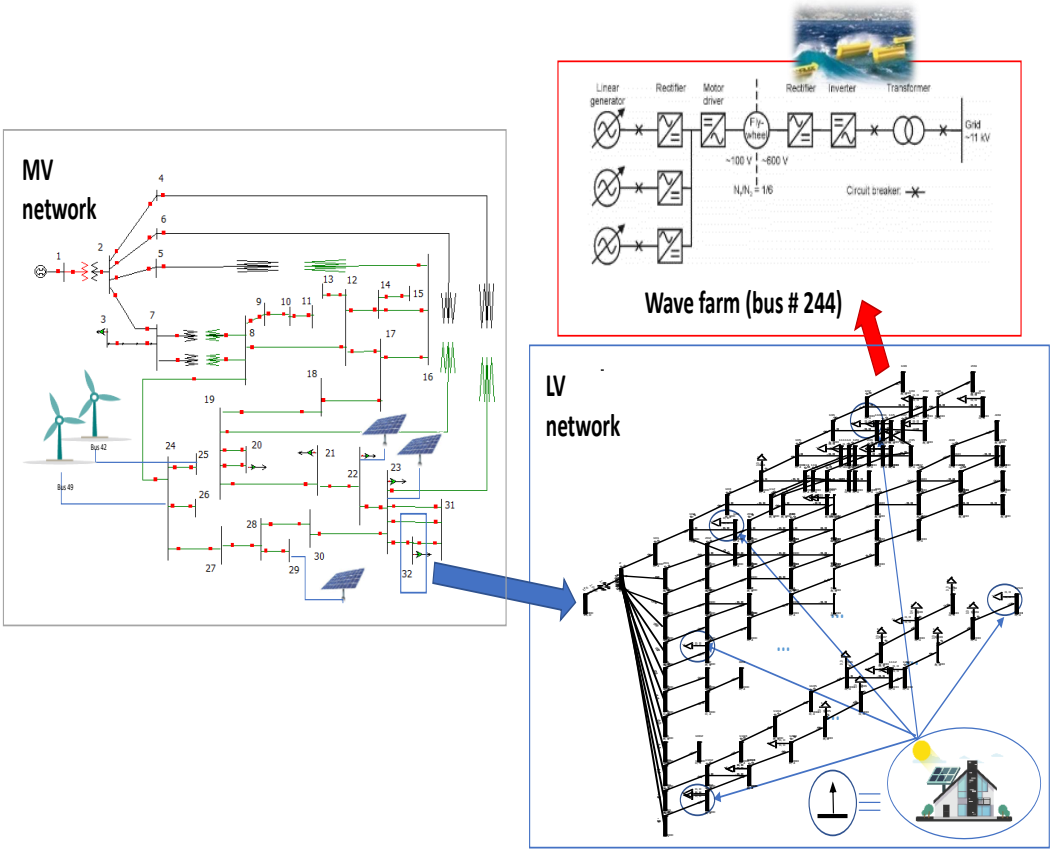

Fig. 5.8. Reduced scheme of the MV-LV studied system

– As shown in figure 5.8, nodes from Nodes #8 to #32 of 45-kV level are connected to Nodes #33 to #59 of 15-kV level via transformer substations.

– Node #32 of 45-kV MV level is connected to the Node #59 of 15-kV MV level; at the same time, this latter is connected to the Node #140, where a secondary substation of 15kV/0.380kV is also connected.

– As an example of a LV network, the blue-colored box shows details of the grid connected to the Node #140 of the 15-kV power system (Node #32 of the 45-kV level). Such a LV grid corresponds to a real LV system that is composed of 160 nodes distributed in 8 feeders. The LV grid comprises 56 loads and has a PV farm connected to each load, which has rated power that is equal to the rated load demand. In addition, the grid has a wave generator of 40 kVA, which is supplied with a FESS to compensate for the oscillations of the wave farm, which is connected to the Node #244 of the LV system. The total load aggregated at all the secondary substations (MV-LV) amounts to 45.29 MW and 17.38 Mvar, and the aggregated capacity of the DG (PV units and wave generator) of the LV system's set is 46 MVA. Each LV grid's prosumer is represented by an arrow, and its equivalent would be the load

demanded at the node and the PV unit connected to the same node.

– Finally, the red-colored box shows the scheme corresponding to the wave farm that is connected to the Node #244 of the LV grid.

5.4.1. Description of the MV network

The system that is named "MV network" is composed of 140 nodes with voltage levels ranged from 380 kV to 0.380 kV, as well as 114 loads with a total nominal power of 185.46 MV and 12.58 Mvar are also connected to the system. Table 5.4 depicts the information on the nodes and the rated power of the loads of the MV system for each voltage level. Nodes #60 to #140 correspond to the 15KV/0.380kV secondary substations.

Voltage level	Number of nodes MV network	Load		
		Number of loads	P (MW)	Q (Mvar)
380 kV	#1	-	-	-
132 kV	#2 - #7	1	46.56	-31.04
45 kV	#8 - #32	5	32.22	10.04
15 kV	#33 - #59	27	43.94	14.26
Secondary substation 15kV/0.380kV	#60 - #140	81	45.13	17.45

TABLE 5.4. LOAD DISTRIBUTION BY VOLTAGE LEVELS IN THE MV NETWORK

The generation mix of the MV system is composed of three PV emplacements of 7.5 MVA, 5 MVA and 10 MVA that are situated at Nodes #22, #23 and #29, respectively. Two wind farms of 31.5 MVA each are connected to the 15-kV grid Nodes #42 and #49.

To compensate for the system's reactive power and to improve the MV grid's voltage profile, two D-FACTS devices of 5 and 3 Mvar have been connected to the Nodes #28 (45 kV) and #35 (15 kV), respectively.

Table 5.5 shows a summary of the RES devices that are present in the MV system with voltage levels from 380 kV to 15 kV.

5.4.2. Description of the LV network

As mentioned in the description of the grid under study, there is a LV grid connected to a 15kV/0.380kV secondary substation. This subsection provides a brief description of the LV network connected to a 15kV/0.380kV secondary substation (Node #140) as this substation uses PV and a wave farm as generation systems. The power of the 15kV/0.380kV secondary substation is 1.26 MVA, and this is connected to the 15-kV Node #59. The

Voltage level	Nodes	Load			
		Nº DG	S (MVA)	Nº D-FACTS	Q (Mvar)
380 kV	#1	-	-	-	-
132 kV	#2 - #7	-	-	-	-
45 kV	#8 - #32	3	22.5	1	3
15 kV	#33 - #59	2	63	1	5

TABLE 5.5. DISTRIBUTION OF RES DEVICES BY VOLTAGE LEVELS IN THE MV NETWORK

aggregated demand of the LV system being studied is 821.1 kW and 392.4 kvar, which is spread among the 56 loads, as shown in Table 5.6.

Each load present in the system has associated a PV generation unit that is capable of providing all the power demand of the customer. Thus, the load customers of the LV system can be considered as prosumers.

Apart from the PV installations that are connected to the load nodes, the LV system has a wave power plant that is connected to the 0.380-kV Node #244, which corresponds to Feeder 2. The wave power plant comprises three WECs and has a rated power of 40 kVA. To improve the power output oscillations associated with the wave emplacement, the study incorporates a non-physically-structured filtering stage coupled with a flywheel system. The complete wave plant model and the power output signal improvement was described in the Chapter 4 and it was adapted to the voltage level of the LV system under study.

Lastly, with the aim of improving the grid's voltage profiles, the LV system being studied is supplied with a 35-kVA CB that is located in the Node #1210 of the Feeder 12.

	Nº of buses	Load		DG	CB
		P (kW)	Q(kvar)	S (kVA)	(kvar)
Substation	56	822.04	392.38		35.00
Feeder 1	7	65.25	31.14	72.30	0.00
Feeder 2	14	193.05	92.18	213.93	0.00
Feeder 4	13	189.60	90.49	210.08	0.00
Feeder 5	1	23.12	11.04	25.62	0.00
Feeder 6	2	8.52	4.06	9.44	0.00
Feeder 7	1	23.12	11.04	25.62	0.00
Feeder 11	9	162.91	77.75	180.51	0.00
Feeder 12	9	156.46	74.68	213.37	35.00

TABLE 5.6. DISTRIBUTION OF LOADS, DG UNITS AND CAPACITOR BANKS BY FEEDERS OF THE LV SYSTEM UNDER STUDY

5.5. Application of the coordinated control algorithm under normal operating conditions

This section describes the behaviour of the proposed coordinated control algorithm applied on both the MV and LV power systems being studied, which was described in the Section 5.4 for normal working conditions. To prove the effectiveness of the proposed control method, the study considers the following working scenarios of both MV and LV systems, as well as their components:

- The MV grid loads demand a power that correspond to 90% of the rated power of each load, that is, the load take 110.44 MVA and sends 6.06 Mvar to the MV system.
- The availability of wind, wave and solar resource is at 100% of their capacity, so that the DG units in both grids could generate up to 100% of their rated capacity.
- LV grid loads demand 40% of their nominal power, which corresponds to a LV system's total demand as seen from the MV system of 18.5 MW and 6.98 Mvar.
- All DG units, loads, OLTCs and reactive power compensation devices are considered available for their operation.

5.5.1. Working conditions of the MV algorithm

From the characteristics of the variables, the objective function, and the constraints associated with the MV grid's operative coordination algorithm, it can be concluded that the optimization process contains the following characteristics:

- It is continuous, because the nature of the variables used in the MV grid's coordination ($S_{DG}, Q_{D-FACTS}, cos\theta_{LV}$) are continuous.
- It is non-linear because the equations that calculate the objective function power losses are non-linear.
- It is non-convex, because the employed load flows to evaluate the potential optimization algorithm solutions. The non-convexity of the optimization process is internally treated by the *Matpower*® software, for solving load flows [215].

Eq. (5.53) shows the calculation of the number of variables that are used by the MV grid's optimization algorithm. For each DG unit, the same variables establish the optimum active/reactive power generation (2 variables per DG unit), while for the case of D-FACTS, the variables determine the reactive power to be injected (1 variable per D-FACT device). Finally, for the case of the border nodes shared by both the MV grid and

the LV networks, the LV grids optimum flexibility is established according to the required power flexibility exchange (active power and power factor).

$$var_{MV} = 2 * n_{DG}^{MV} + n_{D-FACTS} + 2 * n_{frontier_{MV-LV}} \tag{5.53}$$

Where:

- n_{DG}^{MV} is the number of DG units in the MV system.
- $n_{D-FACTS}$ is the number of D-FACT devices in the MV network.
- $n_{frontier_{MV-LV}}$ is the number of border substations between the MV network and the LV networks.

For the case of the proposed study, 5 DG units and 2 D-FACTS devices are connected to the MV network, while 81 border nodes are shared between the MV grid and the LV networks. Thus, the total number of variables used by the MV grid's coordination algorithm is considered to be 174.

For the resolution of the MV grid's optimization algorithm, the study utilizes the interior point method, which can address the continuous and non-linear optimization problems. The stopping criteria utilized by the optimization algorithm are as follows:

- Tolerance of the objective function: 1e-6
- Tolerance of the solutions: 1e-6
- Maximum number of iterations: 10000

5.5.2. Results of the MV algorithm

This subsection displays the results that are obtained after the application of the MV grid's coordinated control algorithm to the MV power system being studied in normal working conditions.

The optimization algorithm has performed 53 iterations before obtaining an optimum solution of the optimization problem that satisfies the imposed constraints and, also fulfils the stopping criteria established in the previous subsection. The optimum solution entails power losses in the system accounted in (2.97+j19.37)MVA, and a power curtailment of the DG units present in the system is found to be at 1.68%.

Table 5.7 and Figure 5.9 depict the optimum values of the variables that were used in the optimization process. Table 5.7 shows the set-points given by the optimization algorithm for each DG unit and D-FACTS device in the system, as well as the hosting capacity of the first DG units.

RES bus connection	$P_{set-point}$ (MW)	$Q_{set-point}$ (Mvar)	Hosting capacity (%)
DG_{22}	7.46	2.46	99
DG_{23}	4.96	1.64	99
DG_{29}	9.96	-3.29	100
DG_{42}	24.92	-0.87	100
DG_{49}	23.98	3.26	96
$D-FACT_{28}$	-	3.77	75
$D-FACT_{35}$	-	0.97	32

TABLE 5.7. SET-POINTS OF THE DER UNITS PRESENT IN THE MV NETWORK

Figure 5.9 shows the optimum flexibility established by the MV grid's coordination algorithm for each border node that is shared with the LV grids. As it can be observed, the flexibility requested to the LV systems oscillates in the intervals of (0, -0.8) MW and (-0.016, 0.11) Mvar for the active and reactive power exchanged between the MV grid and LV grids, respectively. From the obtained results after applying the CVC-MV and, because the active power interchange between the MV grid and the LV grid is negative (blue-colored bars), it can be concluded that in the optimum operation of the grid being studied, the MV network imports active power from the LV network, which supposes a power flow opposite to the conventional one (i.e., from the MV grid toward the LV grids) and exports reactive power to the LV system (orange-colored bars).

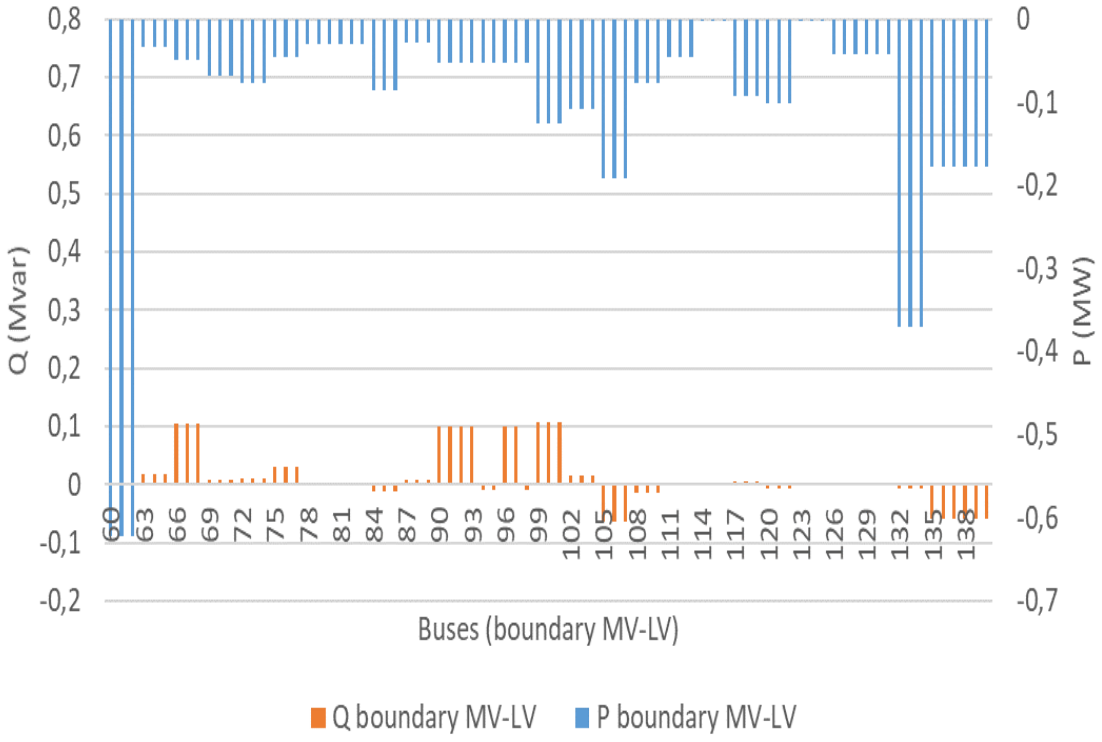

Fig. 5.9. Optimal flexibility at the border nodes between the MV network and the LV networks

Figure 5.10 displays the voltage profile of the solution given by the algorithm for the MV grid. As can be seen, the voltage is situated within the established limits (i.e., 0.95-1.05 p.u.).

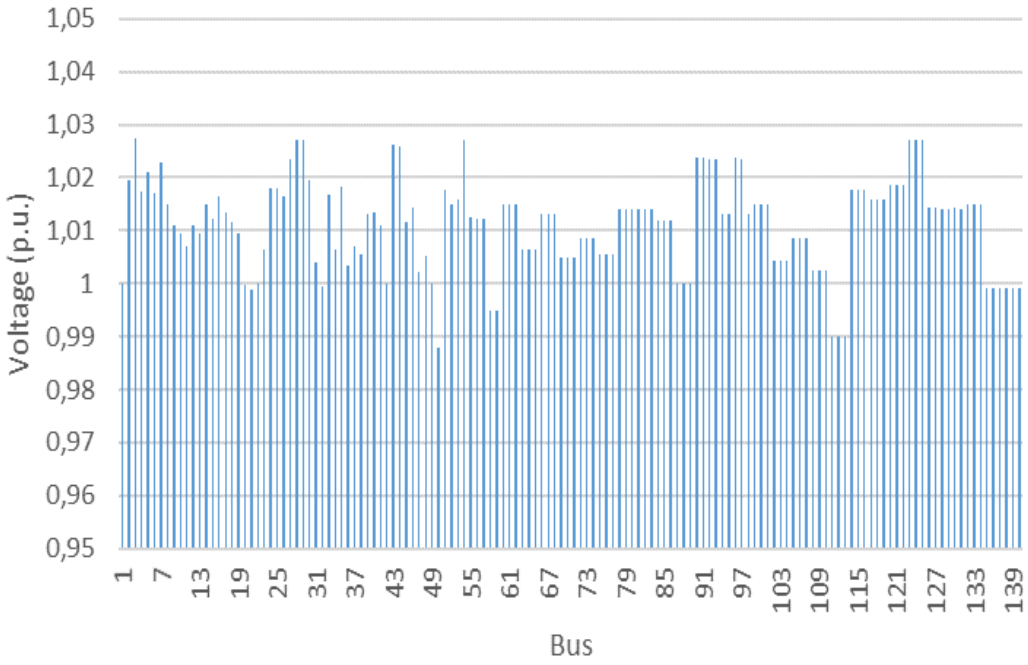

Fig. 5.10. Optimal voltage profile of the MV network

Figure 5.11(a) shows the evolution of the values obtained by the objective function for the 53 iterations performed by the Interior Point algorithm before reaching an optimum solution of the proposed problem. As it can be seen, the objective function value from Iteration 8 stops experiencing huge variations until the finalization of the optimization process. Figure 5.11(b) shows the Pareto front diagram for the two objective functions used during the optimization process, the active power curtailment, and the relative curtailment of the power generated by the DG units in the LV system. As detailed in such sub-figure, small variations in the relative curtailment of the DG units produce great variations in terms of active power losses.

Lastly, Table 5.8 portrays a comparison between the objective function values, and a comparison among the different solving optimization methods of the MV grid's coordinated control algorithm. As it can be seen, the CVC-MV can only be solved with Interior-Point and Pattern-Search solvers. Although the value obtained by using the Pattern Search solver is better than the one by the Interior Point, the computational time and number of iterations are larger and do not justify the 1% improvement obtained in the evaluation function.

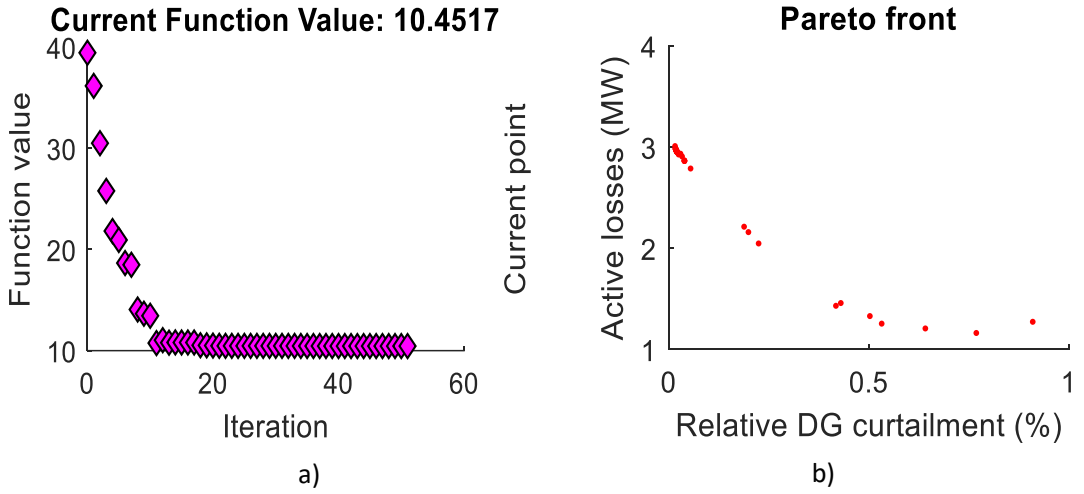

Fig. 5.11. MV algorithm: (a) Evolution of the objective function (b) Pareto front of the objective function

Solver	Execution Time (sec)	Iterations	F_eval
Interior point	119.34	53	10.45
SQP	-	-	-
Active-set	-	-	-
Pattern Search	180.53	156	10.35

TABLE 5.8. COMPARATIVE ANALYSIS OF RESULTS FOR DIFFERENT SOLVERS IN THE CVC-MV

5.5.3. Working conditions of the LV algorithm

The LV grid's optimization algorithm can be considered as discontinuous and non-linear, because the variable associated with CB's generation is noncontinuous, and the calculation of the power losses is a not linear function. In addition, the LV grid's optimization problem is non-convex because of the application of load flows when it comes evaluating the solutions offered by the optimization algorithm. The non-convexity is internally treated by the load flow resolution software *Matpower*®.

The number of variables used by the LV network operation's optimization algorithm is dependent on the number of DG units (n_{DG}^{LV}) and reactive power compensation devices (i.e., CBs, n_{CB}) present in the LV grid, as seen in (5.54).

$$var_{LV} = 2 * n_{DG}^{LV} + n_{CB} \tag{5.54}$$

According to the characteristics of the LV system used in the network being study, there are 114 variables considered in the LV grid's coordinated control algorithm; this

number corresponds to the 56 PV units, the wave farm emplacement and the CBs of Node #1210.

As for the coordinated control algorithm of the MV network, the Interior Point method will be used to solve the optimization problem. The stopping criteria considered by the Interior Point method are as follows:

- Tolerance of the objective function: 1e-6
- Tolerance of the solutions: 1e-6
- Maximum number of iterations: 10000

5.5.4. Results of the LV algorithm

Using the working conditions established by the MV grid's coordinated control algorithm, it is possible to carry out an optimum assignation of the power generated by the DG units in the LV system for the border nodes shared by the MV grid and the LV networks.

The utilization of the LV grid's coordinated control algorithm makes it possible to obtain the working set-points of the PV units, the wave farm, and the CBs in the LV system. This would be based on the flexibility required by the MV grid's coordinated control algorithm in the border nodes between the MV and the LV network. For the LV grid being studied that is connected to the secondary substation corresponding to the Node #140, the optimum flexibility given by the CVC-MV is 0.95 inductive.

When the Interior Point method is used as a solver, the LV grid's coordinated control algorithm can obtain an optimum solution for the LV grid's optimization problem after 11 iterations. The relative error committed in the deviation is 0.52%; this deviation is between the flexibility that is established in the border node between the MV network and the LV network, and the optimal solution established by the LV algorithm.

Figure 5.12 shows the optimum generation for each DG units present in the LV system, and it is established by the LV grid's coordinated control algorithm. Blue-colored and orange-colored bars represent the active and reactive power delivered by each LV-DG unit, respectively. The gray-colored line represents the percentage of generation delivered by each DG units based on, their available capacity. As it can be seen, the PV units are working in the range from 48% to 72% of their maximum installed capacity.

Figure 5.13 depicts the voltage profile of the LV grid based on the optimum generation of the DG units present in the grid being studied. As observed from the figure, the optimum assignation established by the LV grid's control algorithm allows the voltage of the grid nodes to be maintained in the specified range from 0.95 to 1.05 p.u.

Figure 5.14 shows the evolution of the objective function for each iteration carried out by the Interior Point method when it comes to solving the LV grid's optimization problem.

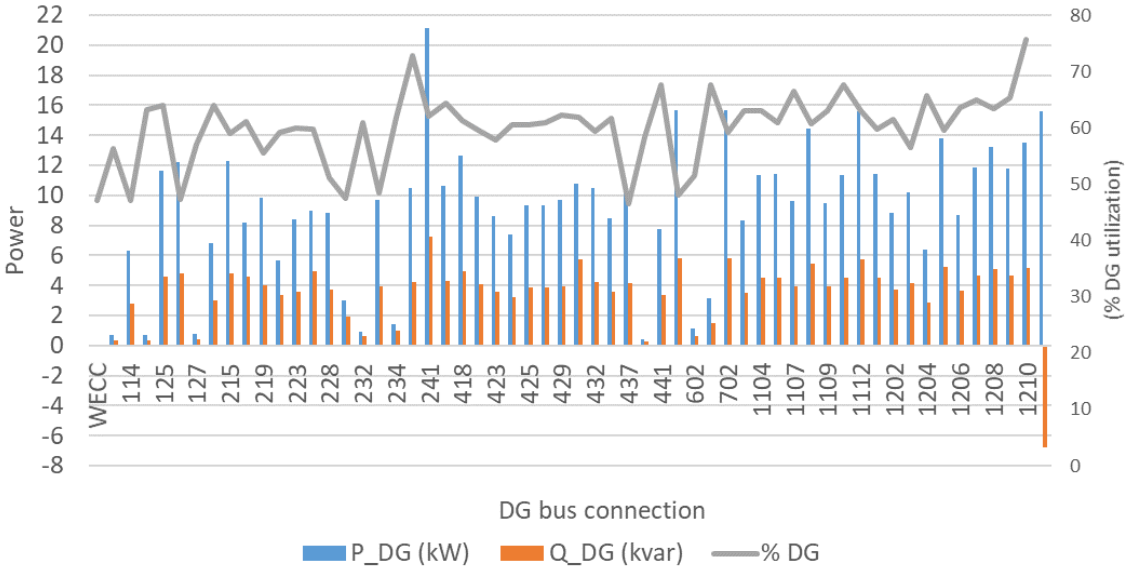

Fig. 5.12. Optimal generation of the PV and WEC units present in the LV system

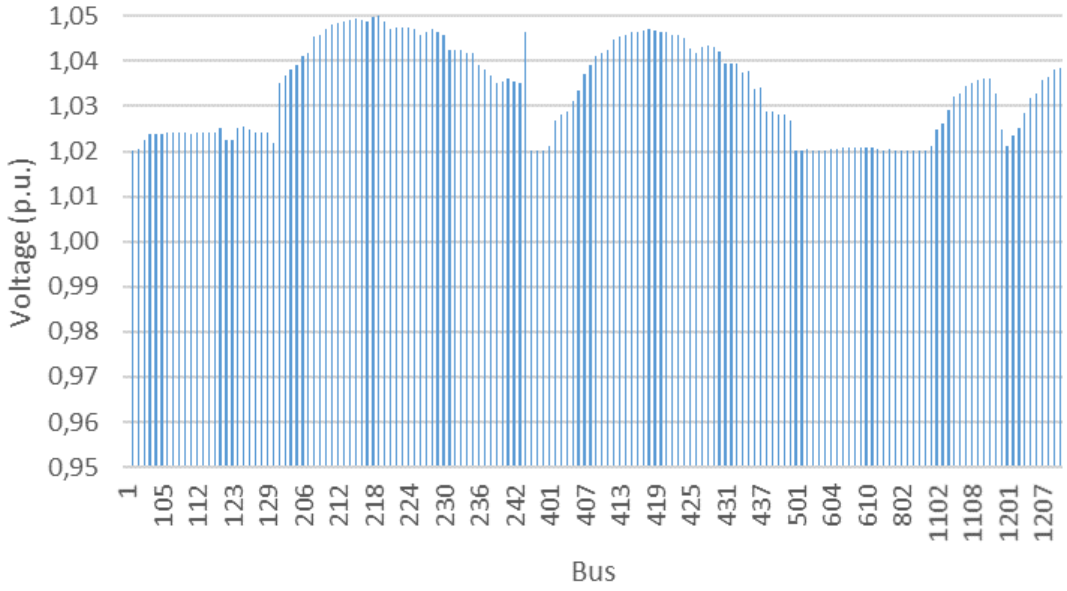

Fig. 5.13. Voltage profile of the LV network

It can be seen that after the first 5 iterations, the value reached by the objective function does not experience significant alterations.

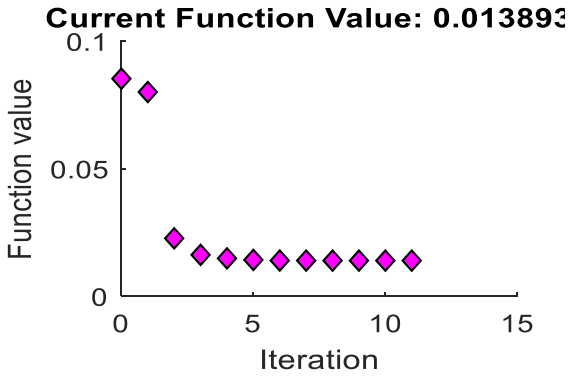

Fig. 5.14. Pareto diagram corresponding to the CVC-LV

Ultimately, Table 5.9 shows a comparative study in terms of the execution time, the number of iterations and the objective function value for different solvers that were used to solve the CVC-LV. Unlike the CVC-MV, it is possible to solve the CVC-LV using all the solvers indicated in the table. On the one hand, the objective function values obtained through the implementation of the SQP and the Pattern Search solvers are equal, and these were obtained after a reduced number of iterations. On the other hand, if the Interior Point and the Patter Search methods are compared with one another, it can be seen that doubling the execution time and multiplying the number of iterations by 10 would improve the value of the objective function up to 40% for the Pattern Search method compared to the Interior Point method.

Solver	Execution Time (sec)	Iterations	F_eval
Interior point	109.03	11	0.0139
SQP	65.5	5	0.0412
Active-set	94.12	9	0.0412
Pattern Search	213.44	110	0.0084

TABLE 5.9. COMPARATIVE ANALYSIS OF RESULTS FOR DIFFERENT SOLVERS IN THE CVC-LV

5.6. Comparative analysis of different control strategies under normal working conditions

Considering the normal operative conditions of the different components of the grid being studied, which was fully described at the beginning of this chapter, as well as the study scenarios categorized in Table 5.10, a comparative analysis of the results obtained for the 4 proposed study scenarios (both MV and LV systems) will be done.

Case	Control strategy	LV network	MV network
A	Local Decentralized	Volt/Watt in all DG units and OLTC	Volt/var in all RES units and OLTC
B	Distributed	Optimal (DG, OLTC, CB)	Optimal (RES, OLTC, CB, D-FACTS)
C	Coordinated		

TABLE 5.10. STUDY SCENARIOS

5.6.1. Scenarios of study

In this subsection, a comparative analysis is performed using the operative conditions established by the proposed coordinated control algorithm, and the comparison is made with respect to the local voltage control and the distributed voltage control methods. Table 5.10 shows a summary of the scenarios being studied, as well as the controllable devices present in the grid at each scenario.

- *Decentralized local control*: This control technique corresponds to the DG's local controllers, namely Volt-Var or Volt-Watt controls. The operation through locally controlling the DG units present in the system allows controlling the power supplied by these units based on the voltage amplitude value at the point they are connected to. In this control method, D units can deliver both active and reactive power to the system. Apart from the voltage control implemented at the RES units, there are OLTCs at the secondary substations (MV-LV).

- *Distributed control*: The distributed control is capable of establishing the working set-points of the DG units present in MV and LV systems independently; it can also control the reactive power compensation devices namely MV-D-FACTS and LV-CBs. The application of the distributed control is performed independently for each MV and LV systems being studied. A more detailed explanation of this operative method is found in Section 5.3.

- *Coordinated control*: The coordinated control of the MV and LV grids is capable of coordinating the operation of such power systems, so that the LV network offers ancillary services to the MV network. The aim of the MV grid controller is to minimize the power losses and the curtailment carried out in the RES units connected to this network. On the other hand, the controller of the LV network aims to minimize the deviation of the power (flexibility) that is injected or consumed to the MV network at the border point of the secondary substation; this is done with respect to the flexibility set-points required by the controller of the MV network at the MV-LV boundary node.

5.6.2. Power losses

Figure 5.15 shows a comparison of the power losses in each of the LV grid's feeders according to the power demanded from the feeder (see Table 5.10). From the obtained results, it can be observed that the highest power losses are registered when a distributed control is used. It should be noted that the losses associated with the distributed control scheme are considerably higher than the losses registered when either a local control or the proposed CVC.

Figures 5.16, 5.17 and 5.18 represent the power losses at each of the lines corresponding to the voltage levels of 132 kV, 45 kV and 15 kV, respectively. Losses are expressed as a percentage with respect to the demand of each line. In looking at the figure's per voltage level, it can be seen that for 132-kV level, the implementation of the MV-grid's distributed or coordinated operation considerably reduces the losses on lines with respect to the local decentralized control strategy. For the case of 15-kV level, the coordinated control algorithm implies a notable reduction of the losses with respect to the local and distributed control strategies.

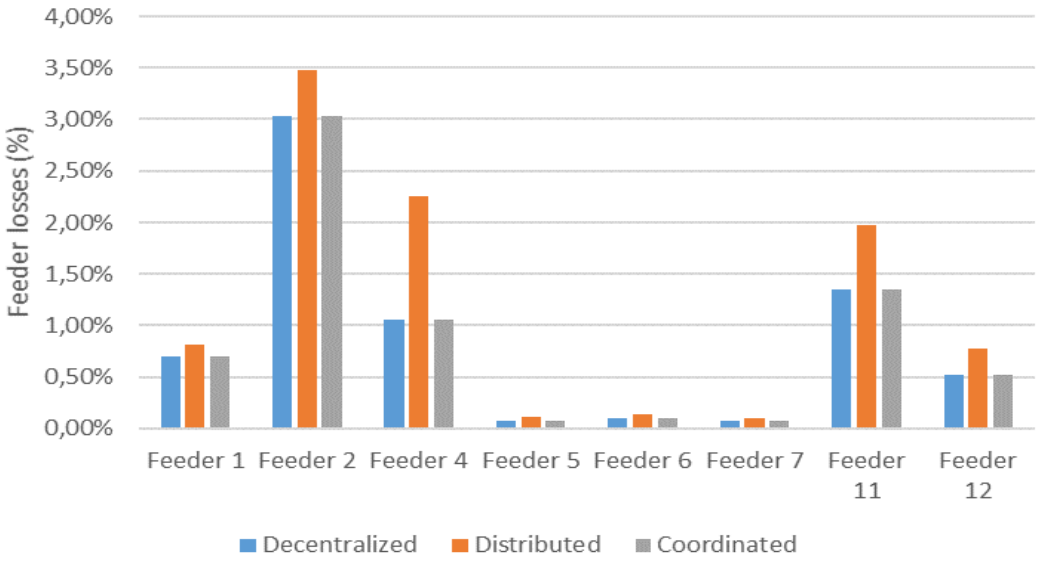

Fig. 5.15. Comparison of power losses for the LV system

5.6.3. Overloads in lines and transformers

Figure 5.19 shows the load level of the LV system's feeders in terms of the percentage with respect to the rated load of each feeder. As it can be seen, operating the LV system in a coordinated way improves the behaviour of the system reducing the load throughout the lines, and better results are obtained this way in comparison to the distributed operation mode.

Figures 5.20, 5.21 and 5.22 show the percentage of the load of the MV system's lines for the voltage levels of 132 kV, 45 kV and 15 kV, respectively.

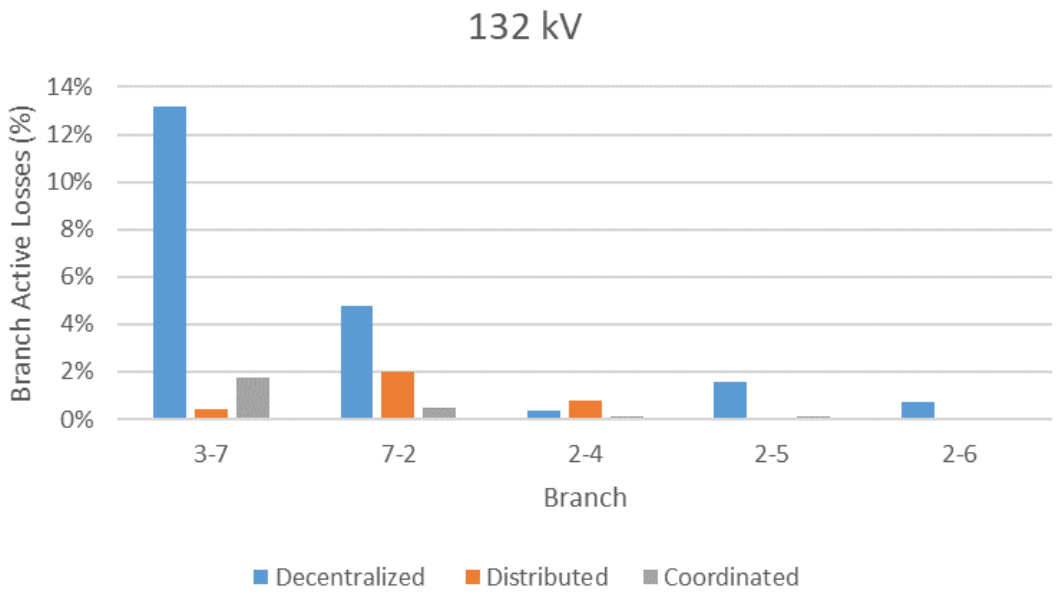

Fig. 5.16. Power losses at the 132-kV level of the MV network

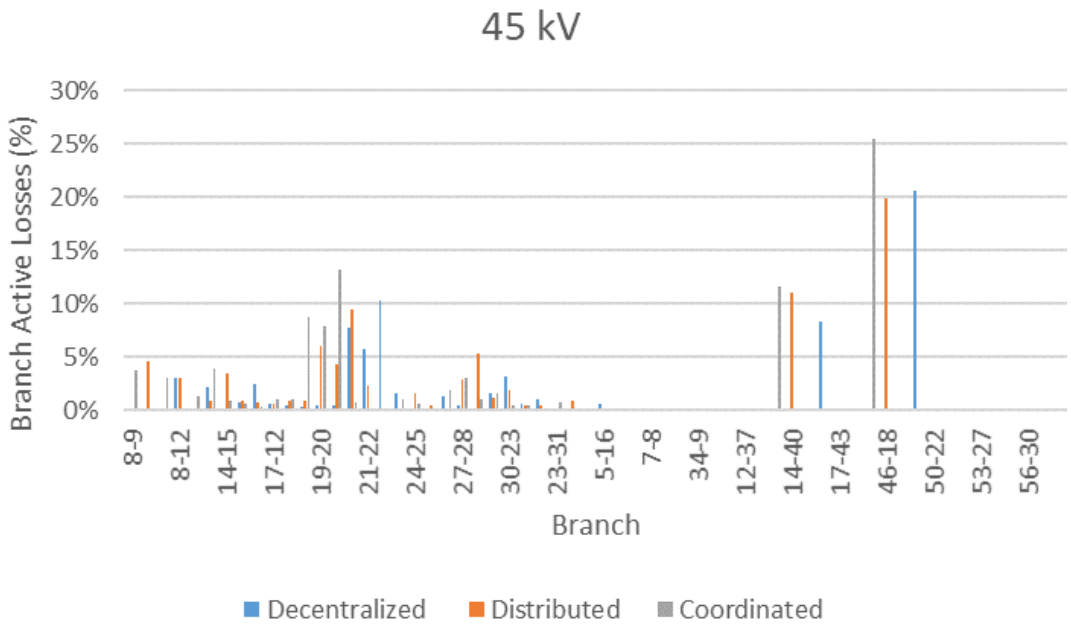

Fig. 5.17. Power losses at the 45-kV level of the MV network

In analysing the 132-kV level, it can be observed that the operation of the MV grid in either a coordinated or distributed mode entails a significant reduction of the power flowing throughout the lines of such voltage levels. For the case of the 45-kV level, none of the studied operative methods show a clear reduction of the loads throughout the lines of such voltage level in general. Finally, by studying the results in Figure 5.22, it can be observed that for the case of the 15-kV level, a clear reduction of the load throughout the lines is detected when compared to the application of the distributed control algorithms.

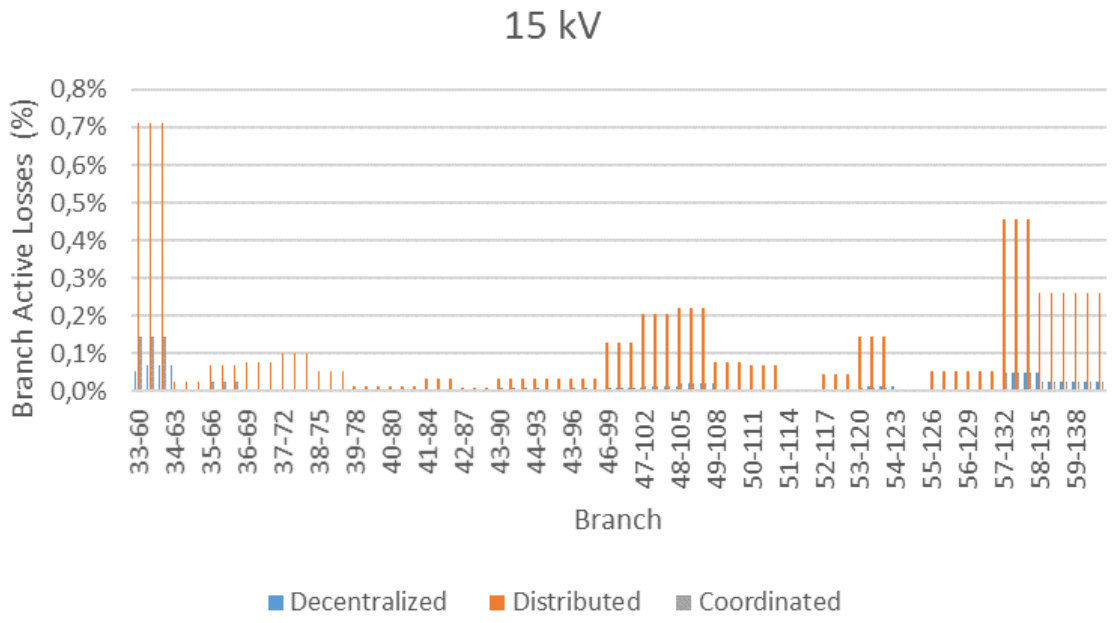

Fig. 5.18. Power losses at the 15-kV level of the MV network

5.6.4. Nodal voltages

Figure 5.23 shows the the nodal voltages (p.u.) for the LV system. This is given for the Scenarios A, B, and C, and they correspond to local decentralized, distributed, and coordinated management control of the same system, respectively. It can be seen that for the three scenarios of study, it is possible to establish an optimum generation of the DG units that allows voltage levels to be maintained within the imposed range from 0.95 to 1.05 p.u.

It should be noted that the use of the coordinated control algorithm between the MV and LV networks makes it possible to minimize the deviation of the voltage profile in the nodes that is, it reduces the oscillations in the nodal voltage between adjacent nodes.

For the case of the MV network, Figure 5.24 shows the nodal voltage profile for the whole grid. It can be observed that the application of the distributed control situates the voltage of Nodes #111 to #113 at the permitted lower level (i.e., 0.95 p.u.). The voltage profile deviation in the nodes of the MV grid with respect to the unity for the local control scheme is 0.17, whereas for the distributed one the deviation is 0.185. Finally, the voltage profile deviation for the voltage control scheme developed throughout this chapter is 0.14, which supposes a reduction of 7% with respect to the less favourable scheme, as in the distributed scheme.

5.6.5. Renewable energy hosting capacity

When it comes to comparing the operation strategies of both MV and LV grids, it becomes interesting to determine what is the percentage of maximum renewable energy that can be

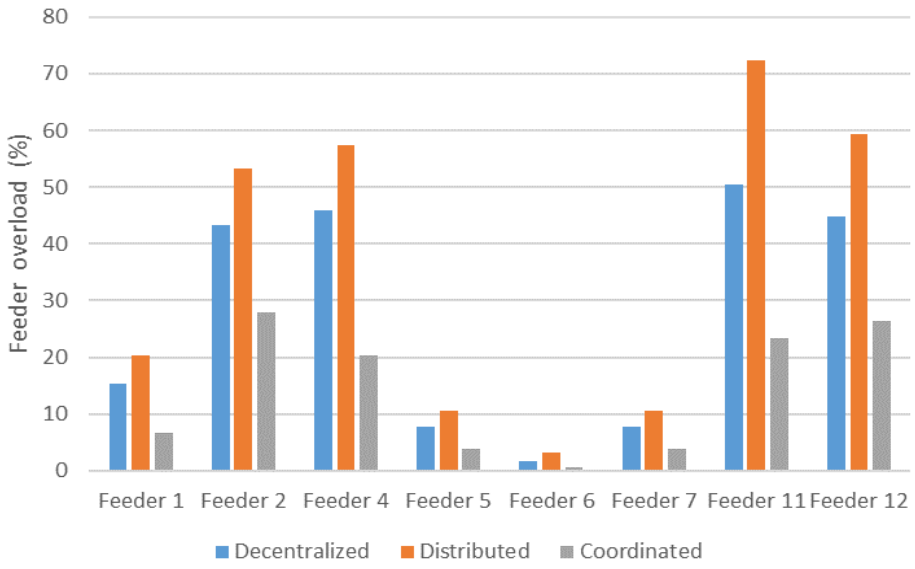

Fig. 5.19. Load percentage of the lines for the studied LV system

grid-integrated under normal working conditions.

Figure 5.25 shows a comparison that is related to the hosting capacity of PV units and the wave farm that are present in the LV system for the selected study conditions and for the three grid operation scenarios. It is observed that when the LV grid is controlled in a way where it offers ancillary services to the MV network, the LV grid's hosting capacity is limited with respect to other control schemes (i.e., local and distributed).

On the other hand, for the case of the MV grid, it is observed that the three controllers offer similar results that are proximal to 100% for the PV units at Nodes #22, #23, and #29.

The biggest difference is encountered in the case of wind farms connected to the 15-kV system corresponding to the MV network at Nodes #42 and #49. For these two DG units, the distributed control algorithm is not capable of integrating all the renewable energy. The park connected to the Node #42 can integrate the 93% of its capacity to the MV grid, whereas at the Node #49 of the same grid it can only integrate 72% of the generation of renewable origin. The coordinated control proposed in this thesis allows the renewable energy hosting capacity of the whole generation to be notably incremented, including the wind farms connected to the MV network (see Figure 5.26).

5.6.6. RES curtailment

Lastly, the study performs a comparative analysis related to the curtailment performed on the generation units of renewable origin present in the grid being studied for each one of the developed grid control techniques.

Figure 5.27 exhibits the curtailment performed for each PV and the WEC unit that

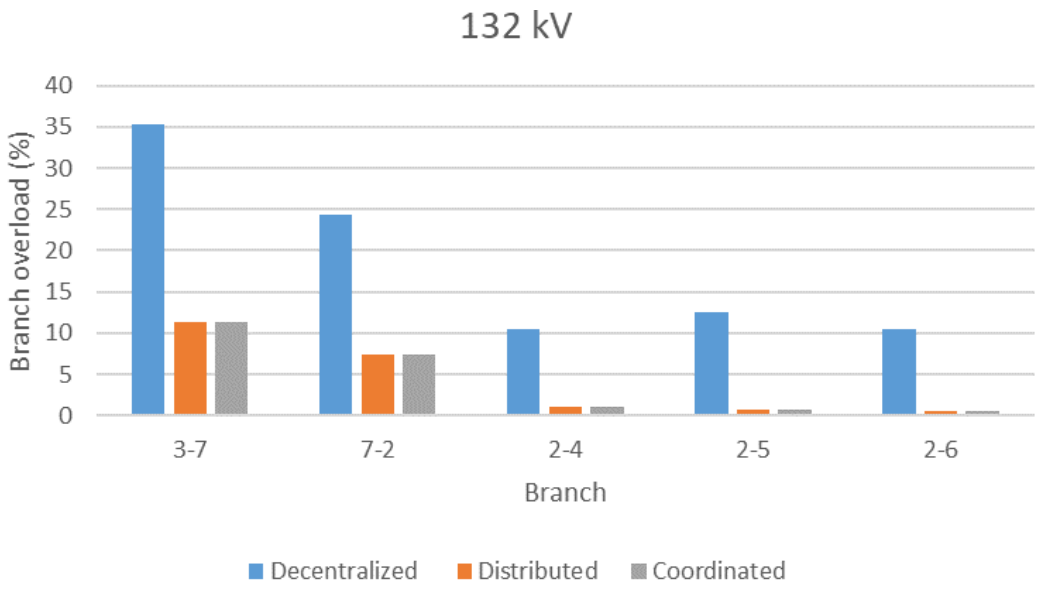

Fig. 5.20. Percentage of branch overload corresponding to the voltage level of 132 kV of the MV system

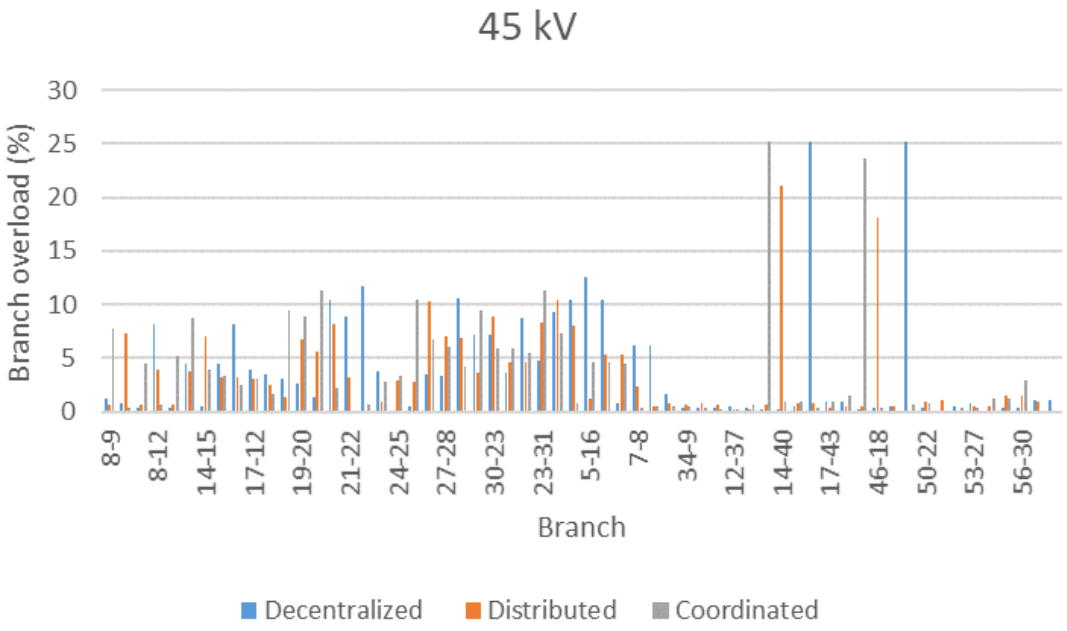

Fig. 5.21. Percentage of branch overload corresponding to the voltage level of 45 kV of the MV system

is connected to the LV system. the value is expressed in terms of a percentage of the curtailed generation with respect to the available resource in the study scenario.

As with the case of determining renewable energy hosting capacity, the greatest curtailment is carried out in the coordinated control scenario when the LV network is controlled to offer ancillary services to the MV power system. Because it is not possible to reduce the demand in favour of a greater renewable generation, it is necessary to perform

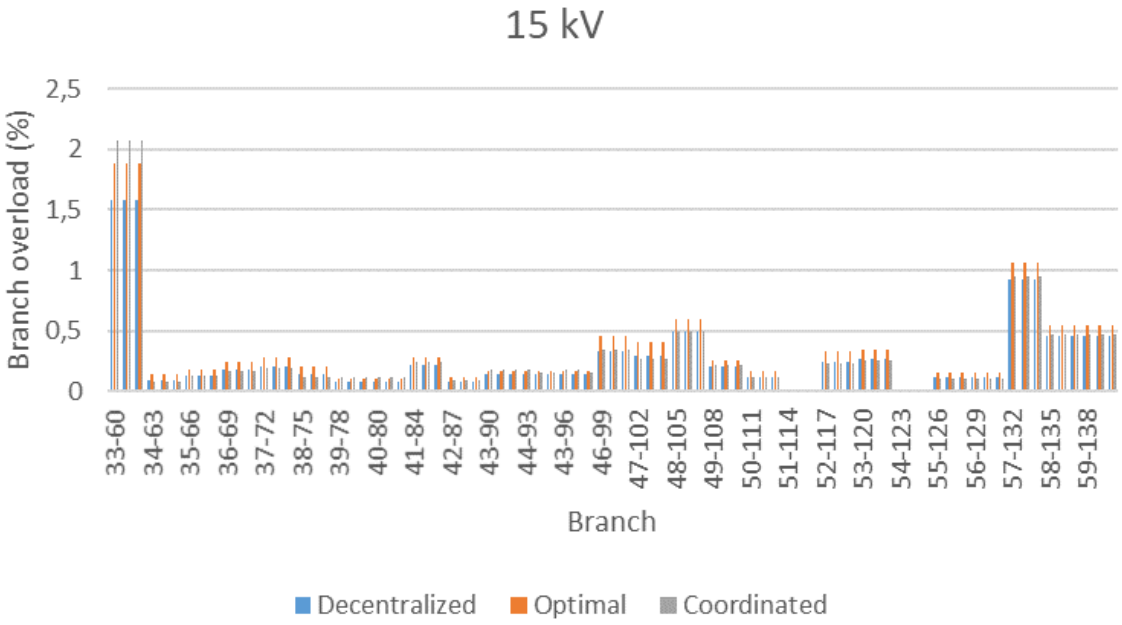

Fig. 5.22. Percentage of branch overload corresponding to the voltage level of 15 kV of the MV system

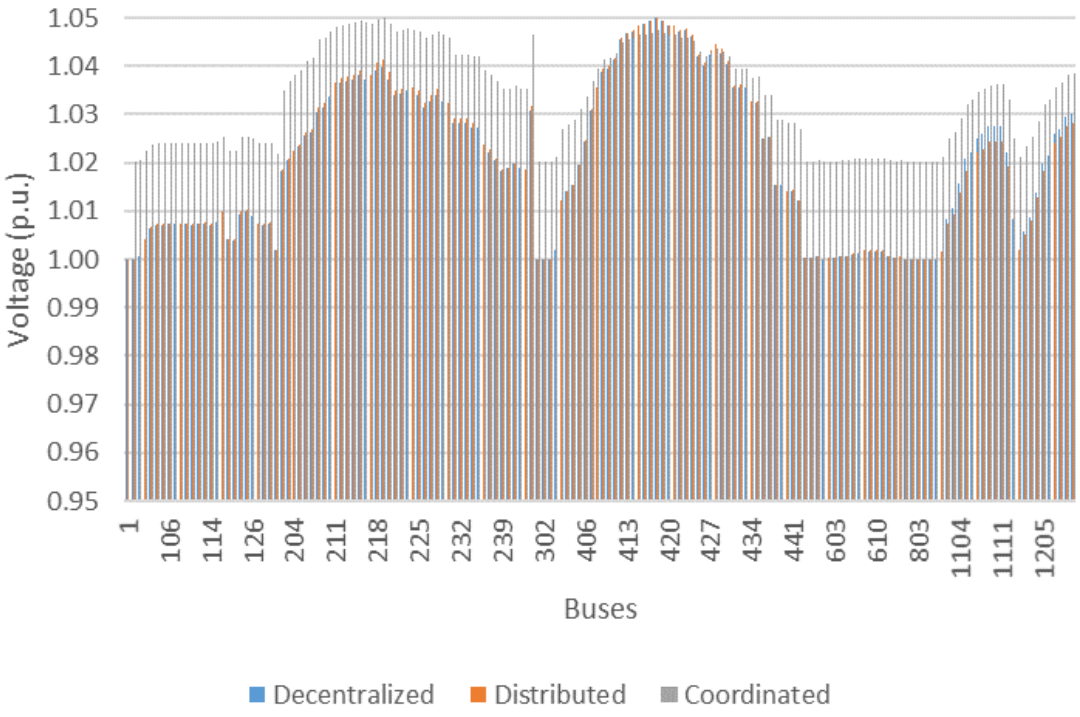

Fig. 5.23. Voltage profile comparison for the LV network under study

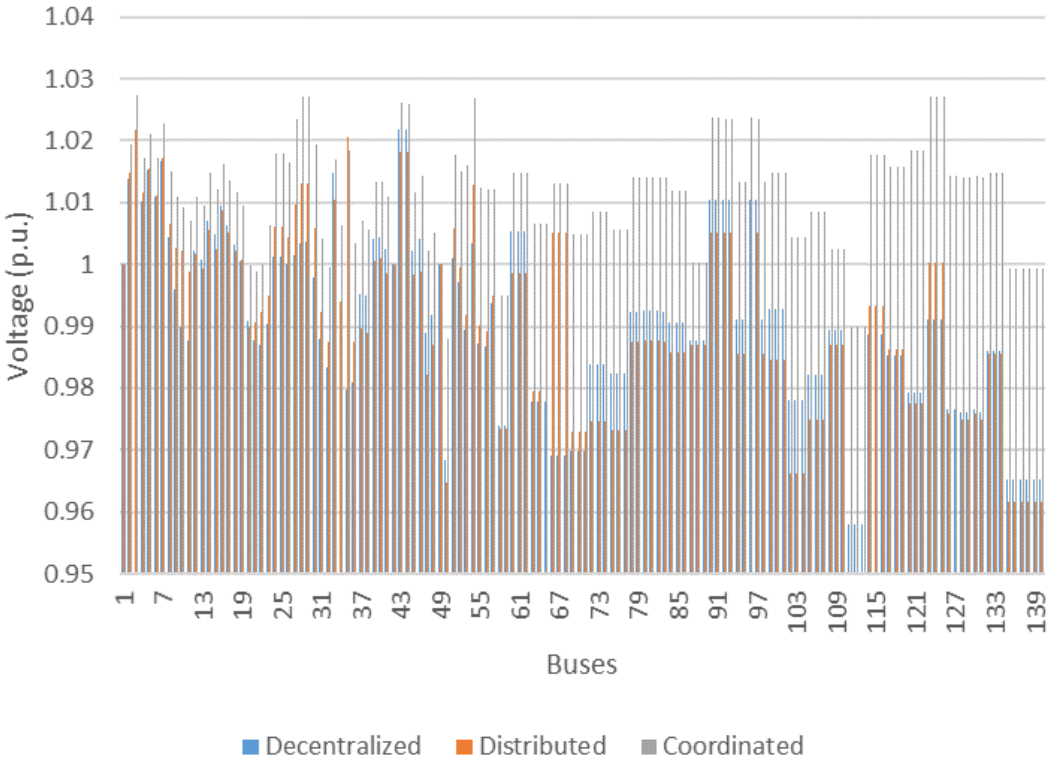

Fig. 5.24. Voltage profile comparison for the MV network under study

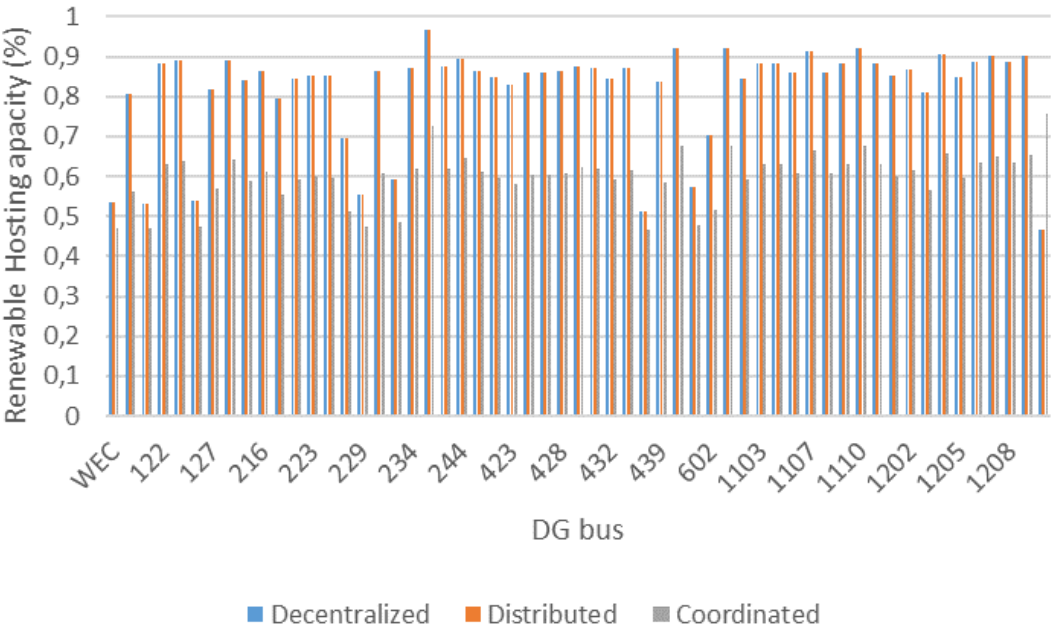

Fig. 5.25. Comparison of the renewable energy hosting capacity for both the PV and WEC units present in the studied LV network

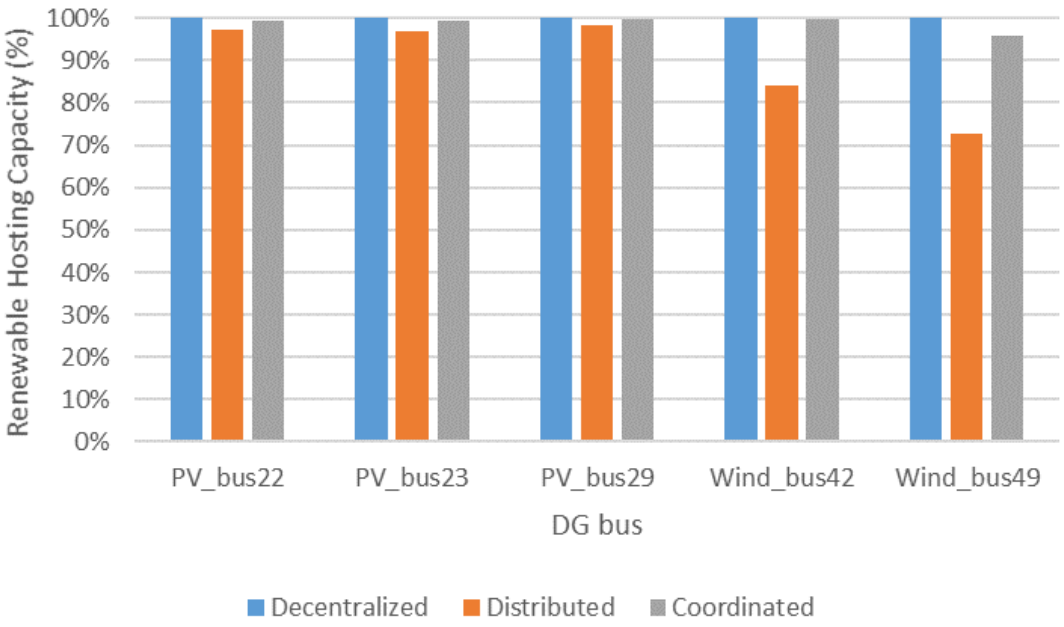

Fig. 5.26. Comparison of the renewable energy hosting capacity for the RES units present in the MV network

a greater curtailment on the DG units of the LV system compared to the results obtained from the local control and distributed voltage control.

With respect to the MV network, it can be seen from Figure 5.28 that applying a local decentralized control scheme on the DG units of the MV system allows all the power available in the scenario of study to be employed, which entails no curtailment. The employment of the distributed control scheme is the factor that supposes a bigger curtailment of the DG units, while the coordinated control algorithm can reduce the curtailment of the both PV and wind power units to nearly 0%. It can also maintain the wind farm curtailment of Node #49 below 5%.

5.6.7. Key performance indicators comparison under normal operation mode

Within the scope of facilitating the comparison among the proposed four operation strategies of both MV and LV power systems, Table 5.11 summarizes their main results.

5.7. Application of the coordinated control algorithm under abnormal working conditions

In this section the behaviour of the CVC proposed in this thesis will be analysed under abnormal working conditions. To do this, the study firstly analysed the case corresponding to a N-1 contingency in which the 45-kV MV grid's line connecting the Nodes #17 and #18 is lost.

Table 5.12 compares the results obtained for the three control schemes proposed in

Control strategy	Local Decentralized	Distributed	Coordinated
$\sum Losses_{LV}$ (%)	5.73	5.73	3.6
$\sum Losses_{MV}$ (%)	1.7	1.5	2.1
Maximum overload LV(%)	50.51	72.33	27.95
Maximum overload MV(%)	35.31	35.31	35.31
LV nodes with voltages out of limits (%)	None	None	None
MV nodes with voltages out of limits (%)	None	None	None
Active power exported from LV to MV grid (kW)	373.3	408.9	196.9
Active power exported from MV to LV grid (MW)	-20.61	-22.56	-9.17
Reactive power exported from LV to MV grid (kvar)	-140.1	-329.2	0.07
Reactive power exported from MV to LV grid (Mvar)	6.21	14.59	2.79
HV-MV Exchange (MVA)	-1.41+j9.24	7.11+j7.74	10.96+j1.13
LV curtailment (%)	21	16	42
MV curtailment (%)	0	15.72	1.68
$\sum D-FACTS_{injection_{MV}}$(Mvar)	0	4.3	4.74
$\sum CB_{LV}$ (kvar)	0	1.75	1.75
LV-DG hosting capacity (%)	79	84	58
OLTC tap changes	-	2	0
MV-RES hosting capacity (%)	100	84.28	98.32
Objective function value for LV grid	0.1077	0.042	0.0139
Objective function value for MV grid	1e-7	12.59	10.45
Execution time for LV grid (sec)	62.09	62.08	109.03
Execution time for MV grid (sec)	29.94	42.76	119.34

TABLE 5.11. KEY PERFORMANCE INDICATORS (KPI) IN NORMAL OPERATION MODE

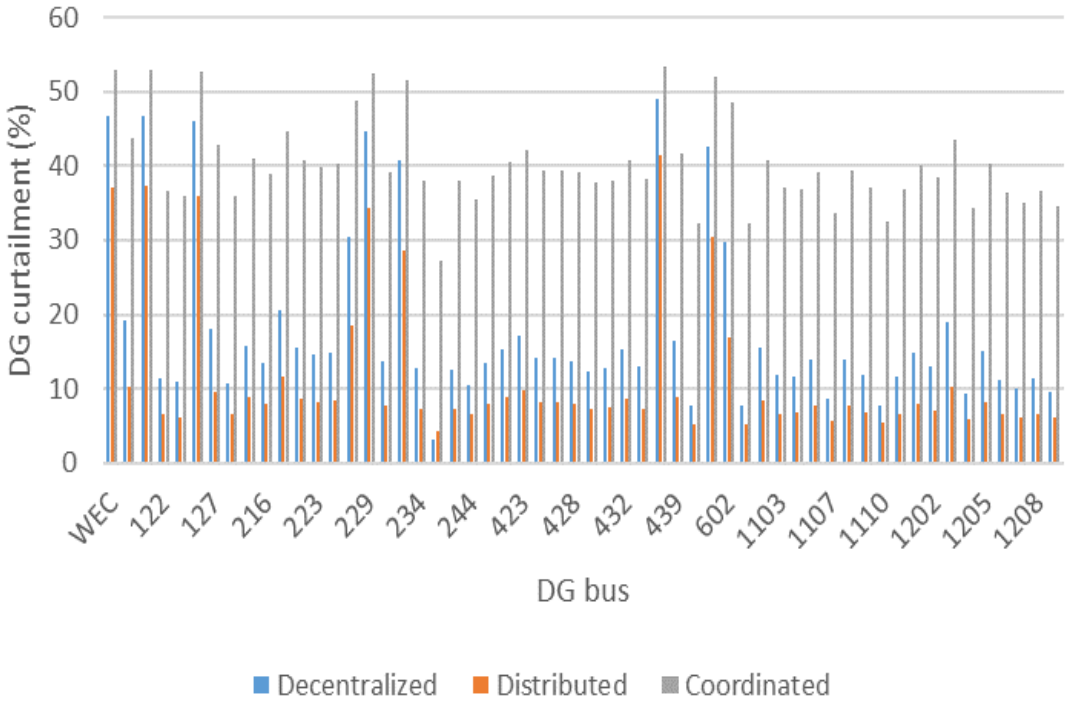

Fig. 5.27. DG curtailment in the PV and WEC units located at LV networks

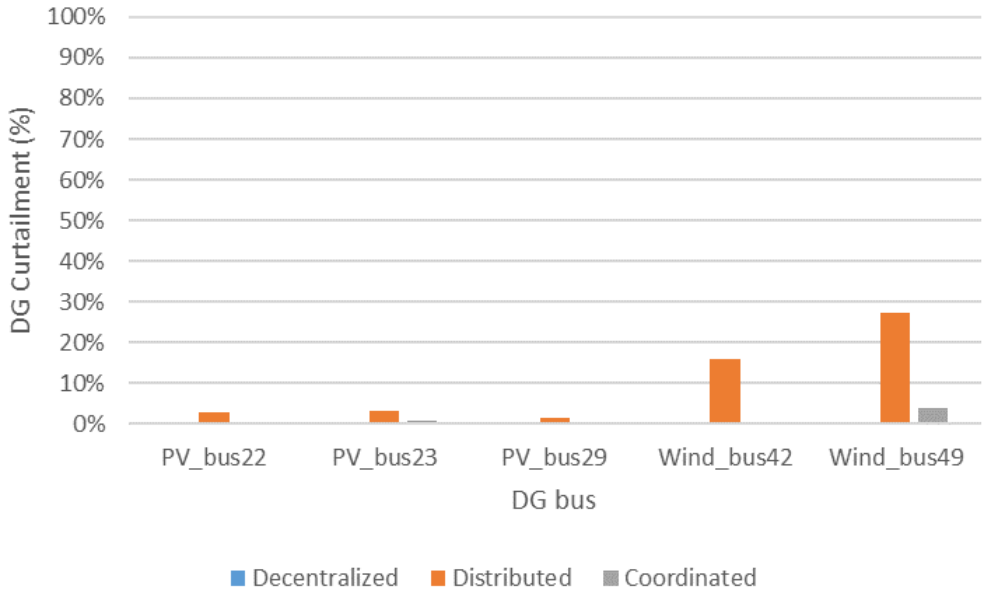

Fig. 5.28. Curtailment of the RES units present in the MV system

this chapter. It can be noted that the decentralized and distributed control schemes are not capable of reaching a solution for the MV grid in a way that would keep grid voltages within the established limits, which would also include the whole system. By contrast, the coordinated voltage control scheme proposed in this thesis can find an optimal solution for both the MV and LV levels under abnormal working conditions, such as losing the line

of an MV system. Under such a situation, the coordinated control algorithm determines the optimal working conditions of the RES devices that are present in the MV system, as well as the conditions of the PV, WEC, and CB units present in the LV grids.

5.8. Analysis of the power exchange between the MV and LV grid for seasonal conditions

The previous sections in this chapter described the undertaken study with respect to the established assignation by the coordinated control algorithm for two load scenarios under normal and abnormal working conditions. In this section, the power exchange between MV and LV grids for four representative seasonal days is investigated.

5.8.1. Analysis of the power exchange between the MV and LV grid for spring

To perform the study for conditions of a spring season, the study used the demand and generation registered on March 28, 2015 as input data. For this date of study, Figure 5.29 shows the demand profile of both MV and LV grids (a), and the values in p.u. of the PV, wind, and wave generation (b); the information is given with respect to the rated power of each used technology. Generation and demand data have been extracted from the website of Red Eléctrica de España.

By employing these profiles as demand and generation forecasts for the inputs of the coordinated control algorithm, the exchange profile among the MV network and the LV grids is compiled, as seen in Figure 5.30. This plot indicates that the positive interchange manifests the necessity of importing energy from the MV grid to the LV grids, whereas negative values indicate energy export from the LV grids to the MV grid. From the obtained results, it is seen that for the conditions of study, it is possible to export energy from the LV networks to the MV ones in 83% of the hours where solar resource is available. Blue and gray-coloured bars represent the optimum generation percentage, with respect of the maximum of the hour due to the application of the coordinated control algorithm. It is proven that for the hours when there is no PV generation, wind power units connected to the MV system work at 100% of their hourly capacity. Nevertheless, as the solar irradiation increases, the optimum assignation established by the coordinated control algorithm sets a generation curtailment of the MV units in favour of the self-supply of the LV networks and a possible power exportation from the LV networks towards the MV one. It is worth highlighting that the optimum assignation given by the coordinated control algorithm carries out the greatest curtailment of the LV-DG units during the hours of greater PV production; this is mainly due to the low demand in both the MV grid and the LV networks.

Figure 5.31 shows the reduction of the active power losses due to the optimum assignation established by the coordinated control algorithm. As it can be seen, at the hours when solar resource is available and when it is possible to export energy from the

Control strategy	Local Decentralized	Distributed	Coordinated
$\sum Losses_{LV}$ (%)	Does not converge	Does not converge	3.6
$\sum Losses_{MV}$ (%)	18	6	16
Maximum overload LV(%)	Does not converge	Does not converge	27.95
Maximum overload MV(%)	28.556	35.31	35.31
LV nodes with voltages out of limits (%)	Does not converge	Does not converge	None
MV nodes with voltages out of limits (%)	None	3($< 0.95 p.u.$)	None
Active power exported from LV to MV grid (kW)	Does not converge	Does not converge	-196.9
Active power exported from MV to LV grid (MW)	-22.68	-22.56	-8.35
Reactive power exported from LV to MV grid (kvar)	Does not converge	Does not converge	-7.03
Reactive power exported from MV to LV grid (Mvar)	6.83	14.59	3.06
HV-MV Exchange (MVA)	-20.46+j11.03	Does not converge	11.70+j1.39
LV curtailment (%)	Does not converge	Does not converge	42
MV curtailment (%)	0	50	1.59
$\sum D-FACTS_{injection_{MV}}$(Mvar)	0	4	4.78
$\sum CB_{LV}$ (kvar)	Does not converge	Does not converge	1.75
LV-DG hosting capacity (%)	Does not converge	Does not converge	58
OLTC tap changes	2	1	0
MV-RES hosting capacity (%)	100	50	98.41
Objective function value for LV grid	Does not converge	Does not converge	0.0256
Objective function value for MV grid	1e-7	100.00	10.5
Execution time for LV grid (sec)	Does not converge	Does not converge	109.99
Execution time for MV grid (sec)	35.55	8.23	96.02

TABLE 5.12. KEY PERFORMANCE INDICATORS (KPI) IN ABNORMAL OPERATION MODE

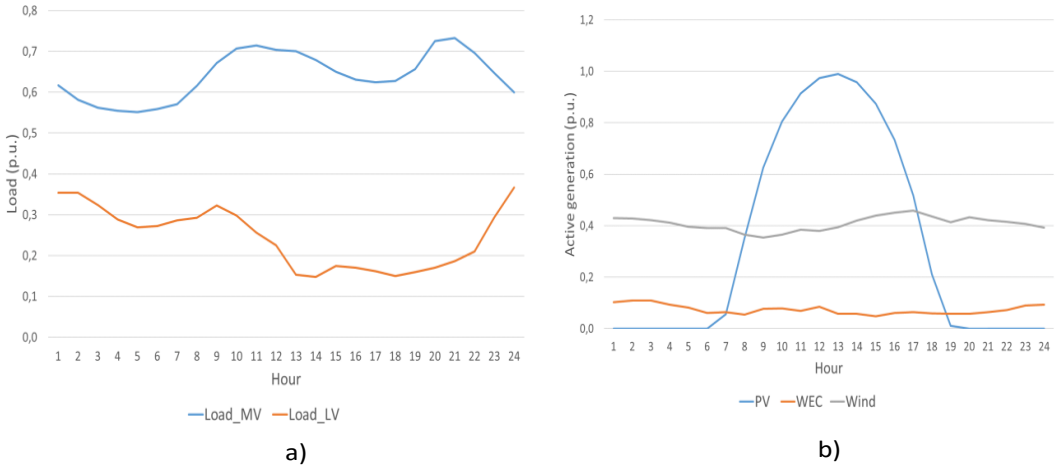

Fig. 5.29. MV and LV load profile (a). PV, WEC, and wind generation profile (b) for Spring case

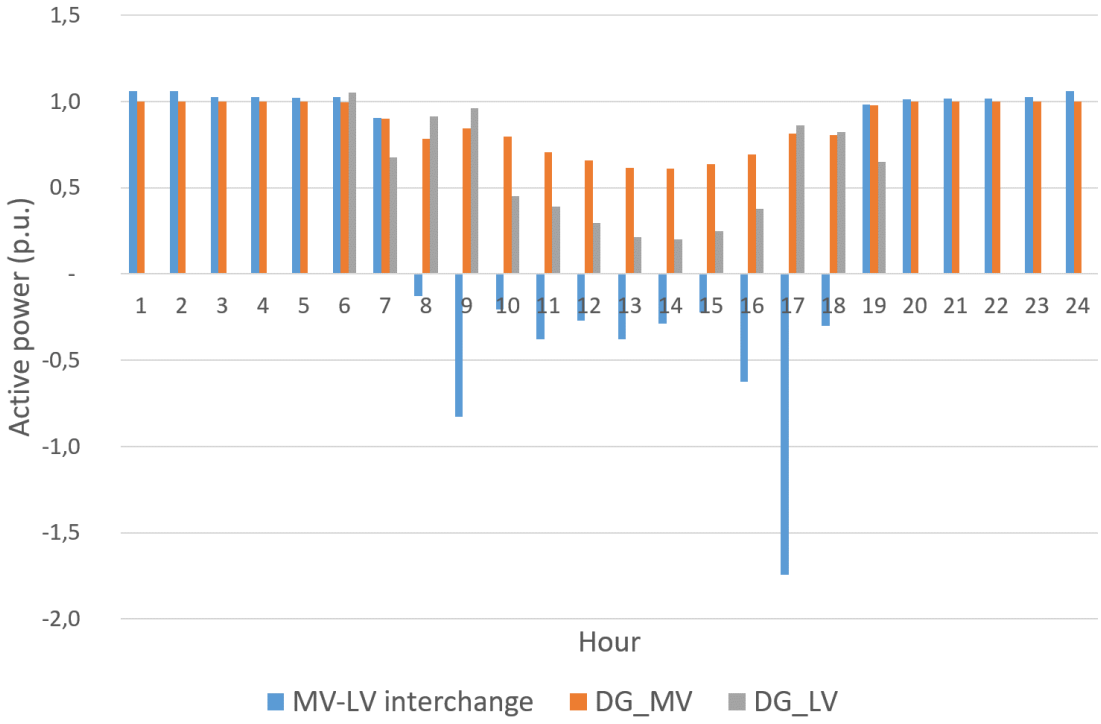

Fig. 5.30. Power exchange from the MV network to the LV network for the Spring case

LV grids to the MV grids (i.e., from 8:00h to 18:00h), the operation of the MV system is carried out by incurring in fewer losses, which allows them to be reduced up 18.5% with respect to the losses registered in the system when this is not optimized. In addition, the application of the coordinated control has allowed the voltage profiles of the MV grid to be improved. This in turn reduces the load transported throughout the MV grid's lines due to the participation of the LV-DG units when it comes to operating the complete system (see Figure 5.32).

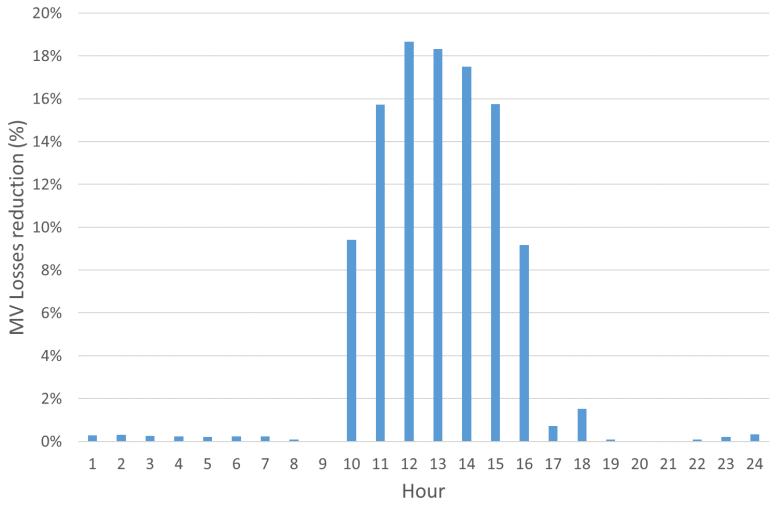

Fig. 5.31. MV active power loss reduction for the Spring case

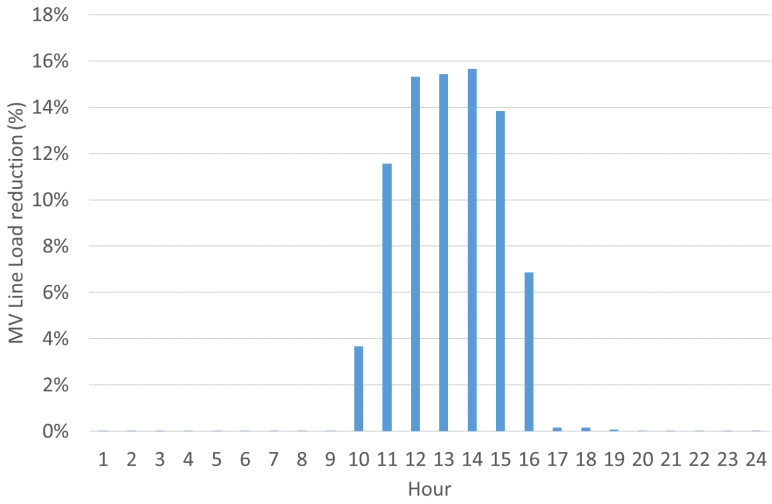

Fig. 5.32. Average load reduction on the lines of the MV system for the Spring case

5.8.2. Analysis of the power exchange between the MV and LV grid for summer

For the study of the summer season, the study used input data corresponding to the generation and demand registered on August 20,2015. Figure 5.33 displays the demand profile in p.u. for both MV and LV grids (a), and the generation of the three technologies of renewable origin (b) that were used to carry out the study on this date.

Figure 5.34 shows the exchanges between the MV and LV grids under these load and generation conditions. These exchanges were established by the coordinated control algorithm, as well as the generation percentage of the DG units connected to both power systems. It is seen that the generation coming from the MV system's units is curtailed up to 30% at thee hours when solar resource is available. For the case of the LV-DG units, the coordinated control algorithm establishes a curtailment that is greater than to the one for the case of MV system; the values here reaches up to 60% at the central hours of the day. For the interchange between the power systems being studied, it can be observed

that, at 16 :00h and 17:00h, the energy export from the LV systems toward the MV grid is double the value of the LV system's demand.

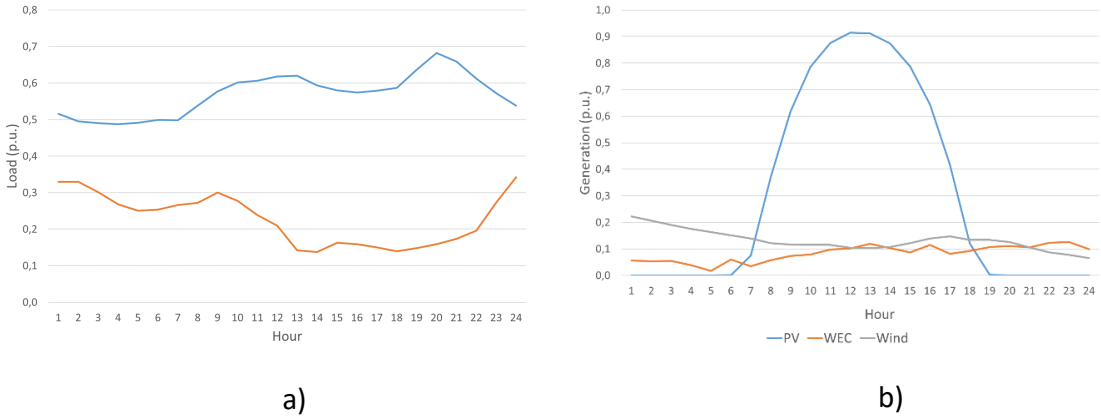

Fig. 5.33. MV and LV load profile (a). PV, WEC, and wind generation profile (b) for the Summer case

Figure 5.35 shows how the coordinated optimization of the operation of the MV and LV grids by means of the proposed control algorithm allows the active power losses to be reduced up to 12% at the hours when solar radiation is greater. The optimization also lessens the mean load that circulates throughout the MV grid's lines; this is done with respect to the operation of the unoptimized system. It can therefore be concluded that having LV grids as generator units by exporting their energy to the MV grid would improve the complete operation of the whole system, and it would also reduce their operative costs decrease the active power losses and the load flows throughout the lines.

5.8.3. Analysis of the power exchange between the MV and LV grid for fall

With the aim of analysing the coordinated control algorithm in the fall season, the study used the generation and demand data registered on November 9, 2015 as input data (seen Figure 5.36). Using the input data, the coordinated control algorithm is applied at each hour in that day. It is concluded that the power exchange from the LV networks toward the MV network is notably increased at central hours, where this exchange is double the demand of the LV grids (seen Figure 5.37). Apart from this, it is observed that the curtailment performed on the LV-DG units do not surpass the 40% mark at such hours.

Figure 5.38 shows the reduction experienced by both the active power losses and the mean load circulating throughout the MV system's lines for the selected fall day. As it can be seen, the maximum reduction of losses reaches a value of 14% as for previous cases. However, optimizing the system's operation by means of the coordinated control algorithm does not imply a substantial improvement of the load flow throughout the MV system's lines.

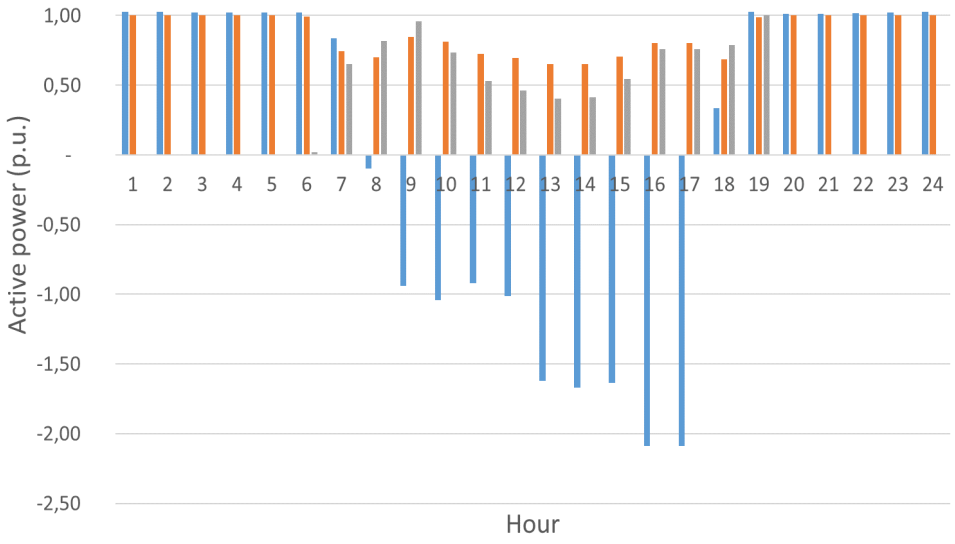

Fig. 5.34. Power exchange from the MV network to the LV network for the Summer case

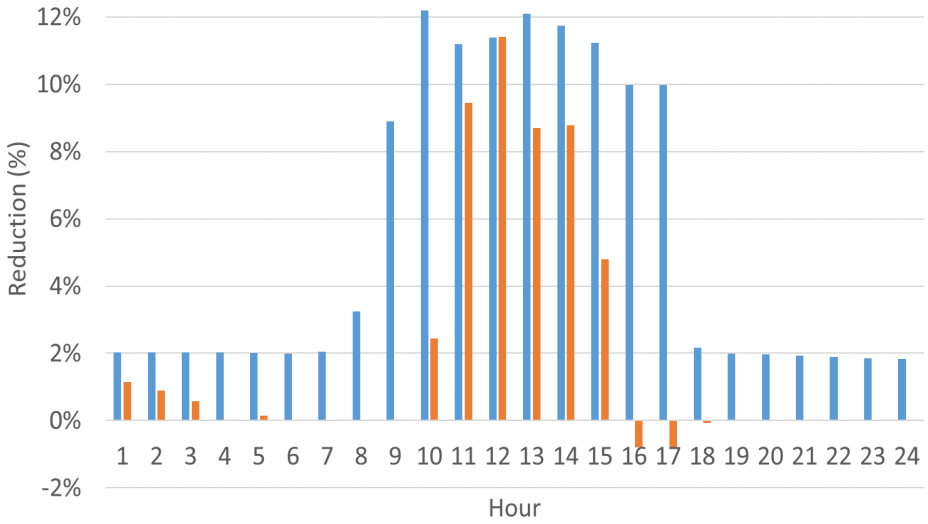

Fig. 5.35. Reduction of the active power losses and average load throughout the lines of the MV network for the Summer case

5.8.4. Analysis of the power exchange between the MV and LV grid for winter

The last analysis that is performed takes the data gathered on February 5, 2015. Figure 5.39 (a) and (b) show the generation and demand for both MV and LV systems on this date, as well as the DG units connected to them. As it can be seen, the wind resource availability is increased, which implies a greater availability for the system to deliver the energy coming from the MV grid's wind farms. It supposes a reduction of the power export from the LV networks towards the MV network at the central hours of the day if compared to the other seasonal days already studied, in which the wind generation is encountered around 40% (seen Figure 5.40).

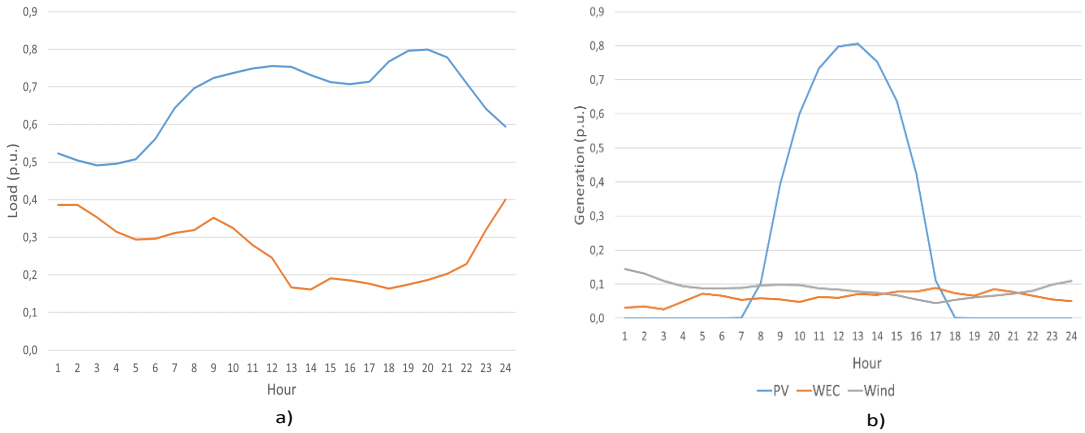

Fig. 5.36. MV and LV load profile (a). PV, WEC, and wind generation profile (b) for the Fall case

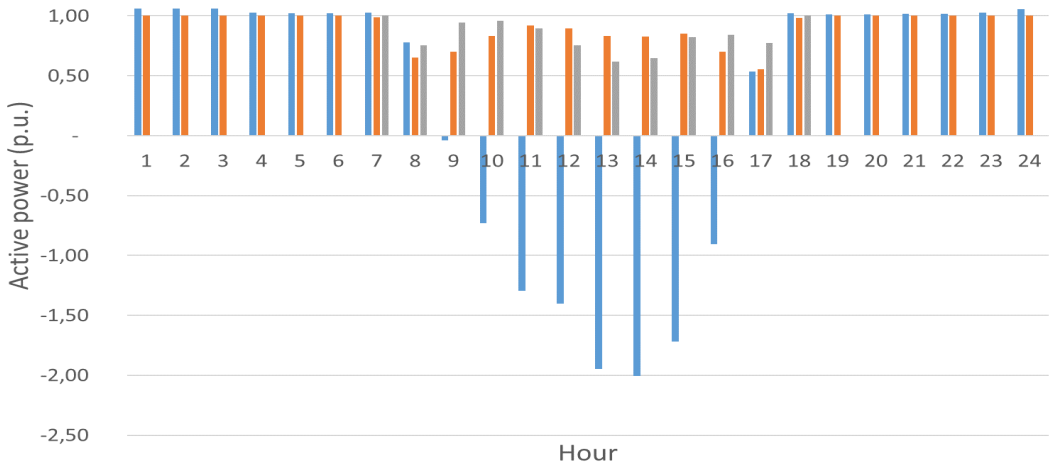

Fig. 5.37. Power exchange from the MV network to the LV network for the Fall case

Finally, Figure 5.41 shows the reduction of both active power losses and mean load throughout the MV system's lines. This is due to the operative optimization of the whole MV-LV system being performed by applying the coordinated control algorithm. For the studied winter day, the average reduction of the active power losses is found at around 2.5%. It can be seen that after analysing the date a reduction of the mean load circulating throughout the MV grid's lines is not always possible.

5.9. Summary

The chapter fully explored to the voltage control of power systems. In particular, the chapter developed a CVC that is capable of interchanging information relative to the optimal power flexibility exchange between MV and LV grids. The proposed CVC comprises two algorithms namely one for the MV grid and other for the LV networks. The objective of each voltage control algorithm is to establish the working set-points of the DER

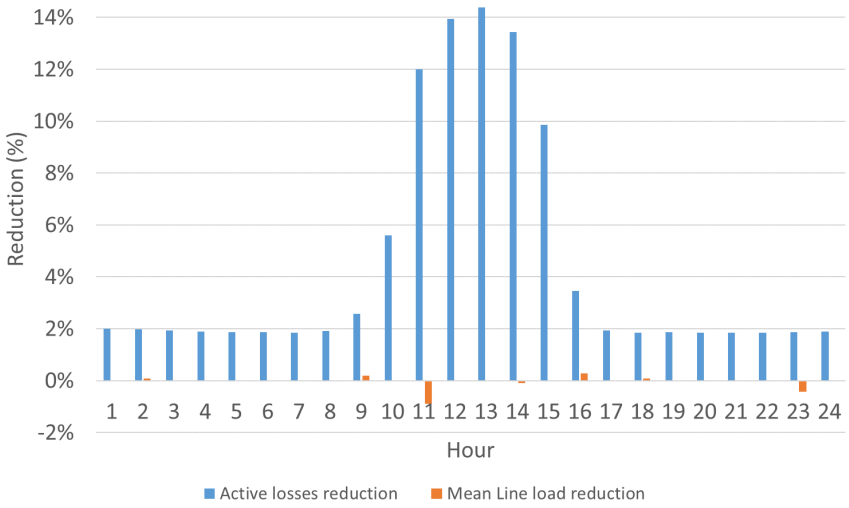

Fig. 5.38. Reduction of the active power losses and average load throughout the lines of the MV network for the Fall case

Fig. 5.39. MV and LV load profile (a). PV, WEC, and wind generation profile (b) for the Winter case

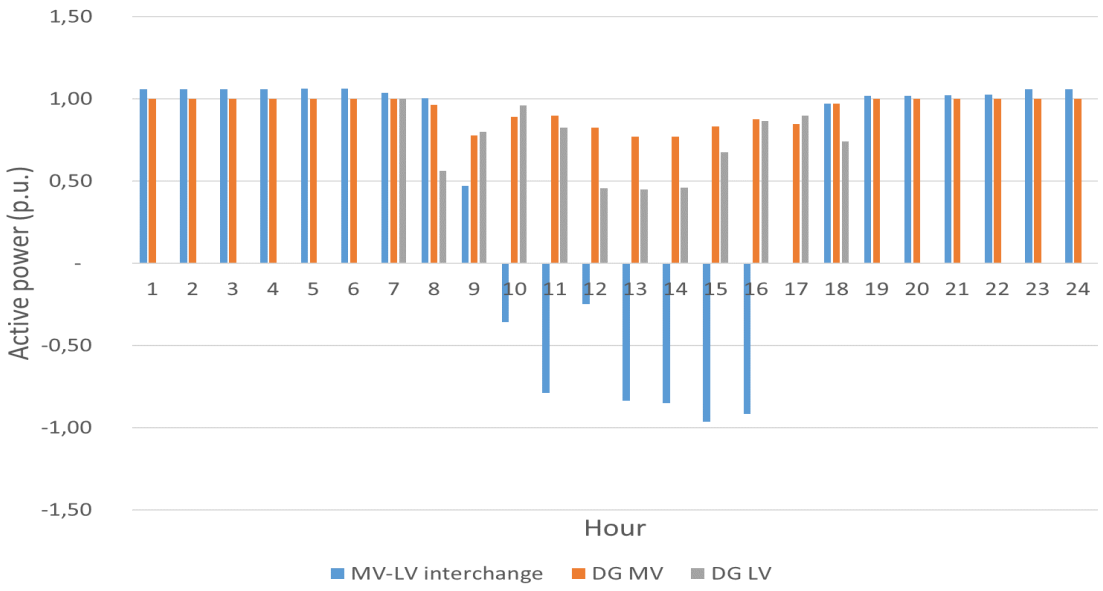

Fig. 5.40. Power exchange from the MV network to the LV network for the Winter case

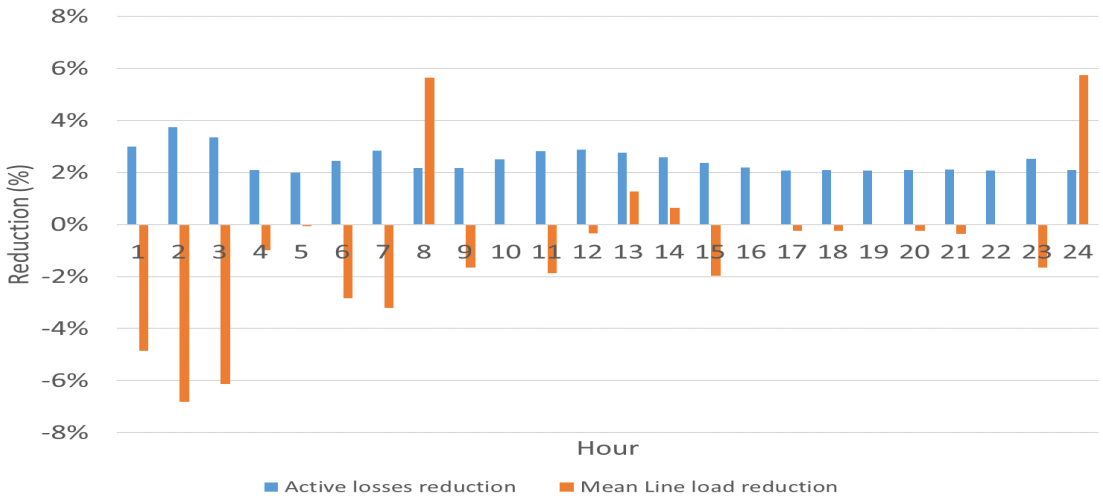

Fig. 5.41. Reduction of the active power losses and average load throughout the lines of the MV network for the Winter case

devices present in the grids. The MV network regards the LV power systems as flexible controllable units that are capable of exchanging either positive or negative power that is, they either act as generators or as loads. The MV grid is seen as a generator for each LV grid, and it has a power output that could be positive or negative, depending on the optimal solution established by the CVC-MV. An optimum voltage at the border nodes shared by both networks is also determined by the CVC-MV. The establishment of the flexibility set-point corresponding to the power exchange among the grids as well as the optimal voltage at the border allows the voltage control scheme to undertake a coordination between the MV and LV levels in the distribution power systems.

The proposed CVC scheme has been compared with two conventional voltage control techniques, namely the local decentralized control in which the interconnection requirements for the RES are defined by the IEEE Standard 1547-2018 and distributed control, which comprises two independent controllers for both MV and LV networks. In the distributed control scheme, there is no information or power exchange between such grids.

The analysis of the results show that the coordinated control scheme allows to optimize the performance of the whole distribution system (MV grid and LV grids) in terms of power losses and curtailment of the DG units.

In addition, the proposed CVC is the only scheme that can determine the optimal working set-points under abnormal working conditions, such as the loss of an MV grid's line.

In looking at the obtained results, the coordinated control algorithm has been applied to the network being studied by considering different load and generation situations. It can be concluded that the application of the proposed algorithm allows power losses in the system to be minimized, and it also reduce the loads carried by the lines if a coordinated optimal assignation of the DG units present in the whole system is performed. Moreover, due to this optimal assignation, the usage of reactive power compensation devices in the MV systems could be eliminated. This can be concluded because with the use of the coordinated voltage control the reactive power compensator units have been used only in one hour of the 96 hours studied and with a required power injection of one fifth of their nominal capacity. Regarding the secondary substation transformer of the LV grids, the application of the coordinated control algorithm allows the number of OLTC tap changes to be minimized because they basically employ two tap ratios. Specifically, one ratio is used for the hours when power is exported toward the MV network, and the other one is used for the hours when power is imported from the MV network instead, which allows them to increase their lifespan.

6. CONCLUSIONS

6.1. Introduction

This chapter presents a summary of the main conclusions obtained in this thesis. A section is dedicated to enumerating the original contributions of this work; future lines of investigation are also explores in the chapter.

6.2. Conclusion

The present doctoral thesis focused on the development of tools that employ the flexibility associated with the DER units that are present in the distribution systems, both at the level of generation units and network operation. The aim of these tools are to improve the voltage control in these systems and the coordination between MV and LV grids.

The main conclusions that arise from the work carried out in each chapters are listed as follows.

Chapter 2 carried out a state-of-the-art review of the Smart Grids corresponding to distribution grids.

- The state-of-the-art analysed all the main actors in a Smart Grids as well as the communication infrastructures and standards developed at the EU.
- The current situation of Smart Grids in the EU-countries in terms of smart meters deployment, demand management mechanisms, implementation of an aggregator figure, and the participation of prosumers in the Smart Grid networks has been analysed.
- Based on the study carried out, it is concluded that there are currently problems and barriers for the full implementation of smart grid networks at the distribution level.

Chapter 3 reviewed the state-of-the-art of the main elements and schemes used for the voltage control of distribution Smart Grids.

- Firstly, the chapter analysed the impact of having active/reactive power variation in the voltage of the grid nodes with a high R/X ratio, that is the case of LV distribution grids. The study found that, unlike in the transmission systems, in distribution grids, where their lines present a noticeable resistive characteristic, active power has a greater impact on bus voltage than the reactive power. It is concluded that the Volt/Watt control mode is the most suitable mode to perform voltage control in LV distribution grids.

- Secondly, the chapter presented a review of the elements traditionally used to perform voltage control, as well as the capacity curves corresponding to PV panels and DFIG wind turbines. To deal with active power - bus voltage relation in distribution grids, two active power control techniques are studied, that are load shedding and demand response mechanisms. Moreover, the usage of storage units is investigated in order to store the energy curtailed. The voltage control mechanisms analysed in Chapter 3 can be used as flexibility services to the DSO.

- Lastly, the chapter analysed the main voltage control schemes used in the distribution grids. The study highlighted the most representative schemes, namely the decentralized, centralized, hierarchical, and coordinated schemes. The study concluded that given the volume of information to be managed by the Smart Grids networks, the most suitable control schemes for this task are the coordinated scheme and the hierarchical control scheme.

Chapter 4 is focused on wave energy. A hybrid wave emplacement coupled to a Flywheel Energy Storage System is modelled. In this chapter:

- The study presents the current state of wave energy, the available resource worldwide, and future perspectives. An analysis of the main components of a wave farm was performed; this included the set of equations that model the wave energy extraction device, as well as the linear generator connected to the wave unit. In order to compensate output power fluctuations of the wave energy installation, a flywheel units it is proposed to store the curtailed energy.

- Following this, a state-of-the-art of flywheel technology is presented, regarding the flywheel components as well as the equations that model it.

- In the final part of the chapter, a hybrid wave-KESS installation model is developed, this model combined the application of clustering and filtering techniques with the utilization of a flywheel in order to improve the power output of the hybrid installation. The study validated the developed model by using real data gathered from the wave farm emplacement owned by Uppsala University and located at Lysekil, Sweden. It has been established that the proposed hybrid plant model smoothens the installation's power output, and let the wave-KESS installation to be connected to the LV grid. Moreover, the hybrid plant can follow a power reference signal imposed by the grid operator. In addition, the study demonstrated that the proposed combination of a wave farm with a KESS unit can be grid-connected as a controllable distributed resource. Such a configuration is capable of offering enough flexibility to the DSO.

Finally, Chapter 5 developed a coordinated voltage control scheme that is suitable for the distribution grids with a high penetration of distributed energy resources.

- First, the study defined the information that must be exchanged between MV and LV networks; knowing this information makes it possible to take advantage of the flexibility offered by DER units located in the LV grid for MV grid voltage support and control purposes.
- The study also found that the absence of information exchange, between operators and devices in both local and distributed voltage control schemes, leads to failure of solving congestions produced for N-1 contingencies which appears in the MV grids (i.e., lost line).
- The study also proved that the utilization of a flexibility set-point for power exchange between MV and LV grids allows for an optimum operation of both grids, when there are normal and abnormal operation conditions.
- From the proposed voltage control scheme, the study demonstrated that the flexibility offered by the LV grid operator, can be used to address voltage deviations or congestions that can arise in MV networks.
- The applicability of the proposed CVC has been demonstrated in a MV-LV network, with 140 nodes at the MV level and 160 nodes at the LV level. Both power systems are real networks located in Spain.
- From the obtained results, the study proved that the proposed coordinated control scheme makes it possible to reduce the number of operations performed on the secondary substation transformer's tap regulations. The study also found that the scheme can reduce the size of the reactive power compensation devices that are connected to both grids.
- Finally, the study concluded that the proposed control scheme allows solving DER integration problems, and it also activates the flexibility resources offered by the DER units in LV systems in order to improve the operation of the MV grid.

6.3. Contributions

The main contributions from the work developed in the doctoral thesis are listed as follows:

- A hybrid wave-Kinetic Energy Storage System (KESS) model is developed.
  - The proposed hybrid wave-KESS plant model is capable of smoothing the power output of the plant, thus allowing the marine installation to be connected to the LV network, as well as following a power reference given by the network operator.

  - The developed wave-KESS model offers flexibility to the DSO in terms of active power. DSO can use this flexibility to participate in voltage control services.

- The development of a Coordinated Voltage Control (CVC) in MV and LV distribution grids, with a high penetration of distributed energy resources.
  - The proposed CVC allows LV grids to offer the aggregated flexibility of their DER units for the optimum operation of the MV grids, and to participate in the voltage control services.
  - The proposed scheme makes it possible to determine the optimum flexibility in the border nodes between the MV and LV grids, as well as the working set-points of both DER and traditional voltage control devices that are in both grids; so that the operation of such networks keeps within the established voltage and overload limits.
  - The developed control scheme is capable of working on both normal and abnormal operation network conditions. In normal operation conditions, the scheme carries out the flexibility planning of the DER devices and the border power exchange for an established time horizon, and on abnormal operation conditions the CVC establishes the necessary flexibility in the border nodes to solve eventual contingencies.

- The definition of the information exchange between the MV and LV operator that it is used by the coordinated control scheme. This information exchange allows the LV operators to offer complimentary voltage services to the MV grid.

6.4. Future work

From the conclusions obtained in this doctoral thesis, a number of future investigation lines can be followed.

- **Integration of electrical vehicle and demand management systems in the coordinated control scheme**. One of the main problems derived from the uncontrolled electric vehicles recharge, in LV grids, is the violation of the admissible voltage lower limits in the nodes of these networks. The active management of both electric vehicles demand and LV grid appliances would allows the operation of such grids to be optimized and would also increase the flexibility offered by the LV grid operator to the MV grid operator.

- **MV grid's control scheme integration into the transmission network control**. At present, the TSO employs the flexibility of the devices that are present in the MV grid without establishing any communication with the DSO, which leads to congestions in the distribution grid. It is therefore necessary to have a greater level

of cooperation between TSOs and DSOs. To do this, there needs to be a development in the control schemes between transmission and distribution grids that employ the flexibility available in the MV grids. This would facilitate the operation of the transmission networks, in both normal and abnormal situations of operation, without incurring congestions of distribution grids.

- Development and incorporation of a new bandpass filter based on Machine Learning techniques. This would be used for the smoothing stage of the output power of the wave emplacement.

BIBLIOGRAPHY

[1] B. Rojas, M. Alonso, H. Amarís, and L. González, "Coordinated management of low voltage power networks with photovoltaic energy sources", *International Journal of Smart Grid and Clean Energy*, vol. 5, no. 5, pp. 2013–220, 2016.

[2] OECD/IEA, "System integration of renewables: Implications for electricity security. report to the g7.29", IEA, Tech. Rep., 2016.

[3] T. G. San Román, "Integration of DERs on power systems: Challenges and opportunities", IEB Working Paper N. 2017/02, Tech. Rep., 2017.

[4] S. E. Michael Schmela, "Global market outlook for solar power 2018–2022", *SolarPower Europe: Brussels, Belgium*, 2018.

[5] Eurelectric/EDSO, "DSO priorities for smart grid standardisation", Joint Task ForceSmart Grid Standardisation. Eurelectric/EDSO, Tech. Rep., 2013.

[6] H. Gerard, E. Rivero, and D. Six, "Basic schemes for TSO-DSO coordination and ancillary services provision", Smartnet Project. D3.1, Tech. Rep., 2016.

[7] "UNE-EN 50160: Voltage characteristics of electricity supplied by public electricity networks", Asociación Española de Normalización, Tech. Rep., 2011/A1:2015.

[8] A. Angioni *et al.*, "Design and implementation of a substation automation unit", *IEEE Transactions on Power Delivery*, vol. 32, no. 2, pp. 1133–1142, 2017.

[9] H. Schuster, J. Kellermann, T. Bongers, V. G. Oñate, and R. Hermes, "Development of methodologies and tools for new and evolving dso roles for efficient dres integration in distribution networks", evolvDSO project. D1.2, Tech. Rep., 2014.

[10] T. Senjyu, Y. Miyazato, A. Yona, N. Urasaki, and T. Funabashi, "Optimal distribution voltage control and coordination with distributed generation", *IEEE Transactions on power delivery*, vol. 23, no. 2, pp. 1236–1242, 2008.

[11] H. J. Liu, W. Shi, and H. Zhu, "Distributed voltage control in distribution networks: Online and robust implementations", *IEEE Transactions on Smart Grid*, vol. 9, no. 6, pp. 6106–6117, 2018.

[12] M. L. Tuballa and M. L. Abundo, "A review of the development of smart grid technologies", *Renewable and Sustainable Energy Reviews*, vol. 59, pp. 710–725, 2016.

[13] IEC, "IEC smart grid standardization roadmap", SMB Smart Grid Strategic Group (SG3), Tech. Rep., 2010.

[14] "Technology Roadmap - Smart Grids". International Energy Agency (IEA)", IEA, Tech. Rep., 2011.

[15] IEA, “How2Guide for smart grids in distribution networks. roadmap development and implementation”, International Energy Agency, Tech. Rep., 2015.

[16] (2018). Grid Modernization and the Smart Grid department of Energy. Office of Electricity. U.S. Department of Energy, [Online]. Available: https://www.energy.gov/oe/activities/technology-development/grid-modernization-and-smart-grid (visited on 05/06/2018).

[17] F. H. Malik and M. Lehtonen, “A review: Agents in smart grids”, *Electric Power Systems Research*, vol. 131, pp. 71–79, 2016.

[18] D. Kolokotsa, “The role of smart grids in the building sector”, *Energy and Buildings*, vol. 116, pp. 703–708, 2016.

[19] G. P. Verbong, S. Beemsterboer, and F. Sengers, “Smart grids or smart users? involving users in developing a low carbon electricity economy”, *Energy Policy*, vol. 52, pp. 117–125, 2013.

[20] R. Belmans, “2035 strategic research agenda, update of the smart grids sra 2007 for the needs by the year 2035”, European Technology Platform Smart Grids, Tech. Rep., 2013.

[21] (2018). Smart Grid Resource Center, [Online]. Available: http://smartgrid.epri.com/ (visited on 10/09/2018).

[22] (2010). Smart grids: Redes eléctricas inteligentes, [Online]. Available: http://www.energiaysociedad.es/pdf/smartgrids.pdf (visited on 05/06/2018).

[23] C. Clastres, “Smart grids: Another step towards competition, energy security and climate change objectives”, *Energy Policy*, vol. 39, no. 9, pp. 5399–5408, 2011.

[24] M. E. El-Hawary, “The smart grid state-of-the-art and future trends”, *Electric Power Components and Systems*, vol. 42, no. 3-4, pp. 239–250, 2014.

[25] F. Gangale, J. Vasiljevska, C. F. Covrig, A. Mengolini, and G. Fulli, “Smart grid projects outlook 2017”, European Commision, 2017.

[26] *Orden IET/290/2012, de 16 de febrero, por la que se modifica la orden ITC/3860/2007, de 28 de diciembre, por la que se revisan las tarifas eléctricas a partir del 1 de enero de 2008 en lo relativo al plan de sustitución de contadores*, Ministerio de Industria, Energía y Turismo, BOE-A-2012-2538, 2012.

[27] S. Repo et al, “D2.1 - Specification of Active Distribution Network Concept”, IDE4L Project, Tech. Rep., 2014.

[28] C. Greer *et al.*, “NIST framework and roadmap for smart grid interoperability standards, release 3.0”, National Institute of Standards and Technology. Special Publication (NIST SP) - 1108r3, Tech. Rep., 2014.

[29] N. E. T. Laboratory, "Appendix B3: A Systems View of the Modern Grid ADVANCED COMPONENTS ", U.S. Department of Energy - Office of Electricity Delivery and Energy Reliability, Tech. Rep., Mar. 2017. [Online]. Available: https://www.smartgrid.gov/files/appendix_b3_advanced_components.pdf (visited on 04/09/2018).

[30] A. Uihlein and D. Magagna, "Wave and tidal current energy–a review of the current state of research beyond technology", *Renewable and Sustainable Energy Reviews*, vol. 58, pp. 1070–1081, 2016.

[31] D. Infield and J. Hill, *Literature Review: Electrical Energy Storage for Scotland*. University of Strathclyde, 2015.

[32] A. Ahadi and X. Liang, "A stand-alone hybrid renewable energy system assessment using cost optimization method", in *2017 IEEE International Conference on Industrial Technology (ICIT)*, Mar. 2017, pp. 376–381. DOI: 10.1109/ICIT.2017.7913260.

[33] EU, "Setting emission performance standards for new passenger cars and for new light commercial vehicles as part of the Union's integrated approach to reduce CO2 emissions from light-duty vehicles and amending regulation (EC)", Parliament, EU. Regulation (EC) N.7, Tech. Rep., 2017.

[34] M. Alonso, H. Amaris, J. G. Germain, and J. M. Galan, "Optimal charging scheduling of electric vehicles in smart grids by heuristic algorithms", *Energies*, vol. 7, no. 4, pp. 2449–2475, 2014.

[35] W. Kempton and J. Tomić, "Vehicle-to-grid power fundamentals: Calculating capacity and net revenue", *Journal of power sources*, vol. 144, no. 1, pp. 268–279, 2005.

[36] D. Hall and N. Lutsey, "Literature review on power utility best practices regarding electric vehicles", International Council on Clean Transportation, Tech. Rep., 2017.

[37] C. Badajoz, S. Dourlens-Quaranta, D. Hernandez-Maldonado, and E. Peirano, "Cooperation between horizon 2020 projects in the field of smart grids and energy storage", European Commision, Tech. Rep., 2018.

[38] N. G. Hingorani, "Introducing custom power", *IEEE spectrum*, vol. 32, no. 6, pp. 41–48, 1995.

[39] "Clean energy for all europeans (CEfAE) package", European Commision, Tech. Rep., 2016.

[40] (2016). Europe 2020 indicators - climate change and energy. Statistical office of the European Union (Eurostat), [Online]. Available: https://ec.europa.eu/eurostat/statistics-explained/index.php?title=Europe_2020_indicators_-_climate_change_and_energy#Renewable_energy_on_the_rise (visited on 10/06/2018).

[41] E. Star and C. Lighting, "Energy Star building upgrade manual", *US Environmental Protection Agency and the US Department of Energy*, 2008.

[42] K. Aduda, "Smart grid-building energy interactions: Demand side power flexibility in office buildings", Eindhoven: Technische Universiteit Eindhoven, Tech. Rep., 2018.

[43] S. Gottwalt, "Managing flexible loads in residential areas", PhD thesis, Dissertation. Karlsruher Instituts für Technologie (KIT), 2015.

[44] GfK Belgium consortium, "Study on Residential Prosumers in the European Energy Union", EU framework JUST/2015/CONS/FW/C006/0127. 2017, Tech. Rep., 2017.

[45] *Real Decreto 900/2015, de 9 de octubre, por el que se regulan las condiciones administrativas, técnicas y económicas de las modalidades de suministro de energía elíctrica con autoconsumo y de producción con autoconsumo*, Ministerio de Industria, Energía y Turismo. BOE» núm. 243, de 10/10/2015.

[46] Smart Energy Demand Coalition (SEDC), "Explicit demand response in europe-mapping the markets 2017", *SEDC: Brussels, Belgium*, 2017.

[47] V. Dehalwar, A. Kalam, M. L. Kolhe, and A. Zayegh, "Review of IEEE 802.22 and IEC 61850 for real-time communication in Smart Grid", in *Computing and Network Communications (CoCoNet), 2015 International Conference on*, IEEE, 2015, pp. 571–575.

[48] T. Considine, T. Principal, and W. T. Cox, "Smart loads and smart grids—creating the smart grid business case", in *Conference: Grid-Interop*, 2009.

[49] J. Babic and V. Podobnik, "An Analysis of Power TAC 2013 Trial", in *AAAI Workshop: Trading Agent Design and Analysis*, 2013.

[50] (2018). Power Tac, [Online]. Available: `http://powertac.org/` (visited on 05/12/2018).

[51] H. Kanchev, D. Lu, F. Colas, V. Lazarov, and B. Francois, "Energy management and operational planning of a microgrid with a pv-based active generator for smart grid applications", *IEEE transactions on industrial electronics*, vol. 58, no. 10, pp. 4583–4592, 2011.

[52] J. A. Momoh, "Smart grid design for efficient and flexible power networks operation and control", in *Power Systems Conference and Exposition, 2009. PSCE'09. IEEE/PES*, IEEE, 2009, pp. 1–8.

[53] A. Mavridou and M. Papa, "A situational awareness architecture for the Smart Grid", in *Global Security, Safety and Sustainability & e-Democracy*, Springer, 2012, pp. 229–236.

[54] National Energy Technology Laboratory, "Methodologies to facilitate Smart Grid system interoperability through standardization, system design and testing ", CEN-CENELEC-ETSI Smart Grid Coordination Group, Tech. Rep., Oct. 2014.

[55] S. Howell, Y. Rezgui, J.-L. Hippolyte, B. Jayan, and H. Li, "Towards the next generation of smart grids: Semantic and holonic multi-agent management of distributed energy resources", *Renewable and Sustainable Energy Reviews*, vol. 77, pp. 193–214, 2017.

[56] C. D'Adamo *et al.*, "Development and operation of active distribution networks: Results of CIGRE C6. 11 working group", in *Proceedings of the CIRED 21st international conference on electricity distribution, Frankfurt, Germany*, 2011, pp. 6–9.

[57] N. Efkarpidis, T. De Rybel, and J. Driesen, "Technical assessment of centralized and localized voltage control strategies in low voltage networks", *Sustainable Energy, Grids and Networks*, vol. 8, pp. 85–97, 2016.

[58] "IEC TR 61000-2-14: Electromagnetic compatibility (EMC) - Part 2-14: Environment - Overvoltages on public electricity distribution networks ", International Electrotechnical Commission, Tech. Rep., 2006.

[59] D. Alcalá González, "Coordinación de protecciones en redes eléctricas con generación distribuida", PhD thesis, Universidad Carlos III de Madrid, 2016.

[60] "Discover the World of FACTS Technology - Technical Compendium", SIEMENS AG, Erlangen, Germany, Tech. Rep., 2011.

[61] F. H. Gandoman *et al.*, "Review of FACTS technologies and applications for power quality in smart grids with renewable energy systems", *Renewable and Sustainable Energy Reviews*, vol. 82, pp. 502–514, 2018.

[62] T. Stetz, M. Rekinger, and I. Theologitis, "Transition from Uni-Directional to Bi-Directional Distribution Grids", *Management Summary of IEA Task*, vol. 14, 2014.

[63] CIGRÉ Working Group 14.19, "Static Synchronous Compensator (STATCOM)", International Council on Large Electric Systems. CIGRE publication, Tech. Rep., 1999.

[64] C. Álvarez Ortega, "Voltage dip mitigation at wind farms", PhD thesis, Universidad Carlos III de Madrid, 2011.

[65] E. F. Camacho, T. Samad, M. Garcia-Sanz, and I. Hiskens, "Control for renewable energy and smart grids", *The Impact of Control Technology, Control Systems Society*, pp. 69–88, 2011.

[66] *IEEE Standard for Interconnection and Interoperability of Distributed Energy Resources with Associated Electric Power Systems Interfaces*, IEEE Std 1547-2018, pp.1-138, 6 April 2018.

[67] *Real Decreto 1565/2010, de 19 de noviembre, por el que se regulan y modifican determinados aspectos relativos a la actividad de producción de energía eléctrica en régimen especial*, Ministerio de Industria, Energía y Turismo. BOE» núm. 283, de 23 de noviembre de 2010, 2010.

[68] *VDE-AR-N 4105:2011-08 Power generation systems connected to the low-voltage distribution network*, 2011.

[69] J. Gómez-González *et al.*, "Reactive power management in photovoltaic installations connected to low-voltage grids to avoid active power curtailment.", *Renewable Energy and Power Quality Journal*, no. 6, pp. 1–7, 2018.

[70] S. Adhikari and F. Li, "Coordinated Vf and PQ Control of Solar Photovoltaic Generators With MPPT and Battery Storage in Microgrids", *IEEE Trans. Smart Grid*, vol. 5, no. 3, pp. 1270–1281, 2014.

[71] H. Abdar, A. Chakraverty, D. Moore, J. Murray, and K. Loparo, "Design and implementation a specific grid-tie inverter for an agent-based microgrid", in *Energytech, 2012 IEEE*, IEEE, 2012, pp. 1–6.

[72] A. Cabrera-Tobar, E. Bullich-Massagué, M. Aragüés-Peñalba, and O. Gomis-Bellmunt, "Capability curve analysis of photovoltaic generation systems", *Solar Energy*, vol. 140, pp. 255–264, 2016.

[73] O. Bertetti, "Benchmarking of Smart Grid Concepts in Low-Voltage Distribution Grids", Master's thesis, KTH, School of Industrial Engineering, Management (ITM), Energy Technology, Heat, and Power Technology., 2017.

[74] T. Xu and P. Taylor, "Voltage control techniques for electrical distribution networks including distributed generation", *IFAC Proceedings Volumes*, vol. 41, no. 2, pp. 11 967–11 971, 2008.

[75] N. Chettibi, A. Mellit, G. Sulligoi, and A. M. Pavan, "Adaptive neural network-based control of a hybrid AC/DC microgrid", *IEEE Transactions on Smart Grid*, vol. 9, no. 3, pp. 1667–1679, 2018.

[76] N. Mahmud and A. Zahedi, "Review of control strategies for voltage regulation of the smart distribution network with high penetration of renewable distributed generation", *Renewable and Sustainable Energy Reviews*, vol. 64, pp. 582–595, 2016.

[77] H. S. Bidgoli and T. Van Cutsem, "Combined local and centralized voltage control in active distribution networks", *IEEE Transactions on Power Systems*, vol. 33, no. 2, pp. 1374–1384, 2018.

[78] D. Zarrilli, A. Giannitrapani, S. Paoletti, and A. Vicino, "Energy storage operation for voltage control in distribution networks: A receding horizon approach", *IEEE Transactions on Control Systems Technology*, vol. 26, no. 2, pp. 599–609, 2018.

[79] M. E. Amiryar and K. R. Pullen, "A review of flywheel energy storage system technologies and their applications", *Applied Sciences*, vol. 7, no. 3, p. 286, 2017.

[80] F. Marra, G. Yang, C. Træholt, J. Ostergaard, and E. Larsen, "A decentralized storage strategy for residential feeders with photovoltaics", *IEEE Transactions on Smart Grid*, vol. 5, no. 2, pp. 974–981, 2014.

[81] S. Ruggeri, "Centralised and decentralised control of active distribution systems: Models, algorithms and applications.", PhD thesis, Universita'degli Studi di Cagliari, 2015.

[82] X. Liu, A. Aichhorn, L. Liu, and H. Li, "Coordinated control of distributed energy storage system with tap changer transformers for voltage rise mitigation under high photovoltaic penetration", *IEEE Transactions on Smart Grid*, vol. 3, no. 2, pp. 897–906, 2012.

[83] Y. P. Agalgaonkar, B. C. Pal, and R. A. Jabr, "Distribution voltage control considering the impact of pv generation on tap changers and autonomous regulators", *IEEE Transactions on Power Systems*, vol. 29, no. 1, pp. 182–192, 2014.

[84] M. A. Azzouz, M. F. Shaaban, and E. F. El-Saadany, "Real-time optimal voltage regulation for distribution networks incorporating high penetration of PEVs", *IEEE Transactions on Power Systems*, vol. 30, no. 6, pp. 3234–3245, 2015.

[85] I. Ranaweera and O.-M. Midtgard, "Centralized control of energy storages for voltage support in low-voltage distribution grids", in *Environment and Electrical Engineering (EEEIC), 2016 IEEE 16th International Conference on*, IEEE, 2016, pp. 1–6.

[86] H. Ji *et al.*, "A centralized-based method to determine the local voltage control strategies of distributed generator operation in active distribution networks", *Applied Energy*, vol. 228, pp. 2024–2036, 2018.

[87] J. Zhao *et al.*, "A review of active management for distribution networks: Current status and future development trends", *Electric Power Components and Systems*, vol. 42, no. 3-4, pp. 280–293, 2014.

[88] M. Yazdanian and A. Mehrizi-Sani, "Distributed control techniques in microgrids", *IEEE Transactions on Smart Grid*, vol. 5, no. 6, pp. 2901–2909, 2014.

[89] M. Andreasson, D. V. Dimarogonas, K. H. Johansson, and H. Sandberg, "Distributed vs. centralized power systems frequency control", in *2013 12th European Control Conference, ECC 2013; Zurich; Switzerland; 17 July 2013 through 19 July 2013*, 2013, pp. 3524–3529.

[90] V. Calderaro, G. Conio, V. Galdi, G. Massa, and A. Piccolo, "Optimal decentralized voltage control for distribution systems with inverter-based distributed generators", *IEEE Transactions on Power Systems*, vol. 29, no. 1, pp. 230–241, 2014.

[91] P. M. Carvalho, P. F. Correia, and L. A. Ferreira, "Distributed reactive power generation control for voltage rise mitigation in distribution networks", *IEEE transactions on Power Systems*, vol. 23, no. 2, pp. 766–772, 2008.

[92] L. F. Ochoa, A. Keane, and G. P. Harrison, "Minimizing the reactive support for distributed generation: Enhanced passive operation and smart distribution networks", *IEEE Transactions on Power Systems*, vol. 26, no. 4, pp. 2134–2142, 2011.

[93] T. Suehiro and T. Namerikawa, "Decentralized control of smart grid by using overlapping information", in *SICE Annual Conference (SICE), 2012 Proceedings of*, IEEE, 2012, pp. 125–130.

[94] P. Khayyer and Ü. Özgüner, "Decentralized control of smart grid with fixed and moving loads", in *Power and Energy Conference at Illinois (PECI), 2013 IEEE*, IEEE, 2013, pp. 72–75.

[95] Q. Zhang, J. He, and D. Zhang, "Coordinated control of energy storage devices and photovoltaic inverters for voltage regulation based on multi-agent system", in *Energy Internet and Energy System Integration (EI2), 2017 IEEE Conference on*, IEEE, 2017, pp. 1–6.

[96] Y. Guo *et al.*, "MPC-Based Coordinated Voltage Regulation for Distribution Networks With Distributed Generation and Energy Storage System", *IEEE Transactions on Sustainable Energy*, 2018. DOI: 10.1109/TSTE.2018.2869932.

[97] Y. Wang, K. Tan, X. Y. Peng, and P. L. So, "Coordinated control of distributed energy-storage systems for voltage regulation in distribution networks", *IEEE Transactions on Power Delivery*, vol. 31, no. 3, pp. 1132–1141, 2016.

[98] D. Hill, T. Liu, and G. Verbic, "Smart grids as distributed learning control", in *2012 IEEE Power and Energy Society General Meeting*, IEEE, 2012, pp. 1–8. DOI: 10.1109/PESGM.2012.6344726.

[99] X. M. Barraguer, "Sistema de Control Distribuido: nuevas soluciones para adaptarse a las exigencias del mercado", *Industria química*, no. 39, pp. 56–60, 2016.

[100] J. H. van Schuppen, "What is Coordination Control?", in *Coordination Control of Distributed Systems*, Springer, 2015, pp. 99–106.

[101] F. Kennel, D. Gorges, and S. Liu, "Energy management for smart grids with electric vehicles based on hierarchical mpc", *IEEE Transactions on industrial informatics*, vol. 9, no. 3, pp. 1528–1537, 2013.

[102] E. Ortjohann *et al.*, "Multi-level hierarchical control strategy for smart grid using clustering concept", in *Clean Electrical Power (ICCEP), 2011 International Conference on*, IEEE, 2011, pp. 648–653.

[103] S.Repo et al, "IDE4L GRID FOR ALL. Finalreport", IDE4L EU Project, Tech. Rep., 2016.

[104] "World Energy Outlook 2016", Organization for Economic Cooperation and Development (OECD). International Energy Agency. ISBN: 978-92-64-26495-3, Tech. Rep., 2016.

[105] H. Schiffer et al, "World Energy Resources: Marine Energy 2016", World Energy Council, Tech. Rep., Mar. 2017. [Online]. Available: https://www.worldenergy.org/wp-content/uploads/2017/03/%20WEResources%5Ctextunderscore%20Marine%5Ctextunderscore%202016.pdf (visited on 04/09/2018).

[106] (2018). How much water is there on Earth, from the USGS Water Science School, [Online]. Available: https://water.usgs.gov/edu/earthhowmuch.html (visited on 04/09/2018).

[107] J. Falnes, "A review of wave-energy extraction", *Marine structures*, vol. 20, no. 4, pp. 185–201, 2007.

[108] A. Clément *et al.*, "Wave energy in Europe: current status and perspectives", *Renewable and sustainable energy reviews*, vol. 6, no. 5, pp. 405–431, 2002.

[109] R. Pelc and R. M. Fujita, "Renewable energy from the ocean", *Marine Policy*, vol. 26, no. 6, pp. 471–479, 2002.

[110] A. M. Howlader, N. Urasaki, A. Yona, T. Senjyu, and A. Y. Saber, "A review of output power smoothing methods for wind energy conversion systems", *Renewable and Sustainable Energy Reviews*, vol. 26, pp. 135–146, 2013.

[111] A. Blavette et al., "Grid Integration of Wave and Tidal Energy", in *International Conference on Offshore Mechanics and Arctic Engineering. Volume 5: Ocean Space Utilization; Ocean Renewable Energy (2011)*, 2011, pp. 749–758.

[112] K. Gunn and C. Stock-Williams, "Quantifying the global wave power resource", *Renewable Energy*, vol. 44, pp. 296–304, 2012.

[113] H. Titah-Benbouzid and M. Benbouzid, "An up-to-date technologies review and evaluation of wave energy converters", *International Review of Electrical Engineering - Iree*, vol. 10, no. 1, pp. 52–61, 2015.

[114] C. Trust, *Future Marine Energy: Results of the Marine Energy Challenge : Cost Competitiveness and Growth of Wave and Tidal Stream Energy*. Carbon Trust, 2006. [Online]. Available: https://books.google.es/books?id=kQx0nQEACAAJ.

[115] R. A. Board, "Marine renewables: current status and implications for R&D funding and the Marine Renewables Deployment Fund", *London, Renewables Advisory Board*, 2008.

[116] D. Vannuci, "ORECCA. WP3 Technologies State of the Art", Tech. Rep., 2011.

[117] (2018). Renewable Energy, [Online]. Available: https://www.boem.gov/Renewable-Energy (visited on 04/09/2018).

[118] (2018). Energy Department Announces Investment in Wave Energy Test Facility. Office of Energy Efficiency and Renewable Energy. US Department of Energy, [Online]. Available: https://www.energy.gov/articles/energy-department-announces-investment-wave-energy-test-facility (visited on 04/09/2018).

[119] A. Curvers and J. Pierik, "ORECCA. WP3: Technologies state of the art. Task 3: Grid integration aspects", *ECN Report. ECN-E–11-014. 2011*, 2011.

[120] (2018). ORECCA - Project, [Online]. Available: https://cordis.europa.eu/project/rcn/94058_es.html (visited on 04/09/2018).

[121] (2018). The Project MeyGen, [Online]. Available: http://www.meygen.com/the-project/ (visited on 04/09/2018).

[122] F. António F. de O., "Wave energy utilization: A review of the technologies", *Renewable and sustainable energy reviews*, vol. 14, no. 3, pp. 899–918, 2010.

[123] N. Khan, A. Kalair, N. Abas, and A. Haider, "Review of ocean tidal, wave and thermal energy technologies", *Renewable and Sustainable Energy Reviews*, vol. 72, pp. 590–604, 2017.

[124] P. Moreno-Torres, M. Blanco, G. Navarro, and M. Lafoz, "Power smoothing system for wave energy converters by means of a supercapacitor-based energy storage system", in *Power Electronics and Applications (EPE'15 ECCE-Europe), 2015 17th European Conference on*, IEEE, 2015, pp. 1–9.

[125] A. Çelik and A. Altunkaynak, "Experimental and analytical investigation on chamber water surface fluctuations and motion behaviours of water column type wave energy converter", *Ocean Engineering*, vol. 150, pp. 209–220, 2018.

[126] Z. Zang, Q. Zhang, Y. Qi, and X. Fu, "Hydrodynamic responses and efficiency analyses of a heaving-buoy wave energy converter with pto damping in regular and irregular waves", *Renewable Energy*, vol. 116, pp. 527–542, 2018.

[127] G. Tampier and L. Grueter, "Hydrodynamic analysis of a heaving wave energy converter", *International Journal of Marine Energy*, vol. 19, pp. 304–318, 2017.

[128] D. Yurchenko and P. Alevras, "Parametric pendulum based wave energy converter", *Mechanical Systems and Signal Processing*, vol. 99, pp. 504–515, 2018.

[129] M. Melikoglu, "Current status and future of ocean energy sources: A global review", *Ocean Engineering*, vol. 148, pp. 563–573, 2018.

[130] D. Xu, R. Stuhlmeier, and M. Stiassnie, "Assessing the size of a twin-cylinder wave energy converter designed for real sea-states", *Ocean Engineering*, vol. 147, pp. 243–255, 2018.

[131] Z. Han, Z. Liu, and H. Shi, "Numerical study on overtopping performance of a multi-level breakwater for wave energy conversion", *Ocean Engineering*, vol. 150, pp. 94–101, 2018.

[132] L. Wang, J. Isberg, and E. Tedeschi, "Review of control strategies for wave energy conversion systems and their validation: The wave-to-wire approach", *Renewable and Sustainable Energy Reviews*, vol. 81, pp. 366–379, 2018.

[133] S. Prakash *et al.*, "Wave Energy Converter: A Review of Wave Energy Conversion Technology", in *2016 3rd Asia-Pacific World Congress on Computer Science and Engineering (APWC on CSE)*, IEEE, 2016, pp. 71–77.

[134] (2019). Marine Energy- Wave Device The European Marine Energy Centre, [Online]. Available: http://www.emec.org.uk/marine-energy/wave-devices/ (visited on 02/24/2019).

[135] M. Eriksson, R. Waters, O. Svensson, J. Isberg, and M. Leijon, "Wave power absorption: Experiments in open sea and simulation", *Journal of Applied Physics*, vol. 102, no. 8, p. 084 910, 2007.

[136] (2018). Wave Roller, [Online]. Available: http://aw-energy.com/waveroller/ (visited on 10/04/2018).

[137] (2018). Oyster 800 at EMEC, [Online]. Available: https://tethys.pnnl.gov/annex-iv-sites/oyster-800-emec (visited on 10/04/2018).

[138] (2018). Pelamis Wave Power, [Online]. Available: http://www.emec.org.uk/about-us/wave-clients/pelamis-wave-power/ (visited on 10/04/2018).

[139] Y. Hong *et al.*, "Review on electrical control strategies for wave energy converting systems", *Renewable and Sustainable Energy Reviews*, vol. 31, pp. 329–342, 2014.

[140] E. Lejerskog, C. Boström, L. Hai, R. Waters, and M. Leijon, "Experimental results on power absorption from a wave energy converter at the Lysekil wave energy research site", *Renewable energy*, vol. 77, pp. 9–14, 2015.

[141] J. Leijon, "Simulation of a linear wave energy converter with different damping control strategies for improved wave energy extraction", Master's thesis, Uppsala University, 2016.

[142] W. Leonhard, *Control of electrical drives*. Springer Science & Business Media, 2001.

[143] *Guide to wave analysis and forecasting*, 2nd ed. Geneva, Switzerland: Secretariat of the World Meteorological Organization, 1998.

[144] X. Zhao, Z. Yan, and X.-P. Zhang, "A wind-wave farm system with self-energy storage and smoothed power output", *IEEE Access*, vol. 4, pp. 8634–8642, 2016.

[145] A. Krings and J. Soulard, "Overview and comparison of iron loss models for electrical machines", *Journal of Electrical Engineering*, vol. 10, no. 3, pp. 162–169, 2010.

[146] M. Rahm, O. Svensson, C. Boström, R. Waters, and M. Leijon, "Experimental results from the operation of aggregated wave energy converters", *IET Renewable Power Generation*, vol. 6, no. 3, pp. 149–160, 2012.

[147] J. Barranger, *Hysteresis and eddy-current losses of a transformer lamination viewed as an application of the poynting theorem*, NASA technical note (TN-D-3114). National Aeronautics and Space Administration, 1965.

[148] R. Henderson, "Design, simulation, and testing of a novel hydraulic power take-off system for the pelamis wave energy converter", *Renewable energy*, vol. 31, no. 2, pp. 271–283, 2006.

[149] E. H. Maslen and G. Schweitzer, *Magnetic bearings: theory, design, and application to rotating machinery*. Springer, 2009.

[150] B. Bolund, H. Bernhoff, and M. Leijon, "Flywheel energy and power storage systems", *Renewable and Sustainable Energy Reviews*, vol. 11, no. 2, pp. 235–258, 2007.

[151] H. H. Abdeltawab and Y. A.-R. I. Mohamed, "Robust energy management of a hybrid wind and flywheel energy storage system considering flywheel power losses minimization and grid-code constraints", *IEEE Transactions on Industrial Electronics*, vol. 63, no. 7, pp. 4242–4254, 2016.

[152] T. Yoshida, M. Sanada, S. Morimoto, and Y. Inoue, "Study of flywheel energy storage system for power leveling of wave power generation system", in *Electrical Machines and Systems (ICEMS), 2012 15th International Conference on*, IEEE, 2012, pp. 1–5.

[153] G. Kubin, "Wave digital filters: Voltage, current, or power waves?", in *Acoustics, Speech, and Signal Processing, IEEE International Conference on ICASSP'85.*, IEEE, vol. 10, 1985, pp. 69–72.

[154] M. El-Habrouk, M. K. Darwish, and P. Mehta, "Active power filters: A review", *IEE Proceedings - Electric Power Applications*, vol. 147, no. 5, pp. 403–413, 2000.

[155] V. Venugopal and G. H. Smith, "The effect of wave period filtering on wave power extraction and device tuning", *Ocean engineering*, vol. 34, no. 8-9, pp. 1120–1137, 2007.

[156] R. Godoy-Diana and S. P. Czitrom, "On the tuning of a wave-energy driven oscillating -water-column seawater pump to polychromatic waves", *Ocean Engineering*, vol. 34, no. 17-18, pp. 2374–2384, 2007.

[157] (2018). Power quality, [Online]. Available: `https://www.schaffner.com/products/power-quality/` (visited on 04/09/2018).

[158] R. Bedard and G. Hagerman, "E2I EPRI Assessment Offshore Wave Energy Conversion Devices", *Electricity Innovation Institute E2I EPRI WP–004–US–Rev*, vol. 1, 2004.

[159] A. K. Arani, H. Karami, G. Gharehpetian, and M. Hejazi, "Review of Flywheel Energy Storage Systems structures and applications in power systems and microgrids", *Renewable and Sustainable Energy Reviews*, vol. 69, pp. 9–18, 2017.

[160] F. Diaz-Gonzalez, F. D. Bianchi, A. Sumper, and O. Gomis-Bellmunt, "Control of a flywheel energy storage system for power smoothing in wind power plants", *IEEE Transactions on Energy Conversion*, vol. 29, no. 1, pp. 204–214, 2014.

[161] S. R. Gurumurthy, V. Agarwal, and A. Sharma, "Optimal energy harvesting from a high-speed brushless dc generator-based flywheel energy storage system", *IET Electric Power Applications*, vol. 7, no. 9, pp. 693–700, 2013.

[162] L. Wang, J.-Y. Yu, and Y.-T. Chen, "Dynamic stability improvement of an integrated offshore wind and marine-current farm using a flywheel energy-storage system", *IET Renewable Power Generation*, vol. 5, no. 5, pp. 387–396, 2011.

[163] J.-D. Park, C. Kalev, and H. F. Hofmann, "Control of high-speed solid-rotor synchronous reluctance motor/generator for flywheel-based uninterruptible power supplies", *IEEE Transactions on Industrial Electronics*, vol. 55, no. 8, pp. 3038–3046, 2008.

[164] W. Li, K. Chau, T. Ching, Y. Wang, and M. Chen, "Design of a high-speed superconducting bearingless machine for flywheel energy storage systems", *IEEE Transactions on Applied Superconductivity*, vol. 25, no. 3, pp. 1–4, 2015.

[165] C. Sihler and A. M. Miri, "A stabilizer for oscillating torques in synchronous machines", *IEEE transactions on industry applications*, vol. 41, no. 3, pp. 748–755, 2005.

[166] M. N. Recheis, B. Schweighofer, P. Fulmek, and H. Wegleiter, "Selection of magnetic materials for bearingless high-speed mobile flywheel energy storage systems", *IEEE transactions on magnetics*, vol. 50, no. 4, pp. 1–4, 2014.

[167] F. Faraji, A. Majazi, K. Al-Haddad, *et al.*, "A comprehensive review of flywheel energy storage system technology", *Renewable and Sustainable Energy Reviews*, vol. 67, pp. 477–490, 2017.

[168] J. Abrahamsson, M. Hedlund, T. Kamf, and H. Bernhoff, "High-speed kinetic energy buffer: Optimization of composite shell and magnetic bearings", *IEEE Transactions on Industrial Electronics*, vol. 61, no. 6, pp. 3012–3021, 2014.

[169] G. Ibarra-Berastegi *et al.*, "Electricity production, capacity factor, and plant efficiency index at the mutriku wave farm (2014–2016)", *Ocean Engineering*, vol. 147, pp. 20–29, 2018.

[170] E. Tedeschi and M. Santos-Mugica, "Modeling and control of a wave energy farm including energy storage for power quality enhancement: The bimep case study", *IEEE Transactions on Power Systems*, vol. 29, no. 3, pp. 1489–1497, 2014.

[171] R. Hebner, J. Beno, and A. Walls, "Flywheel batteries come around again", *IEEE spectrum*, vol. 39, no. 4, pp. 46–51, 2002.

[172] H. Bleuler, J. Sandtner, Y.-J. Regamey, and A. F Barrot, "Passive magnetic bearings for flywheels", Jan. 2005.

[173] W. Wang, H. Hofmann, and C. E. Bakis, "Ultrahigh speed permanent magnet motor/generator for aerospace flywheel energy storage applications", in *IEEE International Conference on Electric Machines and Drives, 2005.*, IEEE, 2005, pp. 1494–1500.

[174] I. Boldea and S. A. Nasar, *The induction machines design handbook*. CRC press, 2009.

[175] S. Amodeo, A. Leon, H. Chiacchiarini, J. Solsona, and C. Busada, "Nonlinear control strategies of a flywheel driven by a synchronous homopolar machine", in *Industrial Electronics, 2007. ISIE 2007. IEEE International Symposium on*, IEEE, 2007, pp. 227–232.

[176] International Energy Agency, "Implementing Agreement on Ocean Energy Systems, OES-IA, Annual Report 2009", IEA-OES executive committee, Tech. Rep., 2009.

[177] C. Boström, "Electrical systems for wave energy conversion", PhD thesis, Uppsala University, 2011.

[178] R. Waters, J. Engström, J. Isberg, and M. Leijon, "Wave climate of the swedish west coast", *Renewable Energy*, vol. 34, no. 6, pp. 1600–1606, 2009.

[179] M. Rahm *et al.*, "Offshore underwater substation for wave energy converter arrays", *IET Renewable Power Generation*, vol. 4, no. 6, pp. 602–612, 2010.

[180] F. Rémouit *et al.*, "Deployment and maintenance of wave energy converters at the lysekil research site: A comparative study on the use of divers and remotely-operated vehicles", *Journal of Marine Science and Engineering*, vol. 6, no. 2, p. 39, 2018.

[181] A. Brito e Melo and J. L. Villate, "Annual report 2016", Executive Committee of Ocean Energy Systems, Tech. Rep., 2016.

[182] (2018). Lysekil Wave Energy Site, [Online]. Available: `https://tethys.pnnl.gov/annex-iv-sites/lysekil-wave-energy-site` (visited on 05/06/2018).

[183] M. Leijon *et al.*, "Wave energy from the north sea: Experiences from the lysekil research site", *Surveys in geophysics*, vol. 29, no. 3, pp. 221–240, 2008.

[184] E. Lejerskog *et al.*, "Lysekil research site, Sweden: A status update", in *9th European Wave and Tidal Energy Conference, Southampton, UK, 5-9 September 2011*, 2011.

[185] O. Svensson, C. Boström, M. Rahm, and M. Leijon, "Description of the control and measurement system used in the low voltage marine substation at the Lysekil research site", in *Proceedings of the 8th European Wave and Tidal Energy Conference, Uppsala, Sweden*, 2009.

[186] C. Boström *et al.*, "Study of a wave energy converter connected to a nonlinear load", *IEEE Journal of Oceanic Engineering*, vol. 34, no. 2, pp. 123–127, 2009.

[187] V. Castellucci, J. García-Terán, M. Eriksson, L. Padman, and R. Waters, "Influence of sea state and tidal height on wave power absorption", *IEEE Journal of Oceanic Engineering*, vol. 42, no. 3, pp. 566–573, 2017.

[188] R. Waters *et al.*, "Experimental results from sea trials of an offshore wave energy system", *Applied Physics Letters*, vol. 90, no. 3, p. 034 105, 2007.

[189] (2018). Mätdata - Islandsberg. Significant Wave Height Uppsala University, [Online]. Available: `http://islandsberg.angstrom.uu.se/` (visited on 05/06/2018).

[190] M. Hedlund, J. Abrahamsson, J. J. Pérez-Loya, J. Lundin, and H. Bernhoff, "Eddy currents in a passive magnetic axial thrust bearing for a flywheel energy storage system", *International Journal of Applied Electromagnetics and Mechanics*, vol. 54, no. 3, pp. 389–404, 2017.

[191] M. Hedlund, J. Lundin, J. de Santiago, J. Abrahamsson, and H. Bernhoff, "Flywheel energy storage for automotive applications", *Energies*, vol. 8, no. 10, pp. 10 636–10 663, 2015.

[192] S. H. Gorland, E. E. Kempke Jr, and S. Lumannick, "Experimental windage losses for close clearance rotating cylinders in the turbulent flow regime", NASA technical memorandum, Tech. Rep., 1970.

[193] M. Hedlund, "Electrified integrated kinetic energy storage", PhD thesis, Uppsala University, 2017.

[194] K. Larsson, "Investigation of a wave energy converter with a flywheel and a corresponding generator design", Master's thesis, Chalmers University of Technology, Göteborg, 2012.

[195] N. J. Abram *et al.*, "Early onset of industrial-era warming across the oceans and continents", *Nature*, vol. 536, no. 7617, p. 411, 2016.

[196] "Key requirements for future control room functionality", The ELECTRA EU research project, Tech. Rep., 2015.

[197] D. Li and D. L. Lubkeman, "Simulation of integrated volt/var control for pv penetration studies", in *Power & Energy Society General Meeting, 2017 IEEE*, IEEE, 2017, pp. 1–5.

[198] A. Majumdar, Y. P. Agalgaonkar, B. C. Pal, and R. Gottschalg, "Centralized volt–var optimization strategy considering malicious attack on distributed energy resources control", *IEEE Transactions on Sustainable Energy*, vol. 9, no. 1, pp. 148–156, 2018.

[199] "Application of Automated Controls for Voltage and Reactive Power Management - Initial Results", U.S. Department of Energy, Tech. Rep., Nov. 2012. [Online]. Available: `https://www.smartgrid.gov/document/application_automated_controls_voltage_and_reactive_power_management_initial_results.html` (visited on 01/28/2019).

[200] R. Anilkumar, G. Devriese, and A. K. Srivastava, "Voltage and Reactive Power Control to Maximize the Energy Savings in Power Distribution System With Wind Energy", *IEEE Transactions on Industry Applications*, vol. 54, no. 1, pp. 656–664, 2018.

[201] R. A. Jabr, "Robust Volt/VAr Control with Photovoltaics", *IEEE Transactions on Power Systems*, vol. doi: 10.1109/TPWRS.2018.2890767, pp. 1–1, 2019.

[202] K. E. Antoniadou-Plytaria, I. N. Kouveliotis-Lysikatos, P. S. Georgilakis, and N. D. Hatziargyriou, "Distributed and decentralized voltage control of smart distribution networks: Models, methods, and future research", *IEEE Transactions on Smart Grid*, vol. 8, no. 6, pp. 2999–3008, 2017.

[203] *ANSI C84.1-2016. American National Standard for Electric Power Systems and Equipment—Voltage Ratings (60 Hz)*, 2016.

[204] *Resolución de 30 de julio de 1998, de la Secretaría de Estado de Energía y Recursos Minerales, por la que se aprueba un conjunto de procedimientos de carácter técnico e instrumental necesarios para realizar la adecuada gestión técnica del sistema eléctrico*, Ministerio de Industria y Energía.«BOE» núm. 197, de 18 de agosto de 1998.

[205] Z. Li, Q. Guo, H. Sun, and J. Wang, "Coordinated transmission and distribution AC optimal power flow", *IEEE Transactions on Smart Grid*, vol. 9, no. 2, pp. 1228–1240, 2018.

[206] R. A. Jabr and I. Džafić, "Sensitivity-based discrete coordinate-descent for Volt/-VAr control in distribution networks", *IEEE Transactions on Power Systems*, vol. 31, no. 6, pp. 4670–4678, 2016.

[207] C. Masters, "Voltage rise: the big issue when connecting embedded generation to long 11 kV overhead lines", *Power engineering journal*, vol. 16, no. 1, pp. 5–12, 2002.

[208] P. N. Vovos, A. E. Kiprakis, A. R. Wallace, and G. P. Harrison, "Centralized and distributed voltage control: Impact on distributed generation penetration", *IEEE Transactions on power systems*, vol. 22, no. 1, pp. 476–483, 2007.

[209] "EXISTING AND FUTURE PV PROSUMER CONCEPTS. Deliverable D2.1. PV-Prosumers4Grid (PVP4Grid)", EU project, Tech. Rep., 2018.

[210] R. Tonkoski, D. Turcotte, and T. H. El-Fouly, "Impact of high pv penetration on voltage profiles in residential neighborhoods", *IEEE Transactions on Sustainable Energy*, vol. 3, no. 3, pp. 518–527, 2012.

[211] O. Samuelsson et al, "Active distribution network-Demonstration project ADINE", in *2010 IEEE PES Innovative Smart Grid Technologies Conference Europe (ISGT Europe), Gothenberg*, IEEE, 2010, pp. 1–8.

[212] R. Walling, R. Saint, R. C. Dugan, J. Burke, and L. A. Kojovic, "Summary of distributed resources impact on power delivery systems", *IEEE Transactions on power delivery*, vol. 23, no. 3, pp. 1636–1644, 2008.

[213] J. Zhao, Z. Zhang, J. Yao, S. Yang, and K. Wang, "A distributed optimal reactive power flow for global transmission and distribution network", *International Journal of Electrical Power & Energy Systems*, vol. 104, pp. 524–536, 2019.

[214] M. Manbachi, H. Farhangi, A. Palizban, and S. Arzanpour, "Maintenance Scheduling of VoltVAR Control Assets in Smart Distribution Networks Using Advanced Metering Infrastructure", *Canadian Journal of Electrical and Computer Engineering*, vol. 39, no. 1, pp. 26–33, 2016.

[215] R. D. Zimmerman, C. E. Murillo-Sánchez, R. J. Thomas, *et al.*, "Matpower: Steady-state operations, planning, and analysis tools for power systems research and education", *IEEE Transactions on power systems*, vol. 26, no. 1, pp. 12–19, 2011.

[216] M. Alonso Martínez, "Gestión óptima de potencia reactiva en sistemas eléctricos con generación eólica", PhD thesis, Universidad Carlos III de Madrid, 2010.

Appendices

A. LYSEKIL RESEARCH SITE DATA

A.1. WECs units data [177]

A.1.1. L1, L2 and L3 main parameters

Main parameters of L1	
Nominal power at 0.7 m/s	10 kW
Voltage, line-to-line, rms at 0.7 m/s, V_d	200 V
Generator resistance, R_G	0.44±1.5% Ω
Generator inductance, L_S	11.7 mH
Air gap	3 mm
Size of magnet block	6.5x35x100 mm^3
Pole width, w_p	50 mm
Number of stator sides	4
Vertical stator length	1264 mm
Vertical translator length	1867 mm
Translator resp. stator width	400 mm
Translator weight	1000 kg

A.1.2. L9 main parameters

Main parameters of L9	
Nominal power at 0.7 m/s	20 kW
Voltage, line-to-line, rms at 0.7 m/s, V_d	450 V
Generator resistance R_G	1±1.5% Ω
Generator inductance L_S	20 mH
Air gap	3 mm
Size of magnet block	6.5x47x230 mm^3
Pole width, w_p	55 mm
Number of stator sides 4	
Vertical stator length	2000 mm
Vertical translator length	2000 mm
Translator resp. stator width	230x2 mm
Translator weight	2700 kg

A.2. Linear generator [193]

Power	5 kW
Voltage (line-to-line)	100 V
Current	28.9 A
Speed	0.67 m/s
Conductor area (Cu)	16 mm^2
Slots per pole and phase	6/5
Pole width	50 mm
Air-gap	3 mm
Stator length	700 mm (14 poles)
Translator length	650 mm (13 poles)
No. of stator sides	4
Width of stator side	400 mm
Active gen. area	1.04 m^2

A.3. Marine substation and cable parameters

A.3.1. Marine substation [179]

substation power	96 kVA
maximum water depth for present design	30 m
vessel volume	3 m^3
concrete foundation weight	5 tonne
substation output voltage	1 kV
max. DC voltage	500 V
DC-link capacitance (DC+ to DC−)	0.24 F
transformer winding ratios	1000/250, 180, 125,100, 80
tap changing mechanism	circuit breakers (off-load)

A.3.2. Marine cable [177]

Main parameters of the sea cable	
Sea cable resistance R_C	0.54±1.5% Ω
Sea cable inductance L_C	<0.01 mH
Sea cable capacitance C_C	145 μF

A.4. Uppsala University Flywheel Prototype

Max. kinetic energy (Wh)	Low power side phase-voltage (Vrms)	High power side phase-voltage (Vrms)	Operating speed range (rpm)	Moment of inertia (kg*m^2)	Rotor mass (kg)	Outer diameter (m)
867.7	116	269	15-30k	0.636	46.7	0.345

More information about the Uppsala University Flywheel Prototype can be found at [168].

B. POWER SYSTEMS DATA

B.1. MV power system data [216]

TABLE B.1 MV POWER SYSTEM: BUSES AND LOAD DATA

Bus	Name	P_d(p.u.)	Q_d(p.u.)
380 kV Network			
1	Lastras	0	0
132 kV Network			
2	Lastras	0	0
3	Burguillo	24	-16
4	Perogordo	0	0
5	Langa	0	0
6	Puente de Piedra	0	0
7	Ávila	0	0
45 kV Network			
8	Ávila	0	0
9	Muñana	0	0
10	Piedrahita	0	0
11	Barco de Ávila	0	0
12	Gotarrendura	0	0
13	Riolanza	0	0
14	Fontiveros	0	0
15	Madrigal	0	0
16	Langa	0	0
17	Arévalo	0	0
18	Nava de la Asunción	0	0
19	Puente de Piedra	0	0
20	Cuéllar	2,7	0,3
21	Cantalejo	6,3	3,052
22	Turégano	3,106	1,323
23	Perogordo	4,5	0,5
24	Punto1	0	0
25	Campo,AZ	0	0
26	Navalperal de Pinares	0	0
27	Cristo del Caloco	0	0
28	Punto2	0	0
29	V, de Matutue	0	0
30	Otero	0	0
31	Cerro de la Horca	0	0
32	Batanes	9	1

TABLE B.2 MV POWER SYSTEM: BUSES AND LOAD DATA (continuation)

Bus	Name	P_d(p.u.)	Q_d(p.u.)
15 kV Network			
33	Ávila	5,068	1,5237
34	Muñana	0,2667	0,1997
35	Piedrahita	0,3945	0,2147
36	Barco de Ávila	0,5518	0,1472
37	Gotarrendura	0,627	0,1675
38	Riolanza	0,3793	0,1128
39	Fontiveros 1	0,2521	0,0653
40	Fontiveros 2	0,2521	0,0653
41	Madrigal	0,698	0,1776
42	Langa	0,2382	0,0658
43	Arévalo 1	0,428	0,1
44	Arévalo 2	0,428	0,108
45	Arévalo 1	0,428	0,108
46	Nava de la Asunción	1,0177	0,5493
47	Puente de Piedra	0,8785	0,322
48	Cuéllar	1,573	0,5169
49	Cantalejo	0,626	0,2477
50	Turégano	0,3723	0,191
51	Campo A,	0,0027	0
52	Navalperal de Pinares	0,7479	0,1973
53	Cristo del Caloco	0,8183	0,373
54	V, de Matutue	0,0037	0,0023
55	Otero -1	0,3447	0,167
56	Otero -2	0,3447	0,167
57	Cerro de la Horca	3,0113	0,6113
58	Batanes -1	1,4473	0,4757
59	Batanes -2	1,4473	0,4757
380V Network			
60	Avila1	3,3789	1,0158
61	Avila2	3,3789	1,0158
62	Avila1	3,3789	1,0158
63	Muñana 1	0,1778	0,1332
64	Muñana 2	0,1778	0,1332
65	Muñana 1	0,1778	0,1332
66	Piedrahita1	0,2631	0,1351
67	Piedrahita2	0,2631	0,1351
68	Piedrahita1	0,2631	0,1351

TABLE B.3 MV POWER SYSTEM: BUSES AND LOAD DATA (continuation)

Bus	Name	P_d(p.u.)	Q_d(p.u.)
380V Network			
69	Barco de Ávila 1	0,3678	0,1981
70	Barco de Ávila 2	0,3678	0,1981
71	Barco de Ávila 1	0,3678	0,1981
72	Gotarrendura 1	0,4175	0,226
73	Gotarrendura 2	0,4175	0,226
74	Gotarrendura 1	0,4175	0,226
75	Riolanza 1	0,2528	0,1962
76	Riolanza 2	0,2528	0,1962
77	Riolanza 3	0,2528	0,1962
78	Fontiveros 11	0,168	0,0812
79	Fontiveros 12	0,168	0,0812
80	Fontiveros 21	0,168	0,0812
81	Fontiveros 22	0,168	0,0812
82	Fontiveros 23	0,168	0,0812
83	Fontiveros 13	0,168	0,0812
84	Madrigal 1	0,4651	0,1941
85	Madrigal 2	0,4651	0,1941
86	Madriga1	0,4651	0,1941
87	Langa 1	0,1588	0,0981
88	Langa 2	0,1588	0,0981
89	Langa 3	0,1588	0,0981
90	Arévalo 11	0,2854	0,1124
91	Arévalo 12	0,2854	0,1124
92	Arévalo 21	0,2854	0,1124
93	Arévalo 22	0,2854	0,1124
94	Arévalo 31	0,2854	0,1124
95	Arévalo 32	0,2854	0,1124
96	Arévalo 13	0,2854	0,1124
97	Arévalo 23	0,2854	0,1124
98	Arévalo 33	0,2854	0,1124
99	Nava Asunción 1	0,6784	0,3662
100	Nava Asunción 2	0,6784	0,3662
101	Nava Asunción 3	0,6784	0,3662
102	Puente de Piedra 1	0,5916	0,322
103	Puente de Piedra 2	0,5916	0,322
104	Puente de Piedra 3	0,5916	0,322
105	Cuéllar 1	1,0407	0,3447

TABLE B.4 MV POWER SYSTEM: BUSES AND LOAD DATA (continuation)

Bus	Name	P_d(p.u.)	Q_d(p.u.)
380V Network			
106	Cuéllar 2	1,0407	0,3447
107	Cuéllar 3	1,0407	0,3447
108	Cantalejo 1	0,4178	0,1651
109	Cantalejo 2	0,4178	0,1651
110	Cantalejo 1	0,4178	0,1651
111	Turégano 1	0,2483	0,1273
112	Turégano 2	0,2483	0,1273
113	Turégano 3	0,2483	0,1273
114	Campo, A, 1	0,0018	0,0014
115	Campo, A, 2	0,0018	0,0014
116	Campo, A, 3	0,0018	0,0014
117	Navalperal 1	0,4985	0,2551
118	Navalperal 2	0,4985	0,2551
119	Navalperal 3	0,4985	0,2551
120	Cristo del Caloco 1	0,5456	0,2487
121	Cristo del Caloco 2	0,5456	0,2487
122	Cristo del Caloco 3	0,5456	0,2487
123	V, de Matutue 1	0,0024	0,0016
124	V, de Matutue 2	0,0024	0,0016
125	V, de Matutue 3	0,0024	0,0016
126	Otero 11	0,2298	0,1114
127	Otero 12	0,2298	0,1114
128	Otero 21	0,2298	0,1114
129	Otero 22	0,2298	0,1114
130	Otero 13	0,2298	0,1114
131	Otero 23	0,2298	0,1114
132	Cerro de la Horca 1	2,0076	0,4076
133	Cerro de la Horca 2	2,0076	0,4076
134	Cerro de la Horca 3	2,0076	0,4076
135	Batanes 11	0,9649	0,3171
136	Batanes 12	0,9649	0,3171
137	Batanes 21	0,9649	0,3171
138	Batanes 22	0,9649	0,3171
139	Batanes 13	0,9649	0,3171
140	Batanes 23	0,9649	0,3171

TABLE B.5 MV POWER SYSTEM: BRANCH DATA

From Bus	To Bus	R (p.u.)	X(p.u.)	B(p.u.)
3	7	0,0359	0,08015	0,01548
7	2	0,0274	0,0927	0,0197
2	4	0,01165	0,0394	0,00837
2	5	0,0329	0,11129	0,0236
2	6	0,0219	0,0742	0,0157
8	9	0,3468	0,578	0,00166
9	10	0,37	0,5916	0,00186
10	11	0,287	0,458	0,00144
8	12	0,1487	0,3887	0,0013
12	13	0,2574	0,331	0,00099
12	14	0,3634	0,4668	0,00141
14	15	0,375	0,3619	0,001
14	16	0,122	0,2506	0,00077
16	17	0,122	0,2506	0,00077
17	12	0,1487	0,3887	0,0013
17	18	0,1416	0,3702	0,00123
18	19	0,122	0,237	0,00082
19	20	0,2533	0,5205	0,0016
19	20	0,909	0,6035	0,0017
19	21	0,23	0,778	0,00223
21	22	0,2332	0,2623	0,000856
22	23	0,2439	0,4888	0,00158
8	24	0,3831	0,4309	0,0014
24	25	0,003	0,00399	0,0000115
24	26	0,1363	0,1764	0,000525
24	27	0,3331	0,3747	0,0012
27	28	0,1261	0,1182	0,00035
28	29	0,00187	0,00385	0,0000118
28	30	0,10506	0,0985	0,00029
30	23	0,1998	0,225	0,00073
23	32	0,1514	0,1945	0,00059
32	31	0,042	0,0394	0,00116
23	31	0,0375	0,0794	0,00023
23	31	0,0375	0,0794	0,00023

TABLE B.6 MV POWER SYSTEM: TRANSFORMER DATA

From Bus	To Bus	R (p.u.)	X(p.u.)	B(p.u.)
132 kV/45 kV and 45 kV/15 kV				
1	2	0,00145	0,07345	0
4	23	0,00683	0,20483	0
5	16	0,01467	0,4163	0
6	19	0,0073	0,1748	0
47	19	0,106	1,4762	0
7	8	0,01467	0,34	0
7	8	0,01467	0,34	0
7	33	0,01467	0,3263	0
34	9	0,106	1,476	0
10	35	0,232	2,388	0
36	11	0,106	1,596	0
12	37	0,106	1,496	0
38	13	0,106	1,596	0
14	39	0,106	1,756	0
14	40	0,106	1,596	0
15	41	0,0267	0,5327	0
16	42	0,044	0,798	0
17	43	0,106	1,596	0
17	44	0,106	1,596	0
17	45	0,106	1,596	0
46	18	0,044	0,798	0
20	48	0,044	0,758	0
49	21	0,106	1,596	0
50	22	0,232	4,712	0
25	51	0,536	5,896	0
26	52	0,0267	0,5327	0
53	27	0,106	1,596	0
29	54	0,536	4,768	0
55	30	0,232	3,1508	0

TABLE B.7 MV POWER SYSTEM: TRANSFORMER DATA (continuation)

From Bus	To Bus	R (p.u.)	X(p.u.)	B(p.u.)
56	30	0,232	3,312	0
32	58	0,06	0,9573	0
32	59	0,06	0,9573	0
31	57	0,0267	0,5193	0
15 kV / 380V				
33	60	0,3472	0,6014	0
33	61	0,3472	0,6014	0
33	62	0,3472	0,6014	0
34	63	2,0833	3,6083	0
34	64	2,0833	3,6083	0
34	65	2,0833	3,6083	0
35	66	4,167	7,2167	0
35	67	4,167	7,2167	0
35	68	4,167	7,2167	0
36	69	2,0833	3,6083	0
36	70	2,0833	3,6083	0
36	71	2,0833	3,6083	0
37	72	2,0833	3,6083	0
37	73	2,0833	3,6083	0
37	74	2,0833	3,6083	0
38	75	2,0833	3,6083	0
38	76	2,0833	3,6083	0
38	77	2,0833	3,6083	0
39	78	2,0833	3,6083	0
39	79	2,0833	3,6083	0
39	83	2,0833	3,6083	0
40	80	2,0833	3,6083	0
40	81	2,0833	3,6083	0
40	82	2,0833	3,6083	0
41	84	0,6944	1,2028	0
41	85	0,6944	1,2028	0
41	86	0,6944	1,2028	0
42	87	1,04167	1,8042	0
42	88	1,04167	1,8042	0
42	89	1,04167	1,8042	0
43	90	2,0833	3,6083	0
43	91	2,0833	3,6083	0
44	92	2,0833	3,6083	0
44	93	2,0833	3,6083	0

TABLE B.8 MV POWER SYSTEM: TRANSFORMER DATA (continuation)

From Bus	To Bus	R (p.u.)	X(p.u.)	B(p.u.)
15 kV / 380V				
45	94	2,0833	3,6083	0
45	95	2,0833	3,6083	0
43	96	2,0833	3,6083	0
44	97	2,0833	3,6083	0
45	98	2,0833	3,6083	0
46	99	1,04167	1,8042	0
46	100	1,04167	1,8042	0
46	101	1,04167	1,8042	0
47	102	2,0833	3,6083	0
47	103	2,0833	3,6083	0
47	104	2,0833	3,6083	0
48	105	1,04167	1,8042	0
48	106	1,04167	1,8042	0
48	107	1,04167	1,8042	0
49	108	2,0833	3,6083	0
49	109	2,0833	3,6083	0
49	110	2,0833	3,6083	0
50	111	4,167	7,2167	0
50	112	4,167	7,2167	0
50	113	4,167	7,2167	0
51	114	8,33	14,43	0
51	115	8,33	14,43	0
51	116	8,33	14,43	0
52	117	0,6944	1,2028	0
52	118	0,6944	1,2028	0
52	119	0,6944	1,2028	0
53	120	2,0833	3,6083	0
53	121	2,0833	3,6083	0
53	122	2,0833	3,6083	0
54	123	8,33	14,43	0
54	124	8,33	14,43	0
54	125	8,33	14,43	0
55	126	4,167	7,2167	0
55	127	4,167	7,2167	0
56	128	4,167	7,2167	0
56	129	4,167	7,2167	0
55	130	4,167	7,2167	0
56	131	4,167	7,2167	0

TABLE B.9 MV POWER SYSTEM: TRANSFORMER DATA (continuation)

From Bus	To Bus	R (p.u.)	X(p.u.)	B(p.u.)
15 kV / 380V				
57	132	0,6944	1,2028	0
57	133	0,6944	1,2028	0
57	134	0,6944	1,2028	0
58	135	1,389	2,405	0
58	136	1,389	2,405	0
59	137	1,389	2,405	0
59	138	1,389	2,405	0
58	139	1,389	2,405	0
59	140	1,389	2,405	0

B.2. LV power system data [34]

TABLE B.10 LV POWER SYSTEM: BRANCH DATA

Branch	Line R (p.u.)	Line X (p.u.)	Branch	Line R (p.u.)	Line X (p.u.)
1	0,714	0,452	41	1,332	0,193
2	0,712	0,450	42	1,848	1,168
3	1,829	1,156	43	2,123	1,342
4	5,851	3,698	44	1,332	0,193
5	11,030	1,600	45	1,336	0,194
6	1,431	0,904	46	1,776	0,258
7	1,652	1,044	47	1,776	0,258
8	5,647	3,569	48	1,776	0,258
9	1,784	1,128	49	1,776	0,258
10	1,674	1,058	50	1,776	0,258
11	1,332	0,193	51	1,776	0,258
12	1,675	1,059	52	1,776	0,258
13	1,332	0,193	53	1,776	0,258
14	1,443	0,912	54	1,776	0,258
15	1,332	0,193	55	1,776	0,258
16	0,368	0,233	56	3,243	2,050
17	1,333	0,194	57	1,332	0,193
18	2,962	1,872	58	4,950	3,129
19	1,339	0,194	59	1,332	0,193
20	2,499	1,580	60	3,712	2,346
21	1,332	0,193	61	1,330	0,193
22	13,322	2,078	62	0,346	0,219
23	0,260	0,164	63	0,346	0,219
24	1,776	0,277	64	1,776	0,258
25	1,776	0,277	65	1,776	0,258
26	0,346	0,219	66	1,776	0,258
27	0,346	0,219	67	1,776	0,258
28	1,776	0,258	68	1,776	0,258
29	1,776	0,258	69	1,776	0,258
30	1,776	0,258	70	1,984	1,254
31	1,776	0,258	71	3,583	0,520
32	1,776	0,258	72	2,376	1,502
33	1,776	0,258	73	0,712	0,450
34	1,776	0,258	74	2,390	1,510
35	1,776	0,258	75	1,332	0,193
36	3,688	2,331	76	0,976	0,617

TABLE B.11 LV POWER SYSTEM: BRANCH DATA (continuation)

Branch	Line R (p.u.)	Line X (p.u.)	Branch	Line R (p.u.)	Line X (p.u.)
37	1,335	0,194	77	1,331	0,193
38	3,581	2,263	78	0,194	0,123
39	1,332	0,193	79	3,297	2,084
40	1,824	1,153	80	4,461	2,820
81	3,009	1,902	125	1,332	0,193
82	1,997	1,262	126	1,564	0,988
83	1,295	0,188	127	1,332	0,193
84	3,743	2,366	128	1,564	0,989
85	1,332	0,193	129	1,332	0,193
86	2,823	1,784	130	1,563	0,988
87	1,332	0,193	131	1,332	0,193
88	1,332	0,193	132	6,533	4,129
89	3,398	2,148	133	1,332	0,193
90	1,776	0,258	134	1,646	1,040
91	1,776	0,258	135	1,332	0,193
92	1,776	0,258	136	1,647	1,041
93	1,776	0,258	137	1,332	0,193
94	2,327	1,471	138	1,623	1,026
95	1,327	0,193	139	1,332	0,193
96	5,825	3,681	140	0,625	0,395
97	1,340	0,194	141	1,776	0,258
98	0,378	0,239	142	1,332	0,193
99	1,310	0,190	143	1,329	0,840
100	4,588	2,899	144	1,776	0,258
101	1,332	0,193	145	1,776	0,258
102	1,776	0,258	146	1,332	0,193
103	1,776	0,258	147	1,617	1,022
104	3,659	2,313	148	1,332	0,193
105	1,332	0,193	149	1,332	0,193
106	2,315	1,463	150	1,610	1,018
107	1,332	0,193	151	1,332	0,193
108	0,564	0,356	152	1,862	1,177
109	1,332	0,193	153	0,346	0,219
110	2,651	1,675	154	0,346	0,219
111	0,260	0,164	155	1,776	0,258
112	1,776	0,258	156	1,776	0,258

TABLE B.12 LV POWER SYSTEM: BRANCH DATA (continuation)

Branch	Line R (p.u.)	Line X (p.u.)	Branch	Line R (p.u.)	Line X (p.u.)
113	1,776	0,258	157	1,776	0,258
114	1,776	0,258	158	1,776	0,258
115	1,776	0,258	159	1,776	0,258
116	1,776	0,258	160	1,776	0,258
117	1,776	0,258	161	1,776	0,258
118	4,883	3,086	162	1,776	0,258
119	0,497	0,314	163	1,776	0,258
120	1,207	0,763	164	1,776	0,258
121	1,332	0,193	165	1,776	0,258
122	5,718	3,614	166	1,776	0,258
123	1,332	0,193	167	1,776	0,258
124	1,559	0,986	168	1,776	0,258
169	1,776	0,258	180	1,574	0,995
170	1,776	0,258	181	1,332	0,193
171	1,776	0,258	182	1,572	0,994
172	1,776	0,258	183	1,332	0,193
173	1,776	0,258	184	1,332	0,193
174	1,776	0,258	185	1,831	1,157
175	1,776	0,258	186	1,776	0,258
176	1,776	0,258	187	1,776	0,258
169	1,776	0,258	188	0,346	0,219
170	1,776	0,258	189	0,346	0,219
171	1,776	0,258	190	1,776	0,258
172	1,776	0,258	191	1,776	0,258
173	1,776	0,258	192	1,776	0,258
174	1,776	0,258	193	1,776	0,258
175	1,776	0,258	194	1,776	0,258
176	1,776	0,258	195	1,776	0,258
177	1,776	0,258	196	1,776	0,258
178	1,570	0,993	197	1,776	0,258
179	1,332	0,193			